

# Parametric Design of Magnetics for Modern Power Electronics Applications

Kapila Warnakulasuriya

School of Computing, Engineering & Digital Technologies Teesside University,  
Middlesbrough, UK

A thesis submitted in partial fulfillment of the requirements of Teesside University for the  
degree of Doctor of Philosophy.

Supervised by Dr. David Hughes  
Dr. Maher Al-Greer  
Prof. Nashwan Dawood

March 2021



## Dedication

I dedicate this thesis to my wife Chathurika, my son Nidula and my daughter Methuki with whom I would have spent the time I devoted to this study.

## Abstract

Magnetic components in a power conversion system or in any power electronics application are responsible for a major part of the volume, weight, and the cost of the systems that they are built in to. It is believed that the size of magnetic components and thereby the cost and the size of power electronics systems can be reduced by the increase of operating frequency. Achieving low switching losses of the semiconductor devices and realizing magnetic components that can operate at high frequencies at high power levels have been identified as the two major challenges.

This research aims to provide a complete set of “parametric solutions” of magnetics for a particular application that enables holistic optimization of power electronics systems. At the start of the research providing a single solution for the power levels and frequency was a not possible. Design variables considered in this study include conductor losses, which included the study of skin effect, proximity effect in different conductor geometries, assemblies and types, core losses in different core geometries, materials and constructions, thermal management of the magnetic components including efficient extraction of heat generated, impacts of inductance, leakage inductance, and losses.

The practical solutions derived from the theoretical studies are evaluated in a number of constructions. Several winding configurations were developed which give the advantage of mitigating the conductor losses at high frequencies and high currents. This includes folded foil windings and transposed wound flat conductor windings which is demonstrated to reduce the conductor losses by a factor of  $>4$ .

The effectiveness of different core materials for  $> 50$  kW was evaluated. Suitability of certain ferrite grades and nanocrystalline grades were identified for different application areas. Even though the findings of the study made it possible achieve theoretically minimum loss levels the compactness achieved results in high-power densities making it difficult to have good thermal management. Novel methods for heat extraction are developed. These provided a drop in hotspot temperature by 10 to 25 degrees. These developments in all the key areas of a magnetic design and the provision of complete set of parametric solutions is presented in this thesis. The design of a 50kW transformer operating at 20kHz was a challenge before this study. With the findings of this study now the design of even 2500 kW transformer is no longer a challenge. The outcome of the research has taken the magnetics industry to the position of a technology enabler rather than being a factor that acts as a barrier for the development of power electronics industry.



## Acknowledgements

I started doing my employer funded PhD at Teesside University in February 2014 under the supervisors Professor Farhad Nabhani and Dr. David Hughes. My research proposal was developed based on my, at that time over 12 years of experience in working as a senior design engineer in the field magnetics for leading companies that were working with cutting edge technologies both in Germany and in the United Kingdom. The research was aimed at finding solutions to overcome barriers that were holding the magnetics industry and eventually the power electronics industry back.

I started my PhD with great enthusiasm and made particularly good progress. Because of the R&D nature of my employment, the maturity in the subject area, the great guidance I received from my supervisors and the Teesside University and its R & D resources I made particularly good progress in my PhD work. I was able to make 12 peer reviewed publications in world leading conferences around the world (in North America, South America, England, Germany etc..) which were very well received by the industry and academic experts in the field.

During the course of my PhD studies, I received a job offer from one of the largest Japanese electronics component manufacturing companies to work as the principal engineer for magnetics in an R& D capacity in one of their R & D centers located in Milton Keynes in the UK. Through I received this offer while I was doing my PhD this was a position advertised for a person who preferably already had a PhD in the field of magnetics. Because of the progress that I had made, the publications that I had done and the demonstration of knowledge in the field of magnetics I had exhibited in the industry I was offered this position.

This was a great opportunity for me to continue my research work. I joined this company leaving the previous company, but I continued my research work very well. I have submitted over 7 patent applications and currently also working as a key researcher in its Milton Keynes R & D center.

My Supervisor Dr. David Hughes was providing advice on a regular basis and guide me to the completion of my PhD.

I would like to make this an opportunity expresses my sincere thanks to Professor Farhad Nabhani, Dr David Hughes and Dr Maher Al-Greer without whom carrying out this research would not be possible.

Kapil Warnakulasuriya

Bsc(Eng) CEng MIET MIEEE Minstp MIMA

Dedication	ii
Abstract	iii
Acknowledgements	v
Abbreviations	xiii
Symbols	xiv
Chapter 1 Introduction	2
1.1 Motivation and overview of the outcome	4
1.2 Current status of the industry and limitations	8
1.3 Current technologies	10
1.31. Research in the development of “Planar” transformers.	10
1.32 Research in the development of “Litz” wire technologies	13
1.33 Research in the development high power high frequency transformers with foil conductors	15
1.4 Novel approach made in this research.	16
1.41 Aim and objectives	17
1.5 Contributions made by the study	19
Patents	19
Publications	22
1.6 Framework for thesis	25
1.7 Summary	27
Chapter 2 Parametric approach for magnetics design	29
2.1 Parametric design	29
2.11 Parametric Design Method	31
2.12 The Realization of Parametric Design	31
Define Parameters	31
Analysis and Calculation of Components Size and Core Parameter Expressions	32
2.2 Parametric design of magnetic components	32
2.21 Design parameters of a magnetic component	33
2.22 Possible transformer constructions	34

2.23 Possible cooling options	35
2.24 Different core and conductor material options	35
2.3 Design tool that facilitates the parametric design of magnetics.	36
2.4 Summary of design options arrived for a 100 kW 50 kHz transformer application.	39
2.5 Summary	41
Chapter 3 Conductor losses in magnetic components	43
3.1 Theoretical background	45
3.11 Skin Effect	45
3.12 Proximity Effect	50
Proximity Effect in the context of foil windings	50
Dowell's Porosity Factor	59
Round wires and "Litz" wires	73
Effects of Twisting Imperfections	97
3.33 Losses in non-current carrying windings.	100
3.4 Experimental results	101
3.41 Inductor applications	101
3.42 transformer applications	103
3.43 High Frequency Transformer 50kW, 50kHz	104
Conductor selection and winding losses estimations.	104
3.44 High Frequency Inductor 8.5μH at 300A, 50kHz	107
3.45 Development of a 100kW, 20 kHz Nanocrystalline Core Transformer for DC / DC Converter Applications	110
Transformer Construction	111
Transformer core selection and turns calculation	112
Conductor selection and winding loss mitigation.	112
3.5 Winding arrangement that enables the handling of high frequency large currents in high frequency magnetics.	116
3.6 Discussion	121
3.7 Summary	124

Chapter 4 Core losses estimation of high-power high frequency magnetics	127
4.1 Magnetic Hysteresis	128
4.1.1 Hysteresis Models	129
Jiles-Atherton Model	129
Preisach Model	131
Chan-Vladimirescu Model	133
Loss Separation Approach	135
4.2 Empirical Methods,	141
4.2.1 Steinmetz Equation	141
4.2.2 Modified Steinmetz Equation	142
4.2.3 Improved Generalized Steinmetz Equation (IGSE)	143
4.2.4 Equivalent Elliptical Loop (EEL)	147
4.2.5 Waveform coefficient Steinmetz Equation (WcSE)	147
4.3 Magnetic material introduction	149
4.3.1 Characteristics of conventional ferri- and ferro-materials	151
4.3.2 Ferrites	151
4.3.3 Amorphous metals	155
4.3.4 Supermalloy	157
4.3.5 Characteristics of nanocrystalline materials	158
4.4 Comparison of Performances of Amorphous and Nanocrystalline	162
4.5 Gap Losses	164
4.5.1 Calculation of gap losses	164
4.6 Performance Comparison of Nanocrystalline Material with Ferrite in a 40kW 20kHz Application	167
4.6.1 Transformer Design	168
Transformer core selection and turns calculation.	168
Conductor selection and winding losses estimations.	171
Control of leakage inductance	171



4.7 Development of High Frequency Transformer 50kW, 50kHz & High Frequency Inductor 8.5μH at 300A, 50kHz	175
4.71 High Frequency Transformer 50kW, 50kHz	176
Transformer Construction	176
Transformer core selection and turns calculation	177
Transformer core loss estimation	177
Conductor selection and winding losses estimations.	178
4.72 High Frequency Inductor 8.5μH at 300A, 50kHz	179
Inductor core selection	179
Effective heat removal of high-density magnetics	180
Prototype development and testing	180
Discussion	182
4.8 Development of a 100kW, 20 kHz Nanocrystalline Core Transformer for DC / DC Converter Applications	184
Transformer core selection and turns calculation	186
Transformer core loss estimation	186
Conductor selection and winding loss mitigation.	187
Effective heat removal of high-density magnetics	187
Construction for the natural convection cooling	187
Prototype development and testing	189
4.9 Comparison of core constructions	192
Discussion	193
4.10 Summary	195
Chapter 5 Thermal management of High-power High Frequency Magnetics	198
5.1 Thermal Investigations for Dry Type Transformers	199
Example calculations for ventilated dry type transformers	201
5.2 Hot spot investigations for liquid filled transformers.	204
Example calculation for liquid filled transformer	205
5.3 Temperature Rise for High Frequency Transformer under Forced-air Convection	207
5.4 Numerical Analysis of Winding Temperature Field for Dry Type Transformer	209

5.41 The simplified model and boundary conditions	209
Heating and Cooling Analysis of Dry-Type Transformers	211
The Governing Equation and Boundary Condition	212
5.5 Effective heat removal of high-density magnetics	213
5.51 Construction for the natural convection cooling	213
5.52 water cooled plate mounting	213
5.6 Estimation of Temperature Rise in MVA Range Dry-Type Transformers and Practical Verification Based on Simulated Loading	216
5.61 Theoretical background	217
Thermal Modeling	217
Transformer core temperature rise	219
5.62 Product construction	222
5.63 Experimental procedure	224
Discussion	227
5.7 Novel thermal management approaches for high power density transformers.	231
5.8 Novel approach to extract heat from the windings of transformers with high isolation requirements.	234
5.9 Summary	237
Chapter 6 Inductance, impedance, leakage inductance	239
6.1 Theoretical Estimation and Practical Verification of the Impedance and Leakage Inductance of MVA Range Single Phase Transformers	241
6.11 Leakage Inductance Calculation	243
Calculation Method	244
Evaluation based on Dowell's Equations.	246
6.12 Short Circuit Impedance Calculation	246
3D Model	246
Calculation Method.	247
6.13 Experimental Results	247
Transformer construction.	247

6.14 Practical measurements	248
6.15 Discussion	249
6.2 Optimization of 12 and 18 pulse rectifier systems by the selection of optimum parameters for magnetics	252
6.21 Magnetics selection	253
Poly phase transformer selection.	253
Interphase transformer for 12 pulse system	255
Interphase transformer for 18 pulse system	256
6.22 Simulations	256
Simulations of a balanced three-phase input	257
Simulations of an unbalanced three-phase input	259
6.23 Prototype development and testing	261
6.24 Discussion	262
6.3 Summary	264
Chapter 7 Summary	266
7.1 Evolution of magnetics	266
7.1 Evolution of magnetics in power electronics applications	267
7.11 Wire wound components.	267
7.12 Planar magnetic components	269
7.13 .PCB Integrated magnetics	271
7.14 Magnetics on silicon	272
7.15 Ultra-high-power magnetics in excess of 100kW	272
7.2 Contributions of the research	273
7.21 Challenges that magnetics industry faced at the beginning of the research.	273
7.22 Overcoming the challenges in mitigating conductor losses	274
7.23 Minimization of core losses and the seclction of appropreae core material	275
7.24 Thermal management of high power high frequency magnetic components	276

7.25 Leakage inductance and other parameters that influence the system optimization.	276
7.26 Parametric design approach	278
7.3 Future work	280
Chapter 8 References	281

## Abbreviations

DEPT	Distribution Power Electronic Transformer
GSE	Generalized Steinmetz Equation
HF	High Frequency
HFHV	High Frequency High Power
HFHPHV	High Frequency High Power High Voltage
HV	High Voltage
IGBT	Insulated Gate Bipolar Transistor
IGCT	Integrated Gate Commutated Thyristors
IGSE	Improved Generalized Steinmetz Equation.
LV	Low Voltage
MF	Medium Frequency
MFT	Medium-Frequency Transformer
MSE	Modified Steinmetz Equation
MV	Medium Voltage
NSE	Natural Steinmetz Extension
PE	Power Electronics
PET	Power Electronic Transformer
RMS (rms)	Root Mean Square
SST	Solid-State Transformer
SiC	Silicon Carbide.
SiC MOSFET	Silicon Carbide Metal Oxide Substrate Field Effect Transistors
TT	Traction Transformer
WcSE	Waveform coefficient Steinmetz Equation

## Symbols

$k$	Steinmetz equation constant
$a$	Steinmetz equation's frequency parameter
$b$	Steinmetz equation's magnetic induction parameter
$k_h$	Hysteresis loss constant
$k_e$	Eddy current loss constant
$k_a$	Anomalous or excess loss constant
$k_1$	Generalized Steinmetz Equation constant
$k_i$	Improved Generalized Steinmetz Equation constant
$P_v$	Volumetric power loss [W/m <sup>3</sup> ]
$P_s$	Specific power loss [W/kg]
$P_h$	Static hysteresis loss [W/kg]
$P_e$	Classical eddy current loss [W/kg]
$P_a$	Excess or anomalous eddy current loss [W/kg]
$P_w$	Winding total loss [W]
$P$	Foil layer loss [W]
$B$	Magnetic induction [T]
$B_m$	Maximum magnetic induction [T]
$B_s$	Saturation magnetic induction [T]
$B_r$	Remanent magnetic induction [T]
$H$	Magnetic field [A/m]
$H_s$	Saturation magnetic field [A/m]
$H_c$	Coercive magnetic field [A/m]
$H_{irr}$	Irreversible magnetic field [A/m]
$H_{int}$	Internal magnetic field [A/m]
$H_{ext}$	External magnetic field [A/m]
$J$	Current density [A/m <sup>2</sup> ]
$f$	Frequency [1/s]
$f_{eq}$	Equivalent frequency [1/s]
$T$	Period [s]
$T$	Temperature [K]
$d_g$	Interwinding gap thickness [m]
$d_i$	Interlayer gap thickness [m]

$d$	Round conductor diameter [m]
$d_w$	Conductor or layer thickness [m]
$H_w$	Conductor or layer height [m]
$l_w$	Conductor or layer length [m]
$h_c$	Winding window height [m]
$N$	Number of conductors in a winding
$l_s$	Litz strand length [m]
$r_s$	Litz strand radius [m]
$d_s$	Litz strand diameter [m]
$n_s$	Number of strands in a Litz bundle
$r_b$	Litz bundle radius [m]
$d_b$	Litz bundle diameter [m]
$P_f$	Packing or filling factor [m]
$t_b$	Distance between the centers of two adjacent Litz bundles [m]
$t_s$	Distance between the centers of two adjacent Litz strands [m]
$I$	Peak current [A]
$I_n$	Root mean square current [A]
$I_s$	Strand peak current [A]
$m$	Consecutive number of layers
$p$	Consecutively located layer number
$F_r$	Resistance factor
$F_L$	Inductance factor
$R_{ac}$	Ac resistance of a conductor [ $\Omega$ ]
$R_{dc}$	Dc resistance of a conductor [ $\Omega$ ]
$R_{sdc}$	Dc resistance of a single strand [ $\Omega$ ]
$L$	Leakage inductance [H]
$L_w$	Winding leakage inductance [H]
$L_g$	Interwinding leakage inductance [H]
$L_i$	Interlayer leakage inductance [H]
$W_m$	Magnetic energy [J]
$\alpha$	Propagation constant
$\beta$	Coefficient of thermal expansion [1/K]
$\lambda$	Thermal conductivity [W/m K]

$\delta$	Skin depth [m]
$\omega$	Pulsation frequency [rad/s]
$\mu$	Permeability [H/m]
$\mu_0$	Permeability of free space [H/m]
$\mu_r$	Relative permeability
$\sigma$	Electrical conductivity [S/m]
$\rho$	Electrical resistivity [ $\Omega\text{m}$ ]
$\Delta$	Penetration ratio
$\Gamma$	Round conductor penetration ratio
$\eta_w$	Porosity factor
$\eta_1$	External porosity factor
$\eta_2$	Internal porosity factor
$\zeta_1$	Skin effect factor for foil windings
$\zeta_2$	Proximity effect factor for foil windings
$\tau_1$	Resistive skin effect factor in round conductors
$\tau_2$	Resistive proximity effect factor in round conductors
$\varphi_1$	Inductive skin effect factor in round conductors
$\varphi_2$	Inductive proximity effect factor in round conductors
$\Phi$	Magnetic flux [Wb]
$v$	Harmonic number



# Chapter 1

## Introduction

## Chapter 1 Introduction

It is the belief of electronics and magnetic experts in the industry that there is a general reduction in the size and weight of magnetic components with the increase of operating frequency. This reduction of volume, weight and thereby the cost of magnetic components are significant enough to outweigh the cost introduced by the additional electronic components required to develop an electronics application. This has already been brought into practice for low power applications for decades with the advancement of semiconductor devices. The need of applying the same principle for high power applications has also been welcome by end system developers and ultimate users of such electronics systems(Villar, 2010) With the increase of the transformer capacity and converter switching frequency, the transformer efficiency, stray parameters, insulation and heat dissipation should be considered when designing a transformers (Bahmani et al., 2015, Zhang et al., 2018).

Applications like traction, ships and basically any mobile platform with a converter on-board require lightweight and compact converters to exploit the space available on-board more effectively. They often also require galvanic isolation for safety or other reasons. Therefore, high-frequency, high-power transformers which offer galvanic isolation, and a small volume are of increased importance (Pavlovsky et al., 2005). Solid State Transformer (SST) has become lately one of the most popular power electronics converter types. It is a combination of a high- or medium frequency transformer and multiple power electronic converters(EI Shafei et al., 2019)

As a key component of Power Electronic Transformer (PET) and traction transformer, high-power high-frequency transformer has the advantages of reducing transformer weight, volume and increasing its power density (Bahmani et al., 2015) while core loss and winding losses due to the eddy effect and proximity increase. At the same time, the series inductance is usually provided by the leakage inductance of the transformer in high frequency resonant converters (Ren et al., 2016), as a result, the design of the high frequency transformer also needs to consider the influence of parasitic parameters, because they will affect the operating characteristics of the converter. Meanwhile, high voltage high frequency transformers are quite compact, insulation becomes a problem. It is necessary to comprehensively consider the optimization objectives, like transformer losses, heat dissipation, insulation, and stray parasitic parameters problems when designing the transformer. As these optimization objectives cannot

be satisfied simultaneously, the high power high-frequency transformer design is a multi-objective optimization issue (Zhang et al., 2018).

These challenges in the design of high-power high frequency magnetics to be in line with the advancements of semiconductor devices such as Silicon Carbide (SiC) devices became so challenging to the level that some industry experts started to bring forward the argument that the continuous increase of operating frequency is a misdirection of the device engineering; “Ironically, the development of faster switching devices became counterproductive and resulted in Energy Conversion System technology being completely neglected for over 50 years now” (Ćuk, 2017).

However, many researchers took up the challenge of improving the magnetic designs to be in line with the demands of the electronics industry.

In order to optimize the design of high-frequency transformer, it is necessary to optimize the design of high-frequency transformer on the premise of meeting the characteristics of high-frequency transformer. The optimization of high-frequency transformer is an iterative process. The optimum design of high frequency transformer is usually to minimize the volume and weight of high frequency transformer under the basic requirements and conditions (Liu et al., 2019). Most of these developments were limited to about 50 kW with operating frequencies of in the range of 30 kHz at the time of the start of this research.

In this research a wider approach was given with an in-depth study in to all the aspects of the transformer design and patentable technologies were developed for each of the transformer design optimizations after those comprehensive studies. Further a parametric approach was made so that multiple solutions for a particular application could be arrived at depending on the most important application specific optimization requirements. By the end of the study commercially viable designs were arrived at even for transformers with power levels of 2 MW operating over 20 kHz.

## 1.1 Motivation and overview of the outcome

The transformers in electrical systems are responsible approximately to as much as one third of total network losses. These losses are accounted as power quality costs, costs to society and to the environment itself (Picanço et al., 2008). The behavior of the transformers and all other magnetic components significantly changes with the presence of harmonics in their excitation waveforms i.e., non-sinusoidal excitations e.g., Pulse Width Modulation (PWM) excitation, high frequency high power transformers etc. The effect becomes more and more significant as the frequency and the magnitude of the harmonics increase. In addition to the core losses, winding losses in such magnetic components operating at high frequencies can severely limit the performance and prevent size and cost reductions. If appropriate design considerations are not taken based on the increased core and winding losses these excessive losses can cause significantly higher temperatures, eventually leading to the condition of thermal runaway. The major challenges of transformer designers are high loss evaluation, high reliability, low cost, and weight requirements. So they need advanced techniques and tools that lead to optimum design and product performance improvements (Najafi and Iskender, 2015)

With the development of power electronics techniques, pulse-width modulated inverters (PWM) are widely used to control electrical machines, to feed transformers and to interface renewable energy systems. Also, in the future DC electric power systems, high power DC –DC converters will play a major role as they will substitute today's bulky 50/60 Hz transformers. This can already be seen in the industries such as the Electrical Vehicle industry (Liu et al., 2007, Ortiz et al., 2010).

The main purpose of high frequency operation of such power electronics circuits is to reduce the physical size and cost. The implication being that the losses and efficiency become of paramount importance because of the need to remove heat from the small surfaces (Cheng, 2000). High power isolated DC-DC converters are likely to provide solutions for many technical challenges associated with power density, efficiency and reliability in potential applications such as offshore wind farms, inter-connection of DC grids, MVDC in data centers and in future solid state transformer applications. The high power medium frequency transformer (HPMFT) is one of the key elements of such a converter to realize the voltage adaption, isolation requirements, as well as high power density (Bahmani et al., 2016)

Apart from the basic functionalities provided by conventional low-frequency transformers, like voltage adaptation and isolation, the conversion with Power Electronics (PE) structures adds

additional features to transformation systems, like power flow regulation and power quality improvement. Thus, depending on their application and features, they are known as Solid-State Transformers (SST) (Lai et al., 2005, Oates and Bassett, 2006, Villar, 2010), Power Electronic Transformers (PET) (Iman-Eini et al., 2008) Distribution Electronic Power Transformers (DEPT)(Wang et al., 2007), e-Transformers (Taufiq, 2007), dc-dc Electronic Transformers (Filchev et al., 2004), Power Electronic Traction Transformers (TT) (Hugo et al., 2007) or simply Medium-Frequency Topologies(Steiner and Reinold, 2007) or Medium-Frequency Transformers (MFT). Throughout this work the term Power Electronic Transformer (PET) will be used.

High Frequency High Power transformers (HFHP) also referred as Medium Frequency Transformers (MFT) in such power electronics circuits constitute a major proportion of the weight and losses. On board transformers are heavy, expensive, have a low efficiency and take up too much of the narrow space in AC-fed locomotives and in passenger vehicles with under floor housing of the drive power chain. The transformer is one of the main reasons why traction vehicles often exceed the targets for vehicle weight and dimensions, and why they only can fulfil rather modest requirements on the efficiency. Weight reduction of the transformers is therefore a matter of priority for the next generation of modern AC-fed traction vehicles (Steiner and Reinold, 2007, Li et al., 2019).

Compared with conventional line frequency transformers, medium frequency power conversion systems operating at the kilo-hertz range feature significant reduction of weight and size, dynamic control of power flow and power quality improvement. Such a compact system is also attractive for railway applications where space is limited. The Power Electronic Traction Transformer (PETT) deals with the design and analysis of high frequency transformer to reduce the core size and desired power control (Shuai and Biela, 2013, John et al., 2018).

There is a rapid increase in the industry demand for the best optimization of high frequency high power transformers. The importance of looking into all the options of optimization become furthermore significant with the increase of the amount of power handled at a given frequency.

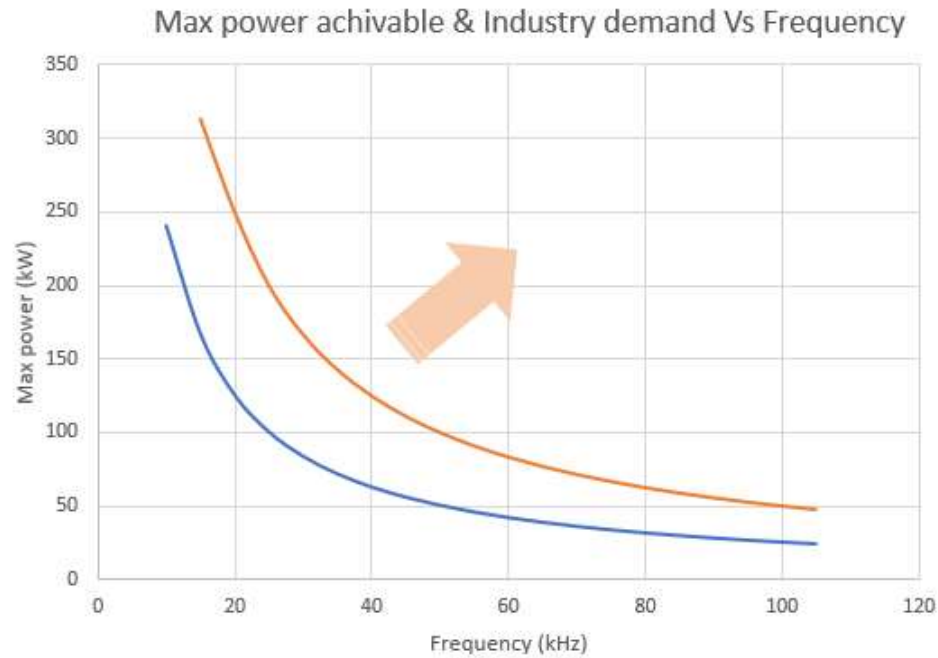


Figure 1-1 Practically achievable power at a given frequency.

As it is illustrated by the graph above there is an upper limit of the power that can be practically achieved at a given frequency in a transformer using the existing technologies. This limit comes due to various reasons such as increase of conductor losses, practical difficulty of making conductors large due to manufacturing difficulties, increased core losses due to increased frequency and large core volume required to accommodate large conductors, extreme aspects ratios of conductors required to minimize the conductor losses etc. However, the demand from the power electronics industry is to achieve higher and higher power levels at higher and higher operating frequencies. This trend continues to rise at an increasing speed with the developments of new semiconductor devices such as SiC MOSFETs.

SiC power devices can be switched at much high frequency than Si counterparts. If they are integrated into power module using the conventional packaging structure, it would lead to dramatically high overshoots during the turn-off/turn-on stages due to parasitic inductance induced by such structure. Therefore, to achieve their full performance with regard to low switching losses and low conduction losses, they can only be used if the module layout is designed with low parasitic inductances and low thermal impedance (Mouawad et al., 2018, Empringham et al., 2013)

SiC technology will have a dramatic effect on power electronics as they are applied to transmission and distribution systems. Their properties of high efficiency and in reducing the complexity of high voltage equipment will lead to new ranges of power electronic systems that

can challenge conventional AC technology on the grounds of cost, efficiency, and size. However, it is also clear that further developments will be required before the use of high frequency converter technology can be justified (Oates and Bassett, 2006).

This has become the major challenge that the magnetics industry has been facing since the rapid development of the power electronics industry. With the recent development of Silicon Carbide devices, the requirement for achieving high power levels increased at a much rapid rate making magnetics components the factor that drags the industry behind. Some experts even believed that the development of power electronics devices to handle high power levels at high frequencies will be of less or even no use as the magnetics technology will not be capable to cope with it. Some industry and academic experts believed that the semiconductor companies developing the semiconductor devices was even a miss direction of the science and engineering as magnetics components will limit the use of them.

This research was aimed at facing this change by carrying out a comprehensive study that extends to the analysis fundamental principles behind these limitations. At the end of this research work it became possible to eliminate the barriers of achieving high power levels and to make the power level that can be achieved in a transformer almost independent from the operating frequency.

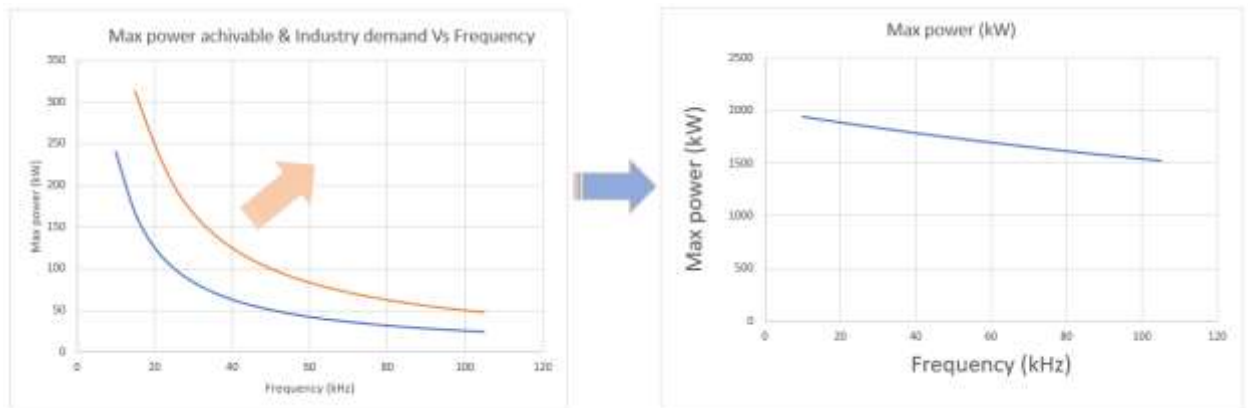


Figure 1-2 Change in power level that can be achieved at a given frequency before and after the research.

The achievement of this condition has made a transformation of the magnetics industry and the commercialization has already started. This achievement is discussed in this thesis. This study does not limit at the level of giving a single solution for a particular application, but also it goes to the extent of providing a whole set of parametric solutions that would fulfill the

requirements of a particular application. Though it was out of the scope of the PhD and was originally seen as a part of future works out of the interest of the researcher an algorithm was developed to automate the magnetic design process which the researcher expects to commercialize in the near future.

## 1.2 Current status of the industry and limitations

Historically the discussions on the non-sinusoidal currents go back 40 about years. A discussion took place in March 1980 during the meeting of IEEE power engineering society on the effect of non-sinusoidal load currents on transformer temperature rise (Pierce, 1996). The study committee formed in May 1980 was later elevated to an IEEE working group of performance. In the paper published by Alexander D. Kline in 1981, he first presented a methodology that was used in the development of IEEE standard C57.110 which defined the K-factor for transformers (Pierce, 1996). The K-factor gives an estimate of the ratio of heating in the transformer due to winding eddy currents when it is loaded with a given non sinusoidal current(a) to the winding eddy current heating caused by a sinusoidal current at the rated frequency(b) (den Bossche et al., 2004, Zheng, 2000). However, K-factor rating is not evaluated for the use with harmonics where the rms currents of any singular harmonic, (h) of a higher order than the 10<sup>th</sup> harmonic is greater than 1/h of the fundamental rms current.

The magnetic components that come under the scope of this research are subjected to much higher order harmonics of significant amplitudes. For example, 400<sup>th</sup> harmonic can be as large as 10% of the fundamental amplitude. Thus, the design considerations go far beyond the guidelines obtained from the K-factor transformer evaluations. Traditionally, transformer design is based on the power transformers with sinusoidal excitation. When the transformer is operated at a high frequency with the practical non-sinusoidal excitation, some loss mechanisms have to be taken into account: skin and proximity effects in windings and the increased eddy current and hysteresis losses in cores (Ma et al., 2007) Increasing the operating frequency can reduce the size of the transformer, but the winding losses caused by high-frequency skin effect and proximity effect also increase. Therefore, it is very important how to select the winding structure, winding size and arrangements which can reduce the winding loss (Zhao et al., 2018, Zhang et al., 2017)

The losses occurring in the core material can be of equal importance to the losses in the windings depending on the excitation waveform (Razak et al., 2005). Further the estimation of losses in the core materials as well as deciding on the best construction that minimizes the



losses in the core and conductors requires an in depth understanding on multi-physical aspects of such magnetic components. Proper knowledge of the transformer core loss is essential for overall design and selection of cooling measures (Joshi and Nath, 2019)

Medium voltage, medium frequency transformers (MFTs) are much smaller in size and weight compared to conventional low frequency transformers. The MFTs are very attractive for applications where full control of the power flow and high-power density are required, such as power electronic interface in smart grids and traction converter system. With reduced size, the optimal design of MFTs becomes more challenging due to the high isolation requirement and thermal stress (Shuai and Biela, 2013) The estimation methods of core loss under sinusoidal excitation in the engineering application mainly cover the iron loss separation method and the Steinmetz empirical formula method. The Steinmetz empirical formula is considered as being of the simplest forms and the fewest parameters in the core loss prediction. However, it is only suitable for the evaluation of core loss under sinusoidal excitation, and the parameters in the model are only dependent on magnitude and frequency of magnetic flux density (He et al., 2018).

Even at the time of the start of the research the industry had understood this requirement. However, the solutions used in the industry were sufficient to handle power levels of a few hundreds of Watts as opposed to the growing demand going several hundreds of kilowatts.

The planar transformer technology was a breakthrough in the design of transformers for high frequency applications. However, these could not reach high power levels at the speeded the demands from the power electronics industry grew due to the constructional limitations of them. The planar windings are usually made as PCB traces. Thus, there is a limitation in the current handling capacity making this approach not suitable power levels typically over 15kW or 20kW. Copper foil technology was developed later in association with planar technology, this was also a breakthrough in the high-power high frequency transformer design. However, there are limitations on the number of turns that can be achieved with this technology due to geometric limitations of such windings. The number of turns that can be achieved under this technology. The percentage of material wastage (mostly copper or aluminum) is also considerably high in these windings. Also, the fabrication cost of such windings is significantly high. This is due to the requirement of using laser technology or high-pressure punching methods.

## 1.3 Current technologies

### 1.31. Research in the development of “Planar” transformers.

Planar transformers are widely used in high- frequency high power density power electronic converters. With the demands of miniaturization, more detailed analysis of thermal stress of the transformers is necessary to enhance its reliability (Shen et al., 2019).

Number of developments took place in the product type of planar transformers. As a result of the research carried out by several industry leading companies and some universities, several planar transformer related technologies were developed that enabled the achievement of power levels of several kilowatts at high frequencies. By about the middle of the first decade of the 21st century planar technologies developed to the level that a few tens of kilowatts could be achieved with them. The efficiency of a planar transformer structure depends on several aspects that are related, considering the working frequency, to core geometry, number of turns, the arrangement of layers and thickness of copper tracks (Ropoteanu et al., 2017).

Multilayer HF planar transformers are widely implemented in power electronic applications (power converters, resonant converters, switching power supplies, etc.) (Zhang et al., 2013, Zhang et al., 2009). Where the advantages of planar technology are; low profile, excellent repeatability, economical assembly, mechanical integrity and superior thermal characteristics (Ouyang et al., 2010, Bernardoni et al., 2010). From a design point of view, planar transformer electrical behavior cannot be precisely predicted by the conventional transformer models. In particular, the skin, the proximity, leakage inductance, the parasitic capacitances and core loss effects are complex devices to model, particularly during large frequency domain. On the other hand, in (Zhang et al., 2014a), based on FEM method, an accurate planar transformer model is introduced. However, this method is not only complicated to implement in circuit simulator but also is time-consuming. Therefore, an analytical approach used to analyze the planar transformer can be a solution aided to design a prototype-less approaches. Based on the geometry parameters of this device, an equivalent circuit model integrated in power converter simulation is preferred. This method allows reducing the time simulation and the cost of achieving a prototype (Ammouri et al., 2015)

Planar-wound structures are generally created by laminating planar copper windings and disk-like dielectrics into multilayer PCBs that are enclosed by a low-profile magnetically permeable core. The planar cores offer high effective areas for the given effective volumes, efficiently using the magnetic material. It must be noted that the rise in effective area for a given volume

is achieved by shrinking the height of the winding window; thus, the window area is reduced. However, the window area is often not fully utilized in a high-frequency design; therefore, shrinking the window area is possible with practically no penalty. The major advantages for the use of planar magnetics are summarized as follows (Ouyang and Andersen, 2013):

- 1) Low profile—planar magnetic components essentially provide lower profiles than conventional wire-wound components, aiding miniaturization. Generally, the height of a planar magnetic component is  $1/4$  to  $1/2$  the height of its wire-wound counterpart.
- 2) Good thermal characteristic and high-power density— planar magnetic cores essentially have a higher surface area to volume ratio than conventional magnetic cores. As a result, they are more efficient to conduct heat and lead to low temperature rises compared with conventional wire-wound components.
- 3) Ease of manufacturability and cost reduction—the fabrication processes used in planar magnetics relies on advanced computer aided techniques. So, it is quite easy to automate the winding of the planar inductors and transformers. PCB techniques are easily adapted for mass production.
- 4) Unrivalled repeatability—the simple automatic assembly process allows planar magnetic components to be fabricated with a high repeatability and accuracy.
- 5) Modularity—because a PCB winding is used for planar magnetic devices, semiconductors and other passive components can also be assembled onto the PCB surfaces. Thus, no extra connections are required.
- 6) Ease of implementation on winding interleaving—as multilayer PCBs allow for an interconnection between arbitrary layers, windings interleaving can be easily implemented. This provides a significant reduction in leakage inductance and high-frequency winding losses.
- 7) Predictable parasitic—it is exceedingly difficult to control the winding layout in wire-wound magnetic components. For planar magnetics, the windings manufactured by PCB machines are more precise and consistent, resulting in magnetic designs with highly controllable and predictable parasitic parameters (Hurley and Wölfle, 2013)

Even though the planar technology was considered as the most suitable candidate to meet the power and operating frequency demand of rapidly advancing power electronics industry due to a number of several limitations.

- 1) Large footprint—the large surface area offered by the flatter cores is used in planar devices. For simple E-type planar cores, if the core window width is fully utilized, nearly one-third of the PCB winding area will be exposed to the ambient air because the PCB windings are situated

in the horizontal direction; this feature will cause a portion of the large footprint. For certain other alternatives, such as ER type cores, the PCB windings can be hidden inside the core; thus, it can have a smaller footprint, but at the expense of reduced core cross section.

2) Low copper fill factor—there are safety standards that dictate the minimum distance between windings, influencing the copper fill factor. A typical dielectric material for PCB fabrication is FR4, a composite material composed of woven fiberglass bond with an epoxy resin. The FR4 material standards show an electric strength (breakdown voltage) of approximately 40 kV/mm. Thus, for offline power converters, a minimum distance of 0.1 mm between primary and secondary windings is required to meet safety standards. Besides the consideration of safety standards, a limited PCB fabrication capability also yields a low copper fill factor. If a rigid PCB is used to implement planar windings, a minimum inner turn spacing of 100  $\mu\text{m}$  and a dielectric thickness of 150  $\mu\text{m}$  are generally required due to the capabilities of PCB fabrication. However, with rapid development of PCB manufacturing and dielectric materials, this limitation can be ameliorated. Copper on a thin flexible polymer substrate (2 MV/mm dielectric strength) gives an improved fill factor, because the dielectric thickness can be made as low as 13  $\mu\text{m}$ . Several single-layer flexible polymer substrates can be laminated together as multiple-layer flexible print circuit board, which results in a similar buildup to a rigid PCB but with higher fill factor.

3) Limited number of turns—a low copper fill factor gives a limited number of turns for PCB winding. Furthermore, an increased number of turns require a large number of layers unless the winding width is reduced at the expense of a high dc resistance. Multilayer lamination is not a cost-effective way of implementing the PCB winding because the cost of PCB manufacturing rises rapidly with an increasing number of layers.

4) High winding capacitance—stacking windings closely provides an increased winding capacitance, and PCB windings have intrinsically larger surface areas than conventional wire-windings, further increasing the winding capacitance(Ouyang and Andersen, 2013).

However, not only these solutions were expensive but also the power levels that could be achieved were still limited to a couple of tens of Kilowatts while the industry demand growing to the level of several hundreds of Kilowatts. The design of a 15 kW planar transformer, operating at 50 kHz. A novel, optimized layer interleaving schema is proposed for reducing its leakage inductance and its parasitic capacitance is presented in the paper published in 2019 (Poveda-Lerma et al., 2019). The paper presented in 2020 single phase planar

transformer for high power application has been investigated. In that study a power losses evaluation of a 20 kW planar transformers has been done (La Ganga et al., 2020) Even at present the Planar transformers have not been able to meet the demand of high-power high frequency industry.

### 1.32 Research in the development of “Litz” wire technologies

The winding power loss of a high frequency transformer is strongly influenced by the high frequency eddy current skin and proximity effects. The litz-wire can effectively reduce the eddy current effects. The precise loss calculation method of litz-wire remains however a difficulty(Liu et al., 2018, Ferreira, 1992).

Due to the rapid increase of switching frequency, the eddy current loss of high-frequency transformer windings becomes more and more significant. The use of litz-wire can reduce the high-frequency loss to some extent (Liu et al., 2018).

Number of research have been carried out to develop an optimal “Litz” wire configuration for handling high power levels at high frequency. Even at present several doctoral studies are carried out for the optimization of “Litz” wires. These include the selection optimal diameter of a conductor, number of conductors for a bundle and number of bundles in a single conductor and even the number of twists and the twisting pattern etc. “Litz” wires still stand to be one of the preferred solutions by many expert magnetics designers. A detailed look and of them is also carried out in this study with an explanation of limitations and practical limitations associated with them specially when it comes to high power applications.

The calculation of skin effect and proximity effect losses on each bundle level requires detailed knowledge of the litz wire geometry. The winding number, the coil size, the insulation layer thickness and the conductor material have to be predefined. The strand diameter, the number of strands or bundles in a bundle and the pitch are subject to the optimization. The diameter of each bundle, the bundle length, the strand length and the specific resistance of the bundles are calculated based on the predefined data. Ideal twisting is assumed, which means that each strand has the same length and its position in the wire is equally distributed. This assumption is valid if the pitch is longer than the bundle diameter, the accepted error is below 0.25%). The average strand length is calculated instead of the exact length of each strand(Barth et al., 2017, Sullivan and Zhang, 2014a)

As expected, the minimum loss is reached using the highest number of strands and a small diameter. In this configuration, eddy current effects are minimized while the conductor cross section is as large as possible. In practice, the strand diameter will be a constraint, because thin strands are expensive in fabrication or even not available. As an example, a strand diameter of 0.08 mm is chosen. Increasing the strand number leads to increasing loss, even though the conductor cross section increases as well. The proximity effect loss, which dominates the ohmic loss in case of high frequencies and the influence of an external magnetic field, causes this behavior (Barth et al., 2017)

Certain research have considered the alternative material options in the development of “Litz” wires arrangements.

An alternative material is aluminum, which has some advantages.

- lower material cost (the actual cost difference varies depending on the commodity market.
- larger skin depth due to larger specific resistance.

In two conductors with the same diameter, proximity effect losses are inversely proportional to the specific resistance. The dc loss is proportional to the specific resistance. Therefore, it depends on the system parameters and the frequency whether an aluminum wire is suitable. The difference between the specific resistance of aluminum therefore the dc loss is about 64 % higher and eddy current losses are about 39 % lower in aluminum single strands compared to copper. The use of aluminum as the conductor material is discussed. Simulation results indicate that it is an alternative to copper under the operating conditions in WPT for electric vehicles. However, the losses strongly depend on the strand diameters, so the available diameter is more important than the conductivity in the design process. Additional to the losses, other parameters like weight, space requirements and cost of the coil must be taken into account (Pryor et al., 2008, Barth et al., 2017)

Paralleling litz wires is often necessary in medium-frequency transformers rated for several hundred Ampères, due to unavailability of wire of large cross-section and the difficulties to bend such wire. Without careful winding design, significant losses may be incurred by circular currents induced between parallel-connected wires. These losses add to the AC losses due to skin and proximity effect on the level of individual strands or bundles within a litz wire (Gradinger and Drofenik, 2018)

Modeling the thermal performance of windings made of litz wire is especially important because litz wire has poor effective thermal conductivity as a result of its individually insulated fine wire strands (Kyaw et al., 2019).

As it has been experienced by many magnetic manufacturers discussed in many studies the mitigation of the conductor loss levels is limited to a certain level in the case of “Litz” wires. Furthermore “Litz” wires have the disadvantages of difficulty in connections and several other manufacturing disadvantages. For example, these wires must be insulated with a sleeve insulation, even though it is possible to do it at a bundle level manufacturing point of view it is a tedious and time-consuming process. Further such insulation process makes the thermal performance extremely poor. Therefore, despite the amount of research carried out in this area “Litz” wires have not become a technology that is strong enough to meet the requirements of the present industry.

### 1.33 Research in the development high power high frequency transformers with foil conductors

The use of conductor foils for the high frequency transformers was an option that industry worked on for almost a decade by now in the development of high-power high frequency transformers. By carrying out the interleaving with proper level of insulation gave the advantage of mitigating conductor losses to a considerable level. However, the level of insulation material required and the construction itself limits its ability to achieve high power levels beyond several tens Kilowatts.

Foil conductors and primary and secondary interleaving are normally used to minimize winding losses in high-frequency (HF) transformers used for high-current power applications (Barrios et al., 2014). Use of foil conductor is attractive for high-power MF/HF transformer designs. It offers the following benefits i.e. (a) The eddy current effects at medium/high frequency are kept low if the ratio of conductor width ( $w$ ) to its skin depth ( $\delta$ ) is unity or less (Dimitrakakis and Tatakis, 2009). Due to its geometry, a rectangular foil offers very low width to height ratio in comparison to a solid round conductor of the same area. Therefore, very low  $w/\delta$  ratio can be attained with foil conductor. It minimizes the eddy current effects, reduces copper loss density and improves the efficiency of a MF/HF transformer. (b) Foil conductor also helps in attaining a good thermal performance of a MF/HF transformer (Das and Fernandes, 2020, Das et al., 2017).

In foil windings of medium-frequency transformers rated for several hundred Amperes and operating at ten or several tens of kHz, parallel connection of foils is necessary to provide sufficient conductor cross-section

However, winding interleaving complicates the transformer assembly, since taps are required to connect the winding sections, and also complicates the transformer design, since it introduces a new tradeoff between minimizing losses and reducing the construction difficulty(Barrios et al., 2014, Gradinger et al., 2020).

The analytical model also indicates rapidly increasing resistance of coil ac losses when the conductor thickness exceeds the skin depth, particularly with a large number of turns(Rios et al., 2016) The thermal management of foil wound high power high frequency transformers is particularly difficult and possibilities using novel approaches are limited by the construction itself. The experimental results in recent studies show that Litz-wound transformer has increased AC resistance and leakage inductance, as compared to the Foil transformer, due to the restriction of core dimensions. Hence, foil windings are preferable over Litz windings for high frequency operations, due to their simpler construction, easier selection and better provision of interleaving(Khan et al., 2018).

As discussed in the above sections each of the approaches in manufacturing high power high frequency transformers have significant limitations. These include manufacturing limitations. Power handling capability limitations, limitations in maintaining dielectric strength between in windings and between the turns of the same windings, limitations in thermal management and heat extraction etc. The details of the above-mentioned limitations of the current research approaches are also discussed with diagrammatic explanations in this thesis.

### 1.4 Novel approach made in this research.

After looking into the studies carried out by number of researchers it was noticeably clear for the researcher that a comprehensive study that looks into the fundamentals of principle and a detail analysis of the situation was necessary to overcome the barriers of achieving high power levels at high frequency.

It was understood that the study must go beyond the standard industry approaches and high-level theoretical study and consideration of multiple design configurations were necessary to take the magnetics industry out from its stagnating situation. Therefore, a parametric approach for the designs were carried out in association with the detail analysis of electromagnetic behavior of high-power high frequency transformers.



### 1.41 Aim and objectives

Magnetic components have not evolved at a compatible rate to semiconductor devices and power electronics topologies. As a result, magnetic components have become the factor that hinders the development power electronics applications, particularly at high power high frequency applications. High need existed to fulfill this requirement by overcoming the challenges in magnetic designs such as mitigating the conductor losses, mitigating the core losses thermal management of the high power density magnetic components and control of leakage inductance and similar parameters and arriving at all the possible set of parametric solution for magnetic designs that will enable the advancement of power electronics industry while making it possible to do overall system optimization with multiple possible solutions.

- In this research it is aimed to provide a solution for the difficulty that magnetics industry faces in providing magnetics solutions for growing and challenging demands that come with the rapid advancement of power electronics industry.
- It is also aimed to take the magnetics industry to the position of a technology enabler for the power electronics industry rather than being a factor that delays the development of power electronics industry.
- It is aimed to develop a basis to have easy access to a complete set of parametric solutions of magnetics for a particular application that enables better optimization of power electronics systems.
- In order to achieve the aims of the research it was intended to evaluate latest methods suggested by the recent researchers in the field and to develop comprehensive mathematical models that give reasonable estimates of core losses and winding losses of the transformers and inductors when subjected to excitation waveforms with higher order harmonics of significant amplitudes.
- It is intended to use these mathematical models to evaluate, quantify and compare the losses associated with the different transformer topologies such as Toroidal, EI, UI, 3UI, 5limb, Hexa, Y cores etc. The mathematical models will be used to research the behavior of different core materials such as Grain oriented Si Steel, non-grain-oriented Si Steel, Amorphous materials, High Si steels when excited by waveforms of higher order harmonics spectrums. The model will be extended to estimate the acoustic noise and losses of energy due to this.
- The mathematical model to be developed for winding loss estimations will investigate the behavior and energy loss patterns of different conductor materials such as Al and Cu and different physical shapes and arrangements of them.

- The researcher also intends to verify the above theoretical findings with Finite Element simulation software. Further practical verification of the results with actual samples will be made to confirm the simulated and calculated results.
- It is also expected to extend the study is to define principles and setting a framework for transformer design for the area of application under discussion in terms of selecting optimum materials, material compositions, geometries and constructions that would minimize the energy losses.
- It is also intended to use the findings of the research to bring suggestions that would contribute to the improvements being done in the modern magnetic materials (eg.6,5% high Si – Japanese steel) used in transformer cores and windings. In order to achieve the research objective a comprehensive study on the theoretical aspects of the subject matter is carried out.

## 1.5 Contributions made by the study

The study carried out under this research and the associated future works have resulted in several patents some of which are already granted at the time of thesis submission and most importantly has eliminated the barriers in achieving high power levels at high frequencies in magnetic components.

After this study there is no limitation or upper threshold in achieving high power levels at high frequencies.

Several i) 50 kW 50 kHz, ii) 100 kW 20 kHz, iii) 100 kW 50 kHz, high power transformers have already been manufactured and tested on very modern applications. A 200 kW 30 kHz transformer was also manufactured and being tested at the time of writing this thesis. A 400 kW 20 kHz transformer design has been completed and waiting for the manufacturing until the developers become confident in managing the power electronics challenges at that power level.

Further designs have been finalized up to 2500 kW (2.5 MW) 20 kHz whenever the power electronics industry demands such extremely high-power levels at high frequencies.

Until this study magnetics industry was dragging the power electronics industry behind in achieving high power levels at high frequencies and miniaturizing power electronics constructions, this study has not only resulted in providing a solution for that but also became a technology enabler that drives the power electronics industry achieving further and further in the direction of high power at high frequencies.

### Patents

1. WARNAKULASURIYA, K., GURWICZ, D. Carroll & Meynell Transformers Ltd 2015, DC power supply GB2536653A

Magnetic approach for power factor correction

A power supply comprises a rectification stage and a plurality of DC output stages (e.g., for charging batteries). The rectification stage comprises a PFC stage including a twelve-pulse transformer generating two three phase AC waveforms phase shifted with respect to each other, two bridge rectifiers, each rectifying a respective three phase AC waveform, and two interphase transformers coupling the rectified DC outputs to provide a combined DC supply, and where each DC output stage has independent current and voltage control. The two interphase transformers coupling the first and second rectified DC outputs have a lower ripple than either of the first or second rectified DC outputs. The rectification stage is arranged to attenuate harmonics transmitted to the power source up to and including the eleventh harmonic of the power line frequency and to provide a total harmonic distortion, THD, of less than 5%.

The power supply circuit may be used for a charger for high power charging, such as charging the batteries of multiple electric vehicles (EVs)

David Gurwicz contributed with the Fundamental concept and electronics verification and Kapila Warnakulasuriya contributed with the magnetic design solution and magnetic option evaluation in parametric scale

Relevance to the study:

Parametric multiple solutions for a given application at high power application.

2. WARNAKULASURIYA, K. Murata Manufacturing Co Ltd 2018, Insulating magnetic components on silicon using PNP or NPN junctions US10756160B2

Insulating magnetic components on silicon using PNP or NPN junctions

A magnetic component includes a semiconductor substrate, a first winding that is located in the semiconductor substrate and that includes at least two turns, and intra-winding insulation located between two adjacent turns of the at least two turns and including doped regions in the semiconductor substrate that define either an NPN-junction or a PNP junction.

Sole invention is by Kapila Warnakulasuriya

Relevance to the study:

Introduction of new approach for miniaturization and optimization of the magnetic design at ultra-low power applications.

3. WARNAKULASURIYA, K. Murata Manufacturing Co Ltd GB 2018, US 2019, US 2021, Multi-phase shift transformer-based ac-dc converter US20200169182A1

Multi-phase shift transformer-based ac-dc converter

A multi-phase shift transformer-based AC-DC converter includes a single transformer that reflects a negative portion of an AC voltage to become a positive voltage by generating multiple phases from a poly-phase input. The multiple phases generated can be separated by as little as 1° to create a well-approximated DC output without the need for a smoothing circuit. The primary and second windings of the transformer are flat wire conductors structured to provide a larger number of windings per core including a larger number of secondary coils, which provides for a large number of output phases.

Sole invention is by Kapila Warnakulasuriya

Relevance to the study:

Introduction of new approach for the magnetic design at ultra-high-power applications in power converter applications.

4. WARNAKULASURIYA, K. Murata Manufacturing Co Ltd US 2019, Inductor US20190378647A1

An inductor includes a core, a plate that holds the core, and a flat copper wire wound around the core in a single layer. The flat copper wire is coated with potting.

Sole invention is by Kapila Warnakulasuriya

Relevance to the study:

Introduction of new winding orientation and construction for an efficient inductor which adds further dimensions for magnetic optimization.

5. WARNAKULASURIYA, K. Murata Manufacturing Co Ltd GB 2018, WO 2019, US2020, Winding arrangement for an electrical transformer WO2019234453A1

Winding arrangement for an electrical transformer

A coil of electrically conductive material is provided, the coil comprising a first and second section, the first section having a first plurality of turns and the second section having a second plurality of turns. Both the first plurality of turns and the second plurality of turns are arranged around a winding axis of the coil. The first plurality of turns are smaller than the second plurality of turns such that when viewed along the winding axis of the coil the first plurality of turns fit within the second plurality of turns. When viewed perpendicular to the winding axis of the coil the first and second sections are adjacent.

Sole invention is by Kapila Warnakulasuriya

Relevance to the study:

Introduction of new winding arrangement that eliminates the difficulties the industry had in achieving high power levels at high currents.

6. WARNAKULASURIYA, K. Murata Manufacturing Co Ltd GB, Novel thermal management approaches for high power density transformers P82227.GB01(M20-02249)

This application relates to thermal management of an electromagnetic device such as a transformer, and in particular to an electromagnetic device and a core assembly suitable for an electromagnetic device.

Sole invention is by Kapila Warnakulasuriya

Relevance to the study:

Introduction of new thermal management approach for efficient removal of heat from high power density high frequency transformers enabling the achievement of high-power levels at high frequencies

7. WARNAKULASURIYA, K. Murata Manufacturing Co Ltd GB, Novel approach to extract heat from the windings of transformers with high isolation requirements.

P82228.GB01 (M20-02413)

The invention relates to a winding assembly for a transformer, and a transformer device including the winding assembly, and to the thermal management of transformer windings.

Relevance to the study:

Introduction of new thermal management approach for efficient removal of heat from high power density high frequency transformers enabling the achievement of high power levels at high frequencies of transformers with high voltage windings ( for High Power High Frequency High Voltage transformers )

#### Publications

1. WARNAKULASURIYA, K., F., ASKARI, V. & NABHANI, F. Determination of Losses in Conductors Carrying Higher Order Harmonics of Significant Amplitudes. WCE (World Congress in Engineering), London, England July, 2014a.

Relevance to the study:

In depth theoretical study of conductor losses which is a main aspect in transformer design. Verification of theoretical predictions by way of physically constructed samples. Suggestions of new approaches for mitigation of losses, details are discussed in the Chapter 3 of the thesis.

2. WARNAKULASURIYA, K., HODGSON, S. & NABHANI, F. Performance Comparison of Nanocrystalline Material with Ferrite in a 40kW 20kHz Application. Power Conversion Intelligent Motion South America 2014, 2014b.

Relevance to the study:

In depth study of the core losses which another main aspect in transformer design. Comparison of different types of materials and grades. Verification of theoretical predictions by way of physically constructed samples. Suggestions of new approaches for minimization of losses, details are discussed in the chapter 4 of the thesis.

3. WARNAKULASURIYA, K., ASKARI, V. & NABHANI, F. Theoretical Estimation and Practical Verification of the Impedance and Leakage Inductance of MVA Range Single Phase Transformers. FAIM (Flexible Automation and Intelligent Manufacturing), Wolverhampton, England 2015, 2015a

Relevance to the study:

Introduction of new thermal management approach for efficient removal of heat from high power density high frequency transformers enabling the achievement of high power levels at high frequencies of transformers with high voltage windings ( for High Power High Frequency High Voltage transformers )

4. WARNAKULASURIYA, K., HODGSON, S. & NABHANI, F. Development of High Power, High Frequency Magnetics for the Future Power Electronics Applications. PCIM 2015, 2016.

Relevance to the study:

Elaboration of the use of developed techniques in the development state of the art transformers. Details are discussed in Chapter 3, 4 and 5

5. WARNAKULASURIYA, K., HODGSON, S. & NABHANI, F. Entwicklung von magnetischen Komponenten für hohe Leistungen und Frequenzen für zukünftige Anwendungen in der Leistungselektronik. PCIM 2015, 2016.

Relevance to the study:

Elaboration of the use of developed techniques in the development state of the art transformers. Details are discussed in Chapter 3, 4 and 5

6. WARNAKULASURIYA, K., HODGSON, S. & NABHANI, F. Estimation of temperature rise in MVA range dry-type transformers and practical verification based on simulated loading. Proceedings of the World Congress on Engineering, 2015. 410-415.

Relevance to the study:

In depth study of the thermal management of high power density transformers. The invention of new thermal management techniques which in combination of other technologies developed make eliminate the challenges that the industry faced in the development of high-power transformers. details are discussed in the chapter 5 of the thesis.

7. WARNAKULASURIYA, K., GURWICZ, D. Magnetics Approach to a Stable Multiple Electric Vehicle Rapid Charger. Darnell's Energy Summit, Los Angeles CA, USA, September, 2015,

Relevance to the study:

Elaboration of the industry demand and how the findings of the study contribute to address them. Details discussed in the Chapter 7

8. WARNAKULASURIYA, K., NABHANI, F. & ASKARI, V. High Power, High Frequency Magnetics for the Future Power Electronics Applications. Darnell's Energy Summit, Los Angeles CA, USA, September, 2015,

Relevance to the study:

Elaboration of the industry demand and how the findings of the study contribute to address them. Details discussed in the Chapter 7

9. WARNAKULASURIYA, K., NABHANI, F. & ASKARI, V. Development of a 100kW, 20 kHz nanocrystalline core transformer for DC/DC converter applications. PCIM Europe 2016; International Exhibition and Conference for Power Electronics, Intelligent Motion, Renewable Energy and Energy Management, 2016. VDE, 1-8.

Relevance to the study:

Proof of the outcome of the contributions for mitigation of conductor losses, core losses and temperature management based on physically constructed samples, details are discussed in the Chapter 3,4,5 and 7

10. WARNAKULASURIYA, K., NABHANI, F. & ASKARI, V. Optimization of 12 and 18 pulse rectifier systems by the selection of optimum parameters for magnetics. PCIM Europe 2016; International Exhibition and Conference for Power Electronics, Intelligent Motion, Renewable Energy and Energy Management, 2016b. VDE, 1-8

Relevance to the study:

Parametric design of magnetics and integration of the application parameters for the design optimization of magnetics, details are discussed in the Chapter 7

11. WARNAKULASURIYA, K., NABHANI, F. & ASKARI, V. Verification of Temperature Rise Estimation of MVA Range Single Phase Dry-Type Transformers Based on Simulated Loading. CWIEME Berlin, Germany, May 2016

Relevance to the study:

Study of the thermal management of high-power density transformers. The invention of new thermal management techniques which in combination of other technologies developed make eliminate the challenges that the industry faced in the development of high-power transformers. details are discussed in the chapter 5 of the thesis.

12. WARNAKULASURIYA, K., POLTI, A. & NABHANI, F. Evolution of Magnetics in Power Electronics Applications and Facing the Challenges of Future Electronics Industry. PCIM Europe 2017; International Exhibition and Conference for Power Electronics, Intelligent Motion, Renewable Energy and Energy Management, 2017. VDE, 1-5.

Relevance to the study:

Evolution of magnetics and how the research contributes for the advancement of the magnetic industry, details are discussed in the chapter 7 of the thesis



## 1.6 Framework for thesis

The research was carried out under four main sections as described above. These sections are explained in the chapters 3 to 6. Under each section a literature survey was carried out to understand the state-of-the-art technologies in the industry which were used to address the challenges in each section. Theoretical solutions were arrived at for finding solutions for the problems in each of the sections and they were verified by simulations. Further, actual physical samples were constructed for the practical verification of the developments which were then tested on real applications. The concept of parametric solution was applied in each section to make it possible to arrive at multiple suitable solutions for a particular application rather than arriving at one single solution This is explained in the chapter 2 and 7.

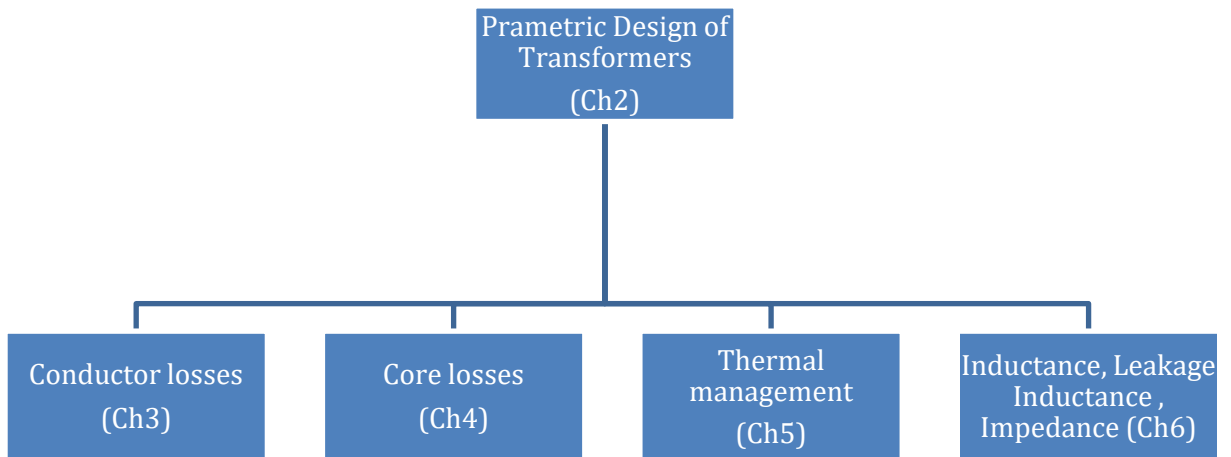


Figure 3 Framework of the Thesis

The framework of the thesis addresses the contents of an entire research separated into different chapters. This thesis is made up of 7 Chapters. The introductory chapter describe Importance of the research, aims and objectives of the study, framework for this thesis and the contributions made by the study. It also describes the general background information and state of the art technologies used in the advanced magnetic design and manufacture giving an overview to the fellow researchers.

Chapter Two explains the concept of parametric design in the context of magnetic design and the contributions that it will bring to the overall advancement magnetics and power electronics industry.

The Third Chapter describes the conductor losses associated with challenging magnetic design and the researcher's approach to mitigate the high frequency losses after an in-depth theoretical study into all the multi-physic phenomena related to the generation of conductor losses. This chapter also explains the work by the researcher that has led to patents in this area of the study.

The Fourth Chapter describes the study into the core losses, core construction and the selection of the optimum magnetic material depending on the nature of the application. The Chapter Five explains about the research carried out in optimizing the constructions to achieve the best thermal management. This Chapter also explains the patent applied by the researcher for the thermal management of high-power high frequency magnetics and for high power high frequency high voltage magnetics.

Chapter six will demonstrate the research carried out in the direction of leakage inductance and inductance of magnetics components which are the other important dimensions in optimizing the magnetic components. This chapter also explains the identified industry weaknesses in specifying the parameters for magnetic components purely based on the consideration of power electronics.

The final chapter, the chapter 7 explains the evolution of magnetics and how the magnetics components had become the factor that hindered the development of power electronics. How this study eliminated such barriers and even made the magnetic components a technology enabler for the advancement of the power electronics industry.

## 1.7 Summary

Magnetic components have become one of the major barriers for the rapid development of the power electronics industry. Semiconductor technologies developed at a rapid rate enabling the power electronics industry to develop at considerably high speed. However, the limitations of magnetic components act as a barrier for these developments.

The state-of-the-art magnetic technologies at the time of the research had significant limitations in handling high power levels at high frequencies.

This research was aimed at finding solutions for this situation by way of doing a detailed theoretical study into the existing technologies and the multi-physical behavior of magnetic components. The generation of conductor losses in different types of conductor types and constructions were studied practically manufacturable technologies were introduced which have led to patents.

Similar studies were carried out and developments were made on the mitigation of core losses and the thermal management of magnetic components which have also led in to patented technologies.

Further, detail studies were carried out in other important areas of magnetic design such as inductance, impedance, and leakage inductance. The importance of doing the magnetic designs in combination with the electronics design was also addressed and the findings of these have also led into patents and publications.

The successful completion of this study has resulted in over 7 patents some of which are already granted and over 12 publications which were well received by the industry and academic experts.

The outcome of the research does not only limit to give a single design solution but also the parametric approach presents a comprehensive set of all the possible solutions for a particular application. Further, though it was out of the scope of this PhD study, out of the researcher's interest an algorithm was developed to automate the complicated magnetic design process and it is planned to commercialize the concept.

## Chapter 2

# Parametric approach for magnetics design

## Chapter 2 Parametric approach for magnetics design

### 2.1 Parametric design

Parametric design is defined as a design process based on algorithmic thinking that enables the expression of parameters and rules that, together, define, encode and clarify the relationship between design intent and design response. As opposed to the conventional design approaches the parametric design approach provides This approach produces multiple solutions for a given situation.

Therefore, this can also be seen as the use of variables and algorithms to generate a hierarchy of mathematical and geometric relations that allow us to generate a certain design, but to explore the whole range of possible solutions that the variability of the initial parameters may allow.

The traditional digital design process is that the design ideas by the designer, create the three-dimensional model and do the analysis. If they cannot meet the design conditions, it is necessary to repeat all the previous process. This process may take several times to succeed, and it must repeat the entire design process even if the same part only makes small changes in the size of the structure(Yong-xiang et al., 2017, 陈建能 et al., 2012, Jian-neng and Ying, 2012).

With the development of computer technology and related application software, mechanical product design has entered the era of digital design. Parametric design which is one important development direction of computer aided design has become an important means for new product design and development and apply. The products that designed by parametric design method can achieve the product components of the size of the relationship between the arbitrary definition of the components, the intelligent association between the assembly. It can greatly reduce the designer's labor and improve design efficiency that the dimensions of the entire part change with a certain degree of association with the changes of base size(DAI et al., 2014, Yong-xiang et al., 2017)

The parametric design can be done by changing one or more design parameters to automatically complete the single part model or the entire assembly changes. This method not only saves a lot of modeling time, but also reduces the probability of human error(Jie et al., 2013).

It can greatly reduce the workload of the designer and effectively shorten the new product development cycle because the parametric design model can be called in the subsequent design of similar products directly. But the previous parametric design is only correlated with the geometric size of the model. For its geometric changes and physical properties of the model did not make a corresponding correlation. It will cause the performance of some or overall unable to meet the design requirements with the change of model geometrical dimensions(Shu-fang, 2011).

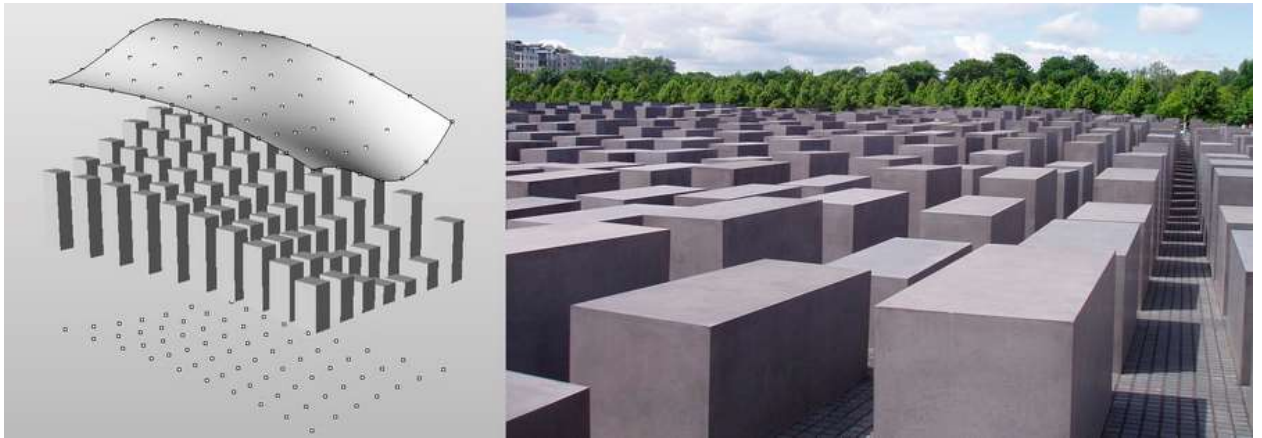


Figure 2-1 Parametric solution of a cuboid satisfying a certain set of constraints.

The above shown example of cuboids of the 28-million-euro second world war memorial that spreads over 20,000 square meters in the center of Berlin is seen as a good example to demonstrate the concept of parametric design. The length, width and the height of each cuboid are selected such that it meets a certain complicated criterion seen by the designer of the monument. Each level of these cuboids is determined by the intersections of the empty field with the grid lines of Berlin's larger urban context. This results in a seemingly faulty shift in the structure of the grid, which causes non-determinable spaces to develop within the seemingly strict order of the monument. The resulting spaces condense, narrow and deepen and open up a multifaceted experience from every point of the field structure.(reference - stiftung-denkmal.de)

In this parametric design that meets the architect's criteria has three parameters in the outcome, which are the length, height and the width of the cuboid. Based on those parameters the cuboids are constructed.

## 2.11 Parametric Design Method

The basic dimensions of the design goals and the main loads must be found which need to be considered in the design before modeling. Take that design a shaft as an example, the diameter and length of the shaft is base size. The keyway and the step shaft diameter on it are the indirect dimensions which are correlated with the base size. After determining the basic dimensions of the entire model to be designed, find the base components that need to be designed with the base dimensions to be designed and define the relevant dimensions for the base part as the parameter. In the process of modeling, sketches must be drawn for the whole constraint. And all dimensions that need to be directly or indirectly correlated with the base size need to be directly or indirectly correlated with the core parameters(Gao et al., 2015, Yongxiang et al., 2017).

Another possibility for the design of industrial devices is the use of topology optimization (TO) techniques. Topology optimization approaches look for the optimal shape of a given device by making free modifications in the distribution of material within the search space, without the need of predefining any parameters (Campelo et al., 2006, Biro et al., 2007). Due to this characteristic, TO-based techniques are able to yield essentially novel, creative solutions for a variety of engineering problems. This approach has been widely used in fields such as structural and mechanical engineering, and also, to a lesser extent, in electromagnetic design (Campelo et al., 2008, Hsu and Hsu, 2005)

## 2.12 The Realization of Parametric Design

### Define Parameters

The main factors that affect the model should be found and defined before modeling. Parameters can be defined in the software after determining the main influencing factors. The model needs to give the initial value in the first modeling.(Gao and Yang, 2012)

In order to establish the initial parametric model, the designer must first obtain a certain amount of understanding about the nature of the device under consideration; otherwise, the search space defined for the optimization procedure may not include potentially good solutions, therefore making it impossible for optimization algorithms to find the most efficient design. However, a long time may be required for the theoretical analysis of many possible models. Also, an initial model based solely on the experience of the designer may not include more unorthodox characteristics, such as holes or other features that could possibly improve the performance of the device (e.g., volume, efficiency, etc.)(Campelo et al., 2008).

### Analysis and Calculation of Components Size and Core Parameter Expressions

The key to parameterization is parameter calculation, determination of parameter reference and realization of parameter transmission, and to ensure its uniqueness. The impact of the size of parameters are found by the analysis and calculation, and it's correlated with calculated mathematical expression(Gao and Yang, 2012, Yong-xiang et al., 2017).

## 2.2 Parametric design of magnetic components

Parametric design is very useful in machine product design, it is the key technology in realizing speediness sculpting for engineering personnel in practical application(Li, 2010).

Increasing the efficiency of Converter devices in secondary power sources is becoming increasingly important, especially for Autonomous power supply systems. It is known that secondary power supplies are based on power electronics elements and electromagnetic elements. Although progress in the development of power electronics elements does not stop, the development of electromagnetic elements of secondary power sources has now almost exhausted itself and is limited only by increasing the operating frequency. New technical solutions in the field of electromagnetic elements appear either very rarely, or when designers return to old practices that were undeservedly forgotten(Styskin and Urazbakhtina, 2020).

In the case of designing magnetics components under given certain constraints there is a large number of parameters that define each possible solution.

Those include, dimensions of the product namely the width, depth and the height of the final solution, the weight, the type of material used such as Silicon steel, Ferrite, Amorphous, High silicon steel, Nanocrystalline magnetic materials, Copper conductors, Aluminum conductors or a combination of these, The temperature rise, insulation class, primary inductance, leakage inductance, interwinding capacitance, winding resistance, voltage regulation, cooling method ( thermal management options), efficiency, noise level, impedance etc.

In this research a detailed study is carried out in optimizing the magnetics design and novel approaches are presented to achieve power levels far beyond what the industry was able to achieve. Further the research and the mathematical models provides the opportunity evaluate a complete array of solutions for multiple solutions for a given application.



## 2.21 Design parameters of a magnetic component

There is a large number of design parameters that are taken into consideration in arriving at the optimum design of a magnetic component. It is rarely the case that the values of all the parameters or at least the suitable range of values for all these parameters are known at the time of the start of the design. In certain applications depending on the level of circuit simulations carried out by the application engineers the ideal values for certain parameters are known. In certain other applications the application engineers and system designers would like to have practically achievable parameters of the magnetic components for them to use as an input for the electronics system design. Below is a list of such design parameters that are taken into consideration.

1. Primary voltage(s), (V)
2. Secondary voltage(s) (V)
3. Rated power (continuous) (W/VA)
4. Operating frequency,  $f$  (Hz)
5. Primary inductance,  $L_P$  (mH)
6. Secondary inductance  $L_S$  (mH)
7. Leakage inductance,  $L_L$  ( $\mu$ H)
8. Primary DC resistance  $R_p$  ( $\Omega$ )
9. Secondary DC resistance  $R_s$  ( $\Omega$ )
10. Primary AC resistance  $R_{pac}$  ( $\Omega$ )
11. Secondary AC resistance  $R_{sac}$  ( $\Omega$ )
12. Interwinding capacitance,  $C_{WW}$  (nF)
13. Turns ratio
14. Primary current,  $I_p$  (A)
15. Secondary current,  $I_s$  (A)
16. Volt-time product/ $E_t$  constant (Vs)
17. Isolation test voltage (kV)
18. Total allowable load loss, (W)
19. Allowable no load loss, (W)
20. Efficiency
21. Primary overvoltage possibility (V)
22. Details of voltage harmonics (V)
23. Details of current harmonics (V)

24. Static shield requirements
25. Magnetic shield requirement
26. Earthing requirements
27. Creepage distance (mm)
28. Clearance (mm)
29. Distance through insulation (mm)
30. Electrical tolerance percentage
31. Dimensions (width, length and height) (mm)
32. Weight, (kg)
33. Ambient temperature °C
34. Allowable temperature rise °C
35. Cooling Method (e.g. natural convention, forced air, active water cooled, passive water cooled, oil natural, forced oil, cold plate mounted etc )
36. Insulation class ( e.g. Class A, Class B, Class F, Class H etc. )
37. Insulation type ( dry type, oil etc )
38. Noise level, (dB)
39. Degree of protection (e.g. IP56 )
40. Pollution degree ( I, II or III)

## 2.22 Possible transformer constructions

In addition to the design optimization possibilities generated by a large number of permutations possible with the above parameters the magnetics designer has a choice of number of constructions.

1. Toroidal core construction
2. Stadium core constructions
3. EI core construction
4. UI core construction
5. 3UI core construction
6. Y core construction
7. Other non-standard core constructions

These different possible constructions provide further design optimization possibilities.

## 2.23 Possible cooling options

There are number of possible cooling methods considered in the design optimization of the transformers, which includes.

1. Natural convection
2. Forced air.
3. Active water cooled.
4. Passive water cooled.
5. Oil natural
6. Forced oil.
7. Cold plate mounted etc.
8. The use of heat conducting channels.
9. Use of heat sink walls for thermal management.

## 2.24 Different core and conductor material options

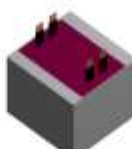

The right choice of different core materials such as grain-oriented Si Steel, non-grain-oriented Si Steel, Amorphous materials, High Si steels, nano-crystalline materials, different ferrite grades etc., is an important factor that makes the transformer design suitable for a particular application. It decides if the required parameters are met, and a commercially viable design is achieved. The details of this aspect and the developments introduced are discussed in the chapter 4 of this thesis.

Similarly, a right choice must be made in the case of selection of the conductor materials. There is a choice between conductor types such as round, rectangular, foil, flat conductor, Litz wires etc., further a choice between copper, aluminum and a combination of them is a possibility. The details and the limitations of conductor selection and associated outcomes are discussed in the chapter 3 of this thesis. Further patented innovations that helps to overcome the limitations of these are discussed in each of these chapters.

## 2.3 Design tool that facilitates the parametric design of magnetics.

In conventional design approaches a significant narrow down of the design options are done based on the experience of the designer. However, the parametric approach gives the designer much more freedom evaluate further possible solution and to come up with multiple solutions or in other words a set of solutions that meets the original requirements. This is a ideal situation for the end product designer.

During the study, this process was carried out by the use of a self-developed developed calculation tool. Based on the findings number of patented technologies were developed which are discussed in detail in the next chapters. However, as a future work the researcher intends to develop a software that would automate this process of finding the most optimized solution(s) in a significantly reduced time.

Parametric Design of HF HP HV Transformers																																							
Design output																																							
Customer	XXXXXX		Schematic																																				
Power	100 kW	Prim Voltage	750 V	Waveform	Square	Frequency	50 kHz	No of Sec.	One	Turns Ratio	1.50																												
														750 V	750 V	Primary Resistance	4.76 mΩ	Primary Inductance	2.144 mH	Working voltage	750 V	Recommended isolation	5 kV	Creepage distance	Recommended Min. 9mm	Insulation Class	H (180 C)	Core loss	110 W	Winding loss	846 W	Efficiency	99.9%	Ambient temperature C	50	Temperature rise C	70	Cooling method	Cold plate mounting - with thermal management
Voltage		Resistance	Width	200 mm	Width	150 mm	Efficiency		99.9%																														
Sec1		750 V	mΩ	Depth	190 mm	Depth	170 mm	Ambient temperature C		50																													
Sec2		0 V	0.00 mΩ	Volume	6.3 l	Volume	4.6 l	Temperature rise C		70																													
Sec3		0 V	0.00 mΩ	Weight Total	14 kg	Weight Total	9 kg																																
Sec4		0 V	0.00 mΩ																																				

2-2 Table 2 1 output of the design tool for parametric design

Design Input

Schematic

Power

100 kW

Prim Voltage

750 V

Waveform

Sinus

Frequency

30 kHz

No of Sec.

One

Turns Ratio

5.65

Sec1 Voltage

750 V

Sec2 Voltage

V

Sec3 Voltage

V

Sec4 Voltage

V

Prim. Current Nominal

133.3 A

Prim. Current Max

135.0 A

Voltage at Max current

0.0 V

Working voltage

750 V

Recommended insulation

5 kV

Creepage distance

Recommended Min. 8 mm

Sec. Power

100 kW

Sec. Current Nominal

133.3 A

Sec. Current Max

134.0 A

Duration

S

Ambient tempara

30

Sec1 Power

0 kW

Sec2 Power

0 kW

Sec3 Power

0 kW

Sec4 Power

0 kW

Sec1 Current

NA A

Sec2 Current

0.0 A

Sec3 Current

0.0 A

Sec4 Current

0.0 A

Sec1 Duration

S

Sec2 Duration

S

Sec3 Duration

S

Sec4 Duration

S

Fourier decomposition available 100

Frequency (Hz)

5 1000 2000 3000 4000 5000 6000 7000 8000 9000 10000 12000 15000 18000 20000 25000 30000 40000 50000 60000 70000 80000 90000 100000

Pri. Current (A)

Pri. Voltage(V)

I<sup>2</sup>(A<sup>2</sup>)

I (A)

W(W)

Power (kW)

Sec 1

Frequency (Hz)

5 1000 2000 3000 4000 5000 6000 7000 8000 9000 10000 12000 15000 18000 20000 25000 30000 40000 50000 60000 70000 80000 90000 100000

Sec. Current (A)

Pri. Voltage(V)

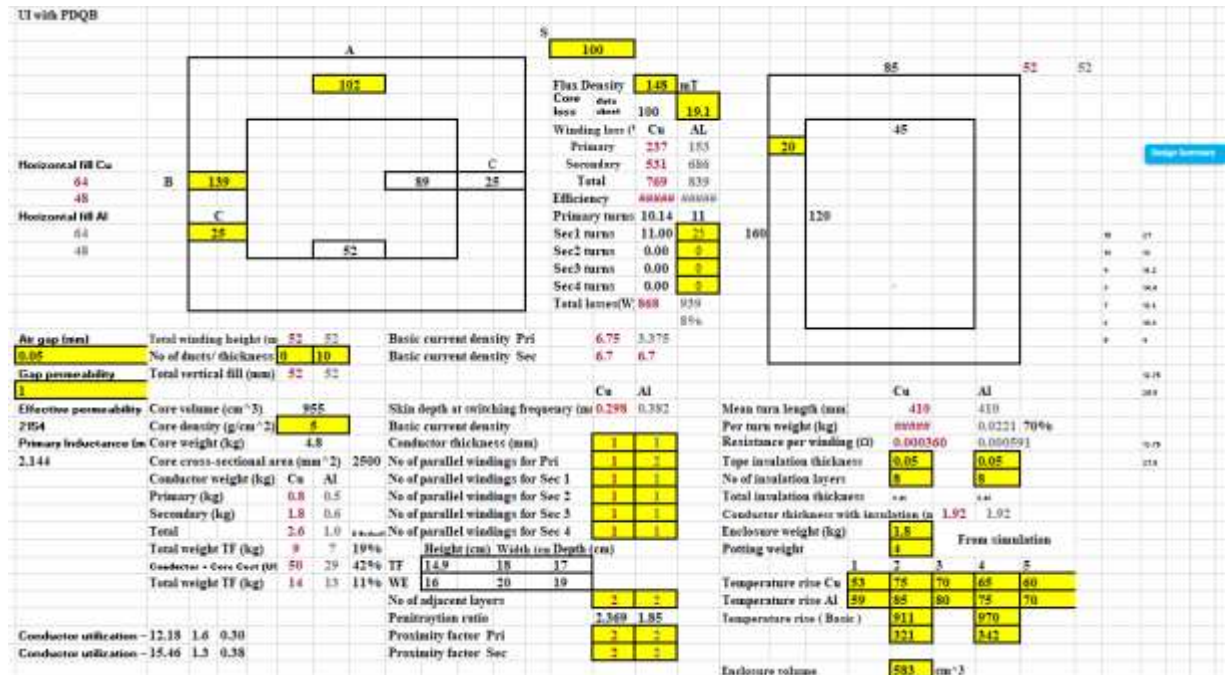
I (A)

W(W)

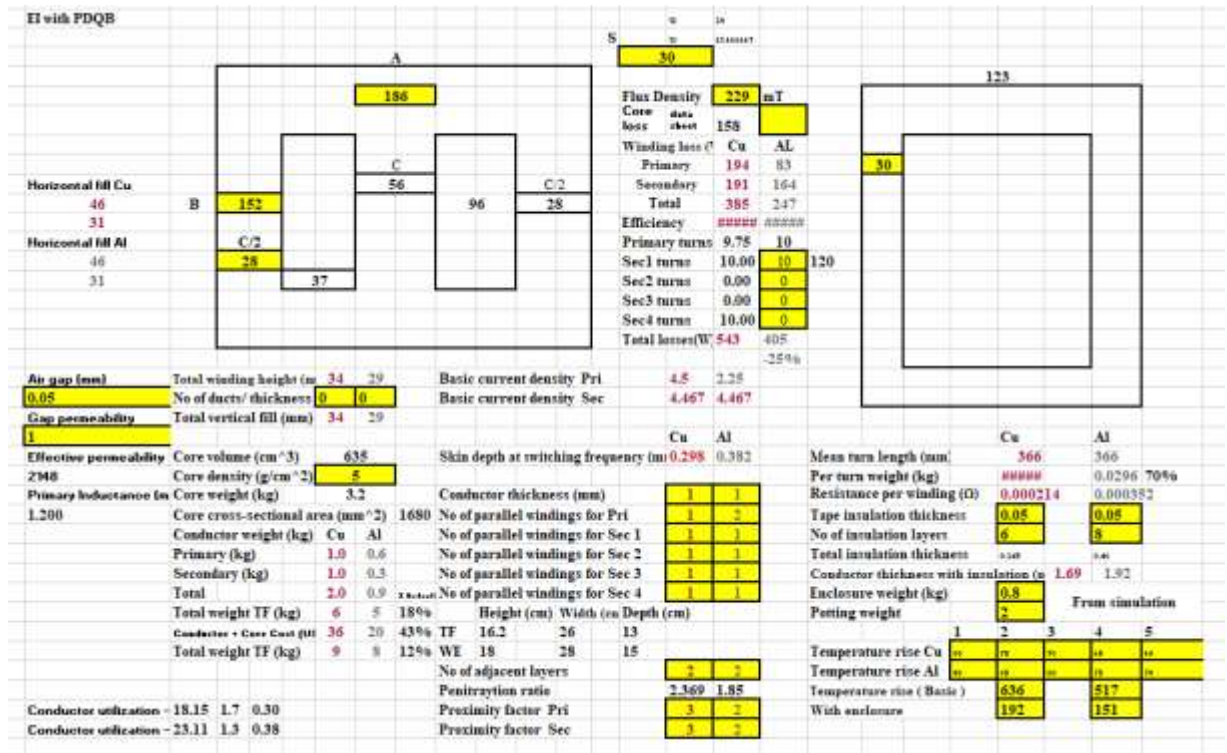
2-3 Input of design parameters

Construction	10 mm thick	15 mm thick	20 mm thick	25 mm thick	30 mm thick	35 mm thick
Conductor type	Cu	Al	Al	Al	Al	Al
Cooling option	1- Natural convection	2- Forced air cooling 2m/s	3- Forced air cooling 4m/s	4- Cold plate mounting-conventional	5- Cold plate mounting-with thermal management	6- Cold plate mounting-with thermal management
Cooling option	1 2 3 4 5	1 2 3 4 5	1 2 3 4 5	1 2 3 4 5	1 2 3 4 5	1 2 3 4 5
Design flux density	1.48	1.48	1.48	1.48	1.48	1.48
Core loss (W)	100	100	100	100	100	100
Winding loss Total	769	839	885	947	980	1000
Pri (W)	237	153	194	83	50	50
Sec (W)	531	686	191	164	50	50
Basic	911	970	636	517	50	50
Efficiency	99.9%	99.1%	99.9%	99.9%	99.9%	99.9%
Temperature rise (S)	53 75 78 65 60	53 75 78 65 60	53 75 78 65 60	53 75 78 65 60	53 75 78 65 60	53 75 78 65 60
Temperature rise (S)	53 59 85 80 75 70	53 59 85 80 75 70	53 59 85 80 75 70	53 59 85 80 75 70	53 59 85 80 75 70	53 59 85 80 75 70
Weight Total (kg)	14	13	9	8	8	8
Conductor weight (kg)	2.6	1.0	2.9	0.9	0.9	0.9
Core weight (kg)	4.8	4.8	3.2	3.2	3.2	3.2
Enclosure weight (kg)	1.3	1.3	0.8	0.8	0.8	0.8
Potting weight (kg)	4	4	2	2	2	2
kg/kVA	0.14	0.09	0.09	0.09	0.09	0.09
Dimensions (TF only)						
Height (mm)	149	149	162	162	162	162
Width (mm)	180	180	256	256	256	256
Depth (mm)	170	170	130	130	130	130
Volume (cm <sup>3</sup> )	4558	4558	5329	5329	5329	5329
cm <sup>3</sup> /kVA	46	46	54	53.9	53.9	53.9
Dimensions (With housing)						
Height (mm)	164	164	177	177	177	177
Width (mm)	200	200	276	276	276	276
Depth (mm)	190	190	160	160	160	160
Volume (cm <sup>3</sup> )	6132	6132	888	888	888	888
cm <sup>3</sup> /kVA	62	62	73	73	73	73
Material cost (USD)						
Labour cost (USD)						
Prime cost (USD)						
USD /kVA						
Selected conductor	Al with PQ26	Al with PQ26	Al with PQ26	Al with PQ26	Al with PQ26	Al with PQ26
Cooling method	Cold plate mounting - with thermal management	Cold plate mounting - with thermal management	Cold plate mounting - with thermal management	Cold plate mounting - with thermal management	Cold plate mounting - with thermal management	Cold plate mounting - with thermal management
Insulation class	B (130 C)	B (130 C)	B (130 C)	B (130 C)	B (130 C)	B (130 C)

2-4 Summary of the different design option comparison



2-5 UI core construction evaluation



2-6 EI construction evaluation



## 2.4 Summary of design options arrived for a 100 kW 50 kHz transformer application.

Below table shows the details of different design solutions arrived at by evaluation of various construction, conductor, core materials and cooling method options. The patented technologies that are discussed in later chapters are also used in arriving at these six designs options for this particular application which is a 100 kW transformer operating at 50 kHz.

Table 2-1 two designs options for 50° C cold plate mounted transformer.

Temperature rise/ Absolute hot spot temperature	45° C / 85° C	80° C / 125° C
Width (cm)	22	22
Depth (cm)	19	16
Height (cm)	13	13
Volume (l)	5.4	4.6
Weight (kg)	12.5	10.5
Calculated Efficiency at 50kHz / 80kHz	99.6% / 99.5%	99.6% / 99.4%

Table 2-2 Two designs options for 4m/s forced air-cooled transformer.

Temperature rise at the hot spot/ Absolute hot spot temperature	45 Deg C / 85 Deg C	80 Deg C / 120 Deg C
Width (cm)	25	22
Depth (cm)	24	24
Height (cm)	13	13
Volume (l)	7.8	6.8
Weight (kg)	16.5	15
Calculated Efficiency at 50kHz / 80kHz	99.6% / 99.5%	99.6% / 99.5%

Table 2-3 Two designs options for a natural convection cooled transformer

Temperature rise at the hot spot/ Absolute hot spot temperature	45 Deg C / 85 Deg C	80 Deg C / 125 Deg C
Width (cm)	25	25
Depth (cm)	26	26
Height (cm)	18	13
Volume (l)	11.7	8.5
Weight (kg)	23.5	18
Calculated Efficiency at 50kHz / 80kHz	99.6% / 99.6%	99.6% / 99.6%



## 2.5 Summary

Parametric design approach is commonly use in the areas of mechanical engineering, structural engineering and in the field of architecture. This approach gives designer to explore and analyze a large number of possible solutions for a certain application. Having a complete set of solution gives the end product designer a large flexibility to optimize the end product design.

The application of the parametric design concept to the design of magnetic components is somewhat difficult due to a large number of design parameters and complex structure of inter connection of them. During this study, this approach was used in evaluating various design inputs. This was carried out in combination with possible constructions, cooling techniques, material options and material combinations etc.

This was a very useful approach in arriving at optimized solutions and developing technologies that led to patents and publications. As a future work the researcher intendeds to automate this approach using latest computer programming techniques.

# Chapter 3

## Conductor Losses in Magnetic Components

## Chapter 3 Conductor losses in magnetic components

The behavior of the magnetic components significantly changes with the presence of harmonics in their excitation waveforms i.e., non-sinusoidal excitations e.g., Pulse Width Modulation (PWM) excitation, high frequency high power transformers etc. The effect becomes more and more significant as the frequency and the magnitude of the harmonics increase. In addition to the core losses winding losses in such magnetic components operating at high frequencies can severely limit the performance and prevent size and cost reductions(Pollock et al., 2003). If appropriate design considerations are not taken based on the increased core and winding losses these excessive losses can cause significantly higher temperatures, eventually leading to the condition of thermal runaway. The impact of this has become one of the major challenges that magnetics designers face at present. The reason for this is there is a rapid increase of the operating frequencies for a given power level due to the advancements of semiconductor technologies and power electronics in general. This can also be seen as an increase of power level for a given frequency. This challenge on magnetics have become to the level that many industry experts even believe that magnetics components as the reason that slows down the development of the power electronics industry.

Historically the discussions on the non-sinusoidal currents go back 35 years. A discussion took place in March 1980 during the meeting of IEEE power engineering society on the effect of non-sinusoidal load currents on transformer temperature rise(Pierce, 1996). The study committee formed in May 1980 was later elevated to an IEEE working group of performance. In the paper published by Alexander D. Kline in 1981, he first presented a methodology that was used in the development of IEEE standard C57.110 which defines K-factor for transformers (Ortiz et al., 2010). The K-factor gives an estimate of the ratio of heating in the transformer due to winding eddy currents when it is loaded with a given non sinusoidal current(a) to the winding eddy current heating caused by a sinusoidal current at the rated frequency(b)(den Bossche et al., 2004) (Zheng, 2000). However K-factor rating is not evaluated for the use with harmonics where the rms currents of any singular harmonic, (h) of a higher order than the 10<sup>th</sup> harmonic is greater than 1/h of the fundamental rms current.

The magnetic components that come under the scope of this study are subjected to much higher order harmonics of significant amplitudes. For example, a 400th harmonic can be as large as 10% of the fundamental amplitude. Thus, the design considerations go far beyond the

guidelines obtained from the K-factor transformer evaluations. The scope of the research has been set such that the solutions found will be able to solve the magnetic components come across for decades.

The losses occurring in the core material can be of equal importance to the losses in the windings depending on the excitation waveform(Zheng, 2000). Further it is necessary that the study of these carries out simultaneously due to their overall interdependent nature. The well-known Steinmetz formula of the form

$$P_c = k_1 \cdot f^{k_2} \cdot B^{k_3}$$

3 -1

where,

$P_c$  is the power losses density,  $f$  is the frequency,  $B$  is the flux density,  $k_1, k_2$ , and  $k_3$  are core material dependent constants, can be used to make an estimate of the contributions of the individual harmonics to the core losses.

However, in this chapter only the losses occurring in the windings are discussed for the various excitation waveforms. The analysis, estimation and the minimization of the core losses are explained in chapter 4 of this thesis.

Winding losses in the foil conductors of high frequency transformers, winding losses in the multi-layer foil wound inductor, winding losses in Litz wire arrangements, winding losses profile conductors, winding losses in flat wire arrangements are taken into consideration in this chapter.

### 3.1 Theoretical background

#### 3.11 Skin Effect

When a conductor carries an ac current, the magnetic field will not only depend on the amplitude of the current and the radial distance from the center of the conductor, but also on the frequency of the waveform; see figure 3-1. The alternating magnetic field generated by the excitation current will induce, according to Lenz's law, an opposing current in the conductor. Therefore, the current density will be reduced inside the conductor and increased in the surface. The total current in the conductor will not suffer any change, however the current density will not be uniform anymore.

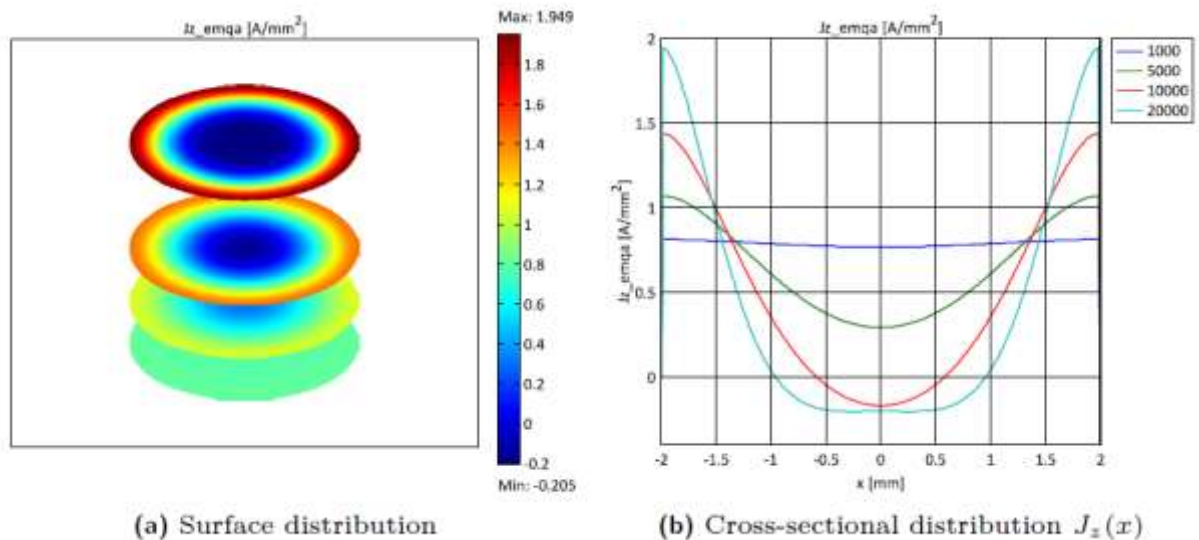


Figure 3-1 Current density in an isolated 4mm round copper conductor with total net current of 10A for various frequencies. a) surface distribution b) Cross-sectional distribution (Villar, 2010)

The non-uniform distribution of the current density will be much more pronounced with higher frequencies; see figure 3-2, due to the linear relationship between frequency and induced current density. This penetration property of conducting materials is known as skin depth, and it is defined as the radial distance from the surface of the conductor where the value of the current density is 37% smaller than its value in the surface; see Table 3-1

$$\delta = \sqrt{\frac{2}{\omega \mu \sigma}}$$

3 - 3

or

$$\delta = \sqrt{\frac{\rho}{\pi \mu f}}$$

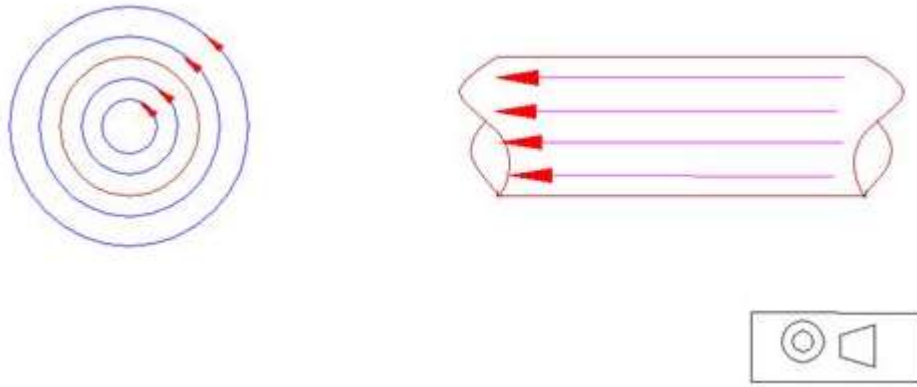
3 - 3

where  $f$  represents the pulsation frequency of the waveform,  $\mu$  is the permeability of the material and the conductivity, or  $f$  represents the frequency of the waveform and is the resistivity of the material.

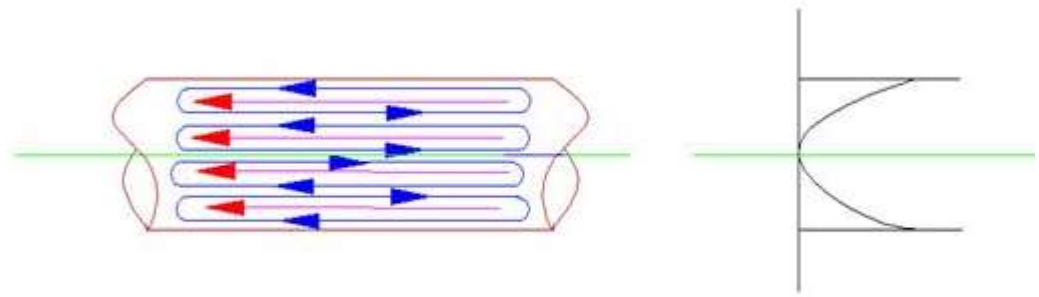
Table 3-1 Skin depth of Copper and Aluminum at different frequencies

Material	Conductivity (25 °C)	Frequency (kHz)					
		1	2	5	10	20	50
Copper	5.688e7	2.11	1.49	0.94	0.66	0.47	0.29
Aluminum	3.478e7	2.69	1.90	1.20	0.85	0.60	0.38

Current carrying conductors try to achieve the condition of minimum losses Figure 3-2 shows the magnetic field inside and around a conductor carrying a DC or low frequency AC current. At low frequencies, the energy associated with the magnetic field of such a conductor is exceedingly small compared to the energy loss in the resistance of the wire. Therefore, the current distributes itself evenly throughout the wire as this gives the condition of minimum loss. However, as the frequency of the current goes up the speed at which the current changes go up resulting in the flux caused by the current changing rapidly(Dixon, 1988).



3-2 Low frequency AC/DC current carrying conductor.



3-3 High frequency current carrying conductor

This rapid change in the current results in induced voltage loops, these voltage loops or the eddies results in circulating currents as shown in figure 3-1b. These current changes reinforce the main current at the surface of the wire but oppose it towards the center(Dixon, 1988). All electromagnetic phenomena are governed by Ampere's law, Faraday's law, Gauss's law etc.(Krawczyk and Tegopoulos, 1993). In the middle of the 19<sup>th</sup> century James Maxwell Published a set of equations giving an analytical approach to electromagnetism(Siegel, 2003). With the use of these equations, which are today known as Maxwell's Equations the above phenomena can be represented in mathematical form as follows.

Consider a homogeneous conducting material with conductivity  $\sigma$  and permeability  $\mu$  and taking the angular frequency of the current to be  $\omega$  and assume the current density vector  $J$  to be parallel to the boundary surface(Popović and Popović, 2000).

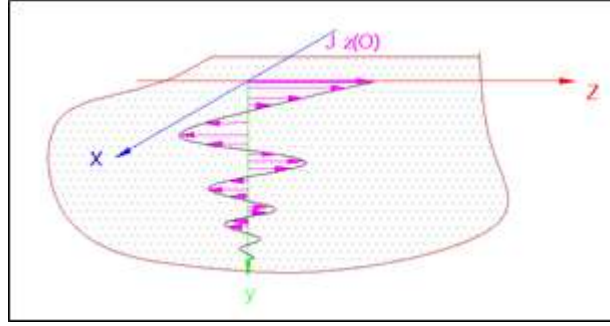


Figure 3-4 Homogeneous conducting material with permeability  $\mu$  and conductivity,  $\sigma$

The differential form of Maxwell's equation for Faraday's law and Ampere's law can be presented as follow (Popović and Popović, 2000).

$$\nabla \times E = -j\omega B$$

3 - 2

and

$$\nabla \times H = J$$

3 - 3

where,

$E$  the electric field strength.

$J$  the current density

$H$  the magnetic field strength.

$B$  the magnetic flux density

$\omega$  the angular frequency of the current.

#### Curl - Physical Interpretation of the Curl

The curl of a vector field measures the tendency for the vector field to swirl around. Imagine that the vector field represents the velocity vectors of water in a lake. If the vector field swirls around, then when a paddle wheel is stuck into the water, it will then tend to spin. The amount of the spin will depend on how it is oriented the paddle. Thus, it is expected for the curl to be vector valued. As other examples, consider the illustrations below. The field on the left, called



$\vec{F}$  has curl with positive  $\hat{k}$  component. To see this, use the right-hand rule. Place the right hand at P. Point the fingers toward the tail of one of the vectors of  $\vec{F}$ . Now curl the fingers around in the direction of the tip of the vector. Stick the thumb out. It points toward the +z axis, so the curl should have positive  $\hat{k}$  component.

These can be rearranged to

$$\nabla \times J = -j\omega\sigma B \quad 3 - 4$$

and

$$\nabla \times B = \mu J \quad 3 - 5$$

$$dJ_z/dy = -j\omega B_x \quad 3 - 6$$

Assuming that the current density vector has only Z component therefore, and

$$-dB_x/dy = \mu J_z \quad 3 - 7$$

Taking a differentiation and by substitution of the equivalent term the following equation can be obtained.

$$\frac{d^2 J_z}{dy^2} = j\omega\mu\sigma J_z \quad 3 - 8$$

Solving this equation gives the result,

$$J_z(y) = J_z(0)e^{-ky}e^{-jky} \quad 3 - 9$$

where,

$$k = \sqrt{\omega\mu\sigma/2}$$

3 - 10

This explains the exponential drop in the current density vector as shown in figure 3-3. This drop becomes more and more rapid as the frequency of the current increases causing more losses in the outer surface of the conductor. In other terms, the high frequency components of the current see (utilizes) only a part of the cross-section of the conductor (Villar, 2010).

### 3.12 Proximity Effect

The ac current that circulates in a wire, generates a magnetic field that enters adjacent conductors and induces voltages on them, resulting in additional current in the conductor. The depth of the penetration will depend on the proximity of the external wire and the frequency of the waveform. The current density in the conductor will be reduced near the external wire and reinforced in the opposite side. The total net current of the conductor does not change; however, the current distribution is altered. Thus, any additional conductor within the same external field will suffer from this current even if there is no net current through it.

#### Proximity Effect in the context of foil windings

Although Dowell was not the first one who solved the one-dimensional Maxwell equations in winding arrangements [Bennet and Larson, 1940], he was actually the first one solving them specifically for transformer windings, and reaching a closed form expression that is nowadays known as Dowell's expression [Dowell,1966]. The resolution of these equations and therefore the validity of Dowell' expression is based on the following considerations (see figure 3-5),

One dimensional analysis is directly applicable to foil conductors closed to each other.

Foil conductors will occupy the whole core window height (y-direction1) assuring one dimensional field along the core window,  $H_y(x)$ .

The magnetic core will have an infinite permeability, thus considering only the field in the transformer window,  $H_{core} = 0$ .

The magnetic field generated by a current carrying conductor enters the adjacent conductors and induces a voltage on them (Figure 3-5). This results in an additional current in the adjacent conductors. The frequency of the waveform and the proximity of the external conductor determine the depth of penetration.

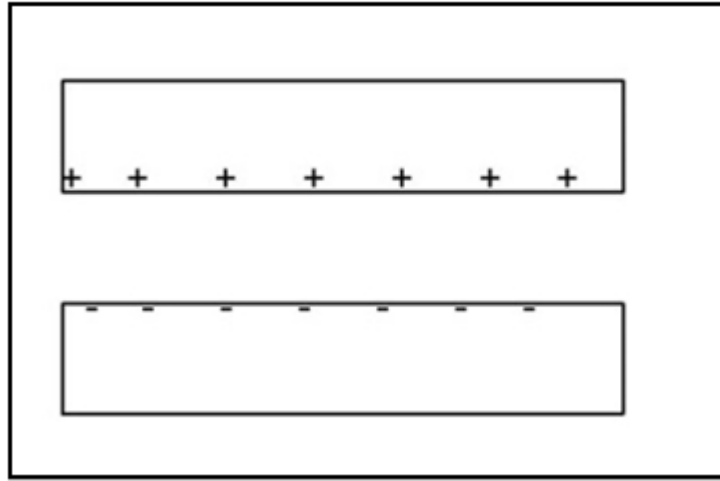


Figure 3-5 Two adjacent current carrying conductors.

The current density of the conductor close to the external wire will reduce and the current density on the opposite side will increase keeping the total current density of the conductor unchanged. This effect becomes more and more significant as the number of conductors in proximity increases. In the typical situation of a multilayer high frequency transformer winding a current density build up as illustrated in the below diagram can be recognized(Dixon, 1988). The general analytical approach to the above phenomena is quite complicated however the use of one-dimensional Maxwell's equations is sufficient to estimate the losses of a multi-layer foil winding. This type of winding is one of the most common winding configurations in high frequency high power transformers and inductors.

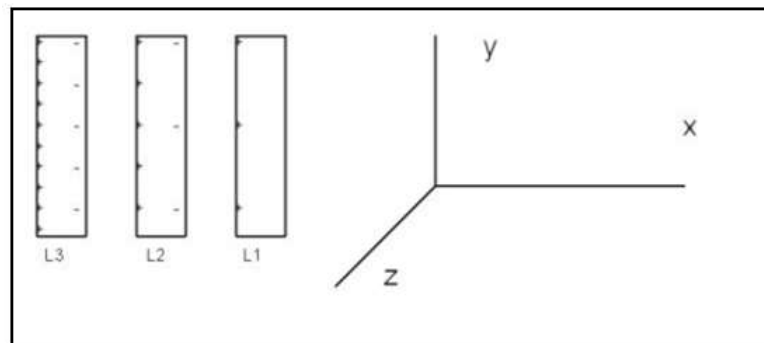


Figure 3-6 Three adjacent foil windings in a magnetic component

In the following formulation, it is assumed that the magnetic field vector has only one component and it is in the direction of y. The magnetic field within the foil depends only on the position along the x-axis; based on the work of Irma Villar (Villar, 2010).

The development of the closed form expression for conduction losses begins with the resolution of the diffusion equation. As conductive materials for winding conductors are linear, the resolution of Maxwell equations is carried out in its time harmonic form using phasors. The magnetic field phasor has only one cartesian component, in this case the y-component

$$H(x) = a_y H_y(x)$$

3 - 11

The magnetic field within foil conductors depends only on the position along the x axis. Therefore, the diffusion equation becomes a second order ordinary differential equation.

By solving the Maxwell equations similar to what was discussed under skin effect analysis it could be shown that

$$\frac{d^2 H_y(x)}{dx^2} = j\omega\mu\sigma H_y(x) = \alpha^2 H_y(x)$$

3 - 12

where,

$$\alpha = (1 + j)/\delta$$

3 - 13

and

$$\delta = \sqrt{2/\omega\mu\sigma}$$

3 - 2

where  $\alpha$  is the propagation constant This gives the general solution of

$$Hy(x) = H1e^{\alpha x} + H2e^{-\alpha x}$$

3 - 14

In order to solve this expression, a single foil conductor within a core window is considered. This conductor carries a peak current  $I$ , has a thickness  $d_w$ , and a height  $h_w$  (much larger than its thickness), a length  $l_w$  surrounding the core with a negligible curvature and general boundary conditions as the ones presented in the figure 3-6

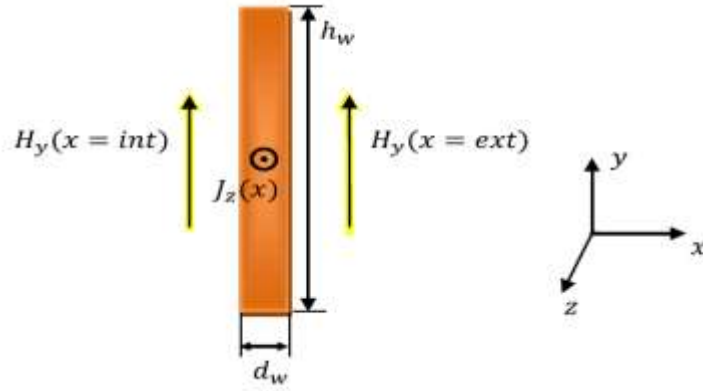


Figure 3-7 With this assumption, a general frequency-dependent expression is reached for the magnetic field distribution within foil conductors.

$$Hy(x) = Hex \cdot \frac{\sinh(\alpha x)}{\sinh(\alpha dw)} - Hin \cdot \frac{\sinh(\alpha(x - dw))}{\sinh(\alpha dw)}$$

3 - 15

Where  $Hex$  and  $Hin$  are the internal and external fields, Once the one-dimensional magnetic field is defined, the current density can be determined.

Since

$$\nabla \times H = J$$

3 - 5

$$a_z \frac{\partial H_x(x)}{\partial x} = J$$

3 - 16

$$\frac{dH_y(x)}{dx} = J_z(x)$$

3 - 17

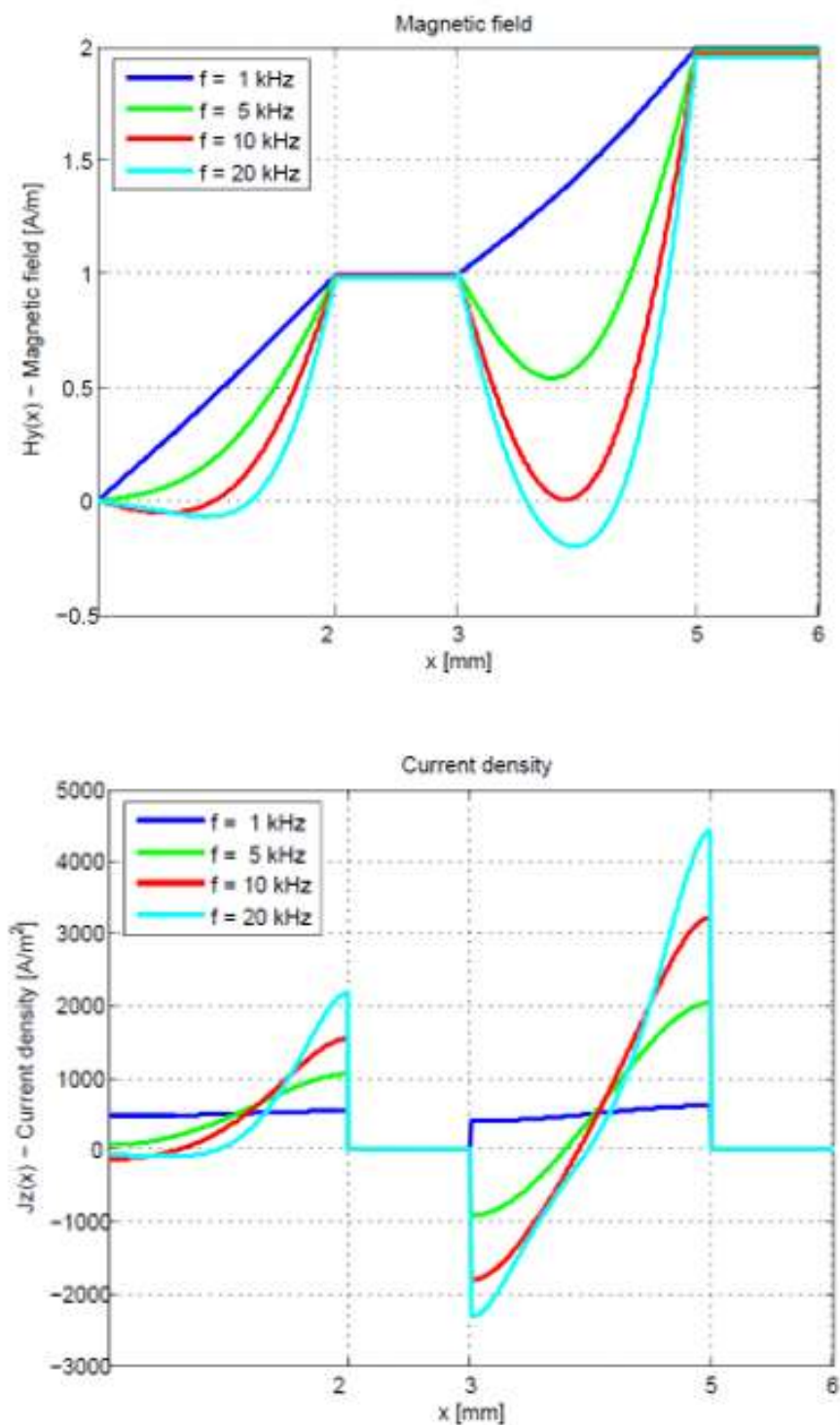
Therefore, deriving the magnetic field expression the frequency-dependent current density in a foil conductor is obtained.

$$J_z(x) = \alpha H_{ex} \cdot \frac{\cosh(\alpha x)}{\sinh(\alpha dw)} - \alpha H_{in} \cdot \frac{\cosh(\alpha(x - dw))}{\sinh(\alpha dw)}$$

3 - 18

In the case of the first foil, the external field is zero and only the internal field determines the current density. When it comes to the second foil it has an external field caused by the field of the first foil and counteracts with an opposite sign current near the first foil. As the total net current does not change, there is a high concentration of current in the opposite side of the second foil in order to balance the total current. This causes a higher current density and at the opposite side to the first foil. This results in an even larger field being applied to the third foil. As this continues through layers the current density at the end of the foils increases significantly (Villar, 2010, Dixon, 1988).

As illustrated in figure 3-8b, the current density increases as the number of foils is also raised. The first conductor does not suffer from an external field on its left-hand side (see figure 3-8a), and consequently the distribution of the current density depends only on its own current (skin effect). In contrast, the second conductor has an external field on its left-hand side and counteracts with an opposed sign current near the first layer. As the total net current does not change, there is a high concentration in the opposite side of the second foil in order to balance the total current (proximity effect).



3-8 Graphical representation of the change in (a) Magnetic Field and (b) Current Density in adjacent foil windings as the frequency of the currents goes high; based on the work of Irma Villar(Villar, 2010)

From the expression of the current density, the frequency-dependent conduction losses in foil windings are determined.

$$P_{\sigma} = \frac{1}{\sigma} \int_v J \cdot J^* dv$$

3 - 19

A simplified expression for ohmic losses P is rewritten and solved.

$$P_{\sigma} = \frac{1}{2\sigma} \int_v |J_z^2(x)| dv = \frac{1}{2\sigma} \int_{x=0}^{x=d_w} |J_z^2(x)| h_w l_w dx$$

3 - 20

Finally, and after some mathematical developments, conduction losses in a conduction layer, placed in a transformer window, are represented with a closed form expression.

$$P_{\sigma} = \frac{l_w h_w}{2\delta\sigma} [(H_{ext} - H_{int})^2] \frac{\sinh(2\Delta) + \sin(2\Delta)}{\cosh(2\Delta) - \cos(2\Delta)} + 2H_{int}H_{ext} \frac{\sinh(\Delta) - \sin(\Delta)}{\cosh(\Delta) + \cos(\Delta)}$$

3 - 21

Where,  $\Delta$  represents the penetration ratio and

$$\Delta = \frac{d_w}{\delta}$$

3 - 22

In this expression two parts can be clearly distinguished, the one generated by the conductor itself representing the skin effect (left-hand side of the expression within the brackets), and the one generated from the interaction of the fields representing the proximity effect (right-hand side). From this expression two factors are determined, the skin and proximity effect factors,  $\varsigma_1$  and  $\varsigma_2$  respectively.

$$\varsigma_1 = \frac{\sinh(2\Delta) + \sin(2\Delta)}{\cosh(2\Delta) - \cos(2\Delta)}$$

3 - 23



$$\zeta_2 = \frac{\sinh(\Delta) - \sin(\Delta)}{\cosh(\Delta) + \cos(\Delta)}$$

3 - 24

Now, if a winding is composed of several consecutive layers, the boundary conditions in each side of the pth foil conductor will be defined with the following two expressions, magnetic field distribution within foil conductors according to Ampere's circuital law.

$$H_{int} = (p - 1) \frac{I}{h_w}$$

3 - 25

$$H_{ext} = p \frac{I}{h_w}$$

3 - 26

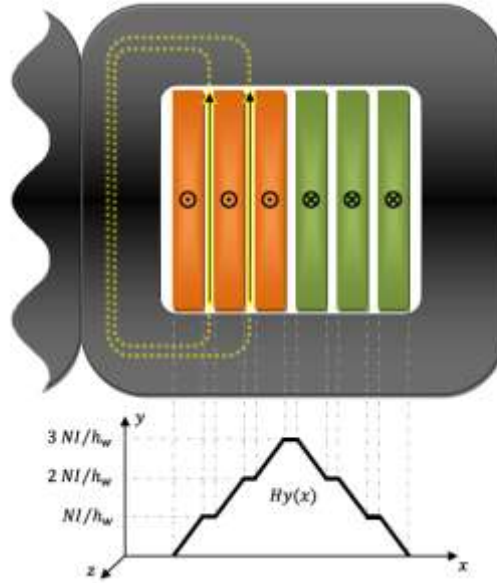


Figure 3-9 Transformer winding with several primary and secondary layers and equivalent dc (Villar, 2010)

where  $H_{int}$  represents the field generated by the previous  $p - 1$  layers and  $H_{ext}$  represents all the field generated by the  $p$  layers, see figure 3-9.

Substituting and simplifying above equations and summing up the losses of all the  $m$  layers of the winding

$$P_w = \sum_{p=1}^m P_{\sigma}$$

3 - 27

the total ohmic losses of a winding will be,

$$P_w = I^2 \frac{l_w}{2\delta\sigma h_w} m \left[ \zeta_1 + \frac{2}{3}(m^2 - 1)\zeta_2 \right]$$

3 - 28

As mentioned before, each foil conductor is carrying a peak current  $I$ . Furthermore, power losses in resistive elements are determined from their resistance  $R_{ac}$  and the rms current through them  $I_n$ .

$$P_w = R_{ac} I_n^2 = R_{ac} \frac{1}{2} I^2$$

3 - 29

Equating the conduction loss expression as explained above, the total ac resistance of the winding is determined.

from these expressions Dowell's resistance factor  $F_r$ , which represents the relationship between total ac resistance and total dc resistance,  $R_{ac} = F_r R_{dc}$ , can be deduced.

$$F_r = \Delta \left[ \zeta_1 + \frac{2}{3}(m^2 - 1)\zeta_2 \right]$$

3 - 30

In figure 3-10 the resistance factor is illustrated for different penetration ratios and for different numbers of layers. For high penetration ratios the total resistance of the winding rapidly increases. Below = 1 losses can be also considerable if windings with large numbers of layers are considered. For example, a four-layer winding composed of  $d_w = 2 \text{ mm}$  copper foil

conductors carrying a sinusoidal current at 1 kHz see Table 3-1 will present 2.7 times higher losses than its dc counterpart.

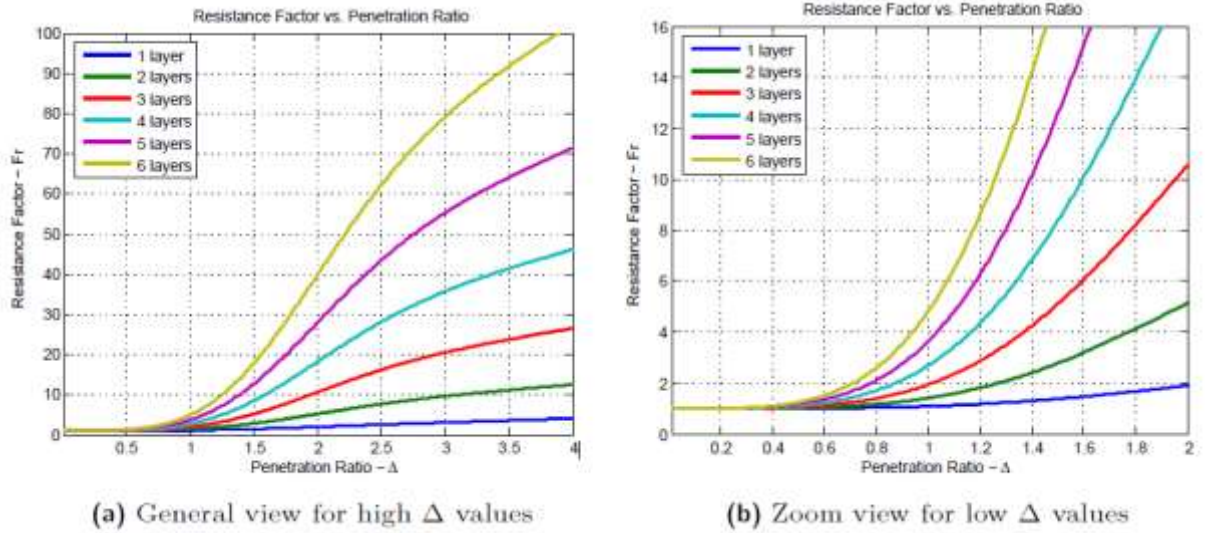


Figure 3-10 Dowell resistance factor expression  $F_r$  versus penetration ratio (Villar, 2010).

The resistance factor expression was introduced by Dowell and equation is one of its variants [Dowell, 1966]. From this closed form expression, losses in foils windings can be directly determined. Nevertheless, it is important to notice that the assumptions made at the beginning of the section must be accomplished in order to achieve a certain level of accuracy. If a different winding arrangement is considered, like interleaving primary and secondary foil conductors, separate consecutive layers can be considered and sum up, or otherwise, expression should be reevaluated, in order to get a new compact expression.

### Dowell's Porosity Factor

Although for some applications foil conductors are practical solutions, winding layers are usually composed of round or rectangular conductors, and sometimes they do not extend the full core window. For those cases Dowell introduced in the same analysis a parameter that accounted for these variations: the porosity factors  $\eta_w$ . This factor relates round, rectangular, or short foil conductors with their equivalent whole window foil conductor see figure. 3-12.

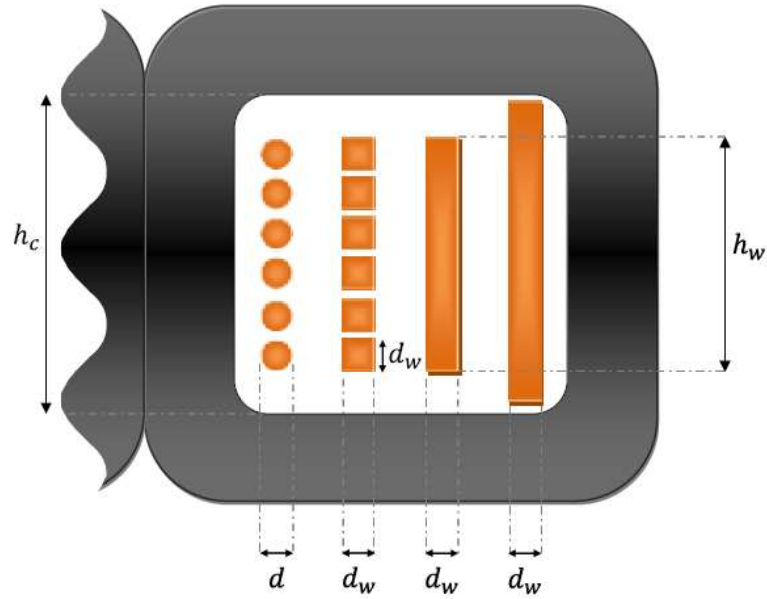


Figure 3-11 Representation of the equivalent foil conductor, from round conductors to equivalent square conductors to equivalent foil conductors and finally to whole window foil conductors(Villar, 2010).

In the case of round conductors, an equivalent square conductor; see figure 3-11, with the same conducting area is defined.

$$d_w = \sqrt{\frac{\pi}{4}} d$$

3 - -31

For equivalent square conductors or rectangular ones, an equivalent foil conductor is determined, which has the same height as the whole conducting layer; see figure. 3-12. However, in this second equivalence, the effective conductive surface is increased, thus an

equivalent conducting material is defined which generates an equal magnetic field along the enclosed winding path.

$$\sigma' = \eta_w \sigma$$

3 - 32

where  $\eta_w$  is known as the porosity factor and it is determined in this case according to.

$$\eta_{w1} = \frac{Nd_w}{h_w}$$

3 - 3-33

where  $N$  represents the number of turns in one layer. Finally, for equivalent or originally short foil conductors, the conductive layer is extended to fill the whole window height and a second porosity factor is determined.

$$\eta_{w2} = \frac{h_w}{h_c}$$

3 - 34

Therefore, equation becomes.

$$F_r = \Delta' \left[ \varsigma'_1 + \frac{2}{3}(m^2 - 1)\varsigma'_2 \right]$$

3 - 35

with

$$\Delta' = \sqrt{\eta_w} \Delta$$

3 - 36

and

$$\varsigma'_1 = \frac{\sinh(2\Delta') + \sin(2\Delta')}{\cosh(2\Delta') - \cos(2\Delta')}$$

3 - 37

and

$$\zeta'_2 = \frac{\sinh(\Delta') - \sin(\Delta')}{\cosh(\Delta') + \cos(\Delta')}$$

3 - 38

The physical validity of the porosity factor has been questioned in several publications (Ferreira, 1994, Robert et al., 2000, Nan and Sullivan, 2003, Reatti and Kazimierczuk, 2002), however its precision as a correction factor has been reinforced.

In (Ferreira, 1990, Villar, 2010), for instance, a remark was made concerning the physical validity of the factor, and it was proposed, if it was to be used, the application of the porosity factor as a compensation term also for the magnetic field, in order to eliminate the geometrical dependency of the skin depth introduced by Dowell.

$$F_r = \Delta' \left[ \zeta'_1 + \eta_w^2 \frac{2}{3} (m^2 - 1) \zeta'_2 \right]$$

3 - 39

Apart from the previous remark, (Ferreira, 1990, Villar, 2010) proposed another closed form expression for round conductors derived from the exact solution of an isolated round conductor (Lammeraner and Štafl, 1966, Villar, 2010) and based on the orthogonality between skin and proximity effects (Ferreira, 1990, Villar, 2010). In the proposed expression the skin effect is characterized with the exact solution of the magnetic field in an isolated round conductor and the proximity effect, with the exact solution of an external magnetic field in a round conductor.

$$F_r = \frac{\gamma}{2} \left[ \tau_1 - 2\pi \frac{4(m^2 - 1)}{3} \tau_2 \right]$$

3 - 40

with

$$\tau_1 = \frac{ber(\gamma)bei'(\gamma) - bei(\gamma)ber'(\gamma)}{ber'(\gamma)^2 + bei'(\gamma)^2}$$

3 - 41

and

$$\tau_2 = \frac{ber_2(\gamma)ber'(\gamma) + bei_2(\gamma)bei'(\gamma)}{ber'(\gamma)^2 + bei'(\gamma)^2}$$

3 - 42

and

$$\gamma = \frac{d}{\delta\sqrt{2}} = \frac{\sqrt{2}r}{\delta}$$

3 - 43

where *bei* and *ber* are Kelvin functions, i.e. real and imaginary parts, respectively, of Bessel functions of the first kind. In order to improve the accuracy of the expression proposed by (Ferreira, 1990, Reatti and Kazimierczuk, 2002) introduced the porosity factor in the equation as a correction term for the magnetic field, like Ferreira himself did for Dowell's expression.

$$F_r = \frac{\gamma}{2} \left[ \tau_1 - 2\pi\eta_w^2 \left[ \frac{4(m^2 - 1)}{3} + 1 \right] \tau_2 \right]$$

3 - 44

The good predictions provided by Dowell's expression and the porosity factor were pointed out already in (Ferreira, 1994, Villar, 2010) for tightly packed windings  $w > 0.7$ . More recently various papers with comparisons and validity ranges have been published (Dimitrakakis et al., 2007, Nan and Sullivan, 2003, Robert et al., 2001, Villar, 2010). The accuracy of Dowell's expression was pointed out once more for tightly packed windings, as well as the overestimation of Ferreira based models, see Table 3-2. The exact solution of Ferreira's method is only accurate for isolated round conductors, when the round conductors are getting close to each other, the effect between turns in each layer is not considered and the representation introduced by Dowell (with its equivalent square and foil conductors) is more precise, and much simpler.

Table 3.2 summarizes the study carried out in (Dimitrakakis et al., 2007, Dimitrakakis and Tataakis, 2008, Villar, 2010). The reduced error in Dowell's expression usually occurs when the skin depth is in the order of the diameter of the conductor ( $\delta \approx 1$ ) (Nan and Sullivan, 2003, Villar,

2010). However, for large penetration ratios the error, as illustrated in Table 2.2, is higher (highest error in each range)(Villar, 2010).

Porosity Factor	Round Conductors		Rectangular Conductors
	Dowell	Ferreira Modified	Dowell
$\eta_w > 0.7$	$< 5\%$	15% – 140%	Accurate
$0.7 > \eta_w > 0.6$	5% – 15%	8% – 70%	$< 15\%$
$0.6 > \eta_w > 0.5$	5% – 30%	5% – 50%	20% – 40%

Table 3-2 Comparison of the relative percentage error of two closed form expressions and for different porosity factors.

Based on these statements, most recent publications related to winding losses, focus on the improvement of Dowell's expression with finite element tools(Dimitrakakis et al., 2007, Nan and Sullivan, 2003, Robert et al., 2001, Villar, 2010). They propose modified expressions with several correction factors or weighting parameters based on tens of finite element simulations, depending on turn-to-turn distance, layer-to-layer distance or edge-to-core distance and skin depth. On the one hand, propositions in are based on complicated look-up tables. On the other hand, in a polynomial expression is introduced, however the conditions in which finite element simulations were carried out make the expression too limited, lacking a real applicability. As a conclusion, it should be noted, if high-power densities are to be reached, windings will be tightly packed and Dowell's expression with the corresponding porosity factor will be precise enough. Nevertheless, for non-conventional winding arrangements, finite element simulations should be used, because even if there are several winding arrangements summarized and characterized in, they do not cover every possible winding arrangement(Villar, 2010).



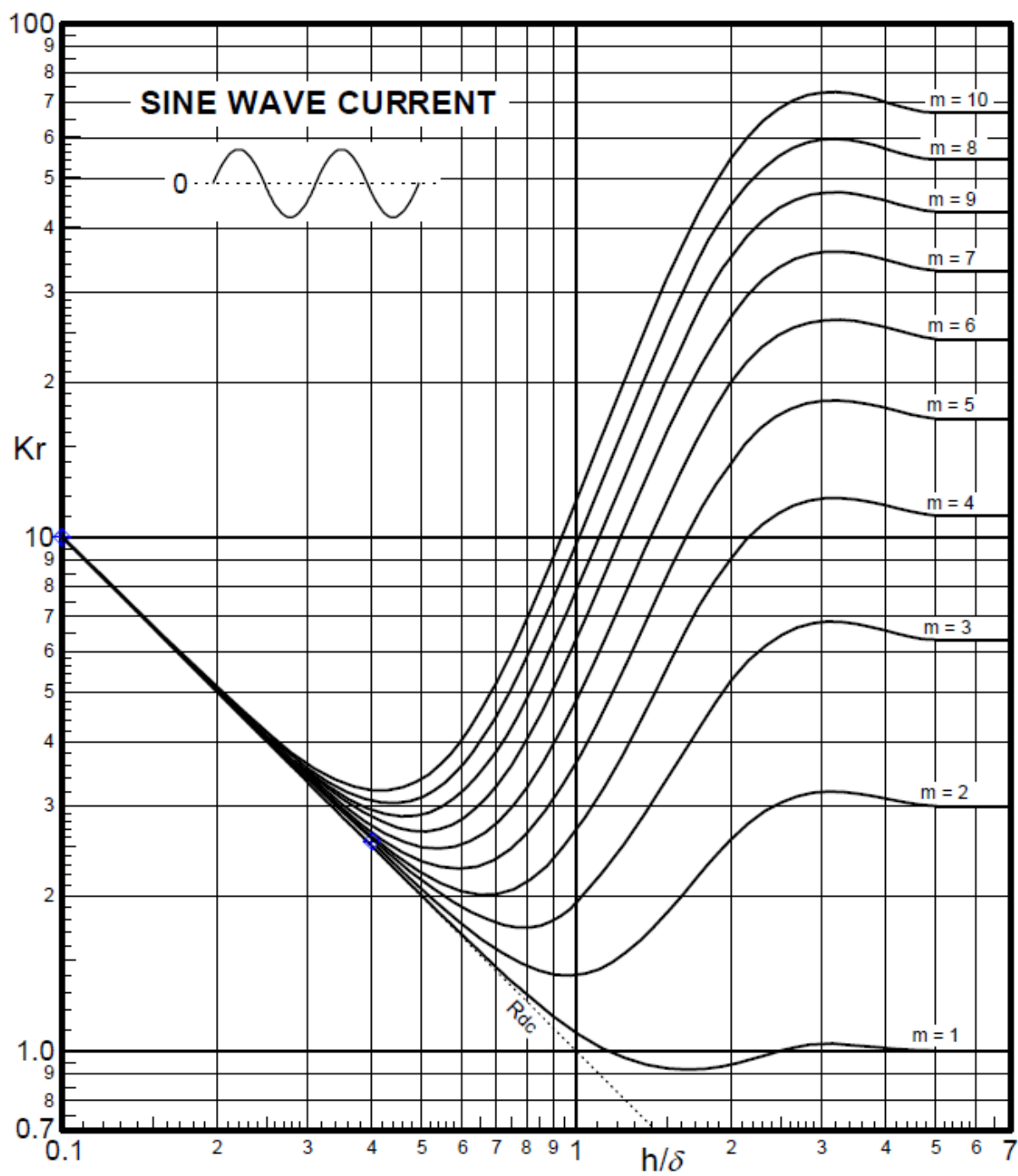


Figure 3-12 Loss Factor for sinusoidal currents and different number of layers(Carsten, 1986)

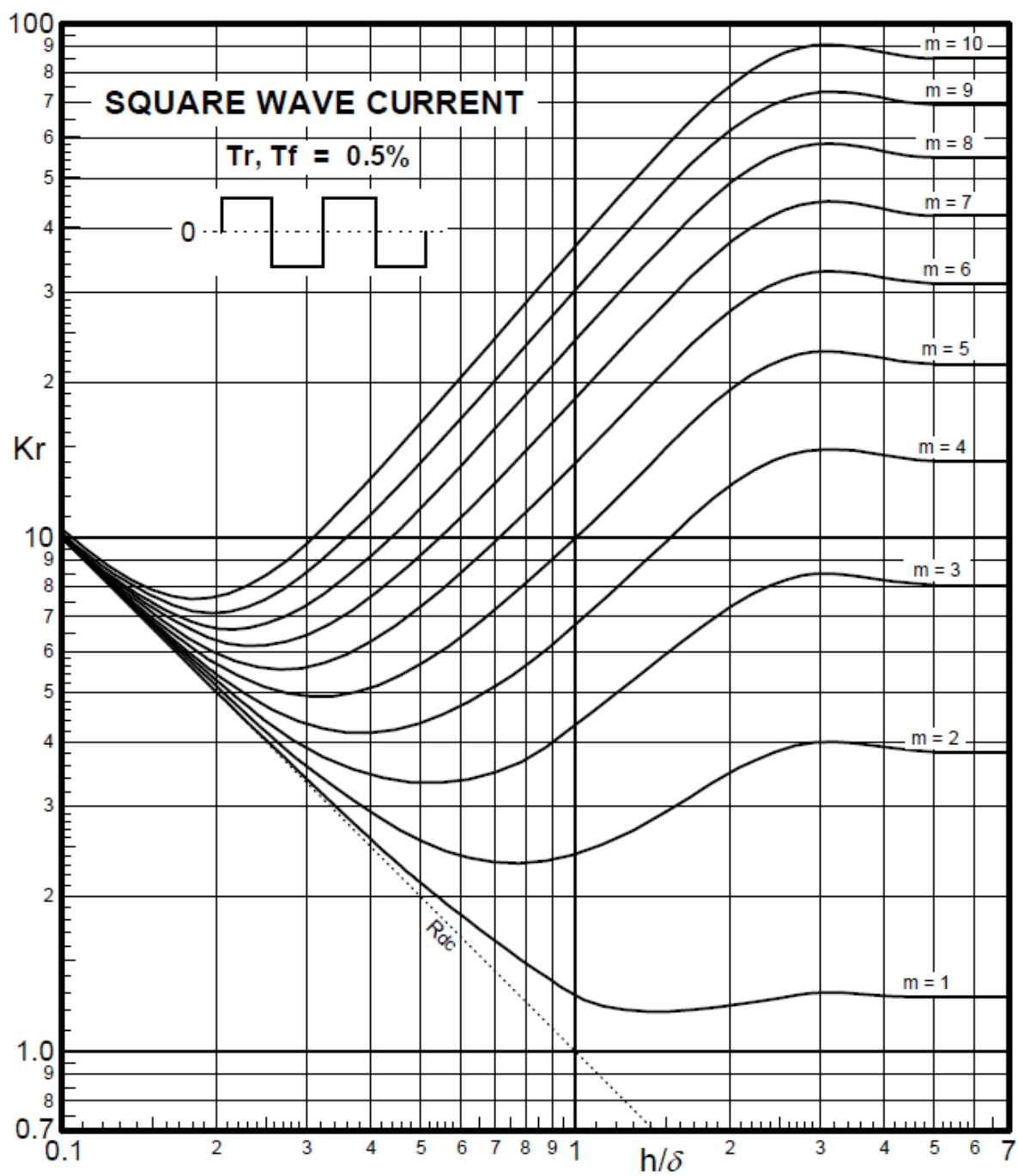


Figure 3-13 Loss Factor for square wave currents and different number of layers(Carsten, 1986)

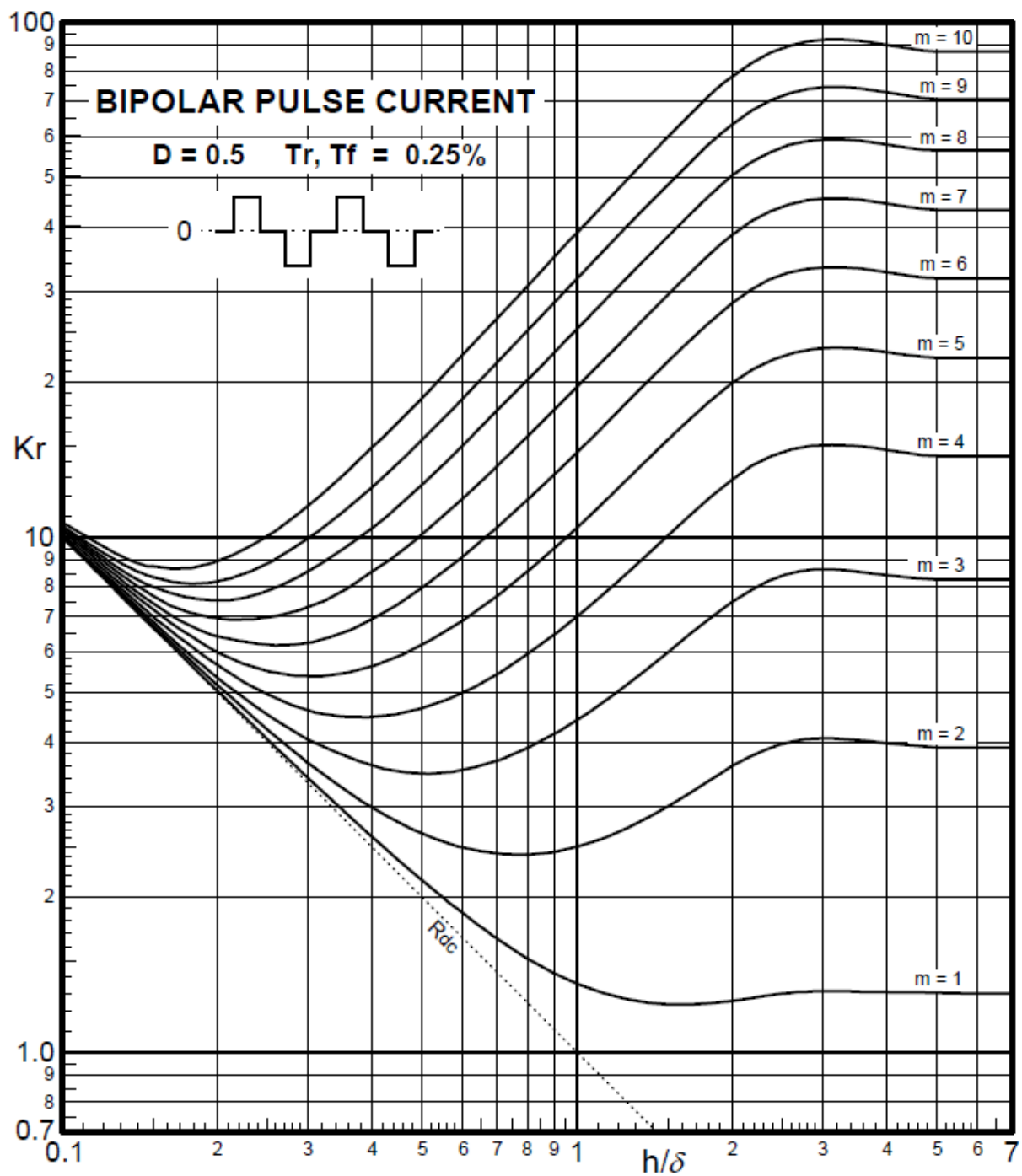


Figure 3-14 Loss Factor for Bi polar pulse currents and different number of layers(Carsten, 1986)

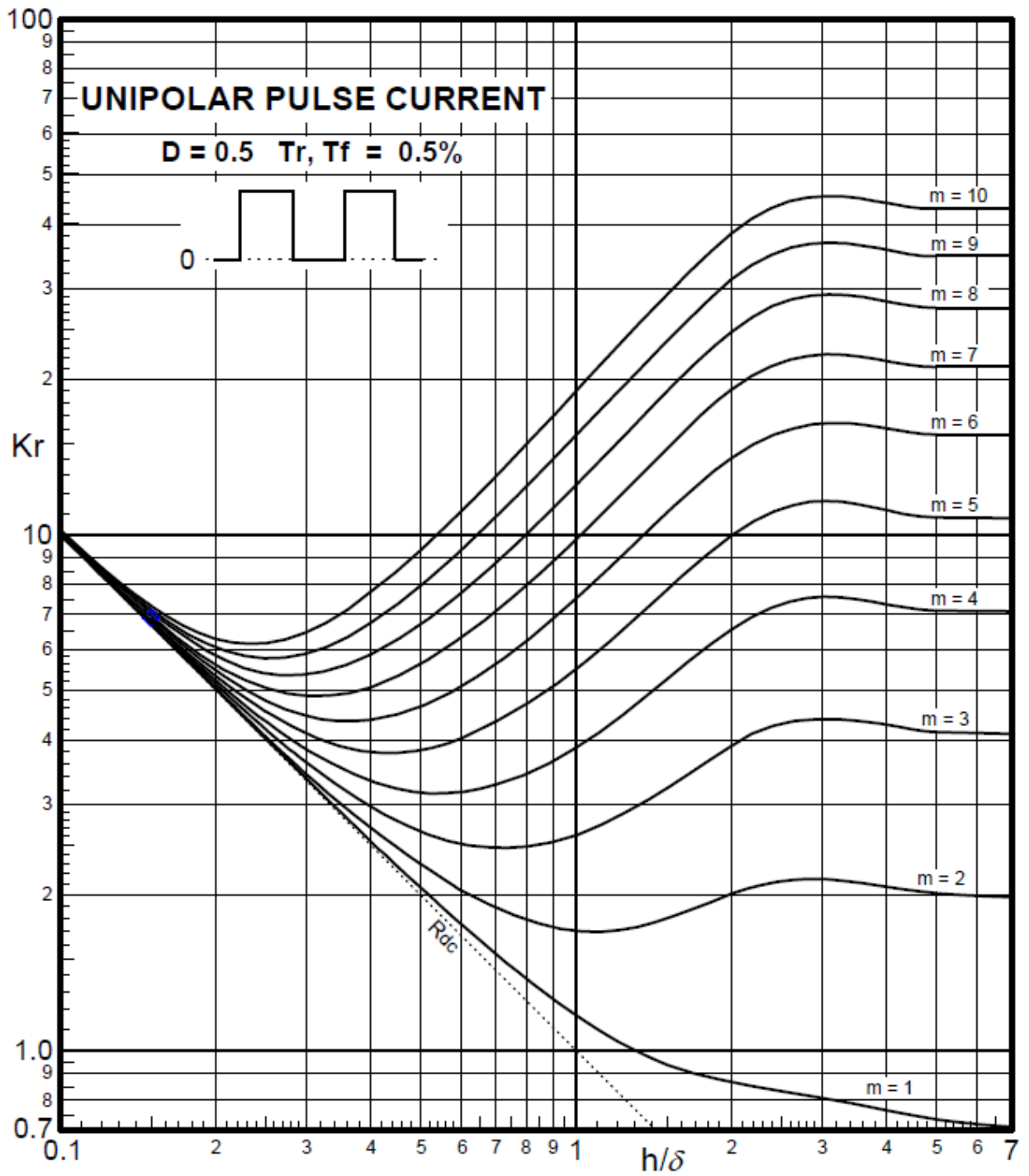


Figure 3-15 Loss Factor for U<sub>i</sub> polar pulse currents and different number of layers(Carsten, 1986)

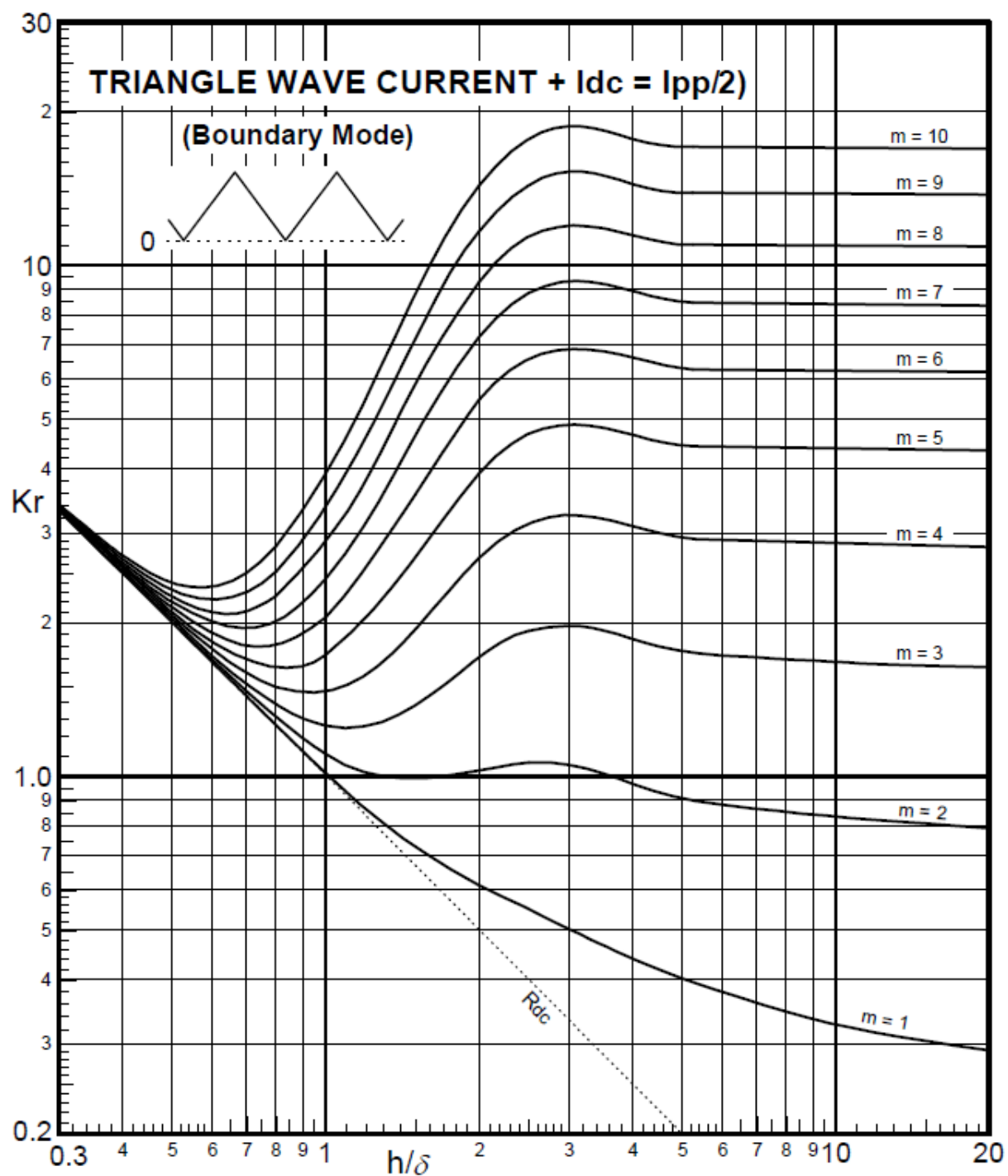


Figure 3-16 Loss Factor for triangular wave currents and different number of layers (Carsten, 1986)

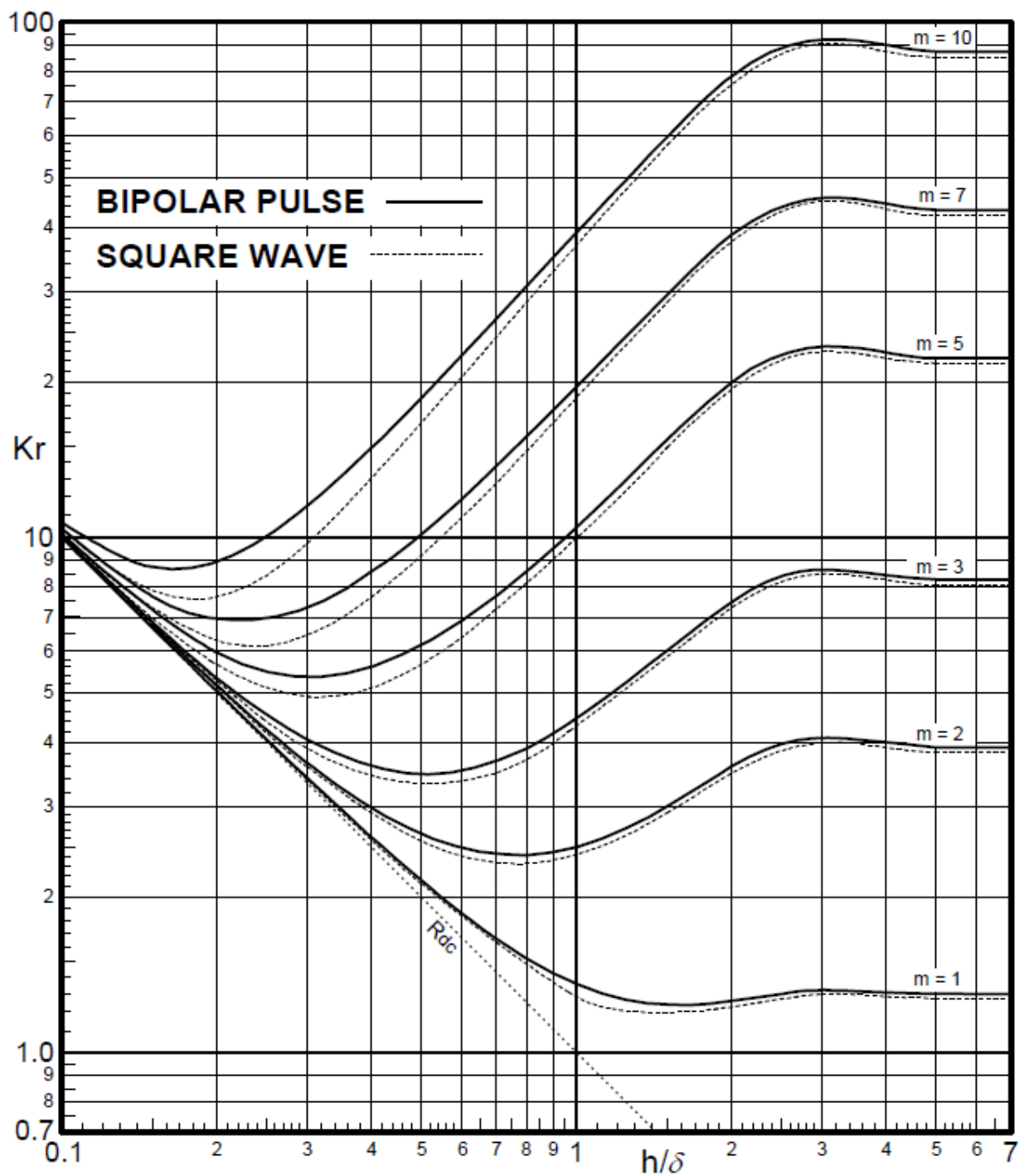


Figure 3-17 Loss Factor for bipolar and square wave currents and different number of layers(Carsten, 1986)

Renormalizing the Loss Factor to  $\frac{K_r}{m}$ , Plotted against the Total Winding Thickness  $mh/\delta$

The Normalized Parameters  $K_r$  and  $h$  were developed to find the effects of changing  $h$  on  $R_{ac}$ , with a fixed No. of Layers  $m$ , but for any number of turns,  $N$ .

The effect of changing the number of Layers  $m$  for a fixed  $N$  is found by plotting with Renormalized Parameters  $\frac{K_r}{m}$  and  $mh/\delta$ .

As an example; doubling the Layers  $m$  for the same turns  $n$  and layer  $h$  doubles the Winding Thickness (hence  $mh/\delta$ ), while the Winding Area is also doubled, halving  $R_{dc}$ , so  $\frac{K_r}{m}$  is used for the renormalized ac/dc Loss Factor(Carsten, 1986).

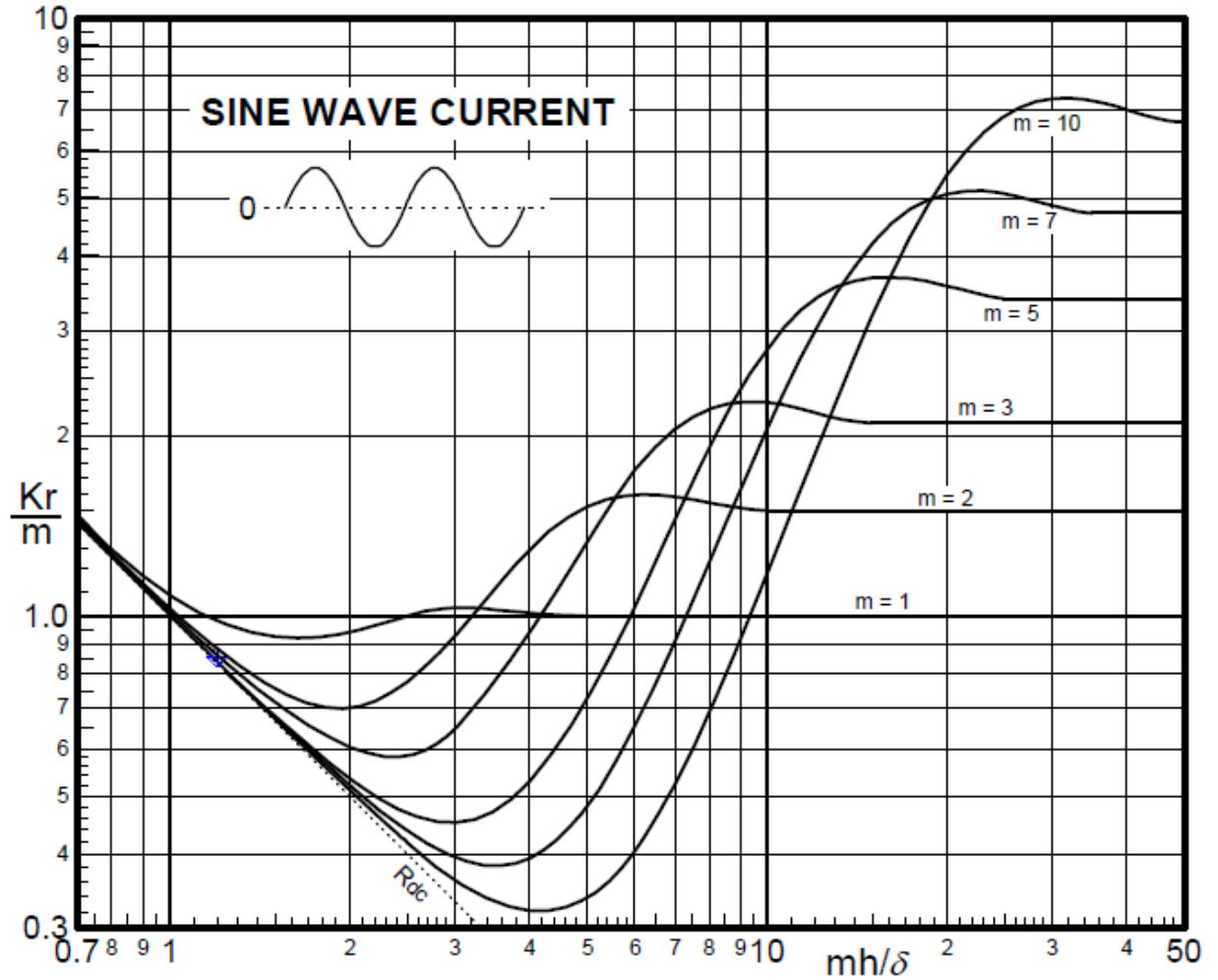


Figure 3-18 For sine wave currents(Carsten, 1986)

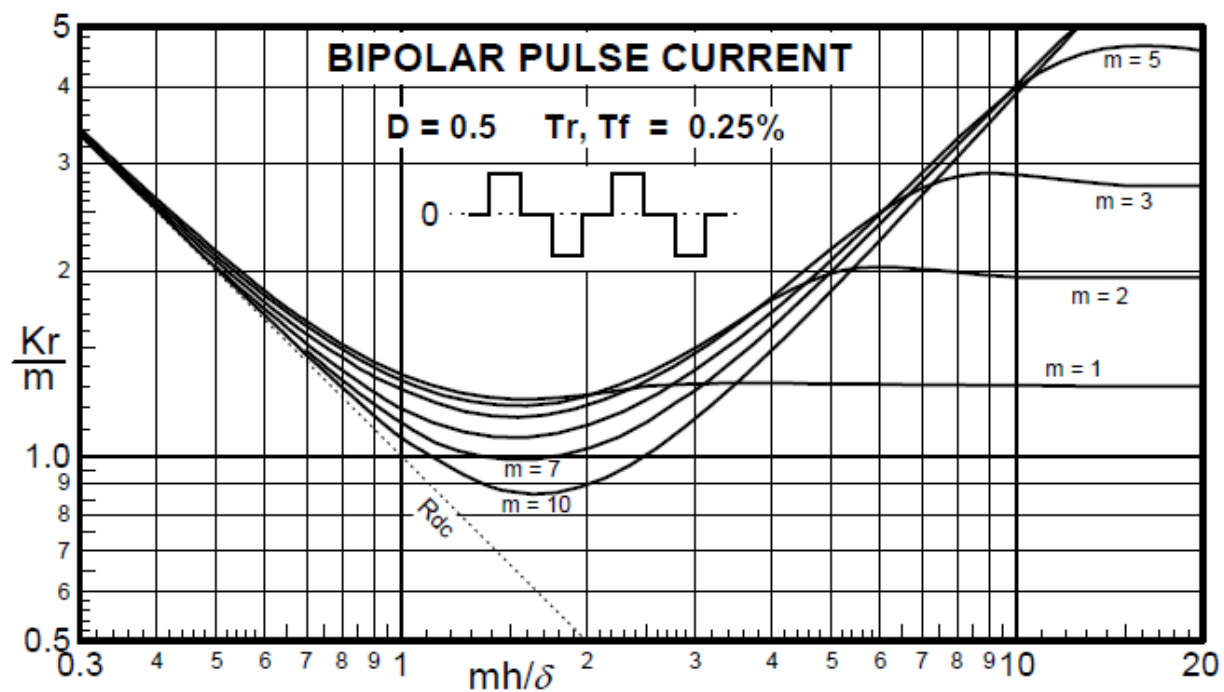


Figure 3-19 For bipolar pulse wave currents(Carsten, 1986)

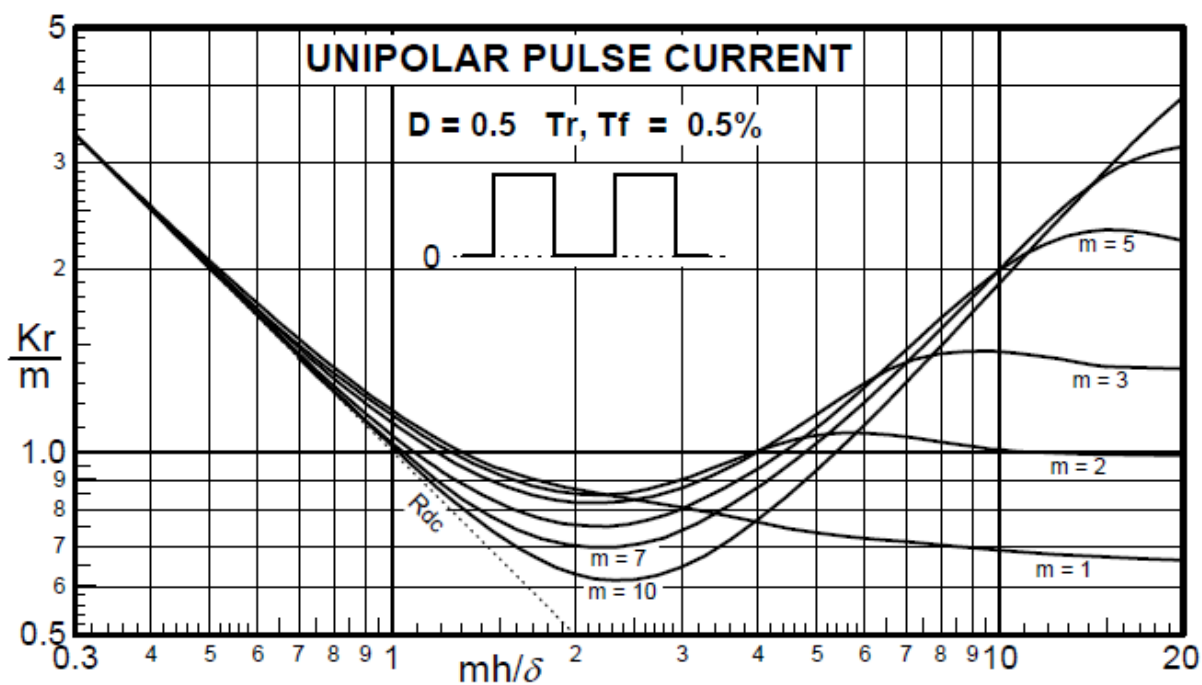


Figure 3-20 For unipolar pulse wave currents(Carsten, 1986)



### Round wires and “Litz” wires

In transformer applications specially in the case of high-power high frequency transformer applications skin and proximity effects can be considerable. Thus, to handle the power density of medium-frequency transformers a certain effective conductor area is necessary. However, this area can be too wide for the frequency of the waveform due to eddy current effects. The use of stranded insulated and twisted wires reduces these effects. If the wire is correctly twisted, each strand takes each of the places in the bundle; see figure 3.21 and therefore the effect between strands is reduced. Moreover, the reduced surface area of each strand reduces the penetration ratio for the same skin depth. Conductors made up of multiple individually insulated strands twisted together are known as “Litz” wires.

In “Litz” wire windings skin and proximity effects can be divided in strand and bundle-level effects(Sullivan, 1999) see figure 3-22. Bundle-level effects, related to currents circulating in paths involving multiple strands, are controlled by the correct construction of the “Litz” wire. Bundle-level proximity loss is controlled by simple twisting, however bundle-level skin effect requires more complex constructions(Sullivan, 1999, Villar, 2010). At strand level, related to individual strands, proximity effect dominates over skin effect in windings with high number of layers, and usually strand-level skin effects are negligible. Strand-level proximity losses can be further divided in internal and external losses. Internal proximity losses are related to the losses generated by the rest of the strands in the bundle, and external proximity losses express the losses generated from current in the rest of the bundles.

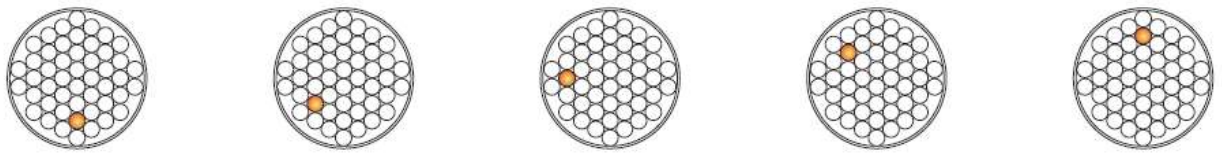


Figure 3-21 Representation of the position variation of a strand in a “Litz” bundle(Villar, 2010).

Usually, equal currents in all strands are assumed in order to calculate losses in “Litz” wire windings. This assumption is equivalent to assuming that the bundle level construction has been chosen properly to control bundle-level proximity and skin effects. Therefore, to calculate the total strand-level proximity-effect loss in a “Litz” winding, the whole winding is supposed to be composed of  $n_s$   $N$  turns, each one carrying an equal current  $I/n_s$ , where  $n_s$  is the number of strands,  $N$  the number of bundle-turns and finally  $I$  the current in a bundle.

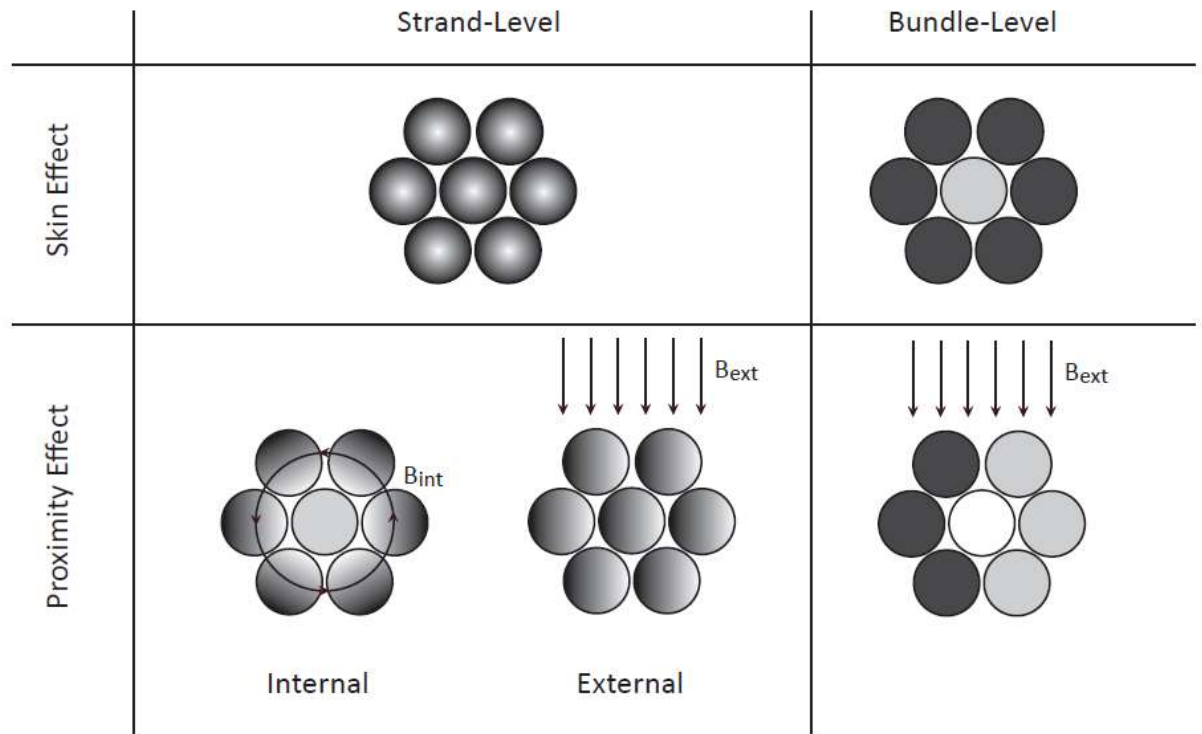
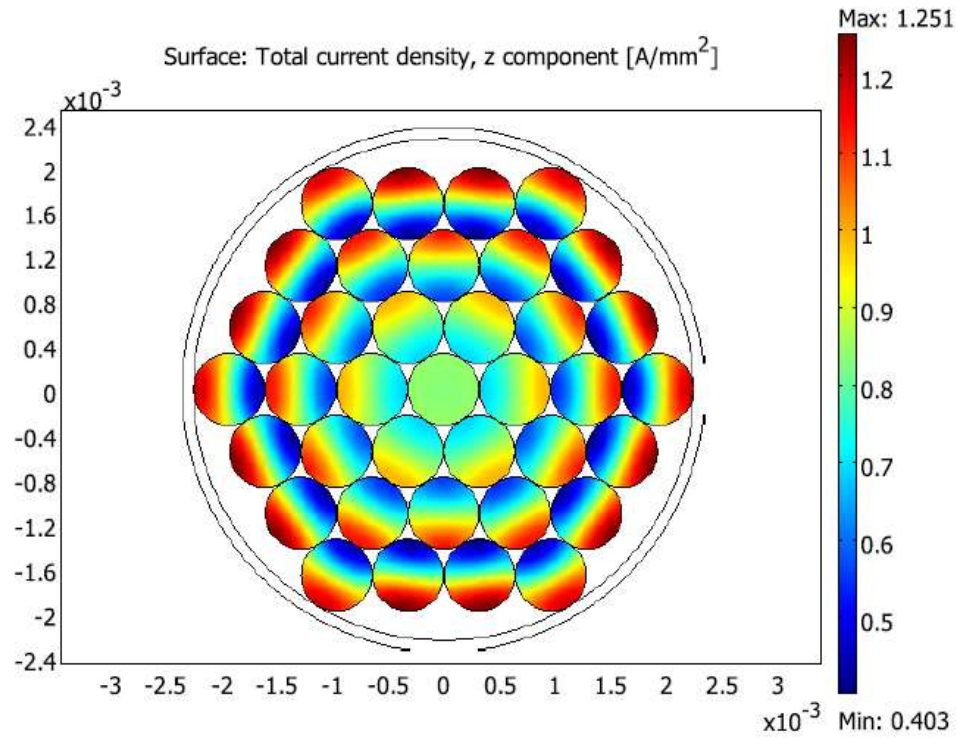


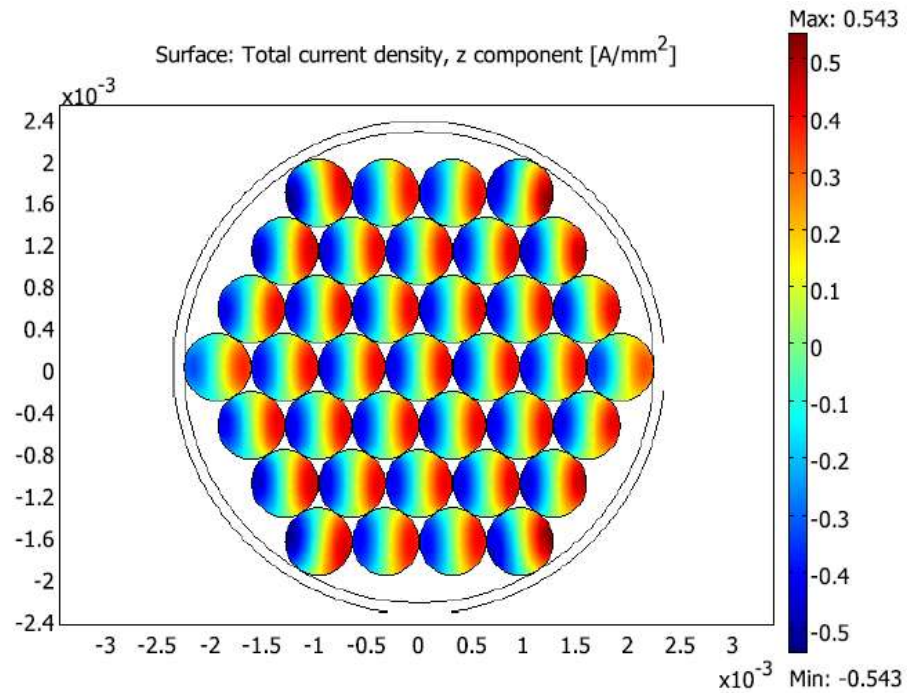
Figure 3-22 Type of eddy currents in Litz conductors. Illustration introduced in(Sullivan, 1999).

In figure 3-24a an isolated “Litz” wire is represented, in which each strand is carrying the same total current, the internal proximity effect is clearly the main eddy current effect and the strand-level skin effect is almost negligible. In figure 3-24b, in contrast, a single “Litz” wire is represented without a net current but within an external magnetic field, in order to illustrate the external proximity effect.

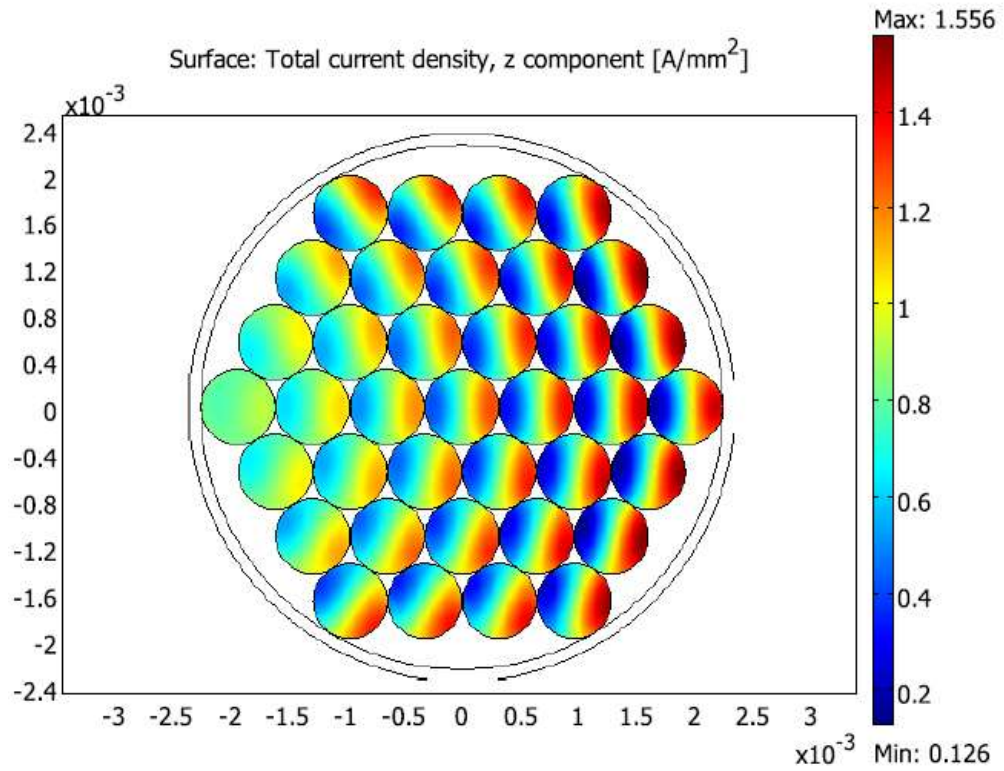
In figure 3-24c the same Litz bundle is carrying a net current within an external magnetic field, and both effects are illustrated.



(a) Internal  $I = 10$  A



(b) External  $H_{ext} \cong 1$  A/mm



(c) Both

Figure 3-23 Total current density in a single round “Litz” wire  $d_b = 4.5\text{mm}$ , with 37 strands of  $d_s = 0.64\text{mm}$  and  $f = 20\text{ kHz}$  (Villar, 2010)

Due to the orthogonality principle between proximity and skin effects, losses in Litz bundles can be calculated separately, an approach followed in several publications. Conduction losses in isolated Litz bundles, i.e. skin effect losses and internal proximity effect losses, were already determined in (Lammeraner and Štafl, 1966). In (Ferreira, 1992) the same approach is followed but instead of reducing the expression to low penetration ratios, the complete equation already developed in for single solid round conductors is used. And finally, in (Lotfi and Lee, 1993) the exact Bessel equations are used, according to (Lotfi and Lee, 1993) in order to improve accuracy in high-frequency applications (Villar, 2010).

Skin Effect Losses are determined from the one-dimensional solution developed for round conductors (Lammeraner and Štafl, 1966), reaching in the case of an isolated strand.

$$P_{skin} = R_{sdc} \frac{\gamma}{4} I_s^2 \tau_1(\gamma)$$

where  $I_s$  represents the current in a single strand and the DC resistance of the strand  $R_{sdc}$  is determined from.

$$R_{sdc} = \frac{l_s}{\pi \sigma r_s^2} \quad 3 - 46$$

where  $l_s$  is the total length and  $r_s$  the radius of a single strand. Therefore, the strand-level skin effect losses in a “Litz” bundle will be

$$P_{skin} = R_{dc} \frac{\gamma}{4} I^2 \tau_1(\gamma) = \frac{R_{sdc} \gamma}{n_s} \frac{\gamma}{4} I^2 \tau_1(\gamma) \quad 3 - 47$$

because all the strands within a “Litz” bundle are in parallel.

The difference between previously mentioned publications lies in the term  $1(\gamma)$ . On the one hand, the expression introduced in (Ferreira, 1992, Villar, 2010) uses the equation already introduced in, where

$$\tau_1(\gamma) = \frac{ber(\gamma)bei'(\gamma) - bei(\gamma)ber'(\gamma)}{ber'(\gamma)^2 + beri'(\gamma)^2} \quad 3 - 48$$

On the other hand and considering the aims of the utilization of Litz wires, (Lammeraner and Štafl, 1966) reduces the expression to low penetration ratios reaching.

$$\tau_1(\gamma) = \frac{2}{\gamma} + \frac{\gamma^3}{96} \quad 3 - 49$$

And finally, in (Lotfi and Lee, 1993, Villar, 2010) the exact solution for solid round conductors is used with modified Bessel functions of the first kind of zero and first order,  $I_0$  and  $I_1$  respectively.

$$\tau_1(\gamma) = \frac{1}{\sqrt{2}} \Re \left[ (1 + j) \frac{I_0(\alpha r_s)}{I_1(\alpha r_s)} \right] \quad 3 - 50$$

A comparison example is illustrated in figure 3-24, where the three expressions are evaluated along with a finite element simulation of a single isolated strand  $d_s = 0.2\text{mm}$ . For low penetration ratios ( $\gamma < 2$ ) all of the expressions are accurate. However, for large penetration

ratios ( $> 2$ ), the error obtained with the reduced expression increases with the increase of the penetration ratio.

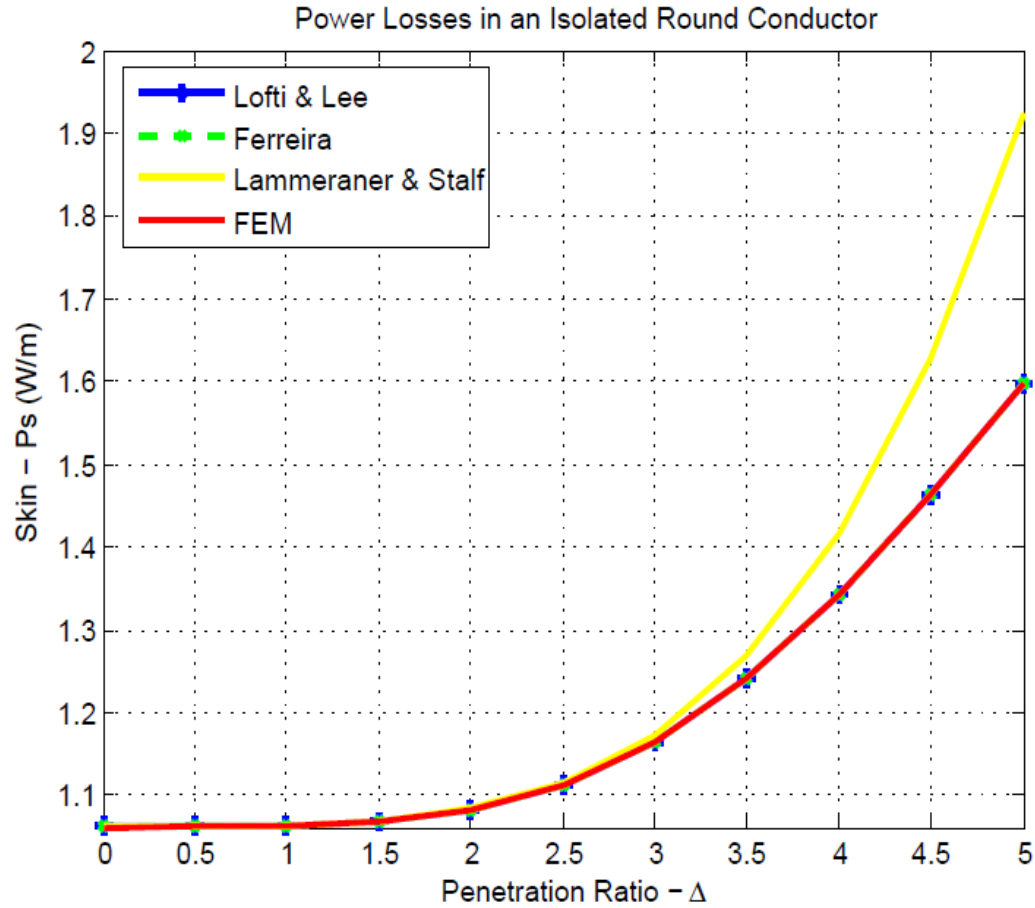


Figure 3-24 Comparison of different expressions for the determination of skin effect losses in an isolated round conductor with  $d_s = 0.2\text{mm}$  (Villar, 2010)

Internal Proximity Effect Losses are also evaluated in previously mentioned publications, and once more they follow the same approach. Internal proximity effects are determined considering the field generated by the strands of the bundle at each radial position  $H_0(r)$ , and applying this field as an external transverse magnetic field to each of the strands (according to their geometrical position as shown in figure 3-24. The general power loss expression for single round conductors subjected to an external transverse magnetic field is (Lammeraner and Štafl, 1966, Villar, 2010),

$$P_{s_{internal}} = -\frac{2\pi\gamma}{\sigma} H_0^2(r) \tau_2(\gamma)$$

3 - 51

The field generated by the strands in the bundle at each radial position can be obtained by modifying the expression for solid round wires

$$H_0(r) = \frac{I}{2\pi r n_s} \left(\frac{r}{r_s}\right)^2 pf$$

3 - 52

where,

$$pf = n_s \left(\frac{r_s}{r_b}\right)^2$$

3 - 53

is the packing factor.

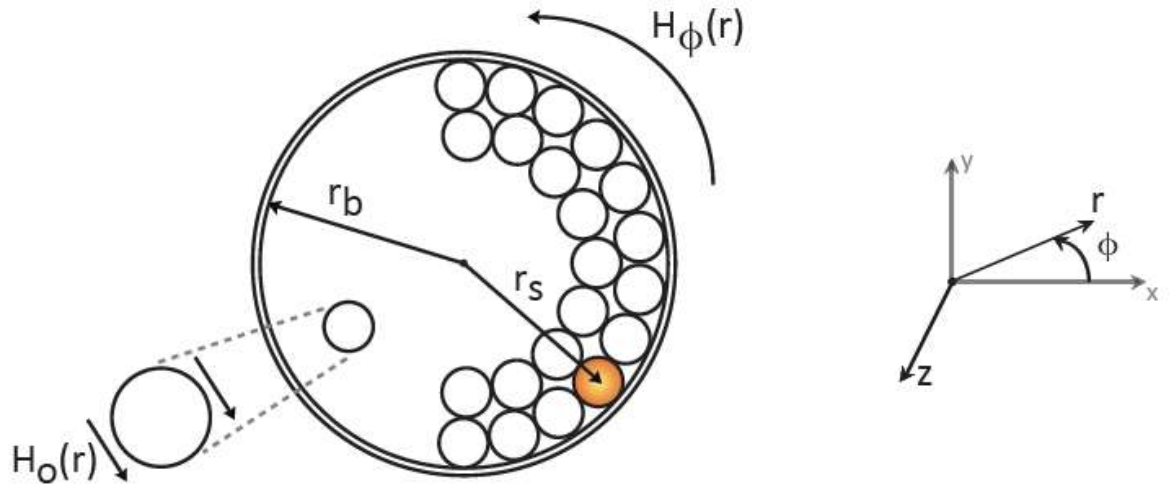


Figure 3-25 “Litz” bundle, the radial position of each strand is considered to apply the radial dependent internal magnetic field(Villar, 2010)

Rather than discrete summation of losses in each strand, the integration of internal losses per unit area results in

$$P_{s_{internal}} = -\frac{2\pi\gamma}{\sigma} \frac{n_s I^2 l_s}{8\pi^2 r_b^2} \tau_2(\gamma)$$

3 - 3-54

Once more, the difference between previously mentioned developments lies in the term  $2()$ . On the one hand, the expression introduced in (Ferreira, 1992, Villar, 2010) uses the equation already introduced in (3-44), where

$$\tau_2 = \frac{ber_2(\gamma)ber'(\gamma) + bei_2(\gamma)bei'(\gamma)}{ber'(\gamma)^2 + beri'(\gamma)^2}$$

3 - 55

On the other hand, (Lammeraner and Štafl, 1966) reduces the expression for low penetration ratios reaching,

$$\tau_2(\gamma) = -\frac{\gamma^3}{16}$$

3 - 56

and finally, in (Lotfi and Lee, 1993) the modified Bessel functions of the first kind of zero and first order are used.

$$\tau_2(\gamma) = \frac{1}{\sqrt{2}} \left[ \frac{\Re(1-j)I_0(\alpha r_s)I_1^*(\alpha r_s)}{|I_0(\alpha r_s)|^2} \right]$$

3 - 57



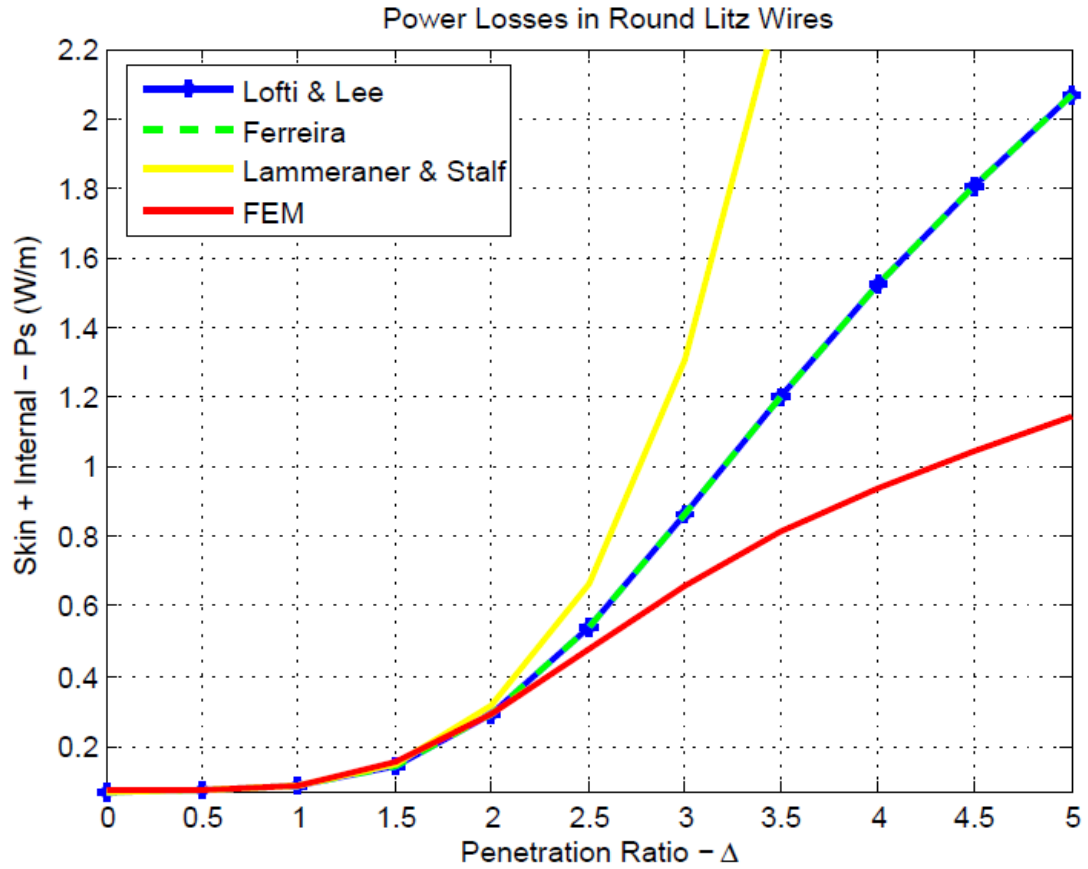
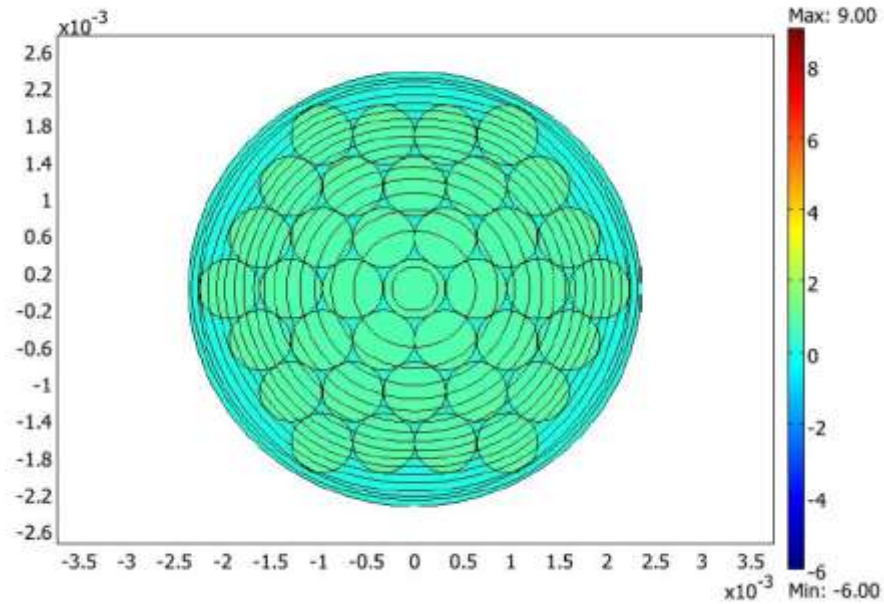


Figure 3-26 Comparison of different expressions for the determination of internal proximity losses in a single isolated “Litz” bundle with  $d_b = 4.5\text{mm}$  and 37 strands of  $d_s = 0.64\text{mm}$  (Villar, 2010).

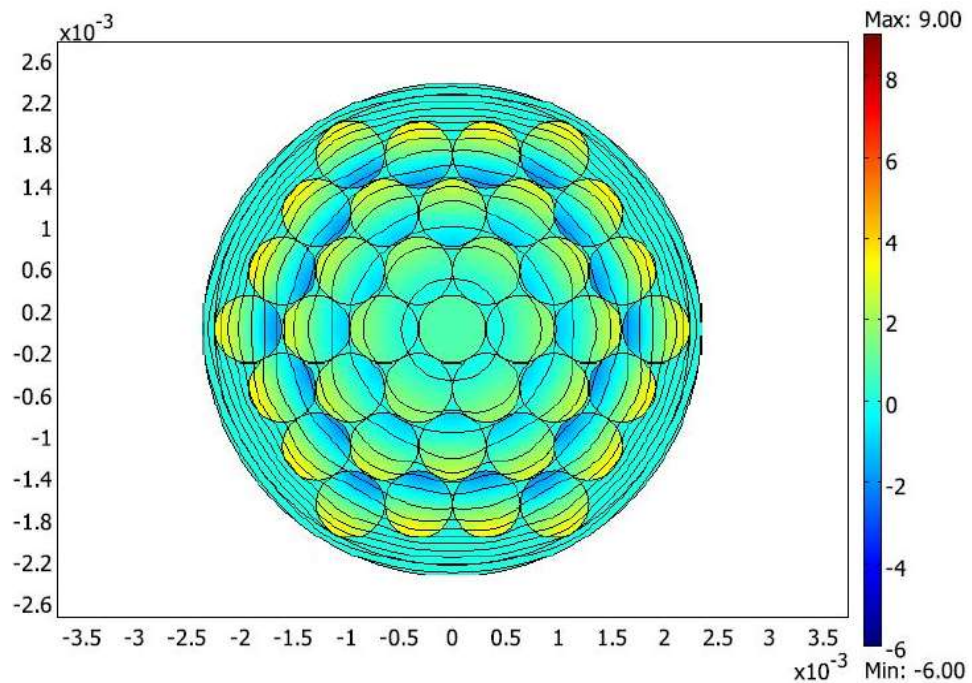
A comparison example is illustrated in figure 3-27, along with a finite element simulation of a single isolated “Litz” bundle with  $d_b = 4.5\text{mm}$  and 37 strands of  $d_s = 0.64\text{mm}$ . For low penetration ratios ( $< 2$ ) all the expressions are precise enough. However, for large penetration ratios even the most detailed of the expressions overestimates the losses. It should be noticed that both the strand level skin effect and the internal proximity effect are evaluated.

In the case of internal proximity effect losses, the simplest of the expressions is accurate enough, large penetration ratio errors are due to the non-circular nature of the field see figure 3-28 to figure 3-30. Therefore, the accuracy in the determination of the losses in an isolated strand does not improve the global prediction, due to the fact that the external magnetic field in each of the strands is no longer one dimensional.



(a)  $\Delta = 1$

Figure 3-27 Total current density and magnetic field lines in a single isolated “Litz” bundle  $d_b = 4.5\text{mm}$ , with 37 strands of  $d_s = 0.64\text{mm}$  for penetration ratio  $\Delta = 1$  (Villar, 2010)



(b)  $\Delta = 2.5$

Figure 3-28 Total current density and magnetic field lines in a single isolated “Litz” bundle  $d_b = 4.5\text{mm}$ , with 37 strands of  $d_s = 0.64\text{mm}$  for penetration ratio  $\Delta = 2.5$  (Villar, 2010)

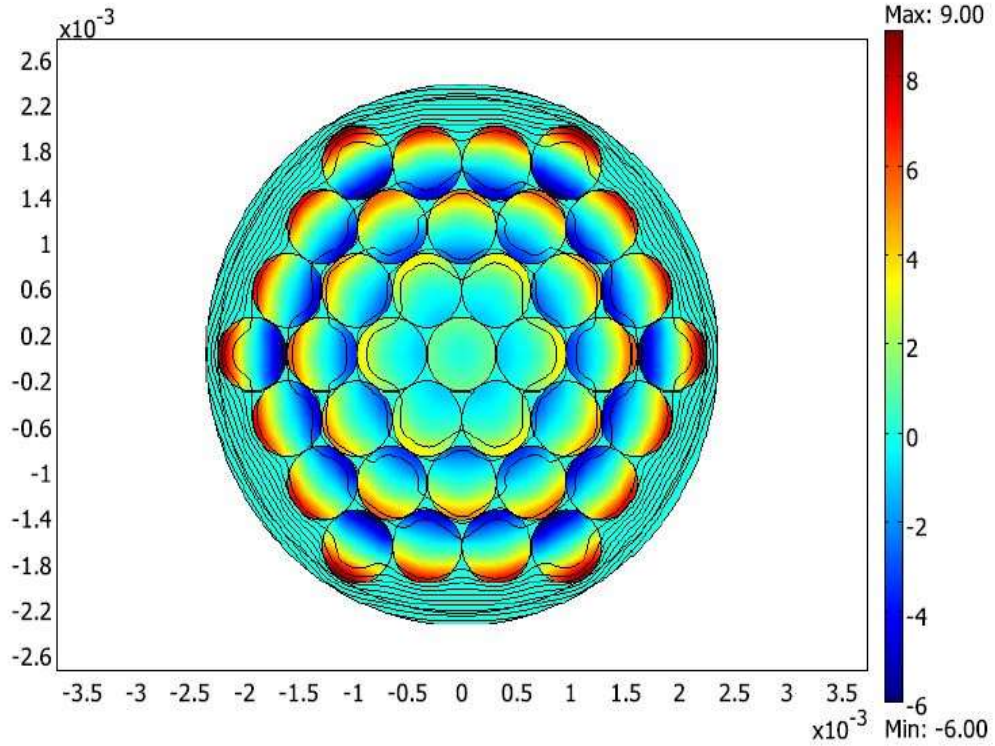

 (c)  $\Delta = 5$ 

Figure 3-29 Total current density and magnetic field lines in a single isolated “Litz” bundle  $d_b = 4.5\text{mm}$ , with 37 strands of  $d_s = 0.64\text{mm}$  for penetration ratio  $\Delta=5$ (Villar, 2010)

External Proximity Effect Losses are determined, from the exact solution of an isolated round conductor within an external field (Ferreira, 1992). Although among previously mentioned publications, external proximity effect losses in Litz bundles are only evaluated in(Ferreira, 1992, Villar, 2010), an extrapolation of the other methods can also be done using each of the expressions for  $2(\gamma)$ . Therefore, the external proximity effect losses in a Litz bundle within an external magnetic field are

$$P_{external} = -\frac{2\pi\gamma}{\sigma} n_s H_e^2 \tau_2(\gamma)$$

3 - 58

A comparison example is illustrated in figure 3-65, where the three expressions are evaluated along with a finite element simulation of a single open circuited Litz bundle  $d_b = 4.5\text{mm}$ , with 37 strands of  $d_s = 0.64\text{mm}$ , within an external magnetic field  $H_e = 1\text{A/mm}$ . For low penetration ratios ( $< 2$ ) all the expressions are precise enough. However, for large penetration ratios, like in the case of skin effect losses, the reduced expression overestimates the losses.

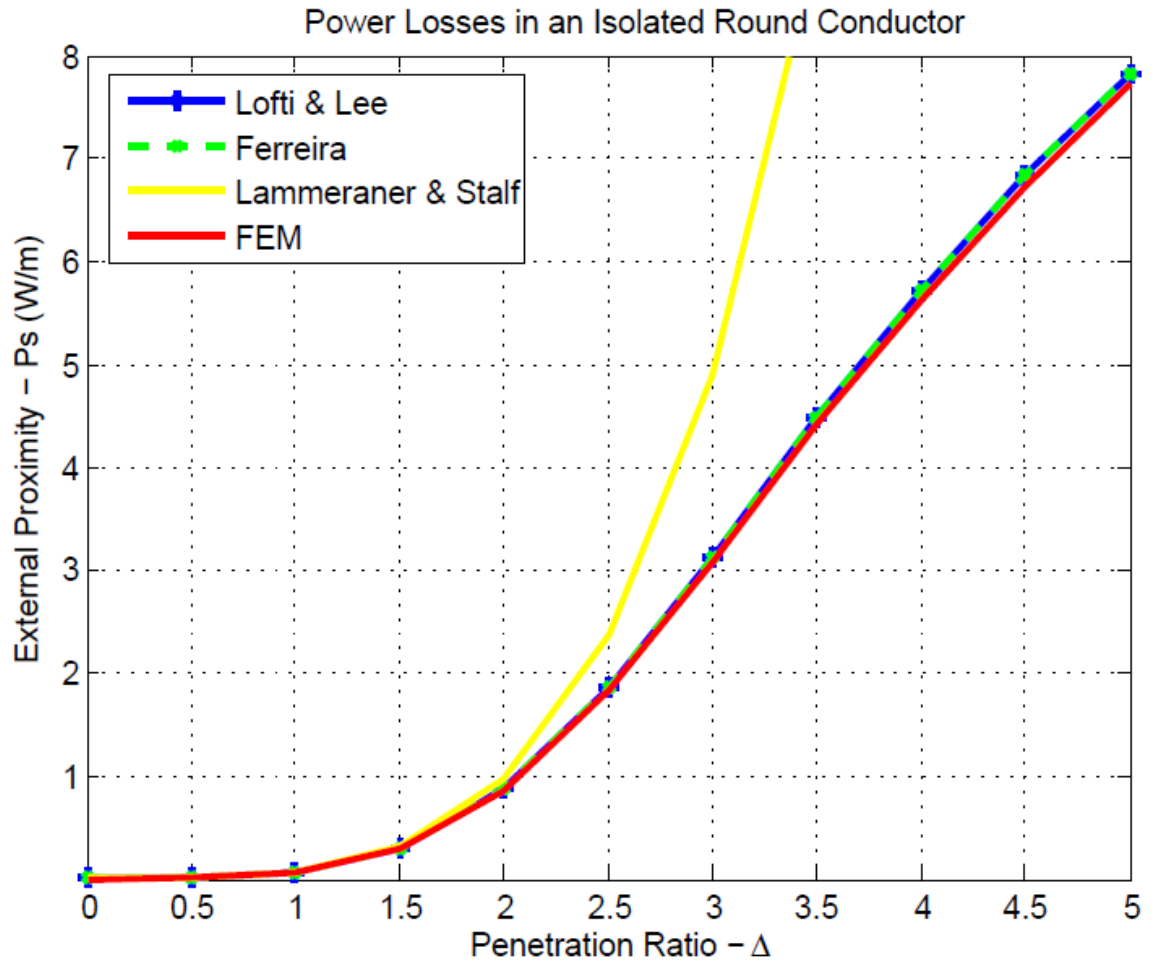
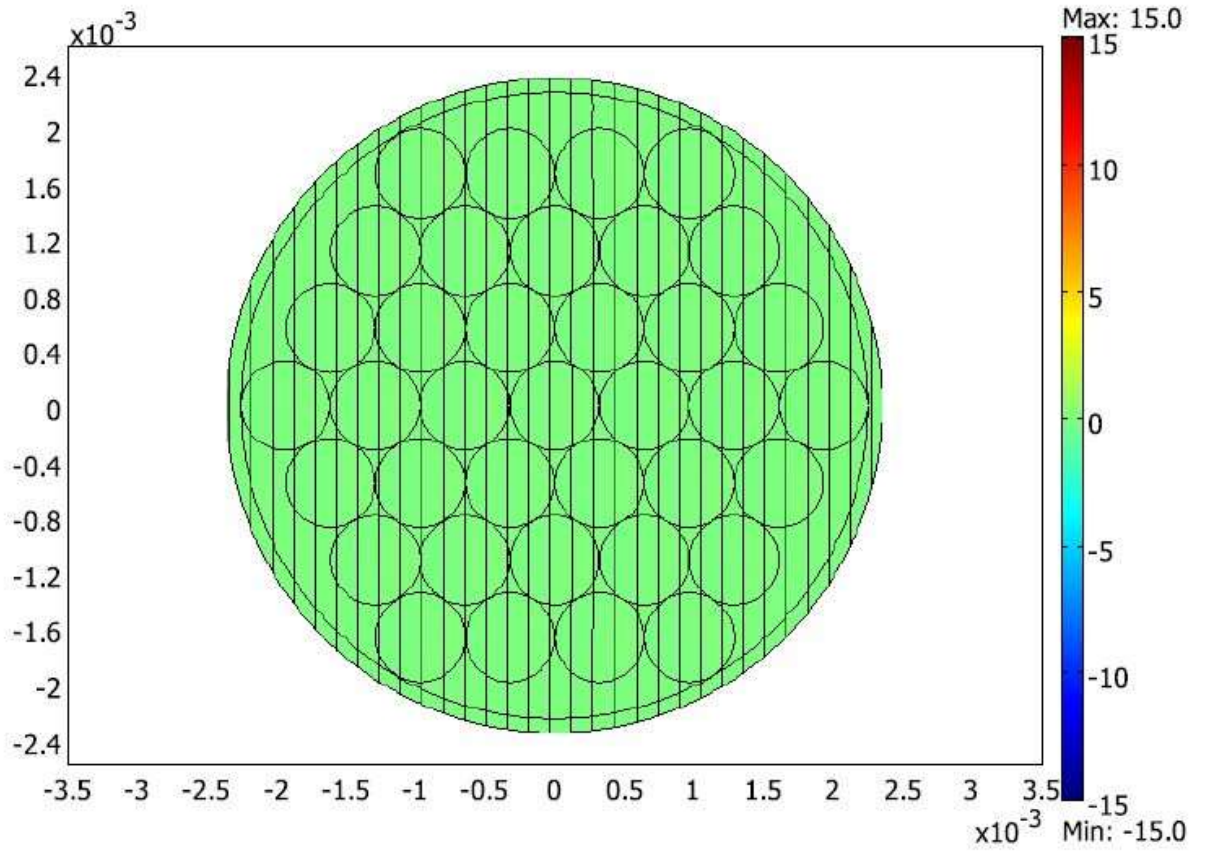


Figure 3-30 Comparison of different expressions for the determination of external proximity losses in an open circuited Litz bundle  $d_b = 4.5\text{mm}$ , with 37 strands of  $d_s = 0.64\text{mm}$ , within an external magnetic field  $H_e = 1\text{ A/mm}$  for different penetration ratios (Villar, 2010).

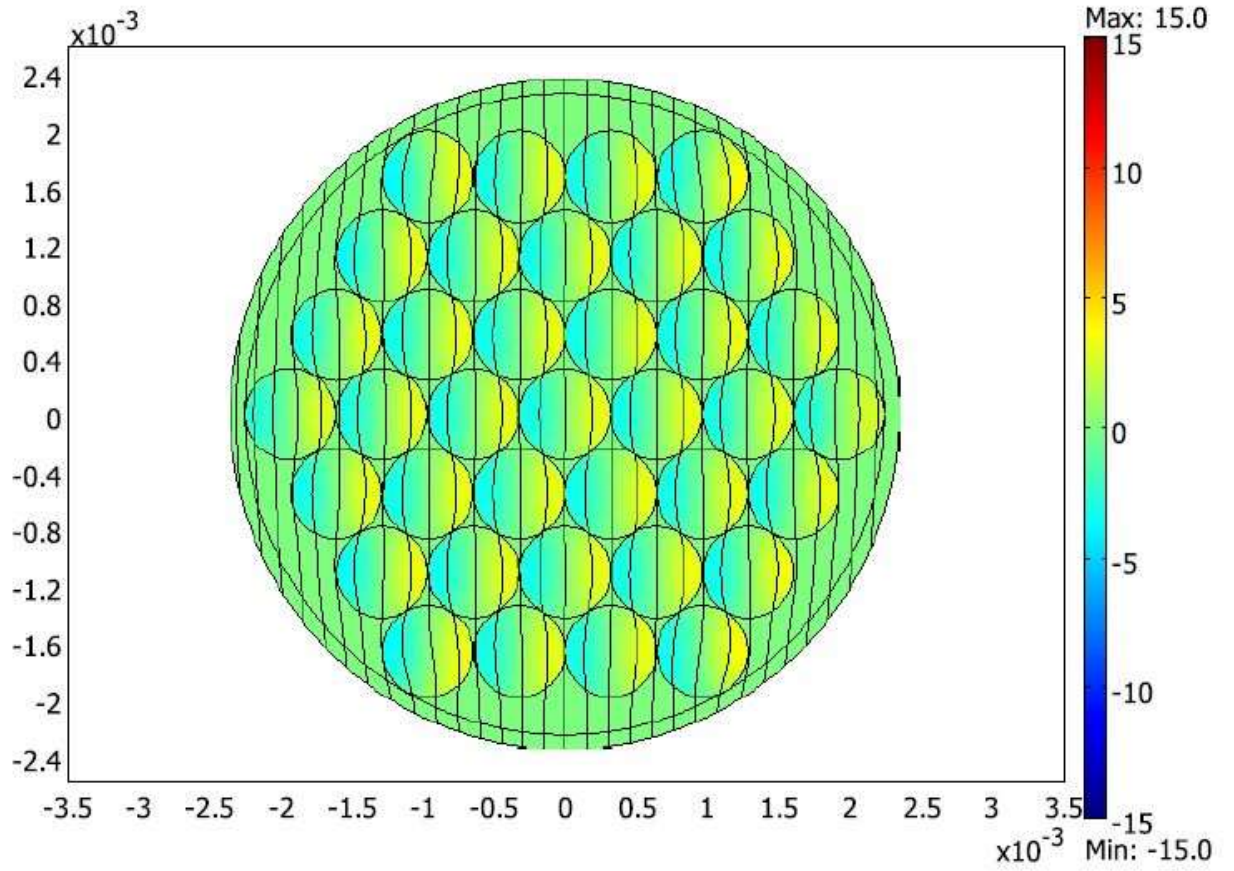
In figure 3-32 to figure 3-34 the difference between several penetration ratios is illustrated for an open circuited Litz bundle within an external magnetic field  $H_e = 1\text{ A/mm}$ .



(a)  $\Delta = 1$

Figure 3-31 Total current density and magnetic field lines in an open circuited Litz bundle  $d_b = 4.5\text{mm}$ , with 37 strands of  $d_s = 0.64\text{mm}$ , within an external magnetic field  $H_e = 1\text{A/mm}$  for penetration ratio  $\Delta = 1$  (Villar, 2010)





(b)  $\Delta = 2.5$

Figure 3-32 Total current density and magnetic field lines in an open circuited Litz bundle  $d_b = 4.5\text{mm}$ , with 37 strands of  $d_s = 0.64\text{mm}$ , within an external magnetic field  $H_e = 1\text{A/mm}$  for penetration ratio  $\Delta$  (Villar, 2010)

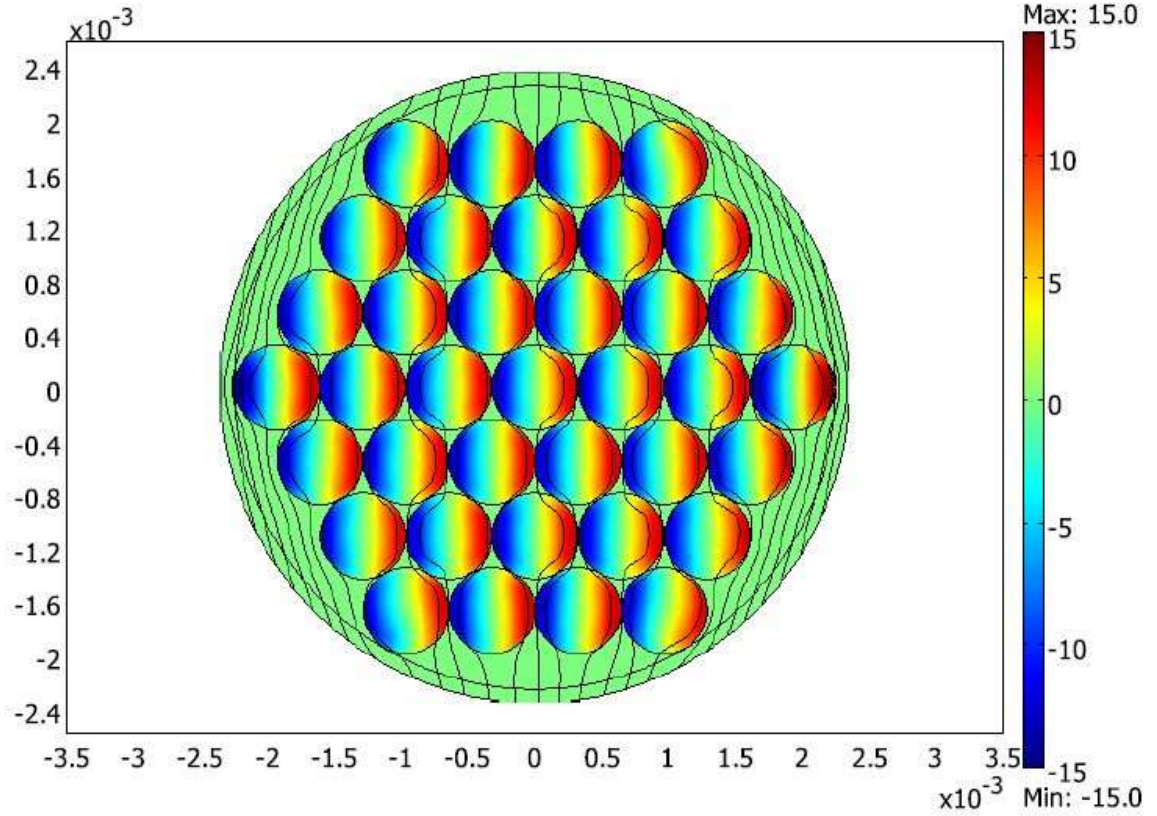

 (c)  $\Delta = 5$ 

Figure 3-33 Total current density and magnetic field lines in an open circuited Litz bundle  $db = 4.5\text{mm}$ , with 37 strands of  $ds = 0.64\text{mm}$ , within an external magnetic field  $H_e = 1\text{A/mm}$  for penetration ratio  $\Delta = 5$  (Villar, 2010)

Although the analysis carried out for external magnetic fields is accurate, the difficulty for its use lies in the fact that first the field within the transformer window has to be evaluated, and then applied in this last expression as an external magnetic field. This case is analyzed in various previous publications, for instance (Bartoli et al., 1996) and (Tourkhani and Viarouge, 2001). The profile of the magnetic field within the transformer window is the same as the one introduced in figure. 3-33, which increases linearly in each layer and remains constant within the inter-layer space. In the former, (Bartoli et al., 1996), the development carried out in (Ferreira, 1992, Villar, 2010) is taken as a reference, and , and two porosity factors are applied, like in the correction proposed for round conductors .

$$P_w = \frac{I^2}{2} R_{dc} \frac{\gamma}{2} \left[ \frac{1}{n_s} \tau_1(\gamma) - 2\pi \left( \frac{4(m^2 - 1)}{3} + 1 \right) n_s \left( n_1^2 + n_2^2 \frac{Pf}{2\pi n_s} \right) \tau_2(\gamma) \right]$$

3 - 3-59

with  $\tau_1$  being the external porosity factor and  $\tau_1$  the internal porosity factor.

$$\eta_1 = \frac{d_s}{t_b} \sqrt{\frac{\pi}{4}} \quad 3 - 60$$

and

$$\eta_2 = \frac{d_s}{t_s} \sqrt{\frac{\pi}{4}} \quad 3 - 61$$

where  $t_b$  is the distance between the centers of two adjacent “Litz” bundles and  $t_s$  is the distance between the centers of two adjacent strands.  $R_{dc}$  refers to the DC resistance of the whole winding, and  $m$  represents the number of layers in the winding.

$$R_{dc} = \frac{Nl_s}{n_s \pi \sigma r_s^2} \quad 3 - 62$$

In the latter, (Tourkhani and Viarouge, 2001, Villar, 2010), like in the previous case, Kelvin functions are used to determine the skin and proximity effect factors,  $1(\gamma)$  and  $2(\gamma)$  respectively. However, in this case, depending of the geometrical position of the “Litz” bundle, the external field is determined in each of the strands and all the losses in all the bundles are added reaching the final expression for the losses in the whole winding.

$$P_w = \frac{I^2}{2} R_{dc} \frac{\gamma}{2} \left[ \tau_1(\gamma) - \frac{\pi^2 n_s P f}{24} \left( 16m^2 - 1 + \frac{24}{\pi^2} \right) \tau_2(\gamma) \right] \quad 3 - 63$$



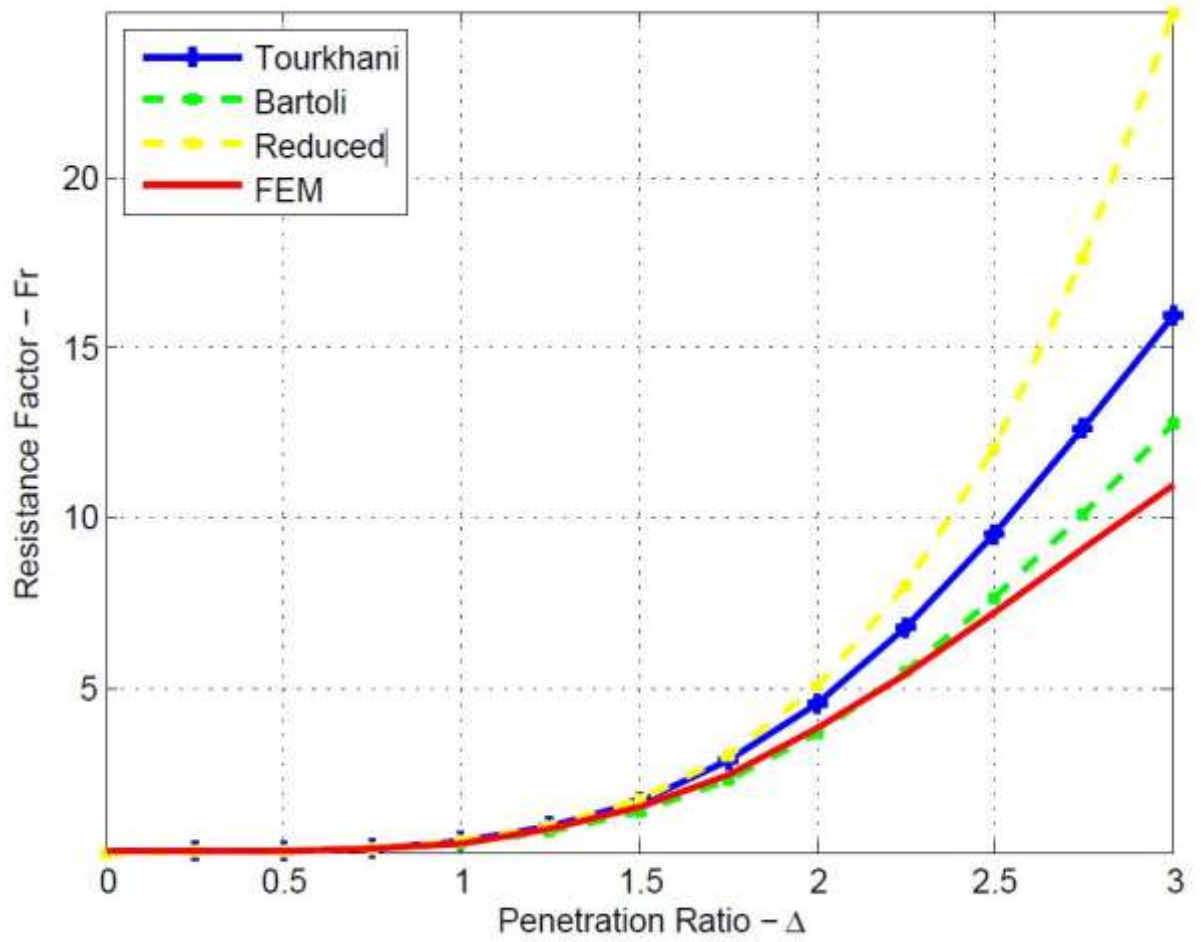
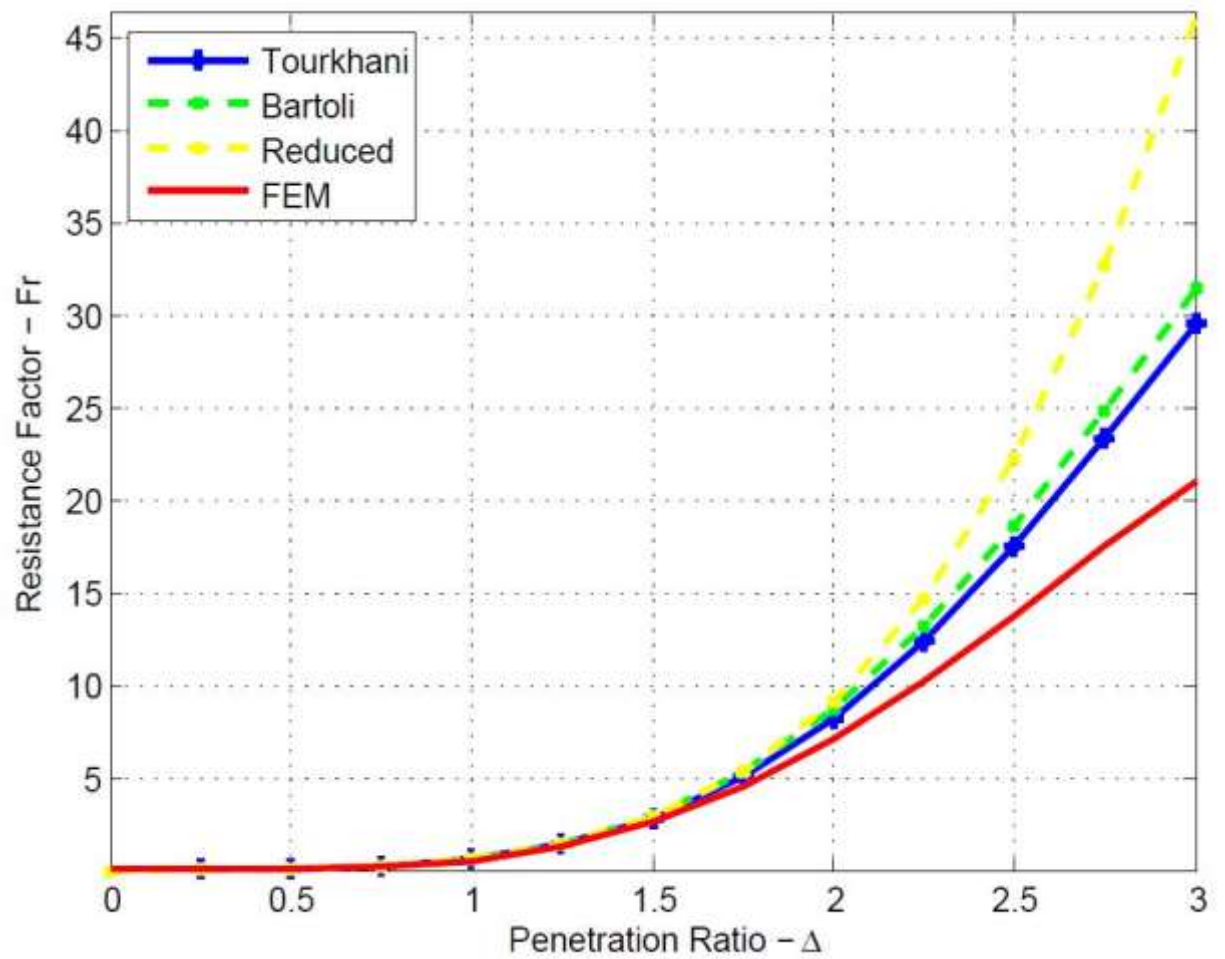
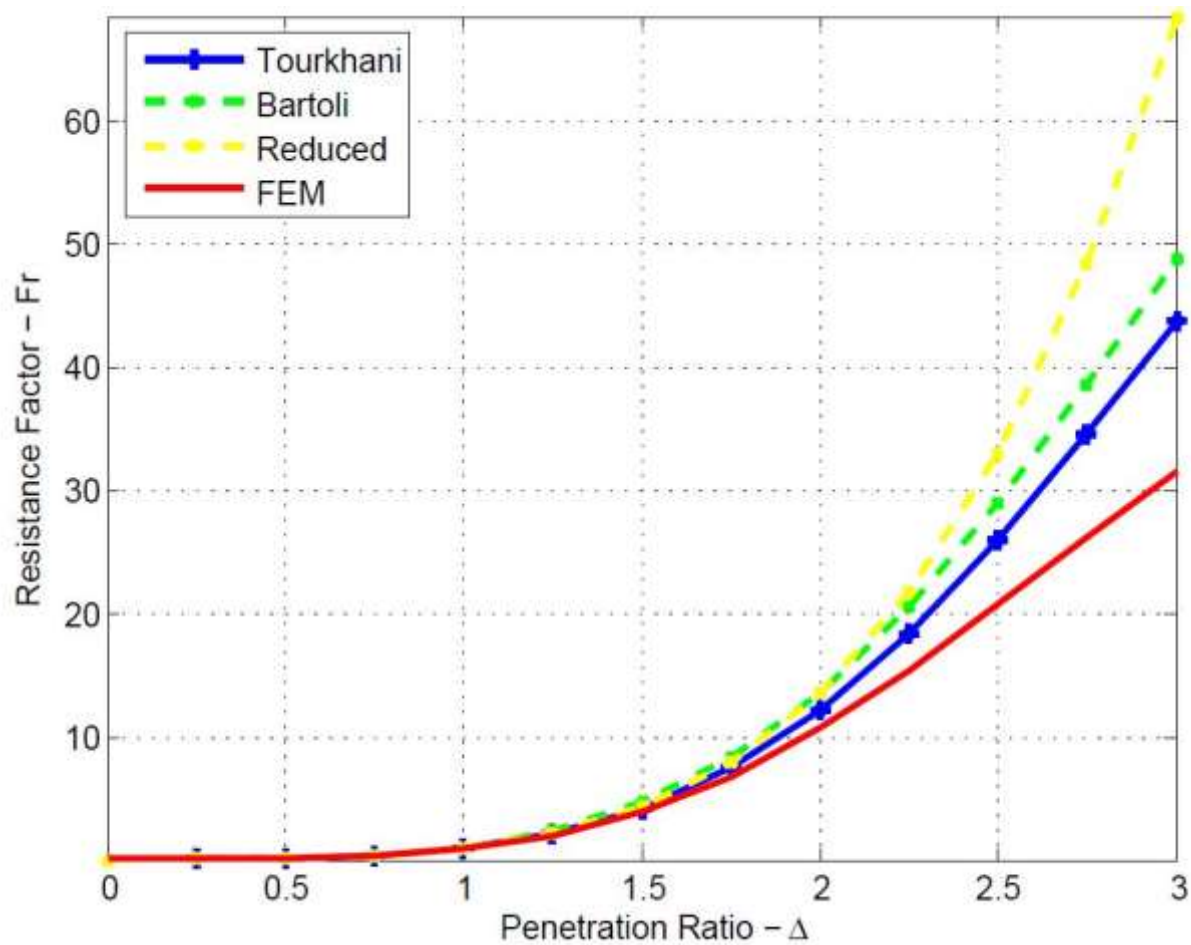

 (a)  $m = 1$ 

Figure 3-34 Comparison of different expressions for the determination of total Litz wire winding losses for different number of layers. Five Litz bundles per layer  $db = 0.54\text{mm}$ , with 37 strands of  $ds = 0.2\text{mm}$ .  $m=1$ (Villar, 2010)



(b)  $m = 2$

Figure 3-35 Comparison of different expressions for the determination of total Litz wire winding losses for different number of layers. Five Litz bundles per layer  $db = 0.54\text{mm}$ , with 37 strands of  $ds = 0.2\text{mm}$ .  $m=2$ (Villar, 2010)



(c)  $m = 3$

Figure 3-36 Comparison of different expressions for the determination of total Litz wire winding losses for different number of layers. Five Litz bundles per layer  $d_b = 0.54\text{mm}$ , with 37 strands of  $d_s = 0.2\text{mm}$ .  $m=3$ (Villar, 2010)

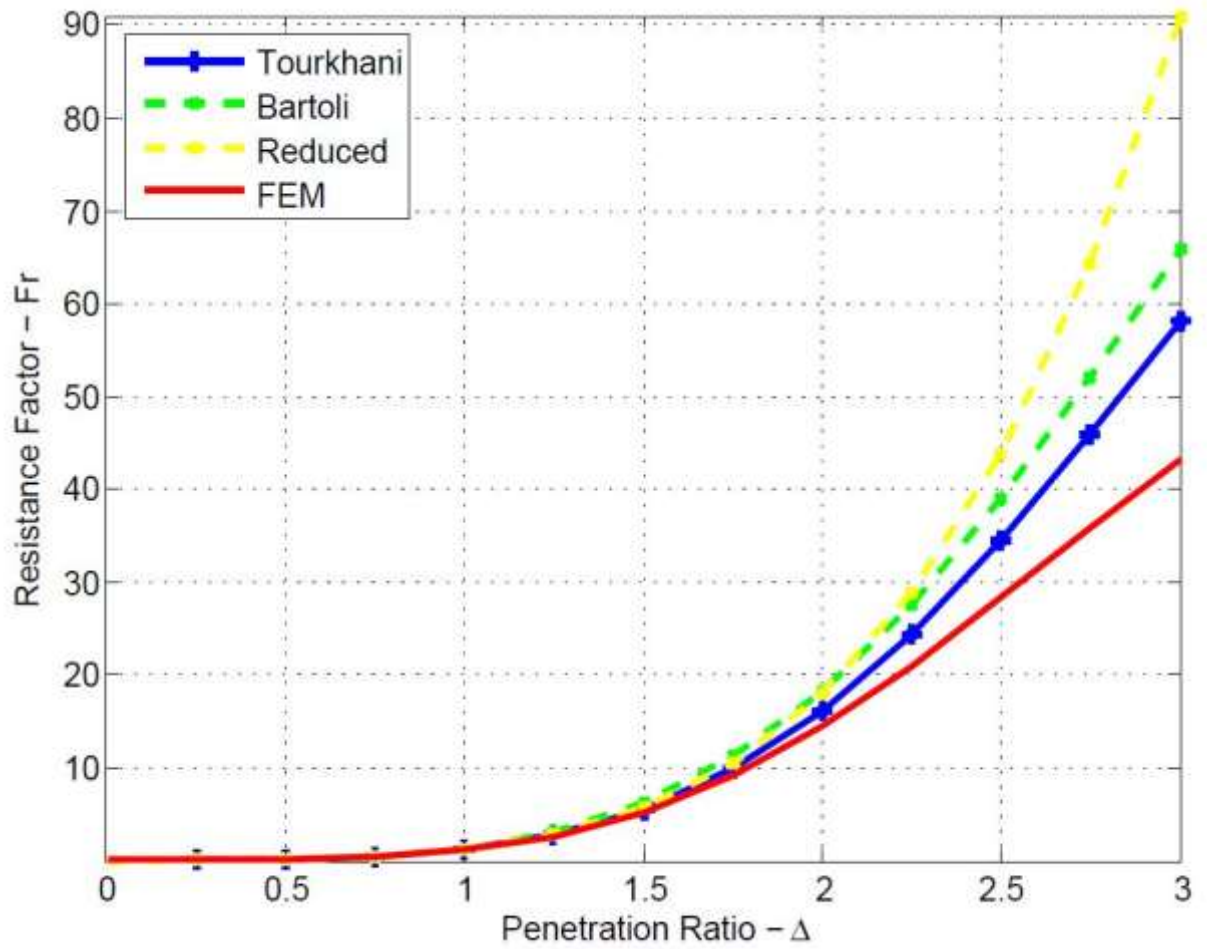

 (d)  $m = 4$ 

Figure 3-37 Comparison of different expressions for the determination of total Litz wire winding losses for different number of layers. Five Litz bundles per layer  $db = 0.54\text{mm}$ , with 37 strands of  $ds = 0.2\text{mm}$ .  $m=4$ (Villar, 2010)

In a preliminary comparison test, a huge underestimation of was detected, which probably comes from a typing error in [Bartoli et al., 1996], (a ns factor is missing). A further comparison has been carried (after correcting the detected error) between the methods for different number of layers (see figures 3-35 to 3-37).

The geometry of some of the compared examples is illustrated in figure 3-37, where the same four layer transformer has been used to determine one layer and two layer losses for various penetration ratios. In the left-hand column example (see figure 3-37a, figure 3-30c and figure

3-20e), the winding is interleaved, which corresponds to a one layer winding-loss estimation while in the right-hand column (see figure 3-30b, figure 3-30d and figure 3-30f), consecutive layers compose the primary or the secondary of the transformer, alternatively.

Apart from above equations, a reduced expression for low penetration ratios using (Lammeraner and Štafl, 1966) approximations, is introduced as mentioned below.

$$P_w = \frac{I^2}{2} R_{dc} \left\{ 1 + \frac{\gamma^4}{192} \left[ \frac{1}{6} + \frac{\pi^2 n_s P f}{4} \left( 16m^2 - 1 + \frac{24}{\pi^2} \right) \right] \right\}$$

3 - 64

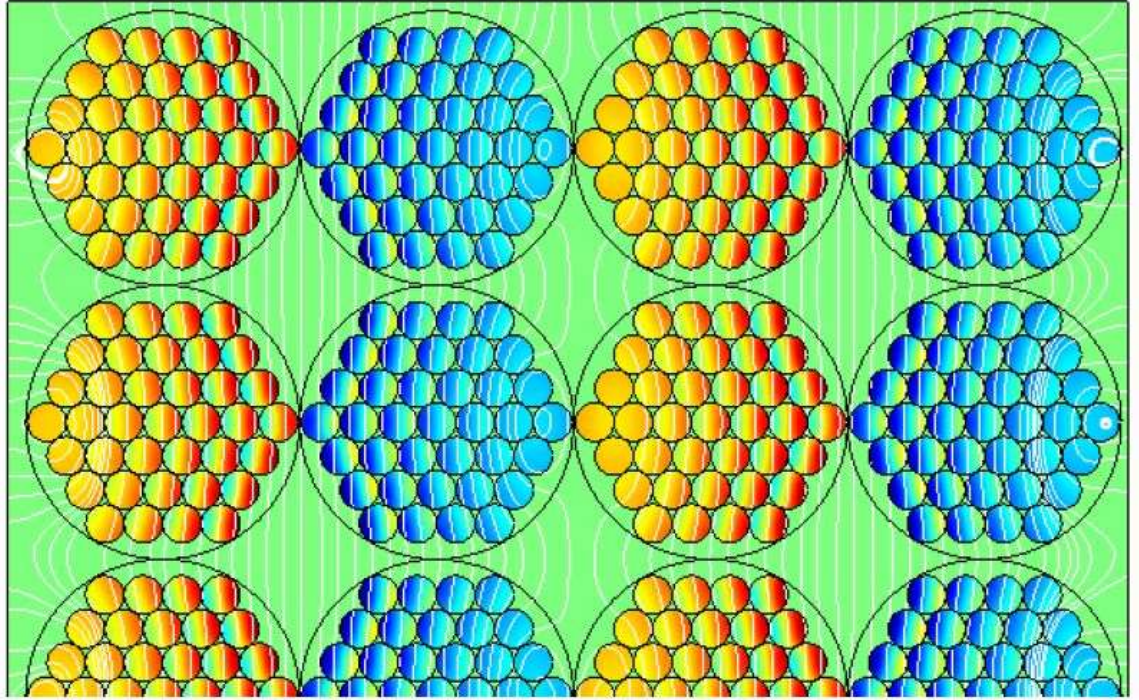


Figure 3-38 Current density and magnetic field lines,  $\Delta=1.5$  (Villar, 2010)



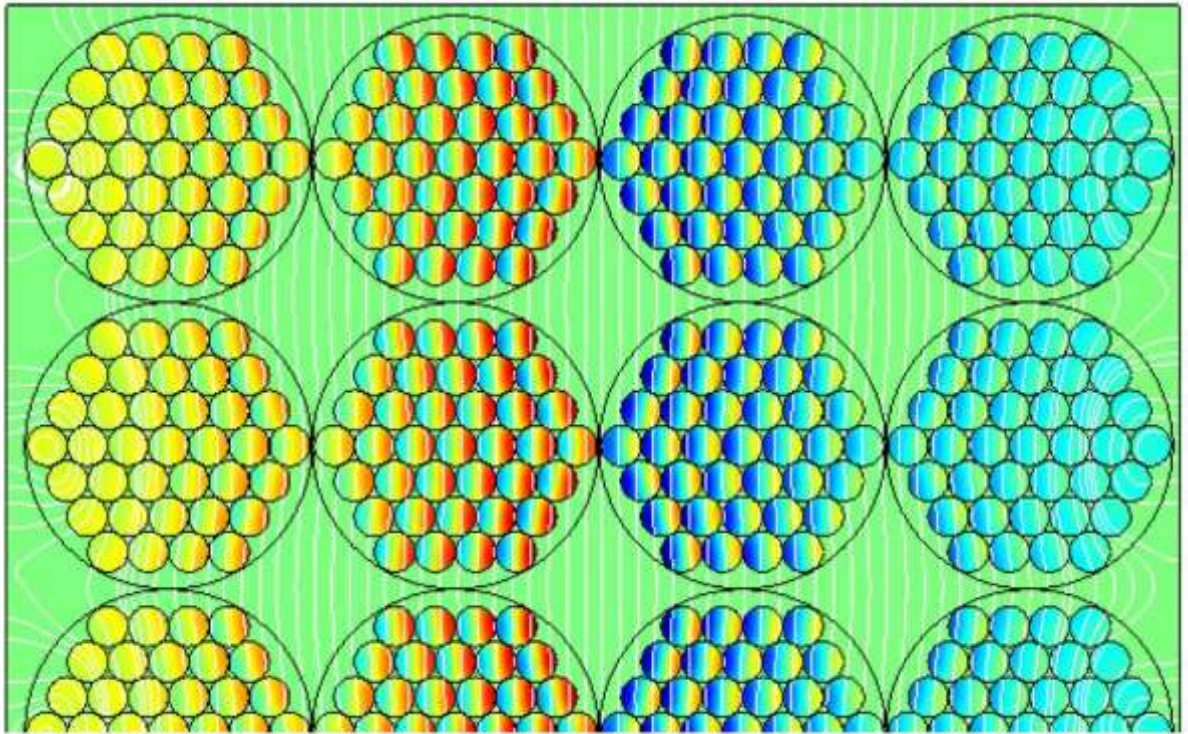


Figure 3-39 Current density and magnetic field lines,  $\Delta=1.5$ (Villar, 2010)

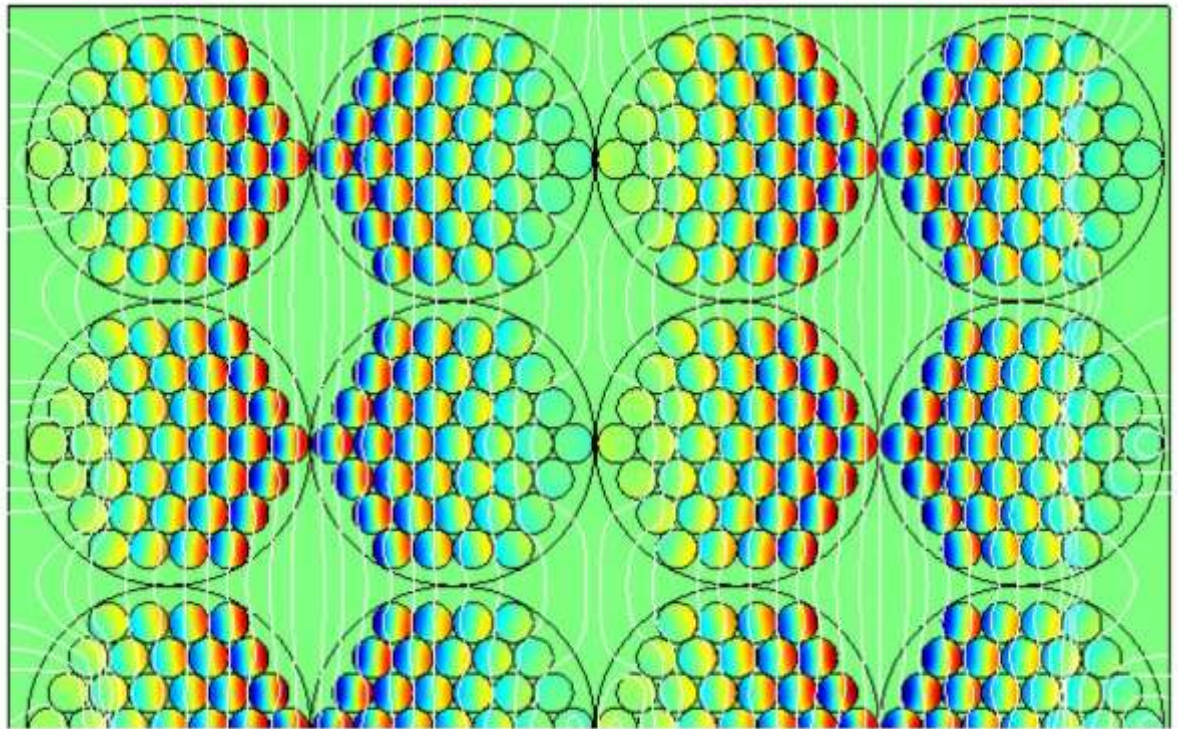


Figure 3-40 Current density and magnetic field lines,  $\Delta=3$ (Villar, 2010)



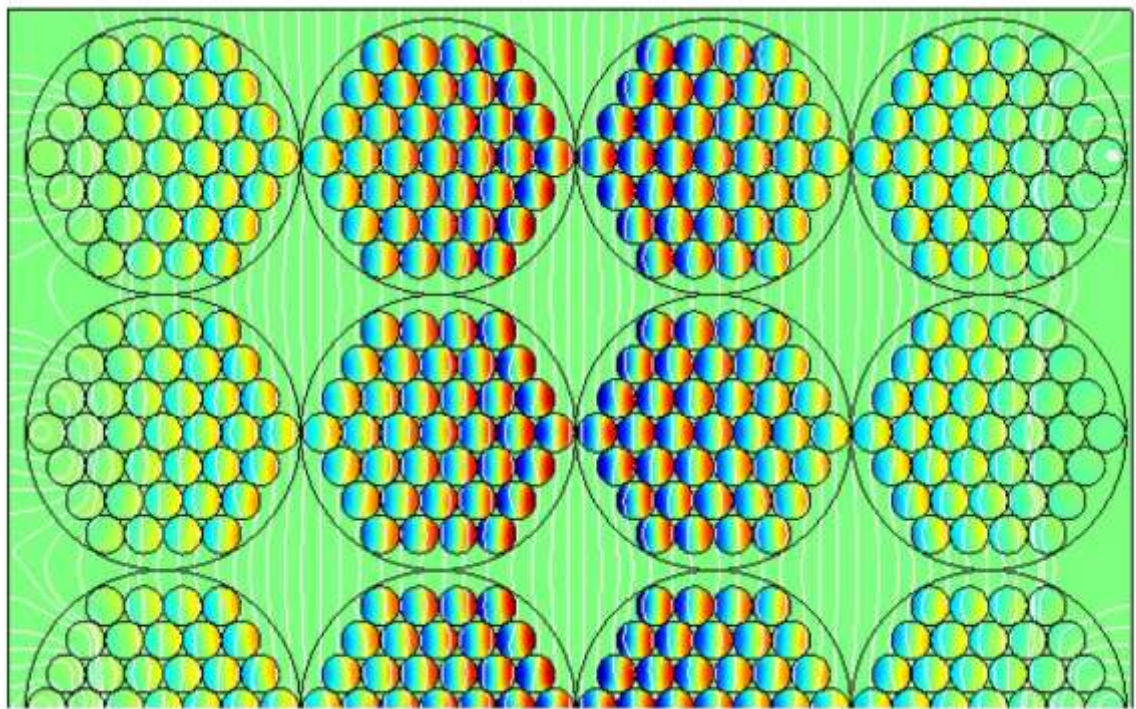


Figure 3-41 Current density and magnetic field lines,  $\Delta=3$ (Villar, 2010)

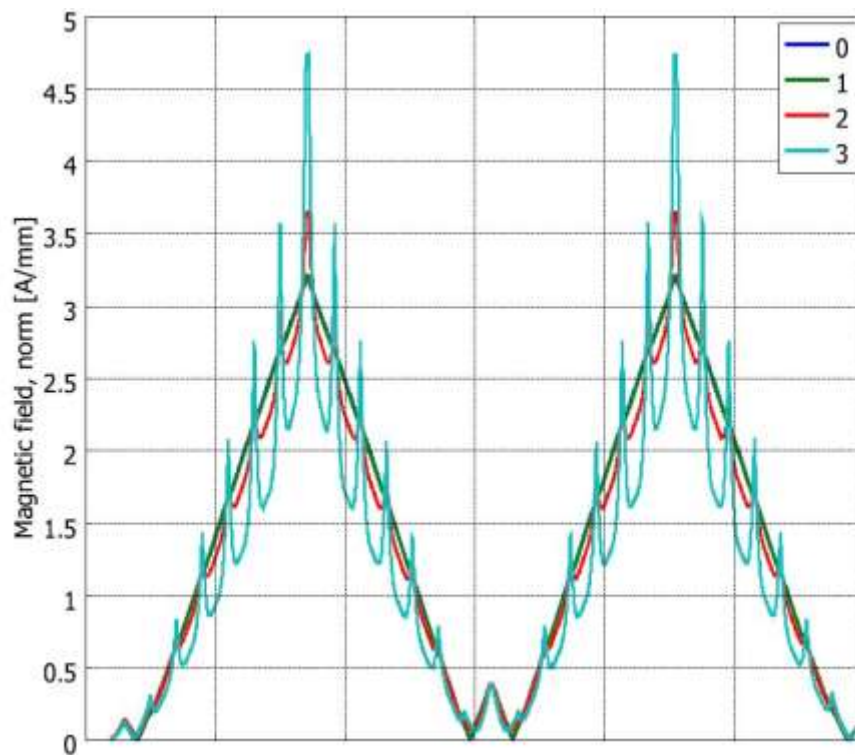


Figure 3-42 Magnetic field through the boundary line for various  $\Delta$ (Villar, 2010)

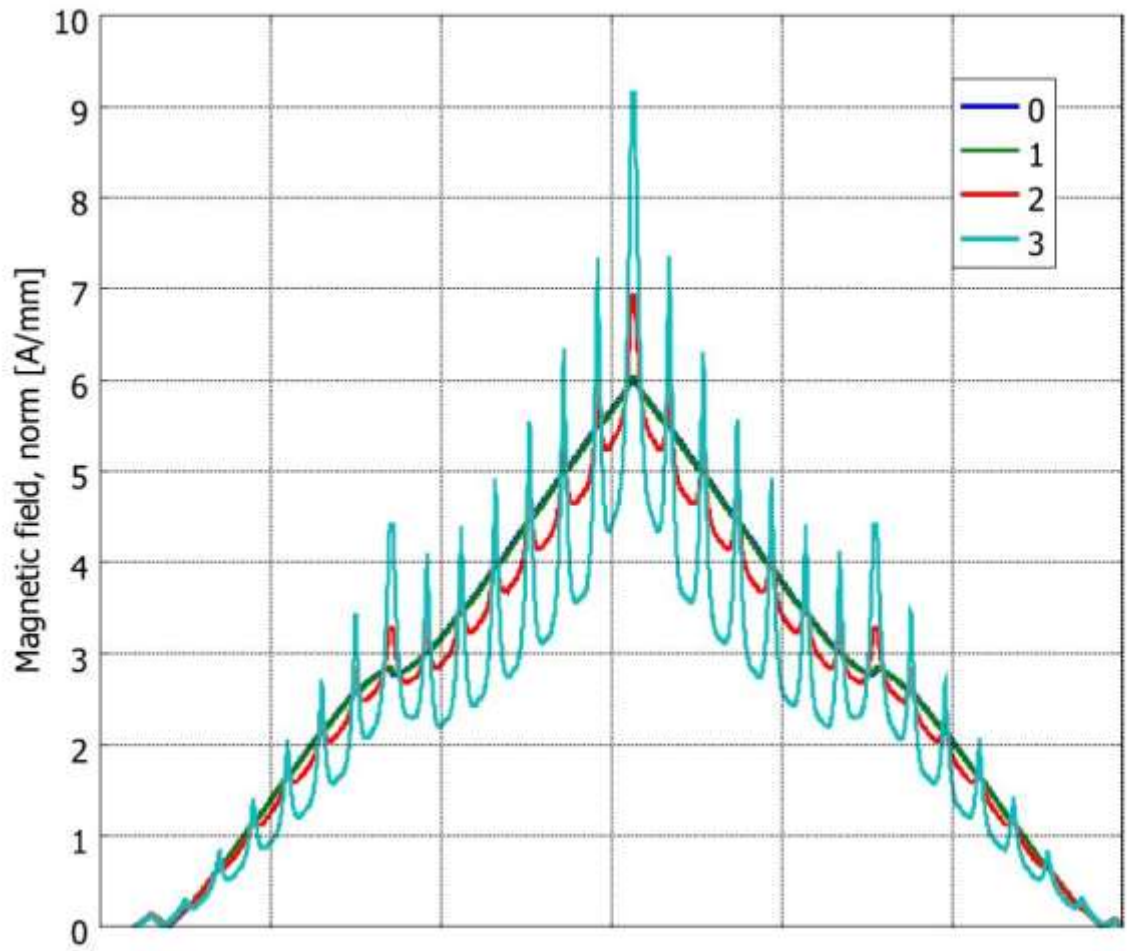


Figure 3-43 Magnetic field through the boundary line for various  $\Delta$  (Villar, 2010)

Four layer winding, two primary and two secondary. First column, layers are interleaved,  $m=1$ .  
Second column, consecutive layers,  $m=2$ .



### Effects of Twisting Imperfections

The computation of winding losses represents an essential part of the modeling process of inductors and transformers. Power electronic converters are usually operating at Medium-Frequency (MF), which can be defined with the power/frequency product (usually  $0.1 \div 1.0 \text{ GHzW}$  for medium-power systems). At MF, the impacts of eddy current losses cannot be neglected any more. Usually, eddy current losses are split up into losses due to skin and proximity effects: the skin effect describes the eddy currents due to the magnetic field created by the current in the conductor itself and the proximity effect characterizes eddy currents that originate from an external magnetic field. In order to obtain efficient MF inductors and transformers, the impacts of losses due to skin and proximity effects need to be mitigated. This is usually achieved with foil conductors or High-Frequency (HF) stranded conductors, e.g., “Roebel” bars or HF “litz” wires. In this regard, HF “litz” wires are extremely popular since they allow for low losses and great flexibility in the design of the magnetic component (Guillod et al., 2017a, Zhao et al., 2017, Leibl et al., 2016, Kieferndorf et al., 2016, Guillod et al., 2017b, Acero et al., 2006). HF “litz” wires are composed of multiple insulated strands, as shown in figure 3-44. Each single strand is subject to skin and proximity effects and thus, the single strand diameter is selected with regard to acceptable losses (Sullivan and Zhang, 2014b). The strands are twisted together in both radial and azimuthal directions (Guillod et al., 2017a, Tang and Sullivan, 2003).

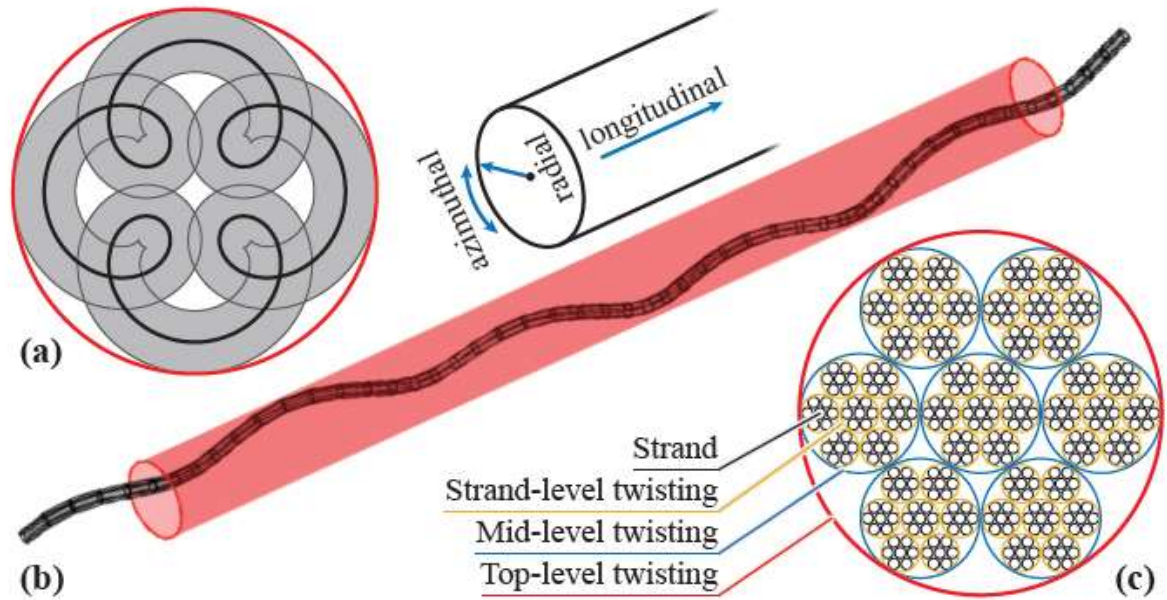


Figure 3-44 (a) Projection and (b) 3D view of the twisting scheme (azimuthal and radial) of a single strand. The depicted path depends on the structure of the bundle, the pitch lengths of the bundles, and the used twisting scheme. (c) Packing structure of a HF “litz” wire with bundles and sub-bundles (Guillod et al., 2017a).

The permutation in radial direction prevents eddy currents in case of an azimuthal magnetic field. An azimuthal field is created by the currents that are present in the considered HF “litz” wire itself. The permutation in azimuthal direction suppresses the oriented area spanned between the strands with respect to an homogeneous external field. The cancellation of the magnetic flux between the strands, prevents the formation of circulating eddy currents. In addition to the number of strands and the diameter of a single strand, the pitch (or length of lay), which is the spatial period length of the twisting (in longitudinal direction), denotes a third important parameter of a HF “litz” wire. For HF “litz” wires with a high number of strands, simultaneous azimuthal and radial twisting is difficult to achieve. Such HF “litz” wires are often constructed in a recursive manner, i.e., the total HF litz wire is composed of twisted bundles of HF “litz” wires and each bundle itself can again be composed of twisted bundles or single strands. In this thesis the first twisting level (twisting of the strands) and the last level (forming the complete HF “litz” wire) are called strand-level and top-level twisting, respectively. Additional twisting levels between the top- and the strand-level are denoted as mid-levels, cf. figure 3-44. With high numbers of strands and complex twisting schemes, the accurate computation of losses in such stranded conductors is a challenging task. Over the years, different calculation methods have been proposed for the calculation of the losses, which rely on analytical and/or numerical

calculations (Guillod et al., 2017a, Sullivan and Zhang, 2014b, Rossmanith et al., 2011, Zhang et al., 2014b, Meeker, 2012, Nan and Sullivan, 2009, Sullivan, 1999, Mühlethaler, 2012).

However, it is found that the measured losses are often larger than the values computed with the afore mentioned methods (Guillod et al., 2017a, Zhao et al., 2017, Leibl et al., 2016, Rossmanith et al., 2011). Different effects can explain such deviations. The (external) magnetic field is inaccurately computed (Roßkopf et al., 2015, Guillod et al., 2017a). Moreover, certain computational methods presuppose the external magnetic field to be homogeneous across the cross section of the HF litz wire (Mühlethaler, 2012). The terminations of the HF “litz” wire are generating losses. Moreover, terminations can add an impedance mismatch between the strands which leads to undesired circulating currents (Leibl et al., 2016, Rossmanith et al., 2011, Roßkopf et al., 2015).

Due to twisting, the length of the strands is greater than the length of the HF “litz” wire (Guillod et al., 2017a). For typical HF “litz” wire, however, this effect is often negligible (less than 10%). The packing (hexagonal, square, etc.) of the strands is not homogeneous and/or not perfectly modeled (Meeker, 2012, Nan and Sullivan, 2009). The exact packing in a HF “litz” wire, which is often not clearly defined, has only a limited impact on the losses (less than 10%). A non-integer number of pitches is used, leading to circulating currents inside the HF “litz” wire (Zhang et al., 2014b, Sullivan, 1999). Alternatively, local variations (a long distances that are similar to the pitch length) of the external magnetic field also create additional losses (Rossmanith et al., 2011).

Such local variations are typically produced by the fringing fields of air gaps. An imperfect twisting scheme is used, leading to an inhomogeneous current distribution in the strands. This includes improper azimuthal and/or radial twisting (at the top-, strand-, or mid-level), poor choices of the ratios of the pitch lengths between twisting levels, etc. The last two effects can lead to significant additional losses and commonly occur in practice. In particular, commercially available HF “litz” wires are frequently found to be subject to imperfect twisting (Leibl et al., 2016). Therefore, this paper analyzes the impact of the twisting scheme on the losses, which, per the information in public domain, has not been studied in detail in the literature. Section II summarizes loss computation methods for perfectly twisted HF “litz” wires. Section III analyzes the implications of twisting imperfections on the losses. Finally, Section IV, compares calculated results to experimental results, using a MF transformer that employs a HF “litz” wire with imperfect twisting (Guillod et al., 2017a).

According to these investigations the implications of imperfections in HF “litz” wires (e.g. number of pitches, twisting) on the losses and particularly focuses on imperfect twisting which is commonly observed in commercially available HF “litz” wires. A fast 2.5D PEEC solver, which is able to simulate HF “litz” wires with thousands of strands, has been implemented to simulate the current distribution among the strands and determine the losses. According to the results obtained from the analysis of different types of imperfect twisting schemes it is found that imperfect twisting, in particular of the top-level bundles, can lead to a significant increase of losses due to eddy currents (up to 100% increase). It is also found that imperfections may be tolerated at sub-bundle-levels. In this context, simple analytical expressions are derived, and the results are summarized in a design guideline for the construction of suitable HF “litz” wires. Furthermore, an increase of the losses is to be expected for windings with low number of pitches and/or non-homogeneous external magnetic fields. The presented method is finally applied to a 7.5 kHz / 65 kW MF transformer, which employs imperfectly twisted HF “litz” wires, for experimental verification. Both, the measured current distribution among the bundles and the losses, are in good agreement with the simulations. The imperfections of the HF “litz” wires lead to an increase of the winding losses by 52%(Guillod et al., 2017a).

### 3.33 Losses in non-current carrying windings.

Eddy current losses will also occur in non-current carrying conductors and shields when they are located in the magnetic fields generated by other windings. Since these windings and shields are not conducting any net current, they cannot be directly assigned a loss resistance and formula similar to Dowell’s formula cannot be applied to calculate the losses.

An alternative approach developed by Perry uses a similar derivation to calculate the losses in a conductive layer (  $\ln W / \text{Area}$  ) based on the thickness layer (  $\ln \text{skin depths}$  ) and the intensity of the H- Field on each surface, but the results are then not transformer to an effective resistance as done by Dowell’s

These formulas were then extended to non - sinusoidal currents by Vandelack & Ziogas. This more general approach can be used to calculate losses in non-current carrying windings and shields as well as those in non-optimum winding portions and for arbitrary layer thicknesses with a winding(Carsten, 1986).

### 3.4 Experimental results

As discussed so far in this thesis the effect of the skin effect and the proximity effect become significant as the frequency of the excitation waveform goes high. The effect of this was practically tested in two applications.

#### 3.41 Inductor applications

The inductors tested were subjected to a considerably larger low frequency current and a high frequency ripple component of considerable amplitudes. These had a construction with a foil winding as seen in the following figures.



Figure 3-45 layers copper foil of thickness 0.7mm separated by interleaving insulation of 0.125mm

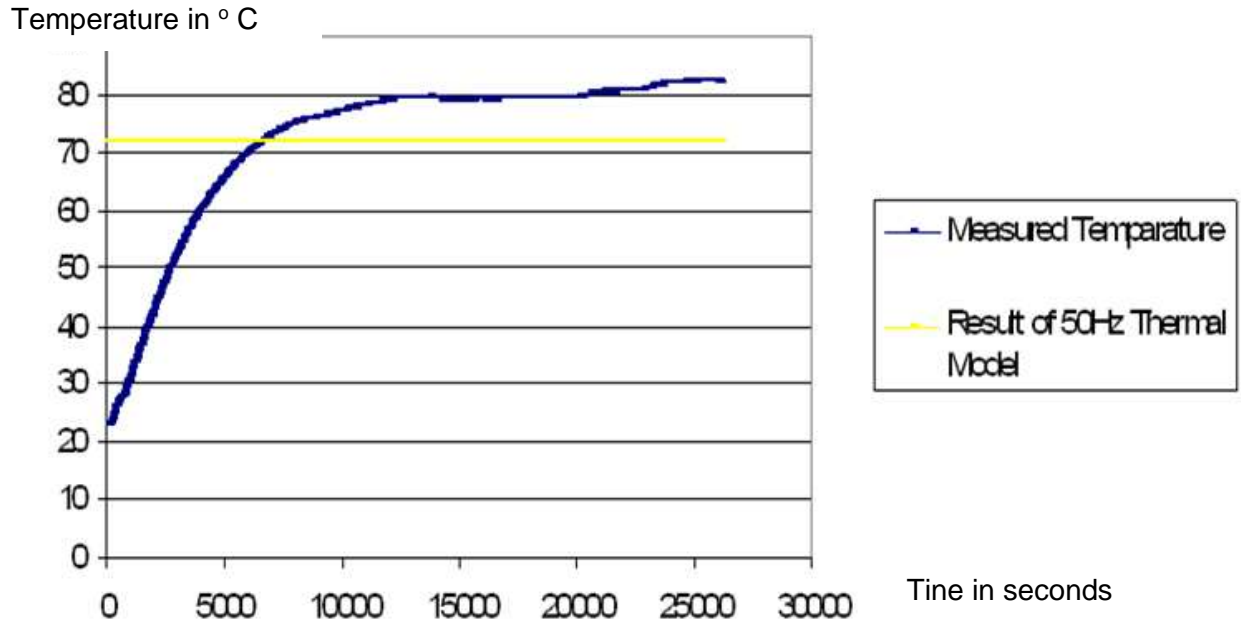


Figure 3-46 Temperature rises under the excitation of a waveform containing significant higher order harmonics.

The above product was subjected to a current waveform of approximately 50A/50Hz, 11A /20kHz and 3A/40kHz. The temperature rise under this condition is shown in figure 3-47. This indicates that the presence of high frequency components in the excitation waveform has resulted in extra losses causing additional temperature rise in the windings which is in line with the indications given by the theoretical predictions.

### 3.42 transformer applications



Figure 3-47 Foil wound HF transformer.

A similar test conducted on a high frequency transformer with foil winding but with secondary winding being sandwiched between two parts of the primary winding. As it could be seen in the below graph this also shows a significantly higher temperature rise compared to a 50Hz current going through the same Cu foils. However, in this case the build-up of extra losses has become less (relative to the number of foil layers) due to the opposite directional flow of current in the secondary windings that are sandwiched.

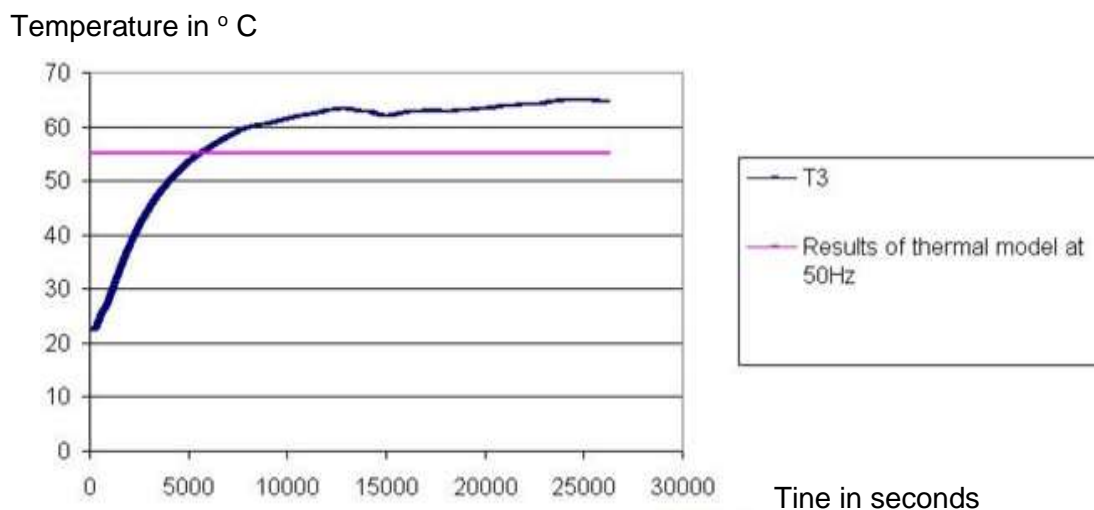


Figure 3-48 Temperature rise under the excitation of a wave form containing significant higher order harmonics.

### 3.43 High Frequency Transformer 50kW, 50kHz

The transformer is designed to handle a power of 50kW at a square wave excitation of 50kHz. The transformer was designed with a primary to secondary turns ratio of 1:2 with a single secondary.

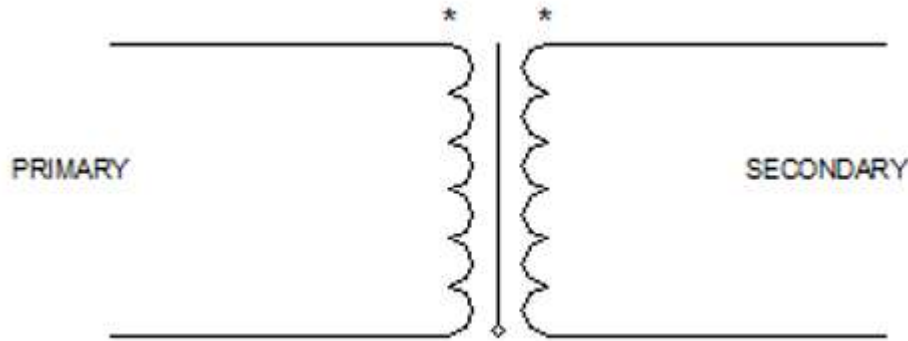


Figure 3-49 Schematic of the 50 kHz, 50kW transformer

Conductor selection and winding losses estimations.

Transformer windings suffer from skin and proximity effects. The current distribution within a conductor depends on its current, the surrounding currents, the type of conductor, the geometry of the winding and finally the frequency of the waveform. Thus, the determination of conductor losses is not always an easy task. If winding configuration is simple enough, like foil or coaxial conductors, the resolution of one-dimensional field equations (Maxwell Equations) is usually sufficient to estimate losses. However, in complex winding arrangements magnetic field distribution, and therefore current density distribution are highly two dimensional and analytical solutions may become too complex to be solved and usually require finite element resolutions [9]. The option of Litz wires and foil conductors were considered for this application. The level of power and the frequency of the current in this particular application make the foil conductors a more attractive choice compared to Litz wires or thin profile conductors. However, the foil conductors carrying high frequency currents result in prominent occurrence of proximity effect as the author pointed out in previous publications. A quick explanation of the increased losses due to the proximity effect in foil windings and its sensitivity to the increase of frequency can be seen from the illustrations below (Villar, 2010, Nabhani et al., 2014).

In a transformer with a conventional winding structure build-up of the magnetic field and thereby increase in the current density occurs as described in the figure 3-36. (Erickson and



Maksimovic, 2001) If a transformer with  $m$  number of layers in each winding is considered the increase in the copper losses can be described by the factor

$$F_r = \Delta \left[ \zeta_1 + \frac{2}{3}(m^2 - 1)\zeta_2 \right]$$

3 - 65

where, skin effect factor

$$\zeta_1 = \frac{\sinh(2\Delta) + \sin(2\Delta)}{\cosh(2\Delta) - \cos(2\Delta)}$$

3 - 66

and proximity effect factor

$$\zeta_2 = \frac{\sinh(\Delta) - \sin(\Delta)}{\cosh(\Delta) + \cos(\Delta)}$$

3 - 67

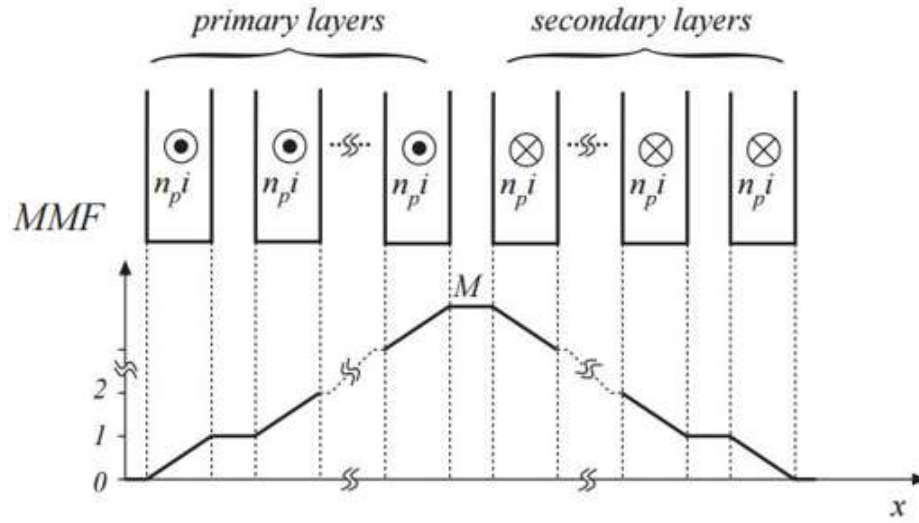
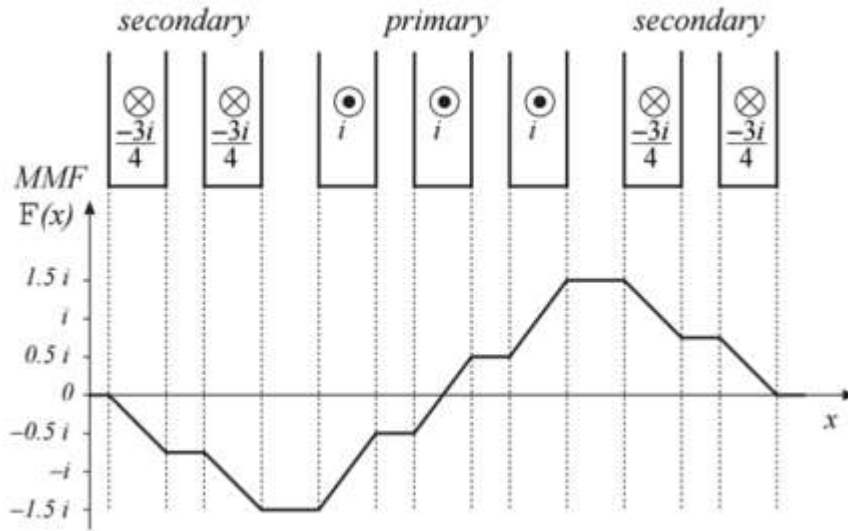
$$\Delta = \frac{d_w}{\delta}$$

3 - 68

$$\delta = \sqrt{2/\omega\mu\sigma}$$

3 - 2

with conductor thickness,  $\omega$  the angular frequency of the current,  $\mu$  permeability and  $\sigma$  conductivity.


 Figure 3-50 MMF Diagram for a conventional wound transformer with *m* number of layers

 Figure 3-51 MMF Diagram for a sandwich wound transformer with *m* number of layers

As it could be seen from the above formula the increase in the losses in foil windings becomes considerably high as the number of foil layers increases. A technique commonly used to minimize this effect is the use of sandwich windings. Author has explained this outcome based on a previous research on a 10 kHz application (Nabhani et al., 2014). Figure 3-51 also explains the MMF pattern of a sandwich wound transformer. However the increase in the losses at

50kHz become significant which demands the need of a further reduction of losses due to skin and proximity effects. As a solution for this in this 50kHz, 50kW transformer a fully interleaved primary and secondary winding was introduced. In the selected construction it was possible to use the bifilar winding technique for the achievement of the perfect interleaving. The change in the MMF pattern with this winding arrangement can be seen in figure 3-52 (Erickson and Maksimovic, 2001).

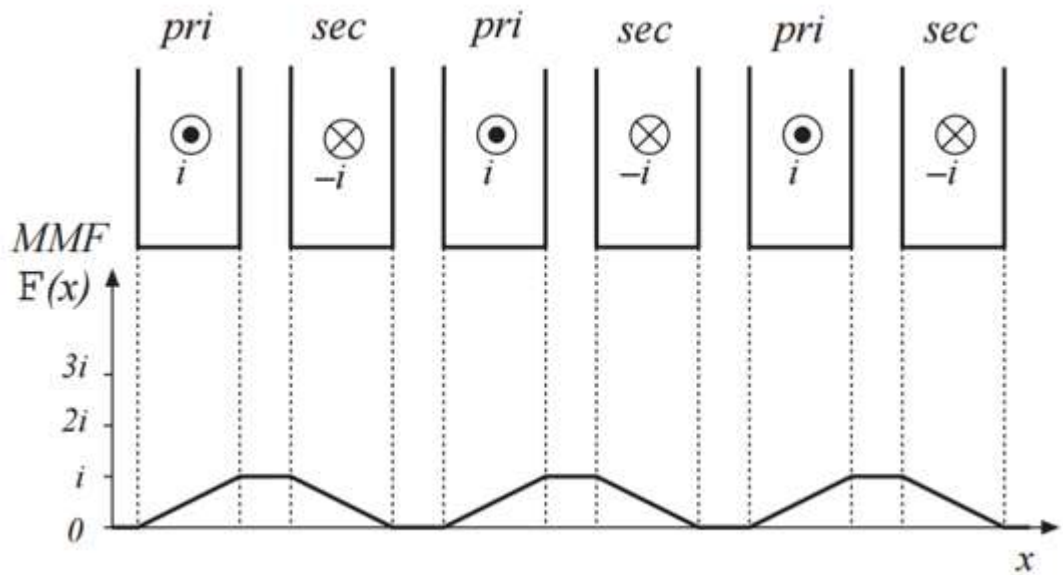


Figure 3-52 MMF Diagram for the fully interleaved winding transformer with number of layers

### 3.44 High Frequency Inductor $8.5\mu\text{H}$ at 300A, 50kHz

The approach discussed under above was possible for the transformers as it is a dual winding component. This approach of minimizing skin effect and the proximity effect is not possible for the inductor applications. In this application the simple approach of maintaining distance between the layers was considered figure 3-54. This provides the means for the reduction of losses due to proximity effect. Further this gives an additional cooling surface for the product. A sample was built up and tested on the 50kHz application.

Prototype development and testing



Figure 3-53 Ferrite HF transformer (50kW,50kHz)

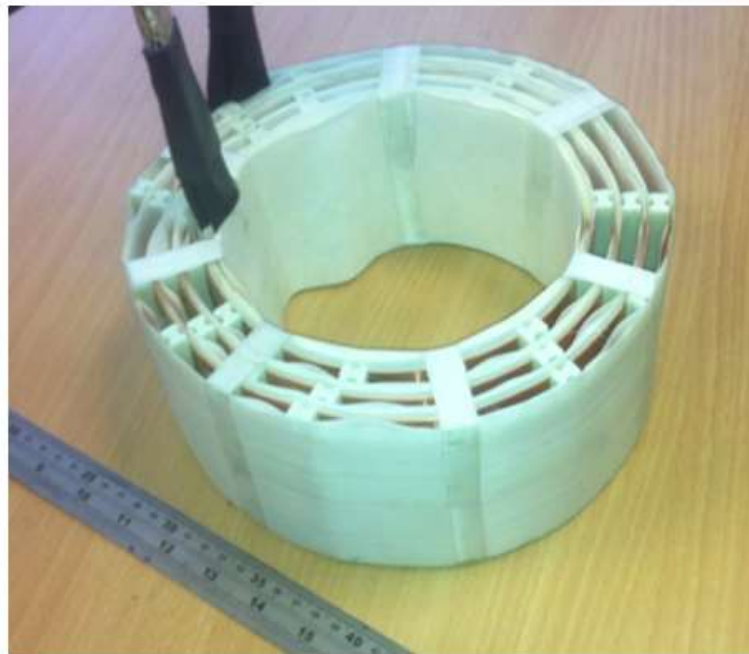


Figure 3-54 Inductor (8.5uH@ 300A, 50kHz)

A 50kHz transformer with the ferrite grade 3C97 was developed, figure 3-53. Bifilar winding technique discussed in this paper was used. The sample comfortably met the standard testing

as per standards including the high voltage test between the primary and the secondary. The heat sink rating was purposely made higher as an addition precaution for avoiding excessive temperatures under the full load conditions. Similarly the inductor was manufactured, figure 3-55. The measured inductance was well within the acceptable tolerance level. Prototypes were tested on a 50kW,50kHz converter application.

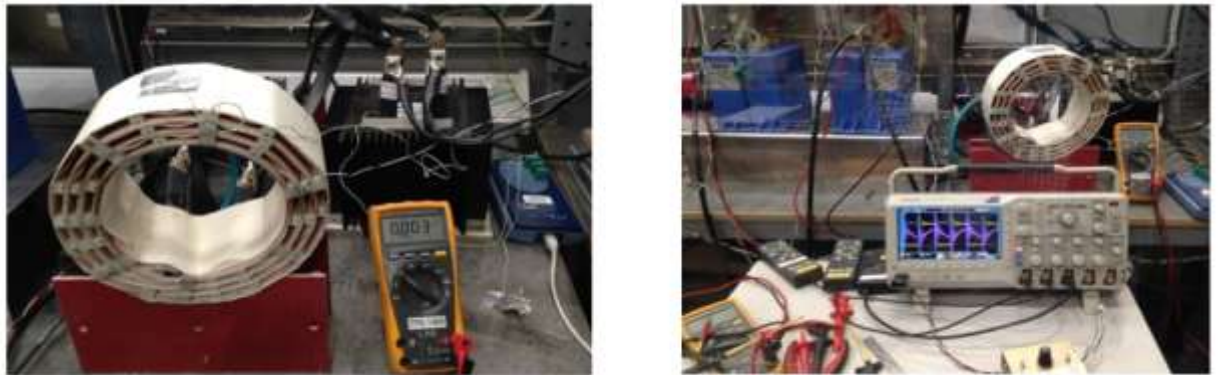


Figure 3-55 Testing arrangement

Due to the difficulty of making accurate loss measurements at 50kHz the temperature rise measurements were made. The temperature rise of each component can be seen in Figure 3-56. There were certain difficulties in arriving at the full power of 50kW in the testing set up. It was identified that certain improvements have to be made in the arrangement in order to arrive at the full power of 50kW at 50kHz. However the testing arrangement was sufficient to make reasonable judgements of the magnetics component performance.

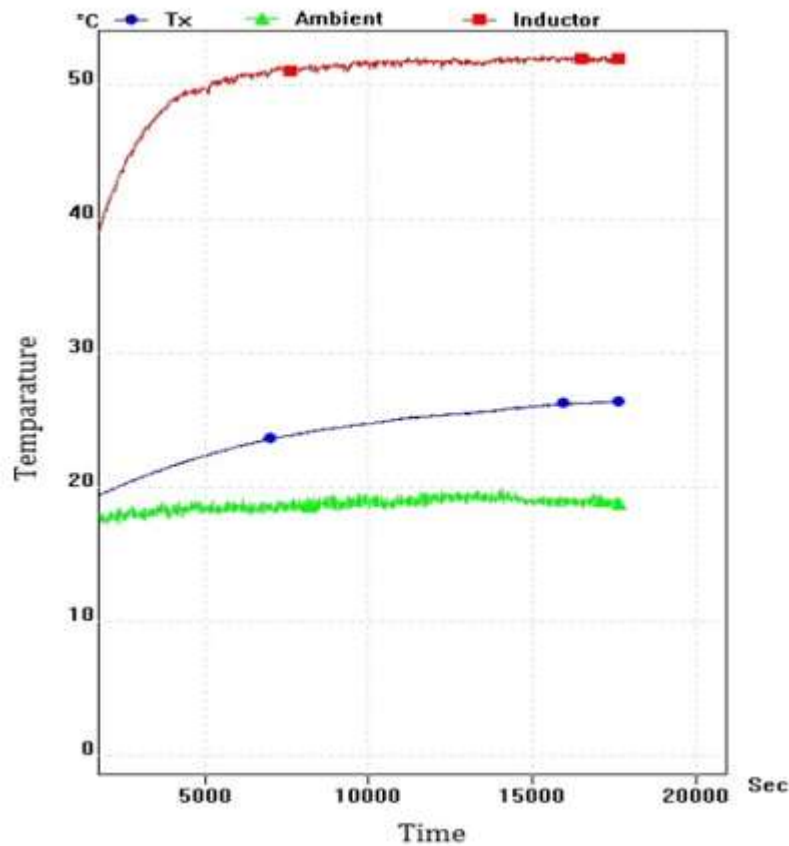


Figure 3-56 Load test temperature rise vs time

### 3.45 Development of a 100kW, 20 kHz Nanocrystalline Core Transformer for DC / DC Converter Applications

In order to achieve a high degree of miniaturization, designers move into significantly high operating (switching) frequencies and high power levels in the development of modern high power converters and inverters. There is also a clear trend that the requirement of achieving high power levels in a single module will increase alongside the operating frequencies used in these applications.

Applications like traction, ship and basically any mobile platform with a converter on board require light weight and compact converters to exploit the space available on board more effectively. They often require galvanic isolation for safety and other reasons. Therefore, high power high frequency transformers which offer galvanic isolation and a small volume are of increased importance (Pavlovsky et al., 2005). In addition to the galvanic isolation magnetic components including transformers and inductors perform functions of harmonics filtering, energy storage and parameter matching for power stages as well as control circuitries in a

power converter. They often determine the converter size (Shen et al., 2008a, Lotfi and Wilkowski, 2001). It has been a long-held view that with a continuous increase in operating and/or switching frequency a continuous decrease in physical size of magnetics would follow. However the heat removal surface of the magnetic components decreases as a result of the higher density design; on the other hand, core and winding loss densities increase correspondingly. Therefore attention needs to be paid to magnetic material selection and associated core loss calculations, especially for high frequency high density magnetics and power converter design(Shen et al., 2008a).

In the initial stages of this research the advantages and disadvantages of Ferrite and Nanocrystalline materials as a core material for high frequency high power transformers were presented. Further mitigation techniques of conductor losses at high power high frequencies with novel winding techniques were presented based on developments such as 40kW,20kHz and 50kW , 50kHz transformers.

Going forward with the findings of these studies an approach was made to achieve 100kW single module transformer that operates at 20kHz, which is used in a DC /DC converter application.

In the selection of suitable core material for this task several Ferrite grades and Nanocrystalline materials were evaluated with modern approaches of estimating core losses in each type under non sinusoidal excitations of high frequencies. The advantages of Nanocrystalline at 20kHz applications reduce to some extent at 50kHz. The challenges of mitigating high frequency conductor losses at these high current levels are explained. A novel winding technique that mitigates the high frequency losses and constructional challenges of this technique are explained.

Two design options are presented with a Nanocrystalline core for natural convection cooling applications and water plate mounting applications. Housings with specially engineered exterior are used for the natural convection cooling applications and one with specially engineered interior is used in water cooled mounting application.

### Transformer Construction

The transformer is designed to handle a power of 100kW at a square wave excitation of 20kHz. The transformer was designed with two parallel operating secondary windings each handling a power of 50kW.

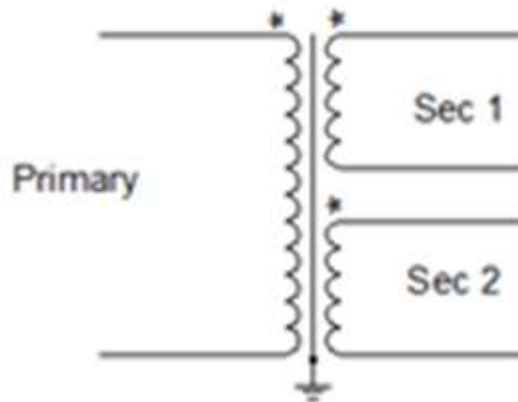


Figure 3-57 Schematic of the 100kHz, 20kW transformer

#### Transformer core selection and turns calculation

The advantage of having a high saturation flux density of Nanocrystalline material was considered. Based on the material properties of Ferrite and Nanocrystalline materials optimal operating flux densities for each material were decided based on the operating frequency of 20 kHz. The Faraday's law with appropriate constants for rectangular wave excitation is used to decide on the primary turns.

#### Transformer core loss estimation

An improved calculation method of core losses for non-sinusoidal waveforms based on recent publications (Venkatachalam et al., 2002, Herbert, 2008) and (Shen et al., 2008a) was carried out. Modified and generalized versions of Steinmetz equations and a simplified graphical method discussed in these publications were used in loss estimations. The core material selection is discussed in the chapter 4 of this thesis

#### Conductor selection and winding loss mitigation.

The option of "Litz" wires and foil conductors were considered. The application under consideration handles a power of 100kW. The suitability of "Litz" wires including rectangular cross-section braided "Litz" wires were considered. However, the initial calculations carried out including poor filling factor of "Litz" wires showed that the foil windings are more suitable for



this application. The increased conductor losses at high frequencies as explained in previous publications were considered and the significance such increased losses at the high-power level of interest were considered.

Two approaches to the windings that minimize the high frequency effect on conductor losses were considered. These approaches to transformer windings make the influence of proximity effect has on conductor losses frequency independent. A mathematical explanation on this concept was presented in the previous publications. Sandwich primary and secondary windings is one of these approaches. The second approach is a specially prepared foil arrangement as described in the diagram below. This second approach also provides the flexibility of adjusting the leakage inductance between primary and secondary windings as required by the rest of the parameters in the converter circuit. The mathematical explanation of the controllability of leakage inductance and the mitigation of conductor losses are beyond the scope of this paper and will be presented in a future publication.

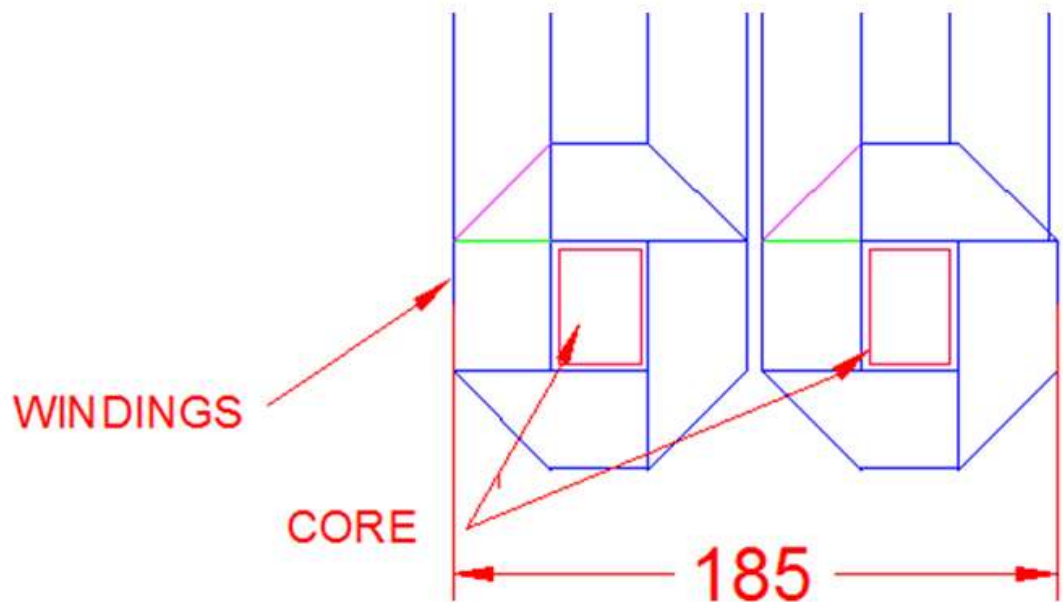


Figure 3-58 Novel winding technique that mitigates the conductor losses

Temperature °C

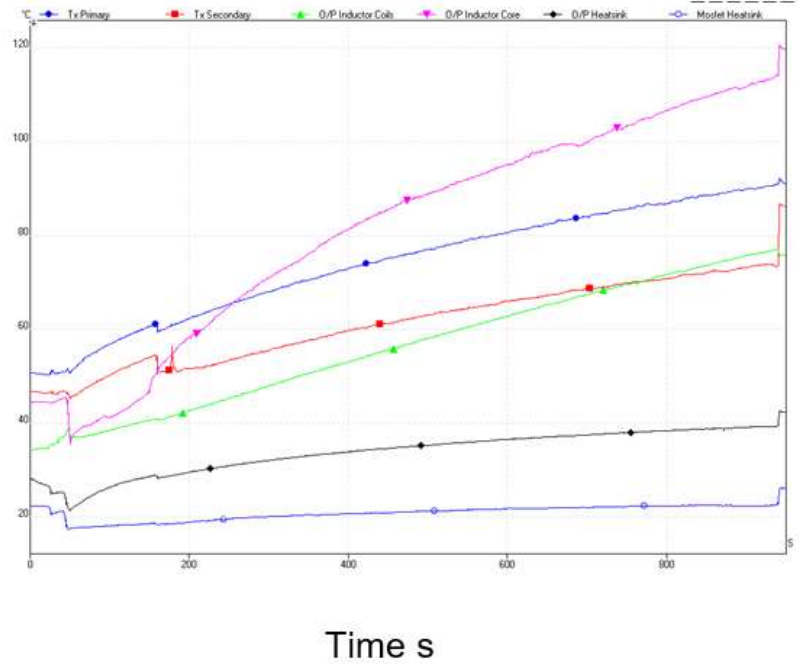


Figure 3-59 Temperature rise with a standard housing

Based on these results it could be concluded that in order to achieve the power of 100kW in the given volume a modified interior housing has to be used. After a further investigation on the thermal model of the arrangement the interior construction of the transformer housing was modified to effectively transfer heat from the hotspots of the transformer towards the water-cooled plate. After these improvements to the housing construction, it could be observed that more than an hour of operation at full power of 100kW was necessary for the transformer temperature to reach 80 Degrees. Further it could be seen that the temperature rise gradient was reducing significantly at this time.

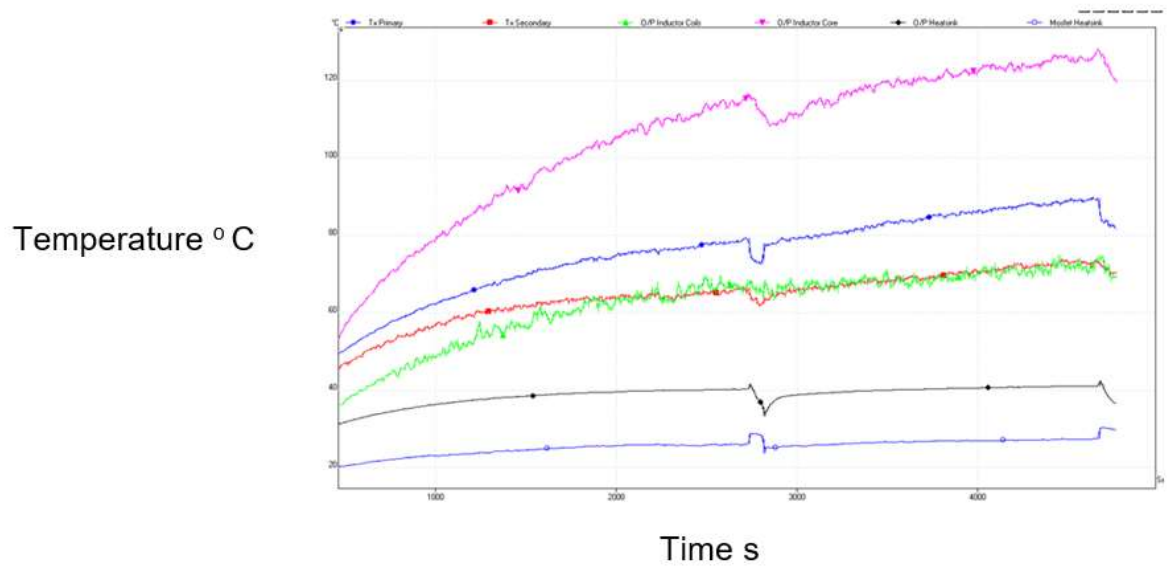


Figure 3-60 Temperature rise with modified interior housing

### 3.5 Winding arrangement that enables the handling of high frequency large currents in high frequency magnetics.

Patented new winding arrangement by the researcher which has already become a game changer in the industry.

Patent No: WO2019234453A1 Winding arrangement for an electrical transformer

*A coil of electrically conductive material is provided, the coil comprising a first and second section, the first section having a first plurality of turns and the second section having a second plurality of turns. Both the first plurality of turns and the second plurality of turns are arranged around a winding axis of the coil. The first plurality of turns are smaller than the second plurality of turns such that when viewed along the winding axis of the coil the first plurality of turns fit within the second plurality of turns. When viewed perpendicular to the winding axis of the coil the first and second sections are adjacent.*

One of the major difficulties in constructing single module high frequency high power magnetics is the difficulty of handling high frequency currents in a compact structure. The nature of the magnetic component construction requires the current carrying conductors to be placed in close proximity to each other. This makes it impossible to avoid one current carrying conductor getting immersed in the magnetic field of neighboring conductor(s). This gives the rise to the phenomena known as the 'proximity effect'.

The design of modern high power high frequency converters requires handling currents such as 250A at 20kHz. There is a physical limitation of having sufficiently thin conductors with a lesser number of layers to accommodate the flow of such high currents. Further there is a machining limitation in doing windings of conductors with such unusual aspect ratios.

The proposed winding configuration will provide the facility to position the conductors carrying current in opposite directions to be placed in close proximity to each other. This mitigates the proximity effect and lowers the high frequency losses significantly. Further this arrangement eliminates the requirement of having to form the windings of conductors with extreme aspect ratios. This basically eliminates the manufacturing limitations of the high frequency high current windings

Interleaved foil windings were used in the old constructions. This has a number of machining difficulties and limits the power that can be achieved in a single unit. Larger overlapping area

in this construction increases the intertwining capacitance and the amount of insulation material required. This also obstructs the flow of heat making it difficult to achieve high power densities. The proposed construction in this patent makes it possible to achieve high power levels at high frequencies. This also eliminates the manufacturing difficulties of constructions that mitigate high frequency losses.

This construction makes it possible to construct high power transformers operating at much higher frequencies than it was possible with conventional constructions. Further it improves the heat flow between windings allowing compact designs with high power densities.

This arrangement eliminates the frequency dependence of the power level that can be achieved in a single module construction.

Eventually this winding arrangement makes the magnetics designs more prepared for the future developments in the power electronics industry.

This increase in the perimeter after half the number of turns makes the resistance of the two windings the same and the amount of magnetic flux enclosed by each of the windings the same, thus the impedance of the each windings the same. This makes it possible to connect these two windings in parallel and increase the current carrying capacity.

This approach is never used in high frequency transformers or planar transformers. This makes it possible to use the advantages of planar construction and to make single module transformers of much higher power levels than otherwise could be achieved.

This concept can be extended to be used in transformers of operating frequencies as high as 200kHz and power levels up to several MW.

This arrangement provides considerable advantages in the development of medium frequency transformers.

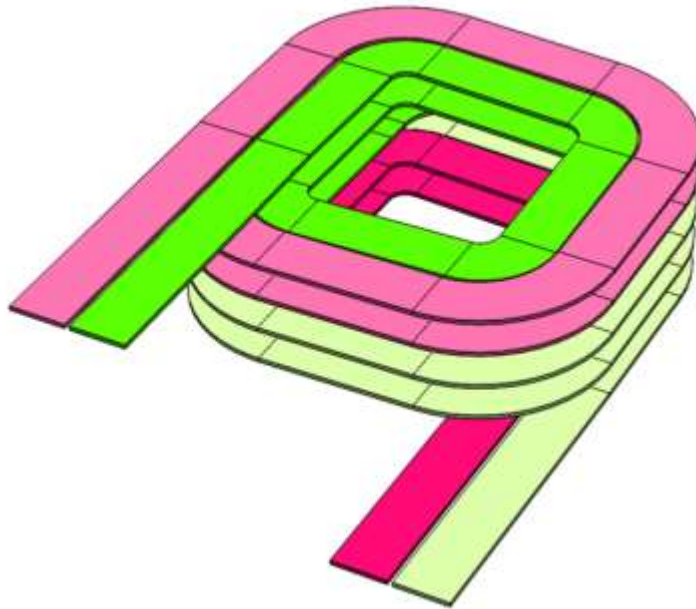


Figure 3-61 the way winding is seen after the assembly of two parts.

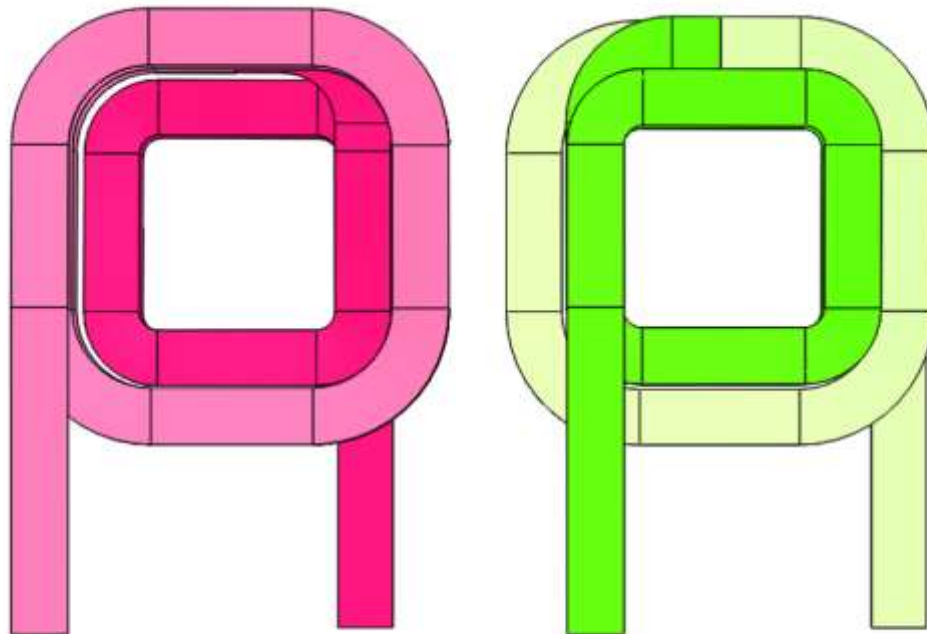


Figure 3-62 The two (identical) constituent winding parts of the winding arrangement with the darker colour showing the part of the winding with smaller periphery

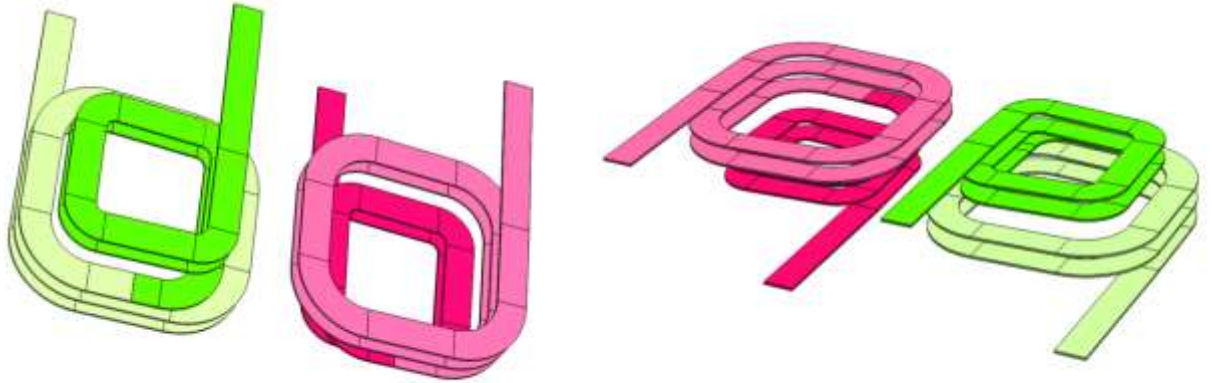


Figure 3-63 Isometric views of the windings

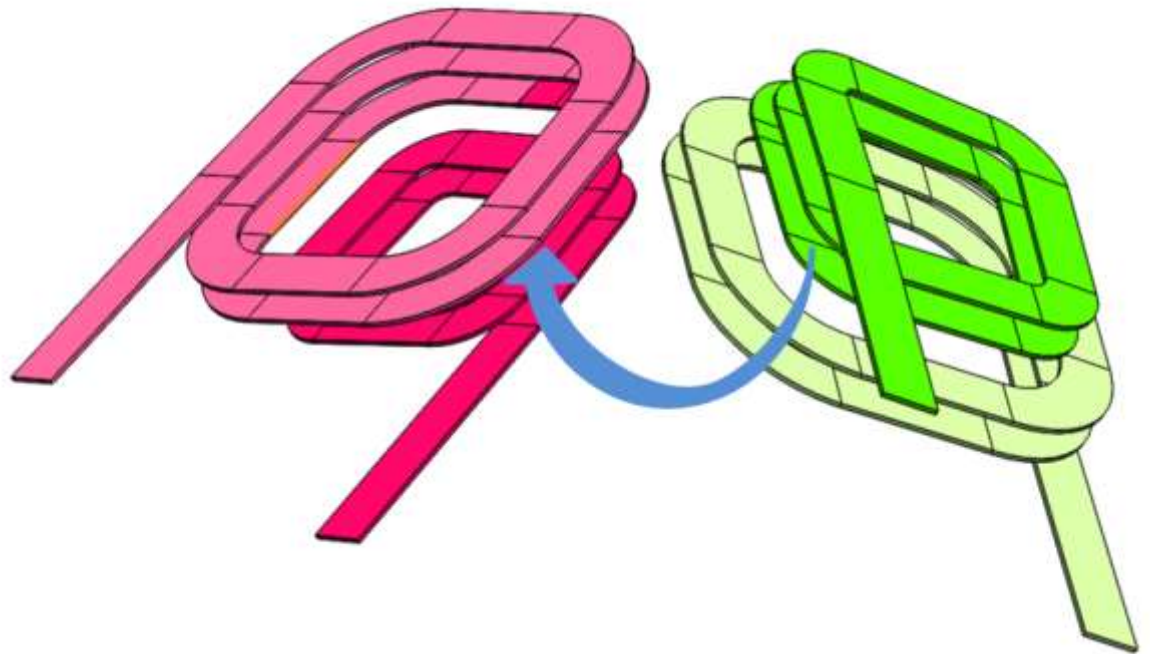


Figure 3-64 Insertion of the two pieces to form the final winding.

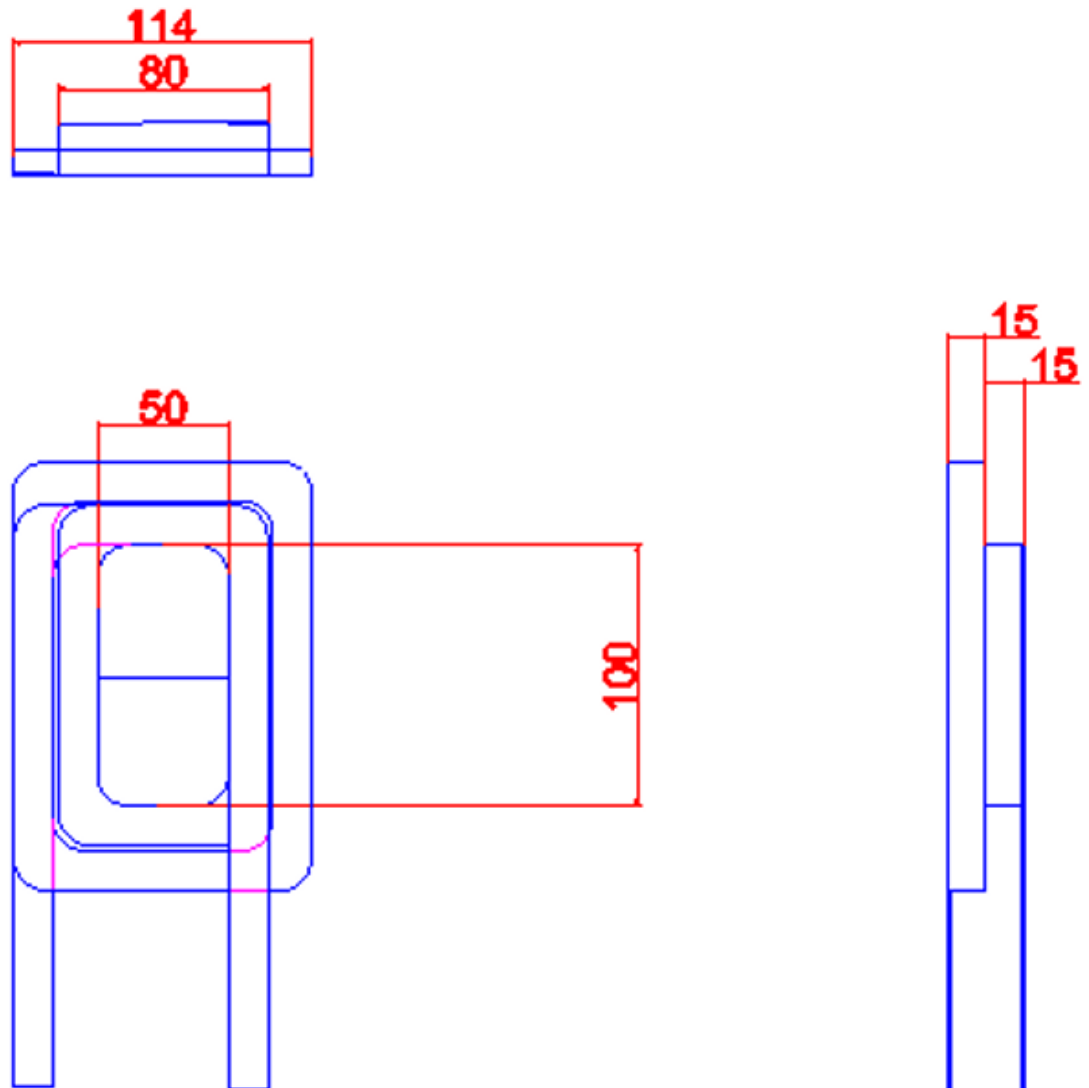


Figure 3-65 Example winding arrangement for a 100kW transformer

The above winding is only a half of the complete winding; two of such windings stacked as shown below make the complete winding.



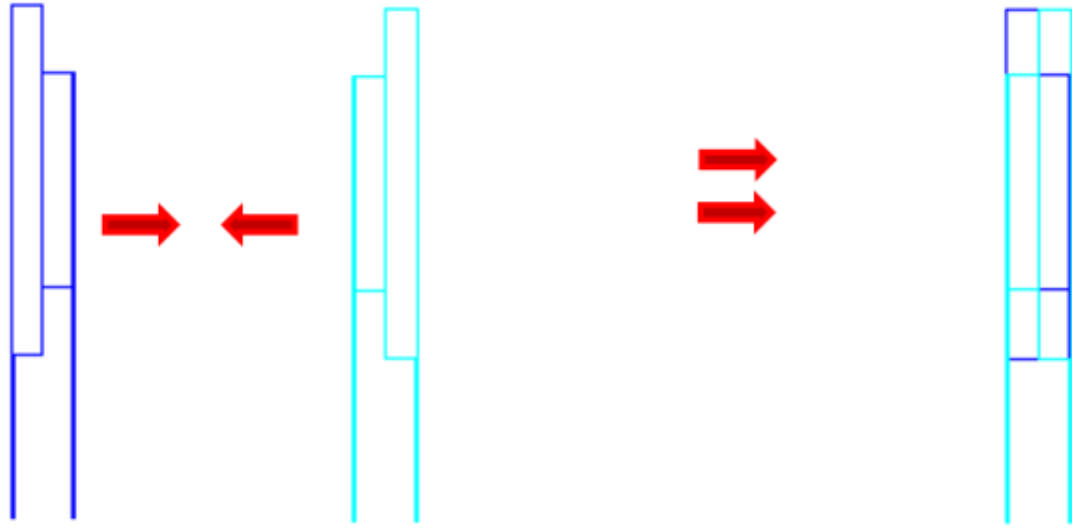


Figure 3-66 Example winding arrangement for a 100kW transformer side view

### 3.6 Discussion

The modern developments such as SiC MOSFETs have considerably low switching losses compared to Silicon MOSFETs and IGBTs. These offer a considerable advantage over conventional silicon devices. These also make it possible to operate at 2 to 5 times higher switching frequencies compared to their conventional counter parts. As the frequency goes high the magnetics components in the power electronics systems become more and more compact. Magnetics components being usually the bulkiest components in a power electronics system and in most of the situations also the most expensive component, it is of high interest of many developers to move in this direction.

However, with the increase of operating frequency accurate approaches have to be taken in the design of magnetic components. Otherwise, these can become high loss-making components in the system generating excessive heat and causing thermal runaway of the complete system. Therefore, it is especially important that the magnetics designers for power electronics applications look into the fundamental theories that govern the electromagnetics behavior in the context of very high frequency levels of interest. In this study which is another step of a series of related research works a detailed investigation was made into magnetic

components to be used in 50kHz high power application going down to Maxwell Equation level analysis. Based on the theoretical findings new constructional techniques were developed to address the challenges of reducing losses, making the product compact and to reduce the weight.

The test results observed on the sample testing was very much encouraging and was reasonably in line with the theoretical predictions. The High frequency transformer shows a considerably low temperature rise and also a considerably low rate of temperature rise. This stands to confirm that the predicted drop in the losses due to interleaved winding has avoided a significant rise of conductor losses at high frequencies. However, when the system reaches the full power the temperature rise of the high frequency transformer can go further high. However, the calculations carried out based on the testing completed it can be concluded that the product will not research the temperature limit of the insulation class. Furthermore, it can be seen that the rating of the heat sinks of the enclosure can be brought down giving the opportunity to further reduce the overall size of the product.

The technique used in the air cored inductor also showed some positive results. However, the need was identified to develop the mathematical model giving the optimum separation of the winding layers based on the frequency and the power it is supposed to handle.

Transformers and inductors in the electrical systems are responsible for approximately one third of the total network losses. These losses can be considered as power utility costs, costs to society and cost to the environment itself (Guillod et al., 2017b). Further with the development of power electronic techniques, pulse-width modulated (PWM) inverters are widely used to control electrical machines, to feed transformers and to interface renewable energy systems (Leibl et al., 2016). The output voltages of PWM inverters contain high frequency harmonics. The presence of these harmonics increases the total losses in the system.

Also, in the future DC electric power systems, high power DC –DC converters will play a major role as they will substitute today's bulky 50/60Hz transformers. The medium frequency transformers operating in the range of 4 kHz is a key component of DC-to-DC converters. They serve the purpose of isolation and voltage step up/ step down function (Acero et al., 2006). The power ratings of these medium frequency transformers easily reach the level of 1 MW. As they operate at a reasonably high frequency for high power applications (4kHz) the importance of considering the effects addressed in this paper become vital.

In depth understanding of the behavior of magnetic components in different applications such as the ones discussed above requires a clear awareness of the fundamental physical laws that govern the operation of them. Maxwell's equations give a comprehensive mathematical

representation to physical laws governing the magnetic behavior. This mathematical approach lays the foundation for the analysis of phenomena like eddy current effect in the windings and in the core materials, proximity effects in the windings etc. Because of the level of complexity, that is present in modern magnetic applications, it is important that magnetic designers carry out detailed analysis on the behavior of magnetic components. Such consideration can save a significant amount of materials and saving of energy especially in the case of high power applications. The facts addressed in this paper needs to be extended further when it come to the application area of litz wires. In litz wire windings, skin and proximity effects needs to be further divided in top strand level and bundle level effects(Kieferndorf et al., 2016).

In this paper the attention is given to the evaluation of winding losses with the increased higher order harmonic presence. The necessity of expanding the model to assess the combined effect of several supper-imposed harmonics was identified. Considering the sum of losses of individual harmonic components would not give the right estimation, i.e. at the microscopic level the materials should be seeing only the combined effect of all the present harmonics. The materials are not subject to each present harmonic separately. Thus the resultant loses may be higher or lower than the sum of individual effects. A detail investigation on this aspect was carried out.

### 3.7 Summary

Rapid developments in the semiconductor technology and the power electronics industry enable the development of power supplies and power converters of significantly higher power levels. Considerably low switching losses of developments like SiC MOSFETs make it possible to operate at 2 to 5 times higher switching frequencies compared to their conventional counterparts. As the frequency goes high the magnetic components in such system become more and more compact. The magnetics components are usually the bulkiest components in a power electronics system and in most of the situations also the most expensive component, therefore it is of high interest of many designers to develop systems that operate at high frequencies.

The achievement of a high-power levels in a single module at high frequencies is next challenge faced by the developers of systems for high power applications. Most often the maximum power achievable with a single module is determined by the magnetic components. As a result, it could be seen that constraints in the development of magnetic components make a significant influence to the miniaturization of the power electronics system. Further it is reasonably accurate to state the magnetics components have a great impact on determining the power level and the operating frequencies of power electronics applications.

In the sections 3.1 to 3.33 theoretical explanation is given for the significant increase of losses in conductors of magnetic components which are excited by waveforms containing high frequency components of considerable magnitudes. Analytical estimation is also made for simplified practical cases. The theoretically looked at situations were tested on actual samples in the sections 3.4. The increase in the number of layers of conductors gives a considerable increase in conductor losses due to current density increases (multi-layer build up). This effect becomes significant as the frequency increases. The sandwiching of the windings in the case of HF transformer showed a contribution towards the reduction of the losses increase. As discussed in the thesis, the current research was focused on the use of analytical evaluations to more complicated and also more practical situations. Due to the significance of this phenomenon in the design of modern magnetic components it is worthwhile to carry out a numerical analysis to be able to address practical situations;

The research discussed in thesis was carried out with the intention of achieving compact, high power, high frequency transformers that are capable of handling power levels in excess of 100kW.

At high power levels the winding design becomes very important for the mitigation of high frequency losses. Two winding constructions are discussed in this paper. The novel method

proposed with folded foils showed very good performance in mitigating the high frequency conductor losses. Further it gives the possibility of controlling the leakage inductance between the primary and secondary windings by adjusting the level of overlap. The disadvantage observed in this method was the time consumed for the proper insulation process. Through several insulating techniques were considered the amount of time savings archived was not sufficient to adopt this method in mass production. Therefor further research is necessary to improve the production process for the successful implementation of this technique.

The second method proposed with sandwich winding could be seen as a good compromise on the performance and the amount of labor consumption.

The tests carried out with a standard enclosure showed that the amount of heat transferred to the cooled plate was not sufficient to maintain the host spot temperature below the desirable level. However, the desirable conditions could be archived with an enclosure with correctly engineered interior.

It could be concluded that with the appropriate material selection, winding techniques and with the thermal management techniques the construction of a 100 kW high frequency transformer could be archived. The product showed very stable performance and presented a very compact construction giving a volume to power density of over 18 W/cm<sup>2</sup> or weight to density of over 6.5kW/kg. This was a considerable reduction in the size and volume against the conventional ferrite construction considered.

Further tests studies carried out showed the possibility of achieving even higher powers such as 150 kW or even 200 kW in a single high frequency transformer operating at a frequency range of 20 kHz to 30 kHz with a compact construction is possible in a similar compact structure. In parallel with the industry demand the research was continued towards these power levels.

As a result of these continued work a winding arrangement that enables the handling of high frequency large currents in high frequency magnetics could be arrived at. Details of this was discussed in this chapter under the section 3.5. this method is now patented and considered as a game changer as this technology very much eliminates the practical difficulties in achieving high power levels even up to MW range at frequencies as high as 50 kHz.

# Chapter 4

## Core Losses Estimation of High-Power High Frequency Magnetics

## Chapter 4 Core losses estimation of high-power high frequency magnetics

In 1892, even before the microscopic magnetization process was defined, Charles Proteus Steinmetz (Steinmetz, 1892, Villar, 2010) introduced an expression for the characterization of magnetic loss density. From the analysis of various loss curves, Steinmetz ended up with this expression.

$$P_s = \eta B_m^b \quad 4 - 1$$

where  $\eta$  and  $b$  are determined by the material characteristic, and  $B_m$  is the peak induction value in a bidirectional magnetization case. Nowadays, a more general expression is widely used in the design of magnetic power devices, like transformers, electric machines or inductors.

$$P_s = K f^a B_m^b \quad 4 - 2$$

where  $K$  and  $a$  and  $b$  are determined by the material characteristic, and  $f$  is the frequency of the sinusoidal waveform. As well as the Steinmetz equation, a usual proceeding to analyze core loss in more detail is to break it up into three separate terms: static hysteresis loss  $P_h$ , classic eddy current loss  $P_e$ , and excess eddy current or anomalous loss  $P_a$ . Therefore, it is assumed that three different physical effects are contributing to magnetization losses. It should be noted that this procedure is mainly applied in the characterization of electric machines.

$$P_s = P_h + P_e + P_a \quad 4 - 3$$

Another usual procedure to get magnetization losses is the determination of the hysteresis model. The static hysteresis model is usually used in combination with the loss separation approach, while more complex models have been proposed lately which consider the dynamic behavior of the magnetic material. Most of the hysteresis models can be sorted out in two model categories, the Jiles-Atherton model (Jiles et al., 1992) and the Preisach model (Preisach, 1935, Villar, 2010), although also other simplified models can be found in the literature. However, in order to understand the variety of characterization methodologies a short description of the hysteresis will be introduced (Villar, 2010).

## 4.1 Magnetic Hysteresis

The phenomenon exhibited by a system, often a ferromagnetic material, in which the reaction of the system to changes is dependent upon its past reactions to change. Magnetization process can be divided into several steps. In the demagnetized state, all domains cancel each other resulting in a zero magnetic field. When an external magnetic field is applied, the magnetic domains change from an initial reversible magnetization state, to an irreversible one. In this state, the domain walls are first displaced and then rotated in another reversible state, and finally a saturation state is reached where all domains are aligned. Depending on the magnetization processes and the history of the material, the magnetic characteristic describes different curves, i.e. different types of hysteresis behaviors, some of them are illustrated in figure 4-1. The major loop is the magnetization curve when the applied field is high enough to force the material into saturation, closing the loop at the tips. Every loop inside the major loop is defined as a minor loop, these loops can be asymmetric or symmetric with respect to the origin. In the case of transformer cores, the magnetization is always symmetric like the minor loops illustrated in figure 4-. The initial magnetization curve is the transition of the magnetization induction from the initial condition of zero flux to the tip of the major loop.

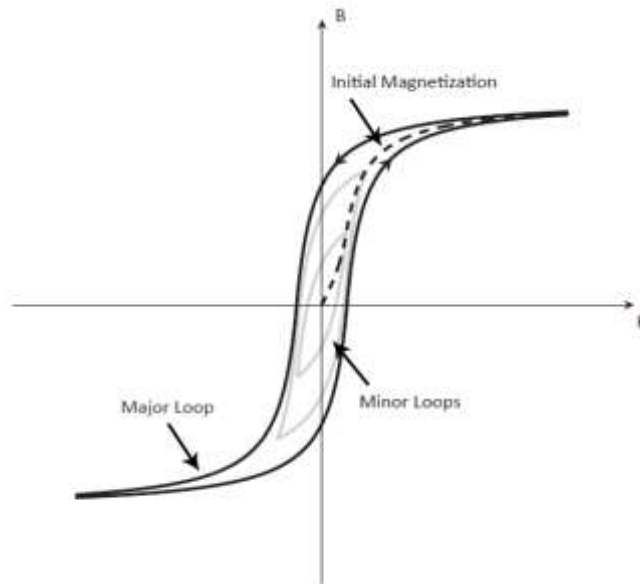


Figure 4-1 Types of hysteresis loops and magnetization curves.



### 4.11 Hysteresis Models

As presented before, there are two main hysteresis models currently applied in circuit simulation or finite element analysis, the Jiles-Atherton (Jiles and Atherton, 1984) model and the Preisach (Preisach, 1935) model. In addition, the simplicity of the Chan-Vladirimescu (Chan et al., 1991) model, makes it an attractive solution to be used with core materials where the steady-state magnetization processes are symmetrical and the hysteresis loop is longitudinal. The main characteristics of the three methods are briefly introduced in the following section.

#### Jiles-Atherton Model

The model of Jiles and Atherton (Jiles and Atherton, 1984) was developed between 1983-1986 and separates the hysteresis loop on the reversible magnetization  $M_{rev}$ , or anhysteretic curve, and the irreversible one  $M_{irr}$ , or the equivalent loss energy.

$$M = M_{rew} + M_{irr}$$

4 - 4

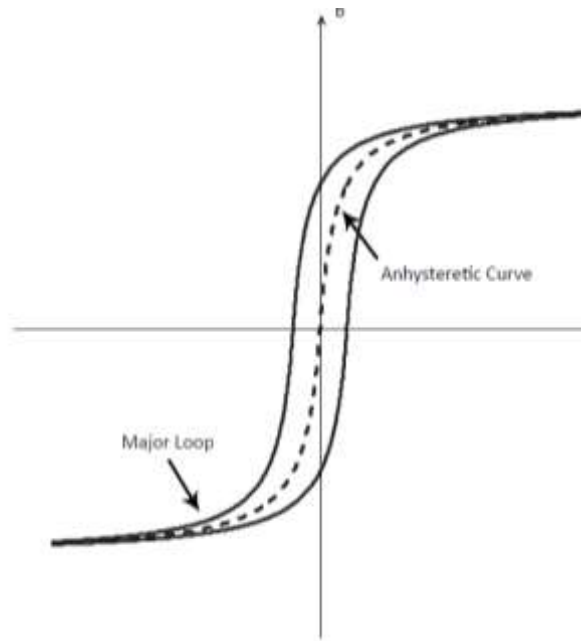


Figure 4-2 Anhysteretic curve and mayor loop(Villar, 2010).

The anhysteretic curve, illustrated in figure 4-2, is characterized by a modified Langevin function.

$$M_{an} = M_s \left[ \coth\left(\frac{H_e}{A}\right) - \frac{A}{H_e} \right] \quad 4 - 5$$

where  $A$  Anhysteretic curve and mayor loop. Anhysteretic curve and mayor loop modifies the curvature of the function and  $H_e$  is the effective applied field,

with

$$H_e = H + M \quad 4 - 6$$

$H$  and  $M$  representing the iteration between domains. The expression of the irreversible magnetization is obtained from a lumped model of the losses determined from the domain wall displacement.

$$\frac{M_{irr}}{dH} = \frac{M_{an} - M}{\frac{\delta k}{\mu} - \alpha(M_{an} - M)} \quad 4 - 7$$

where  $k$  represents the energy dissipation and is the direction of the applied field (+1 for positive and -1 for negative slope). And finally, the total magnetization rate is obtained from the relative ratio, given by  $c$ , between the reversible and the irreversible magnetizations.

$$\frac{dM}{dH} = \frac{1}{1 + c} \frac{M_{an} - M}{\frac{\delta k}{\mu} - \alpha(M_{an} - M)} + \frac{c}{1 + c} \frac{dM_{an}}{dH} \quad 4 - 8$$

One of the difficulties with the Jiles-Atherton model is the extraction of model parameters, already pointed out in (Jiles et al., 1992). The algorithm requires nine experimentally measured parameters. (1) The coercivity  $H_c$ , (2) the remanence  $B_r$ , (3) the initial susceptibility  $\chi_0$ , (4) the initial anhysteretic susceptibility  $\chi_{an}$ , (5) the differential susceptibility at the coercive point  $\chi_0 H_c$ , (6) the differential susceptibility at remanence  $\chi_0 B_r$  and (7)(8) the maximum magnetization points ( $H_{max}$ ,  $M_{max}$ ) on the loop tip, as well as (9) the differential susceptibility of the initial magnetization curve at the same point,  $\chi_0 M_{max}$ . The algorithm yields to the five

previously mentioned model parameters,  $M_s$ ,  $a$ ,  $k$ ,  $\alpha$ , and  $c$ . The model parameters are extracted from the initial magnetization curve, the major loop and the anhysteretic curve, which can be determined from the major hysteresis loop.

## Preisach Model

The model of Ferenc Preisach (Preisach, 1935) has survived to more than 60 years of scientific analysis and competition with other models that have been forgotten. The original Preisach model, or the classical Preisach model, was forgotten until the Russian mathematician Krasnoselskii came across the model and understood the general mathematical idea (Mayergoyz, 1986), introducing the algebraic theory of the model. From the work carried out by Krasnoselskii, Issak D. Mayergoyz introduced and analyzed the properties of the model, as well as the required experimental data for its characterization. One of the greater controversies around the Preisach model is its phenomenological character. Even if the model does not have any relationship with the physical processes occurring in the magnetization process of magnetic materials, it reproduces the hysteresis curve and the field history with a great reliability. Nevertheless, it does not explain what happens in the material. The Preisach method uses a finite number of bistable units which consider the previous state of the material as well as its future evolution, see figure 4-3.

Susceptibility, relationship between magnetization  $M$  and magnetic field  $H$ ,

$$X = \frac{M}{H}$$

4 - 9

The combination of these finite number of bistable units  $(\mu_i, \mu_j)$ , describes the evolution of the magnetic material. If  $H_{sat}$  represents the saturation magnetic field and  $B_{sat}$  the corresponding saturation induction of the material, when the applied field is  $H > H_{sat}$ , all bistable units are positive and the induction is  $B = B_{sat}$ . However, if the applied field is  $H < -H_{sat}$ , all bistable units are negative and the induction is  $B = -B_{sat}$ . Therefore, these bistable units must satisfy  $\mu_i < H_{sat}$  and  $\mu_j > -H_{sat}$ , and as the hysteresis phenomena is dissipative, then  $\mu_i > \mu_j$ . These three conditions define the Preisach plane illustrated in figure 4-3

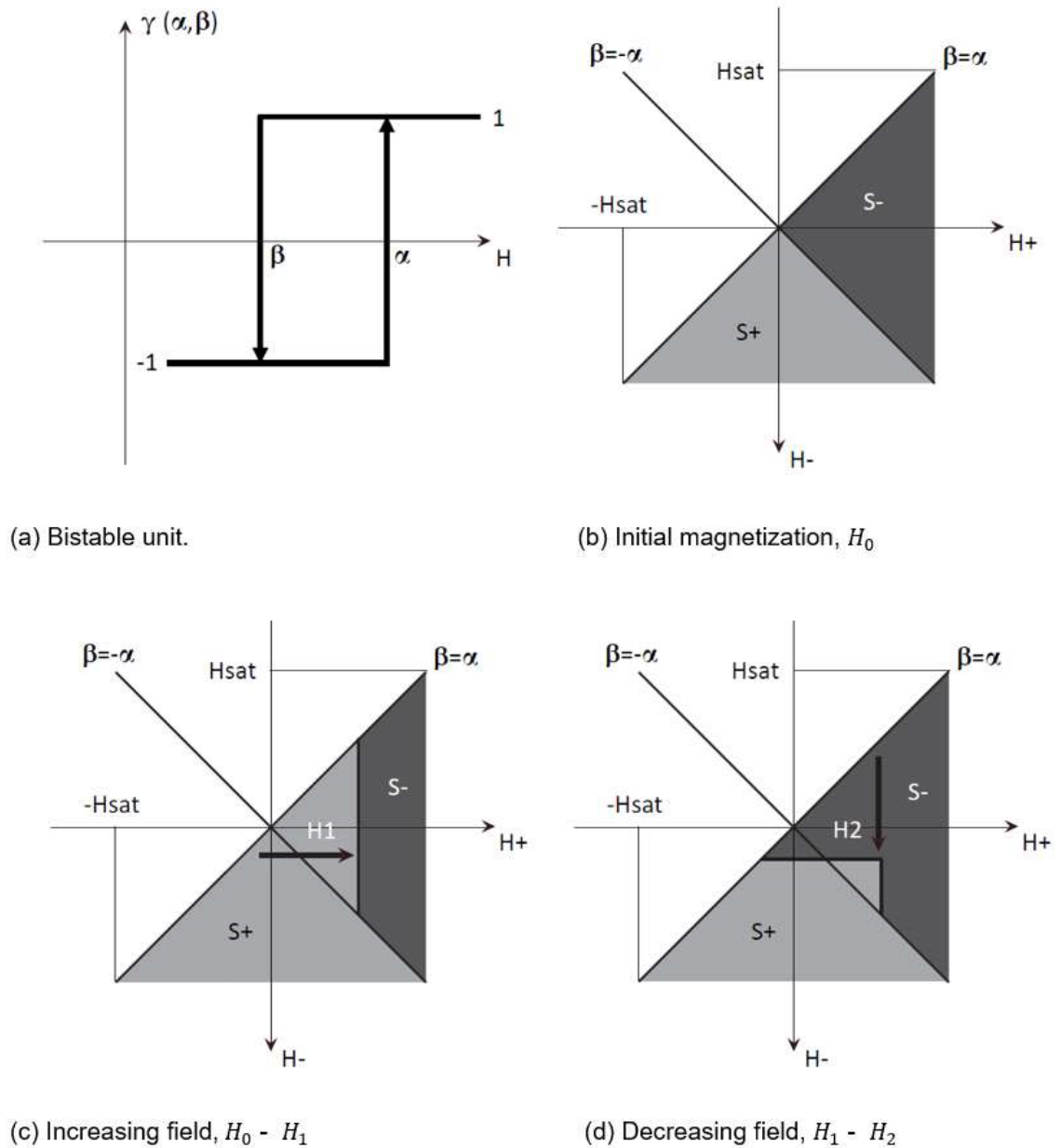


Figure 4-3 Figure 4.3 Preisach bistable unit and Preisach plane, or triangle. (a) Bistable unit. (b) Initial magnetization,  $H_0$  (c) Increasing field,  $H_0 - H_1$  (d) Decreasing field,  $H_1 - H_2$

In the initial magnetization state, zero magnetization, the number of positive and negative bistable units must be the same ( $S^+ = S^-$ ), which is easily represented on the Preisach plane by distributing equally the bistable units within the triangle using the  $\beta = -\alpha$  symmetry line (see Fig.4.3b). When the applied field is increased  $H^+$ , the corresponding  $\alpha$  axis bistable units are switched to their positive state (see Fig. 2.27c,  $S^+ > S^-$ ). On the contrary, if the field is reduced

$H^-$ , the corresponding axis bistable units are switched to their negative state (see Fig. 2.27d,  $S^+ < S^-$ ). The calculation of the net magnetization is the integration of the positive and negative bistable units. A specific magnetic material is characterized with a distribution function  $\mu( , )$ , known as Preisach function or weighting function, that describes the weighting values of each bistable unit in the Preisach plane. The main difficulty with the Preisach model lies on the determination of this density function. The Preisach distribution function can be implemented using an Everett integral (Mayergoyz, 1986, Villar, 2010), which requires several experimental first order reversal curves for its correct characterization. Another way of getting the density function lies on the supposition that the distribution function describes a specific pattern, like a Lorentzian (Bertotti, 1992) or Gaussian function (Della Torre and Vajda, 1994). The simplest of the procedures to determine the distribution function is described in (Hui and Zhu, 1995) where only the mayor loop is required.

#### Chan-Vladimirescu Model

The Chan-Vladimirescu model (Chan et al., 1991) employs only manufacturer supplied data like the coercitivity  $H_c$ , the maximum magnetic induction  $B_s$  and its corresponding magnetic field  $H_s$  as well as the remanence  $B_r$ . The magnetic characteristic is described with two hyperbolic curves. The upper branch of the loop, or the downward part of the loop ( $H_s$  )  $-H_s$ ), is given by:

$$B + (H) = B_s \frac{H + H_c}{|H - H_c| + H_c \left( \frac{B_s}{B_r} - 1 \right)} \quad 4 - 10$$

The lower branch of the loop, or the upward part of the loop ( $-H_s$  )  $H_s$ ), is given by:

$$B - (H) = B_s \frac{H - H_c}{|H - H_c| + H_c \left( \frac{B_s}{B_r} - 1 \right)} \quad 4 - 11$$

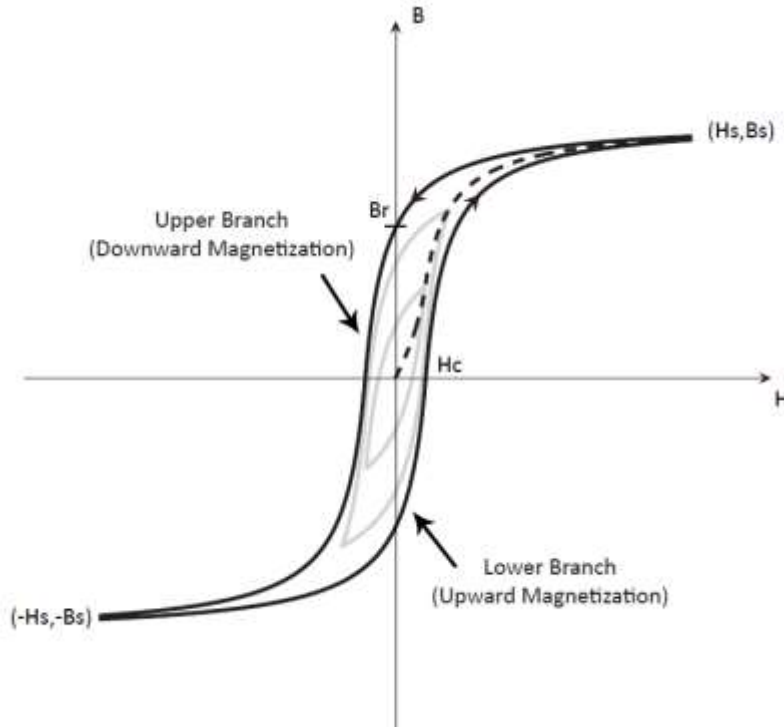


Figure 4-4 Chan-Vladimirescu model with initial magnetization curve, mayor loop and minor symmetrical loops(Chan et al., 1991)

The initial magnetization curve is deduced from the average value of the upper and lower branches.

$$B_{mag}(H) = \frac{B + (H) + B - (H)}{2} \quad 4 - 12$$

In order to characterize the minor loops of the material, the upper branch is reduced by a  $B_d$  magnetization induction value, while the lower branch is increased by the same value.

Upper Branch

$$B(H) = B + (H) - B_d \quad 4 - 13$$

Lower Branch

$$B(H) = B - (H) + B_d \quad 4 - 14$$

The intersection of the upper and lower branches of the minor loop will lie on the magnetization curve  $B_{mag} = H$ . These intersection points are just the extreme points of the minor loop, and

the difference between the upper or lower mayor branches and the magnetization curve in those extreme points will determine the  $B_d$  magnetization induction value.

### Loss Separation Approach

Traditionally core loss has been divided up into two terms: hysteresis loss  $P_h$  and eddy current loss  $P_e$  .

$$P_v = P_h + P_e \quad 4 - 15$$

where

$$P_h = k_h f B_m^b \quad 4 - 16$$

and

$$P_e = k_e f^2 B_m^b \quad 4 - 17$$

However, the traditional two term method assumed that the magnetization process was perfectly homogeneous in space, which was latter on proven to be incorrect. Although there were already some theories about the anomalous behavior of magnetic materials, Bertotti (Bertotti, 1986) introduced a physical explanation of this excess phenomena and a generally approved expression. According to Bertotti, the excess in dynamic loss is a consequence of domain wall motion.

$$P_s = P_h + P_e + P_a \quad 4 - 18$$

with

$$P_a = k_a f^{1.5} B_m^{1.5} \quad 4 - 19$$

$P_a$  is referred to as the excess or anomalous loss and  $k_a$  is related to the material cross-sectional area  $A$ , conductivity and a parameter which describes the material microstructure  $\sigma$ , as well as a numerical constant  $G$ .

$$k_a = 8\sqrt{\sigma G A \eta_0} \quad 4 - 20$$

Excess eddy current loss calculation is not straightforward. Manufacturers do not supply information about the microstructure of the material, so curve fitting is necessary to get the parameter  $k_a$  related to excess loss. Classical eddy current loss expression  $P_e$  derives from Maxwell equations. The time average eddy current loss, per unit volume, is determined by getting a widely used expression.

$$P_e = \frac{\pi^2 d^2}{6\rho} f^2 B_m^2$$

4 - 21

From the average eddy current loss expression, the constant  $k_e$  related with the loss separation approached is established.

$$k_e = \frac{\pi^2 d^2}{6\rho}$$

4 - 22

Usually for the characterization of hysteresis loss the primitive expression of the Steinmetz equation, without frequency parameter, is used.

$$P_h = K f B_m^b$$

4 - 23

If the parameters  $b$  and  $K$  of the primitive Steinmetz equation are not provided by the manufacturer a curve fitting is necessary. As well as the Steinmetz primitive equation, the primitive hysteresis models (static models) are used in some cases.

Time Domain, General Expression

The expressions introduced up to now are only valid for sinusoidal excitation cases, therefore, so as to get magnetic losses for a more general case, a time domain expression has been developed (Lin et al., 2004, Roshen, 2007). This new general expression has to be consistent with the sinusoidal expression in the frequency domain. On the one hand, in the case of excess loss, an expression that will fit correctly with the sinusoidal expression is.

$$P_a(t) = k_2 \left( \frac{dB(t)}{dt} \right)^{1.5}$$

4 -24



The time average value of a sinusoidal flux density for this new expression is equated to the sinusoidal frequency domain expression.

$$P_a = k_2 \frac{1}{T} \int_0^T \left( \frac{dB(t)}{dt} \right)^{1.5} dt \quad 4 - 25$$

$$dt = k_a f^{1.5} B_m^{1.5} \quad 4 - 26$$

From where the new constant parameters will be defined,

$$k_2 = \frac{k_e}{\sqrt{2\pi} \int_0^{2\pi} \cos(\theta)^{1.5} d\theta} \quad 4 - 27$$

On the other hand, in the case of classical eddy current loss, a similar procedure is applied to get the time domain expression.

$$P_e = k_1 \frac{1}{T} \int_0^T \left( \frac{dB(t)}{dt} \right)^2 dt \quad 4 - 28$$

$$dt = k_a f^2 B_m^2 \quad 4 - 29$$

from where,

$$k_1 = \frac{k_e}{2\pi^2} \quad 4 - 4-30$$

Regarding hysteresis loss, the equivalent elliptical loop introduced by Lin (Lin et al., 2004) is used. Magnetic loss density is defined as,

$$P_h = \frac{1}{T} \int_0^T H(t) \frac{dB(t)}{dt} dt \quad 4 - 31$$

The hysteresis loop can be decomposed in two components; a reversible component, and a irreversible component related to the hysteresis loss. Consequently, the instantaneous hysteresis loss will be,

$$P_h(t) = H_{irr}(t) \frac{dB(t)}{dt}$$

4 - 32

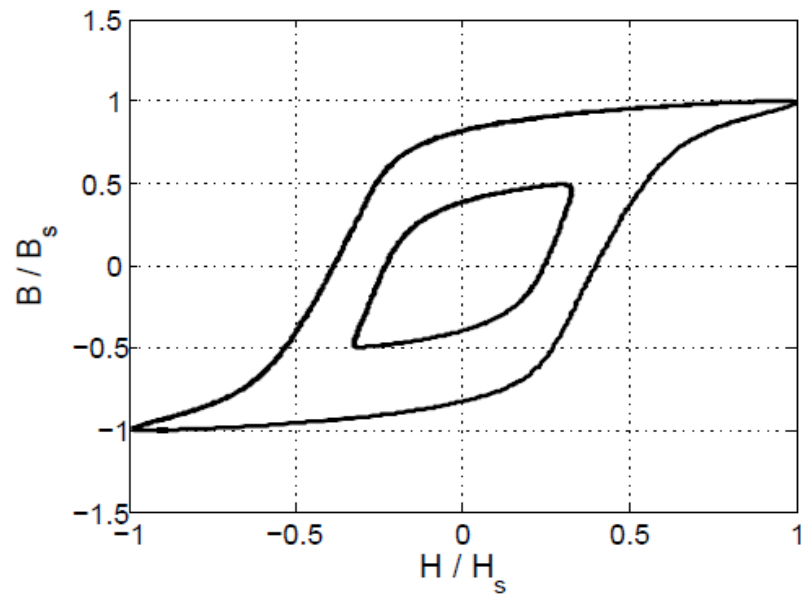


Figure 4-5 Figure 4.5 Magnetic characteristic BH loop.

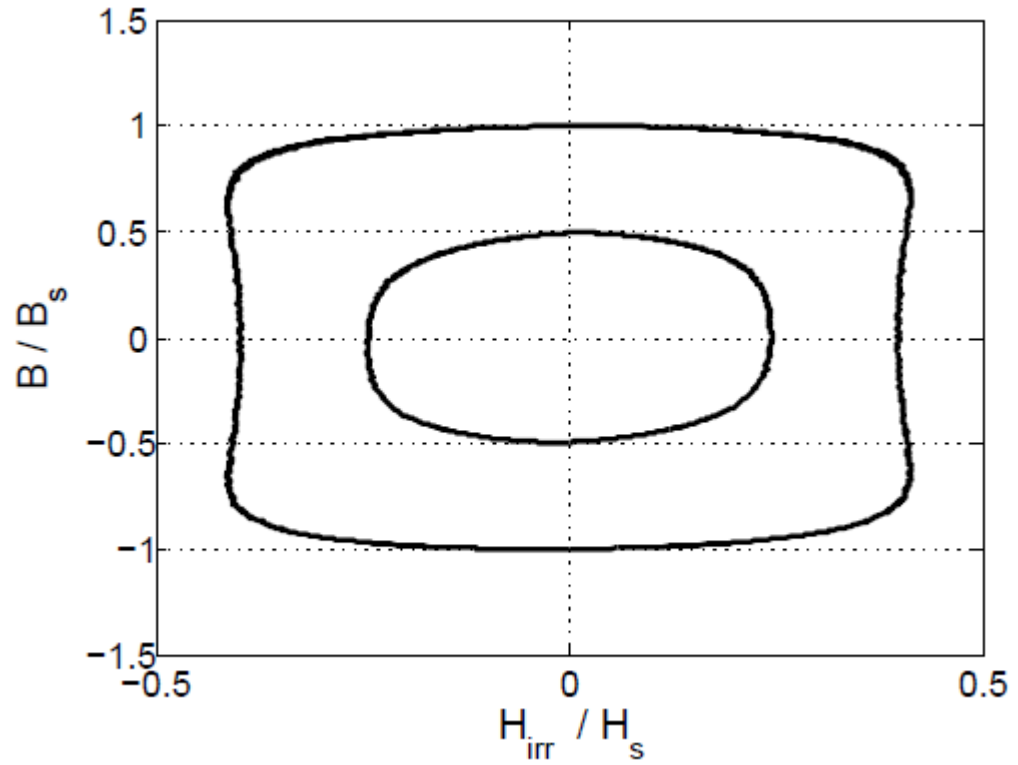


Figure 4-6 Magnetic characteristic and equivalent elliptical loop

The irreversible component of the magnetic loop describes an ellipse see figure 4-6 that can be defined as,

$$B = B_m \sin(\theta) \quad 4 - 33$$

$$H_{irr} = H_m \cos(\theta) \quad 4 - 34$$

Equating the surface of the elliptical loop for a sinusoidal excitation case,

$$P_h = H_m B_m 2\pi \frac{1}{T} \int_0^T \cos^2(2\pi f t) dt \quad 4 - 35$$

$$P_h = H_m B_m \pi f \quad 4 - 36$$

with the time-average hysteresis loss for sinusoidal excitation  $k_h f B_m$ , the representation for  $H_m$  is obtained, and consequently  $H_{irr}$ .

$$H_{irr} = \pm \frac{1}{C_b} k_h |B_m \cos(\theta)|^{b-1}$$

4 - 37

finally, the instantaneous hysteresis loss expression will be,

$$P_h(t) = \pm \frac{1}{C_b} k_h |B_m \cos(\theta)|^{b-1} \left( \frac{dB(t)}{dt} \right)$$

4 - 38

where,

$$C_b = 4 \int_0^{\pi/2} \cos^b(\theta) d\theta$$

Taking into account the developments carried out for each of the loss terms, the time domain general expression for the loss separation approach is reached,

$$P_s = k_0 \frac{1}{T} \int_0^T |B_m \cos(\theta)|^{\beta-1} \left( \frac{dB(t)}{dt} \right) dt + k_1 \frac{1}{T} \int_0^T \left( \frac{dB(t)}{dt} \right)^2 dt + k_2 \frac{1}{T} \int_0^T \left( \frac{dB(t)}{dt} \right)^{1.5} dt$$

4 - 39

where,

$$k_0 = \pm \frac{k_h}{4 \int_0^{\pi/2} \cos^b(\theta) d\theta}$$

4 - 40

$$k_1 = \frac{k_e}{2\pi^2}$$

4 - 41

$$k_2 = \pm \frac{k_a}{\sqrt{2\pi} \int_0^{2\pi} \cos(\theta)^{1.5} d\theta}$$

4 - 42

This three-part expression is usually used in the characterization of electric machines, where the magnetic parts are made of rolled steel and the determination of classical eddy current effects are straightforward.

## 4.2 Empirical Methods,

### 4.21 Steinmetz Equation

Another major group of core-loss calculation methods is based on empirical measurement observations. One of the advantages of these methods is that they are easy to use, especially to designers who do not have much expertise on magnetism. Lacking of physical bases, empirical methods are usually applicable to particular material and operating conditions. Loss in the magnetic material is often predicted using a power law equation:

$$P_s = K f^a B_m^b$$

4 - 43

where  $B_m$  is the peak flux density value of the ac waveform (if the flux density waveform has no time average).  $K$ ,  $a$  and  $b$  are determined by the material characteristic and usually obtained from the manufacturer's datasheet. For different magnetic materials, different values are used. The Steinmetz equation is basically a curve fitting of measured core-loss density under sinusoidal magnetization waveform. Therefore, it can be extracted from the manufacturers data, and without knowing the detailed material characteristics. The empirical Steinmetz equation has proven to be the most useful tool for the calculation of magnetization losses. It requires only three parameters, which are usually provided by the manufacturer. For sinusoidal flux waveform it provides a high accuracy and is quite simple to use. However, the original Steinmetz equation (OSE) and the corresponding set of parameters fail to represent correctly losses for non-sinusoidal waveforms. There is no direct and clear way to extend the Steinmetz equation to arbitrary operating waveforms, like in the case of the loss separation approach. Intuitively, it has been tried to apply a Fourier transform to any arbitrary waveform to obtain a series of sine waves, applying the Steinmetz equation to each frequency component. However, the summation of calculated losses of each frequency is not the total core loss, because there is no orthogonality between different orders of harmonics. Furthermore, it is not universally appropriate to apply the Fourier transform to a magnetic component (Reinert et al., 2001), which is non-linear inherently. Lately, derivations of the Steinmetz equation have been published to deal with non-sinusoidal waveforms, where general time dependent compact expressions have been developed. The Modified Steinmetz Equation (MSE), the Improved Generalized Steinmetz Equation (IGSE) or the Natural Steinmetz Extension (NSE), the Waveform-coefficient Steinmetz Equation (WcSE) and the Equivalent Elliptical Loop (EEL)

have been proposed to extend the original Steinmetz equation to non-sinusoidal applications, using only the Steinmetz parameters provided by the manufacturer.

## 4.22 Modified Steinmetz Equation

According to (Reinert et al., 2001), the macroscopic magnetization rate  $dM/dt$  is directly related to the core losses. The task is then to replace the frequency from the Steinmetz equation with the physical loss parameter  $dM/dt$  which is proportional to the rate of change of magnetic induction,  $dB/dt$ . This method introduces an equivalent frequency which is related to the magnetization rate. Based on physical understanding that loss depends on  $\frac{dB(t)}{dt}$ , (Reinert et al., 2001) averages  $\frac{dB(t)}{dt}$  over a flux excursion to get:

$$\left\langle \frac{dB(t)}{dt} \right\rangle = \frac{1}{\Delta B} \int_0^T \left( \frac{dB(t)}{dt} \right)^2 dt$$

4 - 44

Where  $B$  is the peak-to-peak flux amplitude and  $T$  is the period of the flux waveform. From the averaged magnetization rate an equivalent frequency  $f_{eq}$  can be calculated using the normalization constant  $2/B^2$ :

$$f_{eq} = \frac{2}{\Delta B^2 \pi^2} \int_0^T \left( \frac{dB(t)}{dt} \right)^2 dt$$

4 - 45

Developing the theory, and supposing that the magnetization is repeated with a period of  $T_r = 1/f_r$ , (Reinert et al., 2001) states that the power losses can be described with:

$$P_s = (K f_{eq}^{a-1} B_m^b) f_r$$

4 - 46

### 4.23 Improved Generalized Steinmetz Equation (IGSE)

The improved generalized Steinmetz equation (IGSE) (Venkatachalam et al., 2002) and the natural Steinmetz extension (NSE)(den Bossche et al., 2004), although they have different names , they use the same expression to characterize core losses in case of a non-sinusoidal excitation. They both stem from the generalized Steinmetz equation (GSE) (Li et al., 2001). The generalized Steinmetz equation is developed from a general hypothesis for instantaneous core loss, which assumes that magnetic loss depends on the rate of change of the magnetic flux density and its instantaneous value(Lancarotte and Penteado, 2001).

$$P_s(t) = P_d \left( \frac{dB(t)}{dt}, B(t) \right)$$

4 - 47

The work carried out in this publication analyzes the behavior of FeSi steel sheets under different magnetization rates  $\frac{dB(t)}{dt}$  and induction levels  $B(t)$ . According to(Lancarotte and Penteado, 2001) , finding an expression depending on this two variables would lead to the definition of magnetic losses for all type of waveforms. A careful analysis of the work introduced in this article has to be done, because the term "average dissipated power" can lead to erroneous conclusions. Those waveforms which have the same magnetization rates and induction levels, will describe the same characteristic curve and will have the same average dissipated power. This fact can be verified in figure 4-10. The core of a FeSi transformer has been excited with three different waveforms, see figure 4-7, each of them with the same maximum voltage, which will consequently lead to the same rate of change of the magnetic flux density see figure 4-9. Moreover, the voltages have been applied with different frequencies and different duty cycles to reach the same maximum flux density. Due to the zero-voltage period on the 50Hz wave and the 100Hz wave see figure 4-7, the BH loop presents a slight difference in comparison to the 200Hz wave (see figure 4-10. During the zero voltage period, some of the energy is lost and consequently the area of the loop gets a bit wider. As mentioned before, the term dissipated power can be misunderstood. The conclusion to this test is that the energy (the area of the loop), is the same. However, the power will increase linearly because this loop has to be multiply with the waveform frequency. Based on this fact the proposed generalized Steinmetz equation (GSE) will look like,

$$P_s = \frac{1}{T} \int_0^T k_1 \left| \frac{dB(t)}{dt} \right|^a |B(t)|^{b-a} dt$$

4 - 48

However, according to (Venkatachalam et al., 2002), the dependence of the instantaneous loss on the instantaneous parameters only, is a potential problem, which is solved in the proposed Improved Generalized Steinmetz Equation (IGSE). The Natural Steinmetz Extension (NSE) (den Bossche et al., 2004) is introduced some time later, and although it looks a bit different in a first sight, actually it uses the same expression.

Measurements carried out in a FeSi transformer in order to verify the magnetic induction slope dependency.

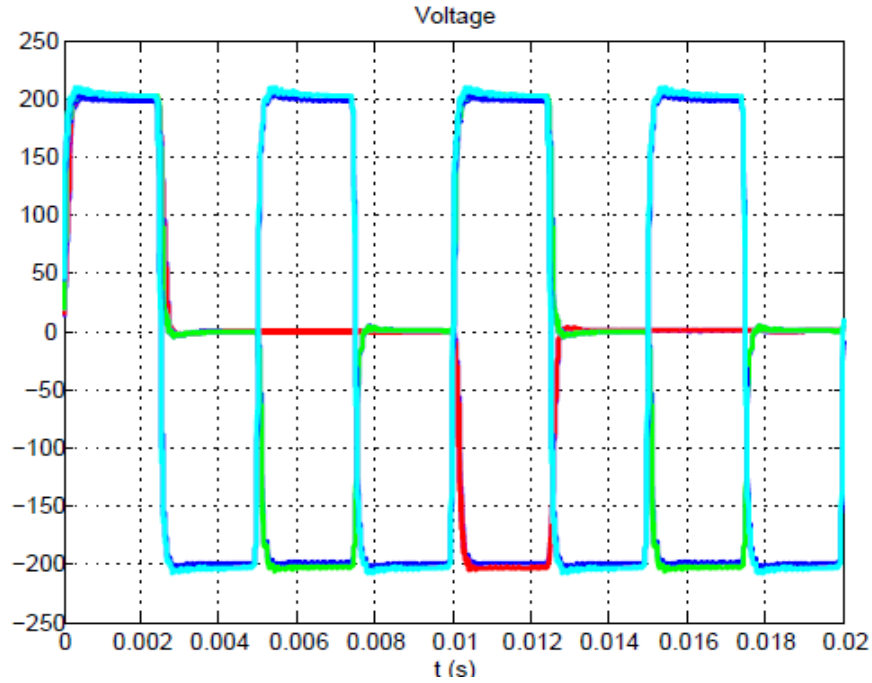


Figure 4-7 Excitation voltage.



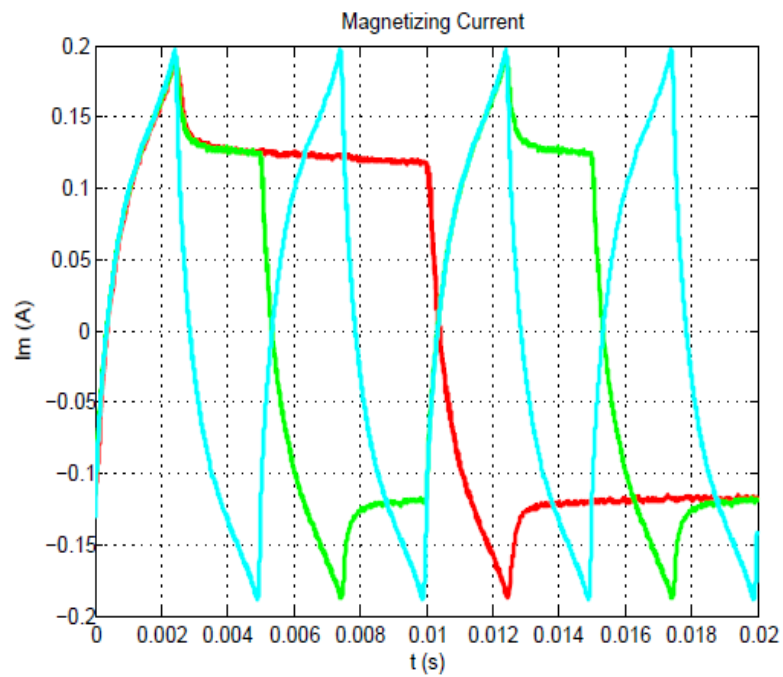


Figure 4-8 Magnetizing current.

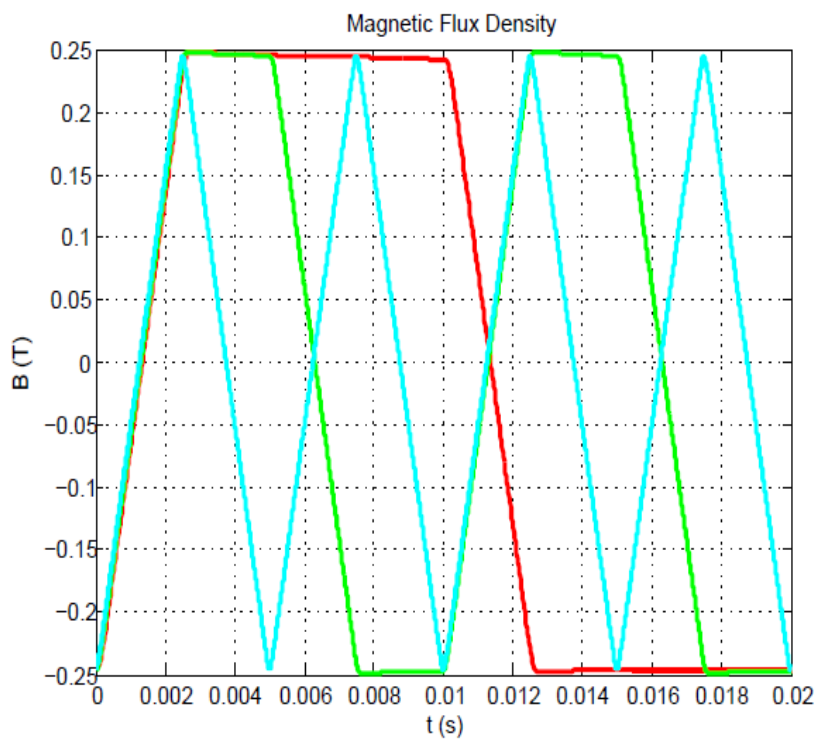


Figure 4-9 Magnetic induction.

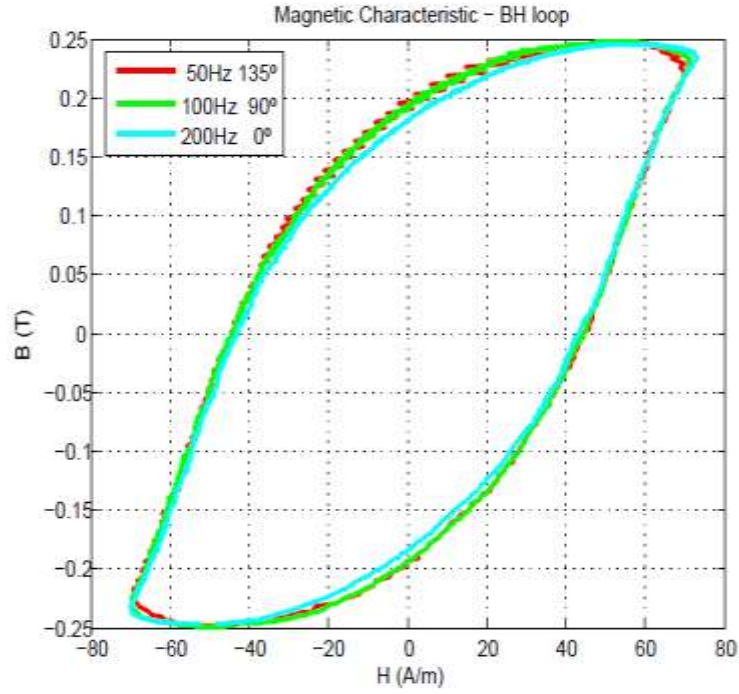


Figure 4-10 BH loop

$$P_s = \frac{1}{T} \int_0^T k_i \left| \frac{dB(t)}{dt} \right|^a (\Delta B)^{b-a} dt$$

4 - 49

where,

$$k_i = \frac{K}{(2\pi)^{a-1} \int_0^{2\pi} |\cos(\theta)|^a 2^{b-a} d\theta}$$

4 - 50

which is determined equating the loss expression for a sinusoidal excitation case with the Steinmetz equation.

$$P_s = \frac{1}{2\pi} k_i (2\pi f)^a B_m^b \int_0^{2\pi} |\cos(\theta)|^a 2^{b-a} d\theta$$

4 - 51

$$P_s = K f^a B_m^b$$

4 - 52

#### 4.24 Equivalent Elliptical Loop (EEL)

Apart from the expression proposed for the time dependent hysteresis loss introduced in the previous section, (Lin et al., 2004) proposes a modified Steinmetz equation based on the same development. The only difference lies in the frequency exponent of the Steinmetz equation that is introduced in this case:

$$P_s(t) = |C| \left| \frac{dB(t)}{dt} \right|^a \quad 4 - 53$$

Where

$$C = \pm \frac{1}{C_{ab}} K |B_m \cos(\theta)|^{b-a} \quad 4 - 54$$

and

$$C_{ab} = \frac{2}{\pi} (2\pi)^a \int_0^{\pi/2} \cos^b(\theta) d\theta \quad 4 - 55$$

#### 4.25 Waveform coefficient Steinmetz Equation (WcSE)

In (Shen, 2006) another concept is used to modify the Steinmetz equation, the waveform coefficient concept which correlates the Steinmetz equation with non-sinusoidal waveforms. This approach attempts to correlate the non-sinusoidal waveforms to the sinusoidal one with the same peak flux density, through calculating the "area" of the flux waveform. First of all, for the sinusoidal flux waveform, the integral of the half cycle is derived.

$$W_{sin} = \frac{1}{TB_m} \int_0^{T/2} B_m \sin(\omega t) dt = \frac{2}{\pi} \quad 4 - 56$$

Similarly, for example in the case of a rectangular voltage waveform and thereby a triangular flux waveform, the "area" of the triangular waveform is found for the same maximum flux density(Villar, 2010),

$$W_{sq} = \frac{4}{TB_m} \int_0^{T/4} \left( \frac{4B_m}{T} t \right) dt = \frac{1}{2}$$

4 - 57

From which the flux waveform coefficient, FWC, of the square voltage waveform (triangular flux waveform) can be defined as:

$$FWC_{sq} = \frac{W_{sq}}{W_{sin}} = \frac{\pi}{4}$$

4 - 58

So, according to(Shen, 2006), the core loss can be obtained from

$$P_s = FWC_{sq} f^a B_m^b$$

4 - 59

### 4.3 Magnetic material introduction

It is always expected that there could be a kind of “perfect” magnetic material with low loss, high saturation density, and high permeability. It can be used as cores of high frequency transformers, which will have a small size and a high efficiency. In reality, there is no such a “perfect” material existing, so a suitable material has to be selected for a particular application. This should be based on the understanding and characterization of different soft magnetic materials. Typical magnetic materials for high frequency transformers are explored in this chapter, and the nanocrystalline material is selected due to its superior loss and saturation characteristics. Magnetic materials have been so extensively used in a diverse range of applications, that the advancement and optimal utilization of magnetic materials would significantly improve the lives. Magnetic materials are classified in terms of their magnetic properties and their uses. If a material is easily magnetized and demagnetized then it is referred to as a soft magnetic material, whereas if it is difficult to demagnetize then it is referred to as a hard (or permanent) magnetic material. Materials in between hard and soft are almost exclusively used as recording media and have no other general term to describe them (Shen, 2006, Fish, 1990).

Table 4-1 Development of magnetism

<b>1600:</b>	<b>Dr. William Gilbert</b> published the first systematic experiments on magnetism in <i>"De Magnete"</i> ( <i>"On the Magnet"</i> ).
<b>1819:</b>	<b>Oersted</b> accidentally made the connection between magnetism and electricity discovering that a current carrying wire deflected a compass needle.
<b>1825:</b>	<b>Sturgeon</b> invented the electromagnet.
<b>1880:</b>	<b>Warburg</b> produced the first hysteresis loop for iron.
<b>1895:</b>	The <b>Curie</b> law was proposed.
<b>1905:</b>	<b>Langevin</b> first explained the theory of diamagnetism and paramagnetism.
<b>1906:</b>	<b>Weiss</b> proposed ferromagnetic theory.
<b>1920's:</b>	The physics of magnetism was developed with theories involving electron spins and exchange interactions; the beginnings of quantum mechanics.

The earliest observations of magnetism can be traced back to the Greek philosopher Thales in the 6th Century B.C (Shen, 2006, Meyer, 1971). However, it was not until 1600 that the modern

understanding of magnetism began (Feldtkeller, 1984). The following table is a brief list out scientists and milestone events significantly influencing the evolution history of magnetic material (Shen, 2006, Overshott, 1991). Transformers and inductors, as energy transmission and storage elements in power electronic converters, usually utilize soft magnetic materials as cores. The soft magnetic material cores perform the crucial task of concentrating and shaping magnetic flux. Power electronics designers need to be familiar with the properties of different kinds of soft magnetic materials, and should be able to choose suitable materials to fulfill specification for certain applications (McLyman, 2018).

“Most of pure elements in the periodic table are either diamagnetic or paramagnetic at room temperature. Since they present very small magnetism under the influence of an applied field, they normally are termed as non-magnetic (Shen, 2006). Another type of magnetism is called anti-ferro-magnetism, and the only pure element presenting this characteristic is Cr in natural environment. Fe, Co, and Ni are called ferro-magnetics, because very high levels of magnetism can be observed if a field is applied to these materials. Actually, pure single element ferromagnetic materials are seldom seen as magnets or cores in practical applications, and alloys composed of these elements and other ingredients are more widely used. Therefore, all of these alloys are also categorized as ferro-magnetics. The last type of magnetic material is classified as ferrimagnetic. Although they cannot be observed in any pure element, they can be found in compounds, such as the mixed oxides, known as ferrites (Albers-Schoenberg, 1958). In general ferri-magnetics exhibit better loss performance but lower saturation flux density, compared with ferro-magnetics. Therefore, material researchers are trying to improve both types of materials, such as, ferrites, amorphous, and silicon steel. Meanwhile, the efforts to discover new materials are ongoing. Characteristics of typical ferrites and amorphous will be discussed in the next section. As a new magnetic material, nanocrystalline material will be characterized, and the advantages and disadvantages will be summarized. Among all electrical, magnetic, and mechanical properties, the following characteristics of soft magnetics are of interests and can help us to select a suitable one for certain application:

- Core loss density (specific core loss) in W/kg ( $\text{W}/\text{cm}^3$ );
- Saturation flux density in Tesla;
- Relative permeability;
- Temperature characteristics.

### 4.31 Characteristics of conventional ferri- and ferro-materials

One decade ago, ferrites and amorphous were the only choices for high-frequency applications, due to their relatively low core loss density. These will be examined in detail from a high-frequency operation perspective.

### 4.32 Ferrites

Since the 1950's, ferrite materials have been developed for high-frequency applications because of their high electrical resistivity and low eddy current losses. The breadth of application of ferrites in electronic circuitry continues to grow. The wide range of possible geometries, the continuing improvements in the material characteristics and their relative cost-effectiveness make ferrite components the choice for both conventional and innovative applications(Albers-Schoenberg, 1958, Shen, 2006).

Ferrite is a class of ceramic material with a cubic crystalline structure; the chemical formula  $\text{MOFe}_2\text{O}_3$ , where  $\text{Fe}_2\text{O}_3$  is iron oxide and MO refers to a combination of two or more divalent metal (i.e. Zinc, Nickel, Manganese and Copper) oxides. The addition of such metal oxides in various amounts allows the creation of many different materials whose properties can be tailored for a variety of uses. Ferrite components are pressed from a powdered precursor and then sintered (fired) in a kiln. The mechanical and electromagnetic properties of the ferrite are heavily affected by the sintering process which is time-temperature-atmosphere dependent. The typical properties of MnZn and NiZn ferrites, according to data from Ferroxcube (previous Philips), are listed in Table 4-2 The saturation flux density ranges from 0.3~0.5 Tesla normally, and permeability varies from thousands to several tens of thousands. Typically, NiZn ferrites have lower saturation flux density and better loss performance, compared to the MnZn ones. Therefore, NiZn ferrites have been used for ultra-high frequency applications.

Table 4-2 Ferrites typical properties at 25°C(Shen, 2006)

Grade / Category	$B_{sat}(T)$	$\mu_i$	$\rho(\Omega m)$	$T_c(^{\circ}C)$	Thermal conductivity (W/(mK))
3F3 (MnZn)	0.45	2000	2	220	3.5 to 5
3C94(MnZn)	0.45	2300	5	220	3.5 to 5
3F45 (MnZn)	0.5	900	10	300	3.5 to 5
4B1 (NiZn)	0.35	250	$10^3$	250	3.5 to 5
4F1 (NiZn)	0.35	80	$10^3$	260	3.5 to 5

As the operating frequency increases, the core loss density of ferrites will increase as shown in figure 4-11, and permeability will reduce as shown in figure 4-12. These two effects must be considered for high-frequency transformer designs, since both of them could cause the designed transformer failure Ferroxcube, “Data sheets - Soft ferrite products and accessories”.

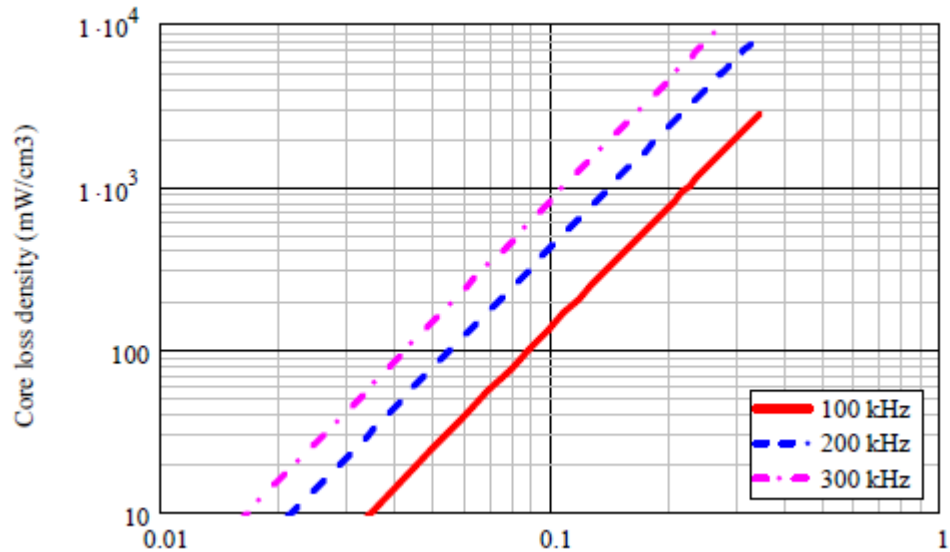


Figure 4-11 Ferrite 3F3 core loss density at 25 °C [65]

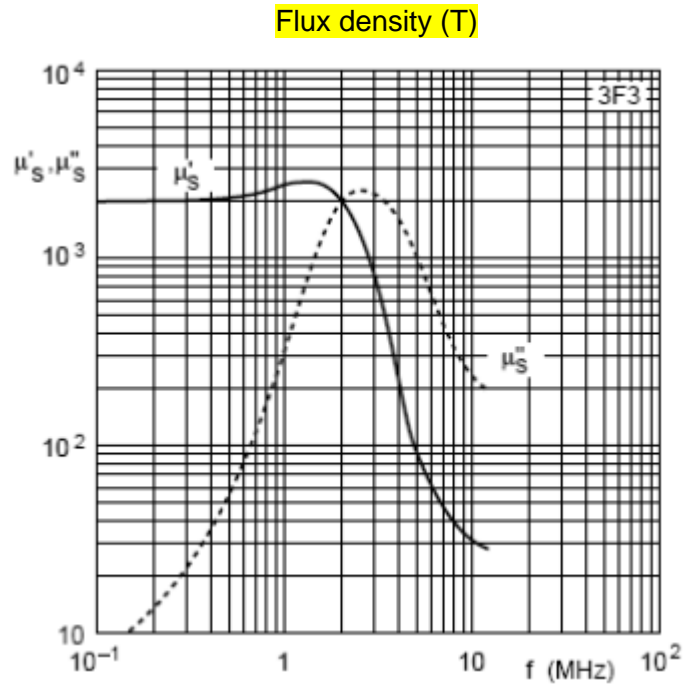


Figure 4-12 Ferrite 3F3 complex permeability as a function of frequency



The operating temperature of the ferrite should be below the Curie temperature where the magnetic material loses magnetic characteristics suddenly. Normally, the maximum continuous operating temperature of ferrites is below 125 °C. The development of high temperature ferrite (300 °C) has gained interests (Spyker et al., 2004), since the high temperature semiconductor devices like SiC was introduced. Within the specified temperature range, temperature dependency of ferrite characteristics concerns designers. Figure 4-13 shows the saturation flux density, initial permeability and core loss density variations of ferrite 3F3 under different temperatures.

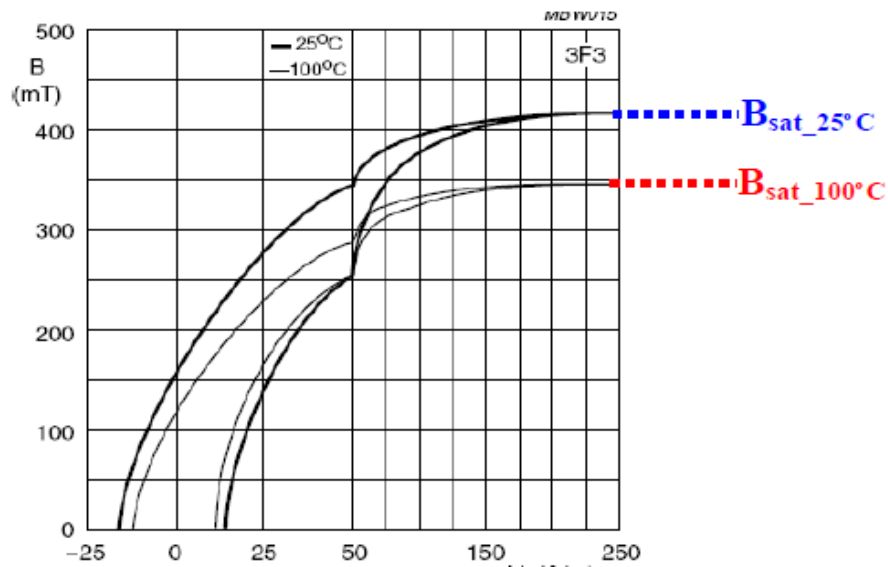


Figure 4-13 Ferrite 3F3 B/H curve

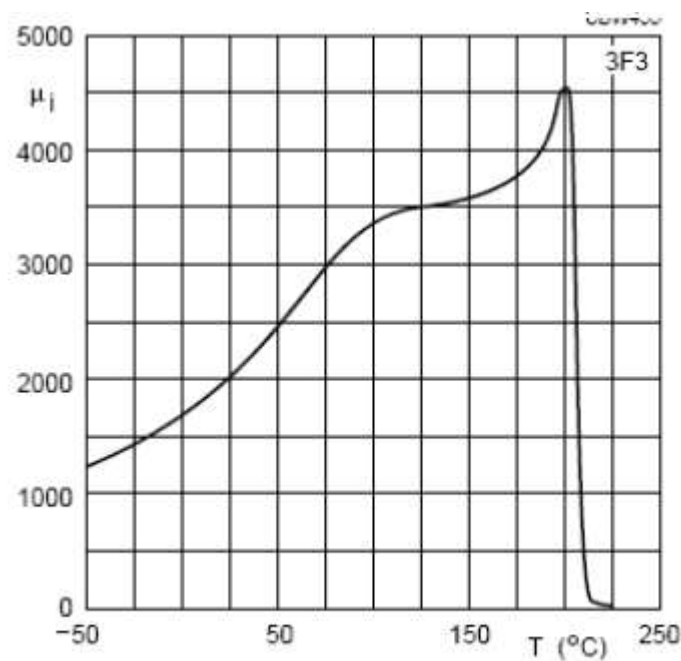


Figure 4-14 Ferrite 3F3 initial permeability as the function of temperature

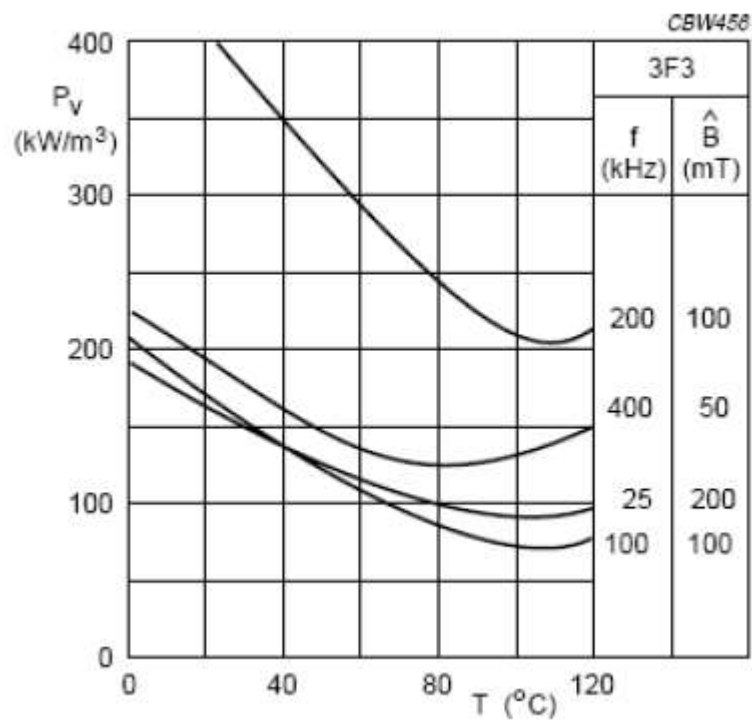


Figure 4-15 Ferrite 3F3 loss density as the function of temperature

The reduction of saturation flux density under higher temperature would consequently result in more margins for a particular design. The permeability variation can cause an inductance change, which will affect the circuit operation. The more sophisticated issue is the loss variation along the temperature. The design would be an iteration process indeed, since the losses have to be calculated under an assumed temperature, and then calculate temperature induced by the amount of loss obtained, and so on. Therefore, all the above-mentioned temperature dependent issues of ferrites actually inherently limit the feasibility of ferrites of high-frequency high density applications.

### 4.33 Amorphous metals

Ferrites have quite low losses at high frequency, but at the sacrifice of saturation flux density. Ferromagnetic materials were too lossy to be used for application above tens kilohertz, until the advent of rapid solidification technology (RST) in 1970s. Amorphous metals produced by RST have markedly improved properties. By quenching the alloy melt at rates of the order 106 K/s, the nucleation and growth of crystals are suppressed. The result is a solid ensemble of atoms that may justly be termed an amorphous metal or metallic glass. Amorphous metals have higher.

concentration of magnetic species than ferrites, promoting high saturation. They also exhibit lower coercivity due to the absence of metallurgical defects related to crystalline structure, have a higher electrical resistivity which requires thinner gauge tape for the higher frequency, if they are compared with conventional ferromagnetic crystalline materials(Overshott, 1979).

The typical properties of Fe-based and Co-based amorphous metals, according to data from Metglas (previous Allied Signals), are listed in Table 4-3. The saturation flux density ranges from 0.5~1.8 Tesla normally, and permeability varies from tens to hundreds of thousands Metglas, “Data sheets – Magnetic alloy”.

Table 4-3 Amorphous material typical properties at 25°C

Grade / Category	$B_{sat}(T)$	$\mu_i$	$\rho (\Omega m)$	$T_c(^{\circ}C)$	Thermal conductivity (W/(mK))
2605CO(Fe(Co))	1.8	400 000	$1.23 \times 10^{-6}$	415	9
2605S-3A(Fe(Cr))	1.41	35 000	$1.38 \times 10^{-6}$	358	9
2826MB(FeNi)	0.88	800 000	$1.38 \times 10^{-6}$	353	-
2705M (Co)	0.77	600 000	$1.36 \times 10^{-6}$	365	9
2714M (Co)	0.57	1 000 000	$1.42 \times 10^{-6}$	225	-

As shown in figure 4 -16, Fe-based amorphous material (Metglas 2605SA1) exhibits a higher loss density than Co-based amorphous (Metglas 2705M), which is similar to MnZn ferrite 3F3. Similar to ferrites, permeability of amorphous materials will reduce as frequency increases, shown in figure 4-11.

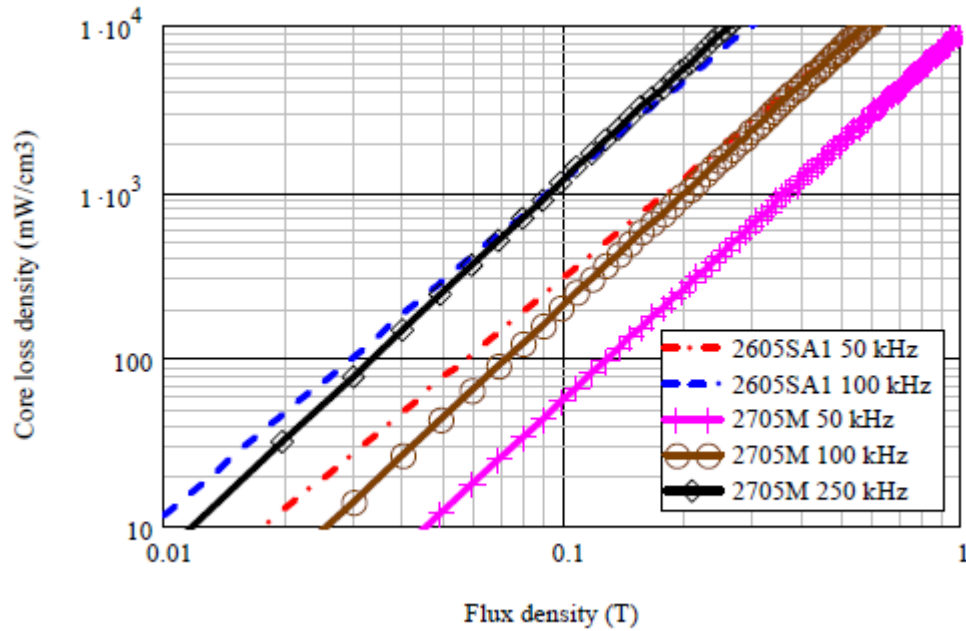


Figure 4-16 Typical Fe- and Co-based amorphous materials core loss density at 25 °C

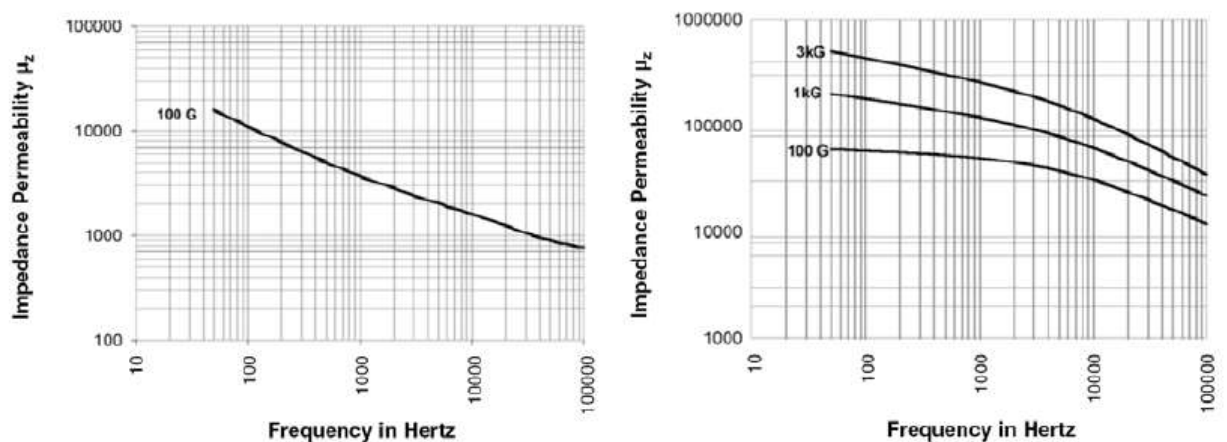


Figure 4-17 Amorphous 2605-3A and 2714A impedance permeability as a function of frequency [69]

The maximum allowed continuous operating temperatures of amorphous magnetic cores are determined mainly by insulation materials, which are applied between amorphous material layers. Amorphous metals also have temperature dependent characteristics to which a designer must pay respects. Since amorphous materials have a much higher permeability than ferrites, The temperature dependency can be suppressed by introducing air gaps into the magnetic loop.

#### 4.34 Supermalloy

One of the early major applications of magnetic devices was the use of transformers in electrical power distribution and telecommunications. In the realm of power distribution, power transfer efficiency is a critical factor. Some ferromagnetic materials lose energy to heat from the physical expansion and contraction of the material, which caused by the magnetic field. This phenomenon, when a material changes physical dimension by an applied magnetic field, is called magnetostriction. A nickel-iron alloy (Ni81Fe19) is found to have essentially zero magnetostriction and is widely used as a transformer core material. Permalloy is the common name for approximately 80-20 nickel-iron alloys, and the name appears to have been coined (or trademarked) by Westinghouse in approximately 1910(Chin, 1971).

Supermalloy has an improved loss characteristic over Permalloy materials, which target a higher operating frequency. It is manufactured to develop the ultimate in high initial permeability and low losses. Initial permeability ranges from 40,000 to 100,000 while the coercive force is about 1/3 that of Permalloy. Supermalloy is very useful in ultra-sensitive transformers, especially pulse transformers, and ultra-sensitive magnetic amplifiers where low loss is mandatory. The composition of Supermalloy is 79%Ni- 15%Fe-5%Mo. The type thickness of the raw material normally in 0.0005”~0.004”, and strip wound cores with case or encapsulation or cut cores can be prepared for the final use. The basic magnetic characteristics are listed in Table 4-4, for Supermalloy.

Table 4-4 Supermalloy material typical properties at 25°C(Villar, 2010)

Grade / Category	$B_{sat}(T)$	$\mu_i$	$\rho (\Omega m)$	$T_c(^{\circ}C)$	Density (kg/m <sup>3</sup> )
Supermalloy	0.66 to 0.75	20 000	$0.57 \times 10^{-6}$	430	$8.72 \times 10^3$

The core loss density of the Supermalloy is plotted in figure 4-18, according to the data from Magnetic Metals Magnetic Metals, “Data sheets: NAM – Wound magnetics”.

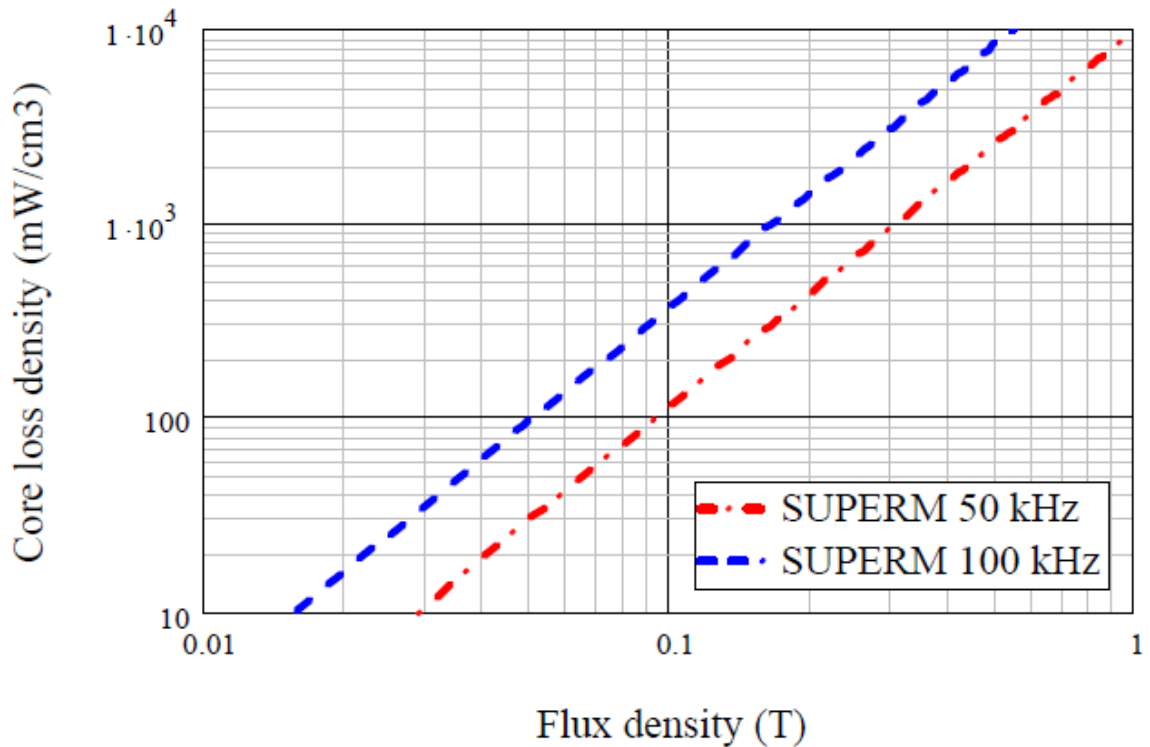


Figure 4-18 Loss density of Supermalloy

#### 4.35 Characteristics of nanocrystalline materials

In 1988, Yoshizawa, etc, (YOSHIZAWA) introduced a new class of iron based alloys, named nanocrystalline, which exhibit superior soft magnetic behavior. Another group of Japanese scientists also found a similar type of magnetic material in 1991 (Suzuki et al., 1991). The properties were a unique combination of the low losses, high permeability and near zero magnetostriction. Compared with all previously known soft magnetic materials, nanocrystalline type materials have higher products of relative permeability and saturation flux density, as in figure 4-19 The higher the value of the product is the smaller size and lighter weight of magnetic components will be used for certain applications. Certainly, good high frequency behavior, low losses and the good thermal stability are also, important factors to affect the component density.

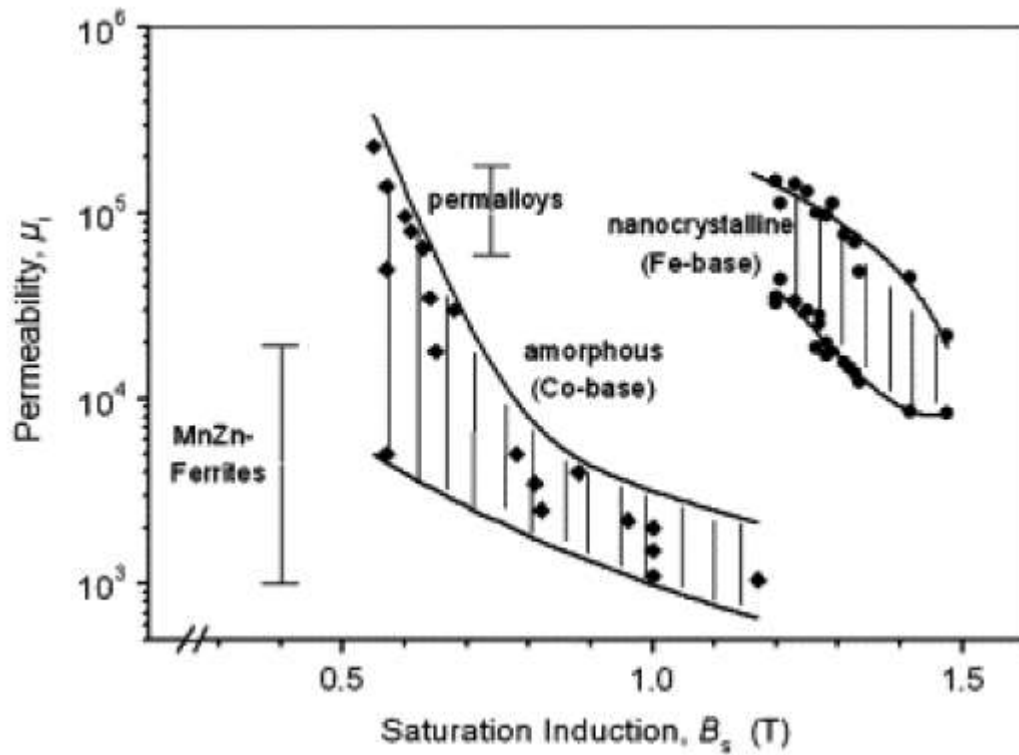


Figure 4-19 Typical initial permeability and saturation flux density for soft magnetic materials(Petzold, 2002)

“The fact that an extremely fine-grained structure leads to good magnetic properties actually came as a surprise, since for conventional crystalline magnetic materials the coercivity increases with decreasing grain size, as illustrated in figure 4-20 Yet excellent soft magnetic properties are re-established when the grain size is below about 20 nm.” Somehow, the nanocrystalline materials are thought fit the blank between the amorphous and crystalline materials(Herzer, 1997).

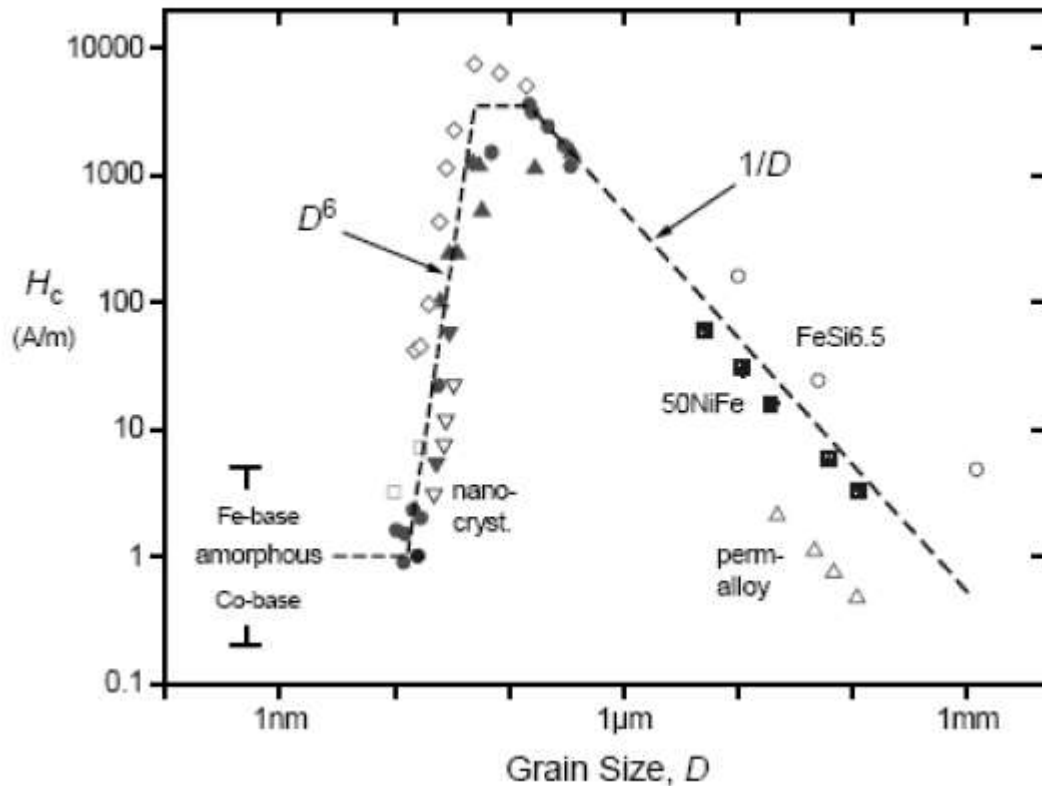


Figure 4-20 The relation between coercivity and grain size of different ferromagnetic materials

Typical and so-far optimal nanocrystalline material composition is Fe-Si-B-Nb-Cu, which is also adopted by two major commercial nanocrystalline materials, Hitachi Finemet® Fe73.5Si13.5B9Nb3Cu1 and Vaccumschmelze Vitroperm® Fe73.5Si15.5B7Nb3Cu1. “Nanocrystalline materials are prepared based on amorphous precursors, and the nanocrystalline state is achieved by annealing at a temperature typically between 500 and 600 °C; this leads to primary crystallization. The resulting microstructure is characterized by randomly oriented, ultra-fine grains of Fe-Si with a typical grain size 10-15 nm embedded in a residual amorphous matrix which occupies about 20-30% of the volume and separates the crystallites at a distance of about 1-2 nm. These features are the basis for the excellent soft magnetic properties indicated by high values of initial permeability of about 105 and correspondingly low coercivity of less than 1A/m.” (Herzer, 1997) The concerned properties of nanocrystalline materials are characterized in the following section, based on the material Finemet® from Hitachi.



Nanocrystalline cores such as Finemet from HitachiMetals and Vitroperm from Vaccumschmelze are attractive for high-frequency high-power applications. They offer a high saturation flux density of over 1 T, and low hysteresis losses that are comparable with figures from some ferrites in the 20-100 kHz frequency range. Typical applications include inductors and transformers for multi-kW DC-DC converters. These cores are wound from a thin (18  $\mu\text{m}$ ) metallic ribbon, each layer of the ribbon being insulated from the stack by a thin coating of epoxy. The cores therefore have a finely laminated structure and are typically available as C-cores. Whilst the hysteresis loss behavior of the cores has been thoroughly characterized (Bertotti, 1988) including the effects of non-sinusoidal excitation and DC bias, the phenomenon of gap losses is less well understood.

## 4.4 Comparison of Performances of Amorphous and Nanocrystalline

Amorphous and nanocrystalline alloys show attractive magnetic properties and can be the excellent choice to develop the cores of high-frequency high-power transformers used in high-power density renewable power generation systems. However, the electromagnetic design of high-frequency power transformers is a multi-physics problem and thereby affects the system efficiency and cost. In this paper, four high frequency transformers are optimally designed with amorphous and nanocrystalline alloy-based cores and electromagnetic performances are evaluated by finite element method. The results are analyzed and found their huge potentiality for future smart grid applications(Liu et al., 2014).

With the growing demand of high-power density power conversion systems, the high-frequency high-power transformers have attracted significant attention in recent years(Islam et al., 2013a, Islam et al., 2014). Operated with a higher frequency, the volume of a magnetic core can be minimized. When the power capacity increases, however, advanced soft magnetic materials of high permeability, high saturation flux densities, and low core losses, such as amorphous and nanocrystalline alloys can be the excellent choice. Metglas amorphous alloys 2605S3A and 2605SA1 are excellent magnetic materials with maximum flux densities of 1.41 T and 1.56 T, and the core losses are 120 W/kg and 650W/kg, respectively at 100 kHz sinusoidal excitation of 0.2 T, 25 oC. The Hitachi magnetic alloys FT-3H and FT-3M are iron-based nanocrystalline alloys with saturation inductions of 1.23 T and 1.23 T, and the core losses are 80 W/kg and 40 W/kg, respectively at 100 kHz sinusoidal excitation of 0.2 T, 25 oC. The main parameters of these four materials are summarized in Table I. Several papers have proposed the application of amorphous and nanocrystalline alloys to design high frequency transformers (Rabiul Islam et al., 2014, Islam et al., 2013b, Shen et al., 2008b), but none of them well focused on their electromagnetic performance comparison, especially in designing multiple secondary winding high-frequency transformers. In this paper, four multi-winding high-frequency transformers with amorphous and nanocrystalline alloy-based cores are optimally designed by finite element method. Transformer parameters are calculated, and electromagnetic performances are compared to choice suitable core materials for high-power high-frequency transformers.

Table 4-5 Parameters of soft magnetic materials

Material	Amorphous		Nanocrystalline	
	2605SA1	2605S3A	FT-3H	FT-3M

Saturation flux density (T)	1.56	1.41	1.23	1.23
Core loss (at 0.2 T, 20 °C and 100kHz) (W/kg)	650	120	80	40
Thickness (μm)	25	18	18	18
Magnetostriction (ppm)	27	20	<1	<1
Curie temperature (°C)	395	358	570	570

The amorphous alloy can reach higher flux density than nanocrystalline material, while nanocrystalline transformer has lower specific core losses, higher efficiency and smaller volume. The optimal core material of amorphous alloys transformer is 2605SA1, while the optimal core material of nanocrystalline alloys transformer is FT-3H. Above all, the nanocrystalline transformer has lower noise level than amorphous transformer.

## 4.5 Gap Losses

These losses occur within the core near the air gap in the magnetic circuit and arise due to the fringing flux around the air gap. The fringe field creates a component of flux,  $B_n$ , which is normal to the surface of the ribbon laminations, figure 4-15, causing eddy currents and losses within the laminations. The effect can be particularly significant in some high-current, high-frequency DC inductors and increases with air gap length(Wang et al., 2016, Fukunaga et al., 1989, Fukunaga et al., 1990). Accurate prediction of these losses is therefore crucial for an optimum design. One approach to mitigate the effect is to place multiple smaller air gaps in the magnetic circuit, however this may be difficult to manufacture and the multiple cuts can degrade the characteristics of the core(Shen et al., 2008a, Rylko et al., 2011). This paper makes a contribution to the understanding and calculation of gap losses in nanocrystalline cores under high-frequency operating conditions. Finite element (FE) modelling is used to examine the distribution and magnitude of the gap loss in a Finemet C-core. A sensitivity study is undertaken using the simulation model to investigate the effects of the inductor design parameters, such as air gap length, frequency, flux density and core lamination width, on the total gap loss. Assuming the gap loss is a power function of these parameters, a convenient design-oriented expression is derived for estimating gap loss at high frequency. Validation is provided by temperature measurements on a 300 A, 60 kHz inductor for a 30 kHz, 25 kW dual-interleaved DC-DC converter. The established gap loss calculation method is first reviewed, and then the inductor component is introduced followed by the details of the FE modelling.

### 4.51 Calculation of gap losses

The prediction of gap losses typically uses an empirical formula, that was originally proposed by Lee in 1947 for steel laminated cores operating at power line frequencies(Lee, 1988).

$$P_g = Gl_g D f B_m^2$$

4 - 60

where  $P_g$  is the gap loss in Watts,  $l_g$  and  $D$  are the total gap length and lamination width in mm respectively,  $B_m$  is the peak

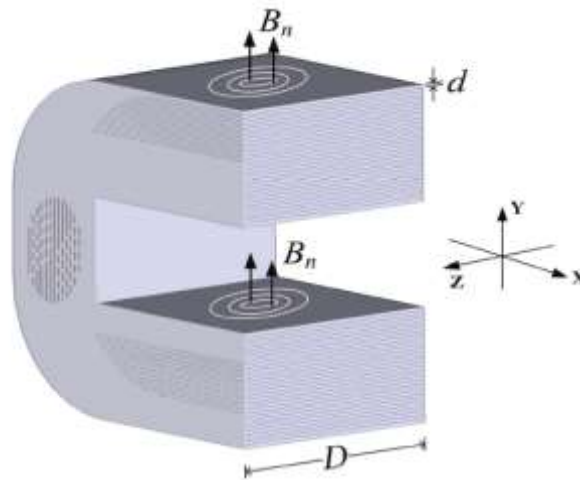


Figure 4-21 Schematic diagram of in-plane eddy currents in one half of a cut core with air gaps

induction in the core in T with frequency  $f$  in kHz, and the term  $G$  is a numerical constant. In the second edition of this book (Lee, 1988) (1955) Lee proposed a change to (1) whereby the frequency term was raised to the power of 0.5 and also the lamination thickness and permeability were included, however in subsequent publications in the 1970s (Lee and Stephans, 1972, Lee and Stephens, 1973) he concluded that the original formulation was most accurate. This was based on testing both stamped laminations.

cores and strip wound cores of silicon steel at frequencies of 60 Hz and 400 Hz. Lamination/Strip thicknesses of 0.36 mm, 0.15 mm, and 51  $\mu\text{m}$  were used. Furthermore, different values were proposed for the constant  $G$  for various configurations of windings and air gaps, for example  $G = 0.388$  for single cut C-cores with two coils. Above equation is generally used to predict gap losses in high frequency inductor cores. The equation appears in McLyman's Transformer and Inductor Design Handbook (McLyman, 2017), and it is used in the DC Reactor Core Design Tool from Metglas. However, some concern has been expressed over the accuracy of the above equation for high frequency inductors using amorphous metal cores, suggesting the losses are likely to be much lower than predicted (Rylko et al., 2011). Other work has also suggested that the air gap fringing flux makes little contribution to the increased loss in cut nanocrystalline cores (Shen et al., 2008a).

A 3D electromagnetic FE model has been developed to predict the gap loss distribution in finely laminated nanocrystalline inductor cores operating at high frequencies. The losses were seen to be highly localised on the edges of the core in the region of the air gap with loss densities approaching 1 W/mm<sup>3</sup> in the design example. Depending on the design parameters the gap loss can be a major part of the total inductor losses and accurate prediction is therefore

important for optimised designs and to prevent localised overheating. Based on the FE analysis an updated approximation formula has been proposed for the estimation of gap losses in nanocrystalline cores. Since current-driven Biot-Savart conductors were used for the windings, the shielding effect of the winding on the gap fringe field is neglected. Therefore, the results are applicable to inductors where the windings are spaced away from the core by approximately the gap length per leg. If the windings were closer to the core, the fringe field and gap loss would be reduced, but at the expense of increased winding loss. The FE model has been validated by measurements on a 5.1  $\mu\text{H}$ , 300 A, DC inductor operating with 60 kHz ripple in a 30 kHz DC-DC converter. Since the FE model assumes single frequency sinusoidal excitation, the total gap loss was determined by adding the losses due to the first three harmonics using the approximation formula. The predicted overall losses matched closely with measurements, and furthermore the measured core temperature distribution corresponded closely with predictions from a 3D FE thermal model.

The updated gap loss approximation formula is considered to provide a sound basis for the design and optimisation of nanocrystalline core, high current DC inductors operating at frequencies up to around 100-200 kHz. The updated formula shows that the gap losses increase with strip width  $D$  to the power 1.65 as opposed to linearly in the established design equation. This suggests that a narrower strip width and a thicker core, having the same cross-sectional area may be beneficial in reducing gap losses.

## 4.6 Performance Comparison of Nanocrystalline Material with Ferrite in a 40kW 20kHz Application

In this study the performance of Nanocrystalline material in comparison with ferrite is evaluated for a high frequency high power transformer core application. The major advantage of Nanocrystalline material over ferrite is its ability to go for higher design flux densities. However, this is limited with increased losses occurring with the increase of operating frequency. The situation is studied for a 40kW, 20 kHz application. Samples of both versions are developed, and a performance evaluation is made on the application. Based on the practical outcome a comparison is made in terms of power density per physical parameters such as weight and volume. The cost and manufacturability were also evaluated.

As it was discussed before the transformers in electrical systems are responsible approximately to one third of total network losses. These losses are accounted as power quality costs, costs to society and to the environment itself (Picanço et al., 2008) and with the development of power electronics techniques, pulse-width modulated inverters (PWM) are widely used to control electrical machines, to feed transformers and to interface renewable energy systems. Also in the future DC electric power systems, high power DC –DC converters will play a major role as they will substitute today's bulky 50/60 Hz transformers (Pollock et al., 2003, Nabhani et al., 2014).

The main purpose of high frequency operation of such power electronics circuits is to reduce the physical size and cost. The implication being that the losses and efficiency become of paramount importance because of the need to remove heat from the small surfaces (Dixon, 1988). High frequency transformers in such a power electronics circuits constitute a major proportion of the weight and losses. Thus, there is a rapid increase in the industry demand for the best optimization of high frequency transformers. The importance of looking into all the options of optimization become furthermore significant with the increase of amount of power handled.

In this paper the design optimization of a 40kW High frequency transformer operating at 20kHz application is discussed. The losses in the core as well as in the windings are analyzed. Theoretical explanations on the principles used in optimizing the core and winding losses are discussed. Attention is given to make a comparison on the performance of Nanocrystalline core and ferrite core. The design approach discussed below is used to arrive at optimal designs with each core material.

## 4.61 Transformer Design

### Transformer Construction

A single phase high frequency transformer was designed to handle a power of 40kW. The transformer is to be fed from an inverter bridge and is subjected to a square wave excitation. The transformer was designed with two parallel operating secondaries each handling a power of 20kW. Each secondary is supposed to feed a full bridge rectifier. The basic schematic diagram of the transformer can be represented as in the figure 4-22

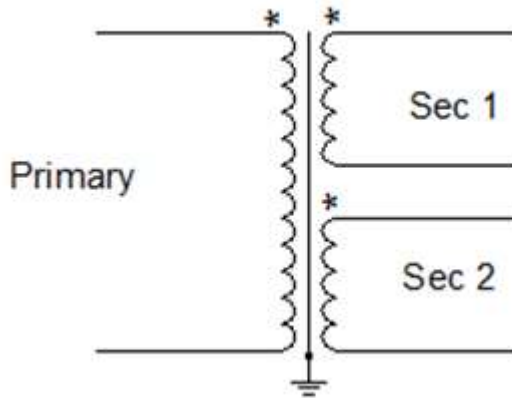


Figure 4-22 Schematic of the high frequency 40kW transformer

### Transformer core selection and turns calculation.

The basic interest of this study was to see the advantages and disadvantages different core materials provide in the application of high power high frequency transformer applications and thereby to arrive at best magnetic solutions for the developing high power high frequency field. A range of high frequency core materials present in the market including several grades of ferrite, such as 3C90, 3C93 and 3C97, three versions of nanocrystalline materials ANTAINAO, FINEMET, VAC, Amorphous materials and high silicon steel e.g. 6.5% Si JFE steel were considered. Based on an initial study on the properties of each material it was decided to consider the ferrite grade 3C90 and two versions of nanocrystalline for the construction of cores for the development of samples for the phase one of the study where a power level of about 40kW is considered. It is intended to consider some other materials mentioned above for subsequent evaluations.



Based on the material properties of selected Ferrite version 3C90 and Nanocrystalline materials and based on the core losses calculated as explained in the next section the optimal operating flux densities for each material were decided. The advantage having a high saturation flux density of nanocrystalline was utilized, However higher losses compared to ferrite avoids going in to much higher flux densities. The Faraday's law with appropriate constants for rectangular wave excitation was used to decide on the primary turns. Secondary turns were decided based on the target voltages of the output voltage

#### Transformer core loss estimation

Most commonly used formula for the calculation of core material losses is the one given below which is known as Steinmetz equation.

$$P_v(t) = k f^\alpha \hat{B}^\beta \quad 4 - 61$$

where  $B$  is the peak flux amplitude,  $P_v$  is the time average power losses per unit volume,  $f$  and  $\beta$  are the frequency of sinusoidal excitation and  $\alpha$  and  $\beta$  are constants calculated based on curve fitting. Similar equation without the frequency component was introduced by Steinmetz back in 1892 therefore this is known Steinmetz equation. However, this equation as well as the data provided by the core materials manufactures so far are only based on sinusoidal excitation (Venkatachalam et al., 2002)

The form of excitation coming into the product under discussion is a square one and the losses differ from a sinusoidal excitation. A detail explanation on losses under non sinusoidal excitations was discussed and experimentally proven mathematical model was presented in IEEE Workshop on "Computers in Power Electronics" in June 2002 under the topic of "Accurate Prediction of Ferrite Core Loss with Nonsinusoidal Waveforms Using Only Steinmetz Parameters", by Venkatachalam, C.R. Sullivan, T. Abdallah and H. Tacca.

However for the simplicity of application the simplified version of this model expressed below (Venkatachalam et al., 2002) which does not require numerical integration was used for the estimation of losses.

$$P_v = k_i (\Delta B)^{\beta-\alpha} / T \sum_j |V_j / (N A_c)|^\alpha (\Delta t_j) \quad 4 - 62$$

Where  $N$  is the number of turns,  $A_c$  is the core cross-sectional area,  $B$  is the peak to peak flux of the loop under consideration and

$$k_i = k / (2^{\beta+1} \pi^{\alpha-1} \left[ 0.2761 + \frac{1.7061}{\alpha + 1.354} \right])$$

4 - 63

The predicted losses were also considered as a fact in deciding the optimum flux density for a particular core material.

The use of this equation gives a reasonable indication of the losses at the initial design stage. Further based on the detailed study described in (Shen et al., 2008a) it was possible to get an estimation of the losses that would be generated in Nanocrystalline material in the application of interest

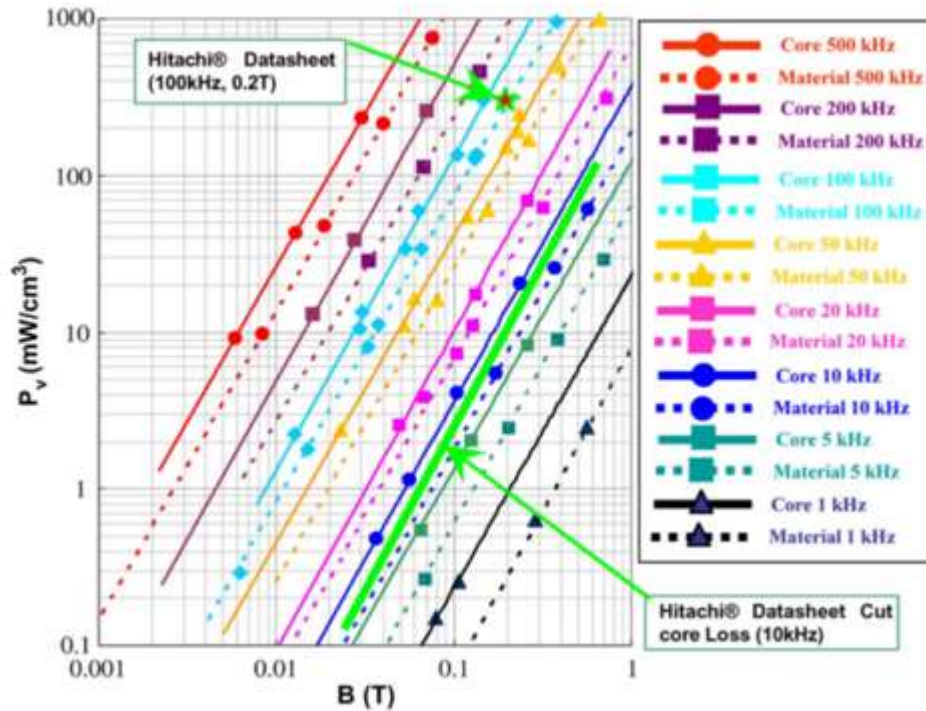


Figure 4-23 Loss densities of Nanocrystalline Material at different frequencies, based on (Shen et al., 2008a)

The values obtained in these calculations suggested that the Ferrite 3C90 or the latest development 3C97 stand to be more suitable in this application. Thus at the initial study it was decided to produce the sample with the Ferrite 3C97. The winding losses estimations described in the below section and the manufacturing conditions suggested that UU construction would give the best advantage in this application. Though the Nanocrystalline option was set aside at this stage it was decided to reinvestigate possibilities further size and weight reductions using different Nanocrystalline grades after the successful completion of the phase 1 of the project.

### Conductor selection and winding losses estimations.

The selection of optimum conductor type and arrangement are crucial in the case of high power high frequency magnetic designs. A careful consideration of the skin effect and the proximity effect needs to be made to arrive at an optimal selection of the conductors in order to avoid the generation of excessive losses and thereby high temperature rises or even in certain cases thermal runaway conditions. These situation is discussed in in detail in Chapter 3 of this thesis the winding loss calculation

The physical constructions of the nonocrystalline core make the Litz wire the The option of Litz wires and foil conductors are discussed. Advantages and disadvantages of each with respect to construction and losses are discussed. The increased conductor losses at high frequencies are discussed. Theoretical aspects of approaches taken to minimise the skin effect and the proximity effect, such as minimising the number of winding layers and sandwiching of windings carrying currents of opposite directions are explained.

### Control of leakage inductance

Two novel methods were used to achieve the required higher leakage inductance that will improve the smooth functioning of the overall circuit. Both these methods give the flexibility of controlling the leakage inductance over a considerable range enabling the meeting of the desirable leakage inductance levels of many inverter /converters manufactures. The theoretical explanation of this aspect goes beyond the intended scope of this paper and will be discussed in a subsequent paper.

### Prototype development and testing



Figure 4-24 Nanocrystalline HF transformer (40kW)



Figure 4-25 Ferrite HF transformer (40kW)

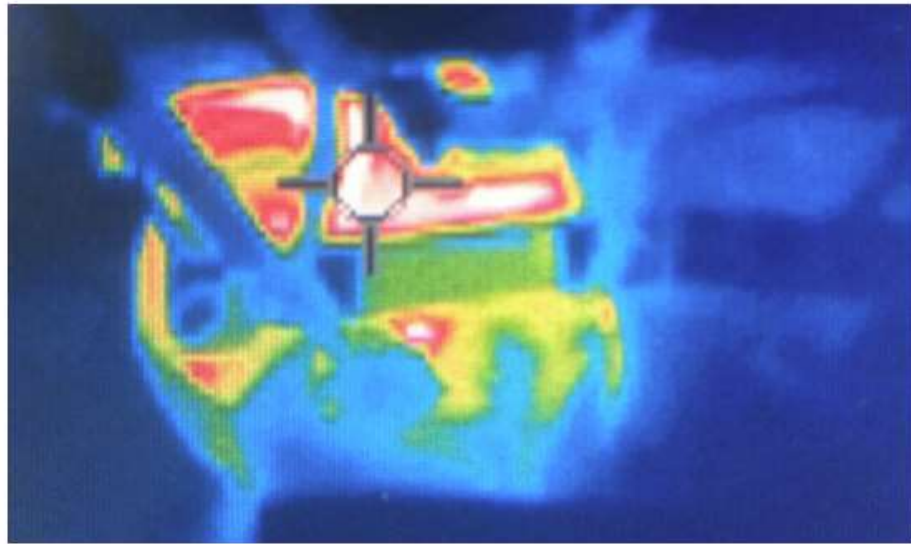


Figure 4-26 Thermal images of 40kW transformer top view

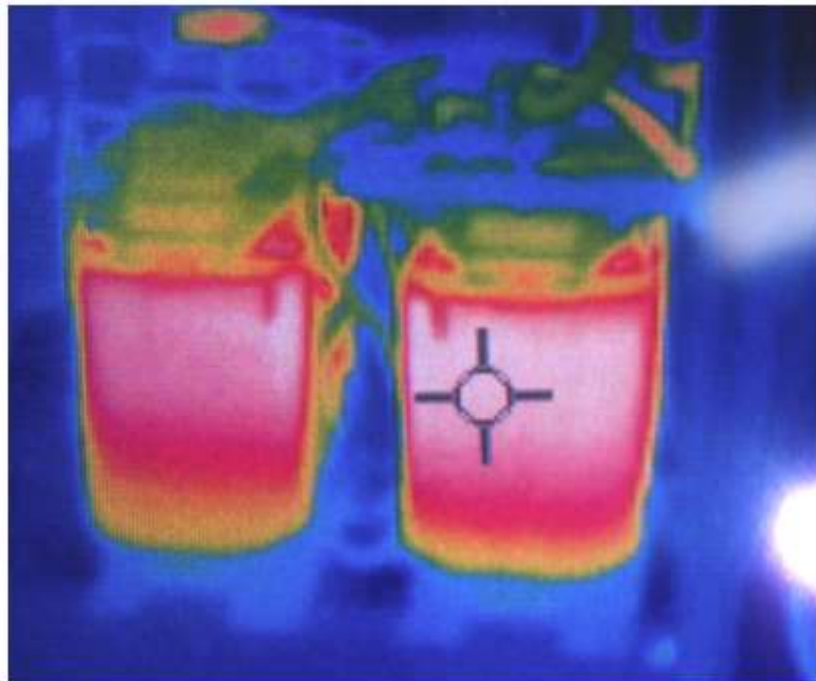


Figure 4-27 Thermal images of 40kW transformer side view

Above two samples were developed and tested in a converter application operating at 20kHz. The temperature rises of each of the products under a load of 40kW could be seen as in the pictures above. The comparison is discussed in the end of the chapter summary.

The test results observed in the discussed high frequency high power application for Nanocrystalline, and Ferrite was very much encouraging and was reasonably in line with the theoretical predictions. In this study nanocrystalline transformer was designed at an approximately three times higher flux density compared to the ferrite one. The temperature rise of the cores under the 20kHz excitation was at a reasonable level and Nanocrystalline version showed only a slight increase in the rate of temperature rise compared to Ferrite version. This proves that the estimation made based on theoretical calculations for the suitable operating flux density for nanocrystalline was reasonable. Further no considerable audible noise was observed in either of the products. This could be partly due to the fact that the significant part of any noise generated goes over the human audible range.

The weight of the nanocrystalline version designed under these criteria was approximately 6kg compared to approximately 15kg of the ferrite version. However large mass and the wider radiating area of the ferrite version give the advantage of reduced overall temperature rise at the condition of thermal equilibrium. In order to account for this fact, it is required that a winding wire with a wider cross section is used for the nanocrystalline version. This results in increase in the weight of the nanocrystalline version slightly reducing the weight ratio advantage over ferrite. Further all the disadvantages of a thicker conductor in high frequency applications discussed in the paper need to be considered in increasing the conductor cross section of nanocrystalline version.

The arrangement used for the control of leakage inductance showed positive results however the temperature rise in the supplementary core parts were slightly higher than what was theoretically predicted. The explanation of this and the theoretical aspects of this concept go beyond the scope of this paper and will be discussed in a chapter 6 of this thesis.

Based on the results obtained in this study it could be concluded that a considerable reduction in the weight and size could be reached by the use of nanocrystalline material as a core for a high-power high frequency transformer and it is intended to construct a 200kW transformer operating at 20kHz as the next step of the study. However, it should also be noted that the cost of each version highly depends on various commercial aspects.

## 4.7 Development of High Frequency Transformer 50kW, 50kHz & High Frequency Inductor 8.5 $\mu$ H at 300A, 50kHz

In this section the optimum design of high power high frequency magnetics is discussed based on a 50kW application operating at 50 kHz. An in depth theoretical explanation on minimizing the losses at high frequency is discussed. Further how this approach will make it possible to develop a new generation of magnetics that enable power electronics designers to go for significantly high operating frequencies is discussed. The challenge of handling high temperature rise due to high power density of such high power high frequency magnetics is addressed in this paper with a practical solution for that. The theoretical findings are verified based on a set of prototypes developed for a 50kW DC DC converter operating at 50kHz.

Energy efficiency, low noise, reduced mass and dimensions are becoming more and more vital factors in designing magnetics for all kinds of modern power electronics applications such as rolling stock, renewable energy and similar applications. In order to achieve a high degree of miniaturization, designers move into significantly high operating (switching) frequencies in the development of modern high-power converters and inverters. There is also a clear trend that the operating frequencies used in these applications will continue to increase.

Applications like traction, ship and basically any mobile platform with a converter on board require lightweight and compact converters to exploit the space available on board more effectively. They often require galvanic isolation for safety or other reasons. Therefore, high power high frequency transformers which offer galvanic isolation and a small volume are of increased importance(Pavlovsky et al., 2005). In addition to the galvanic isolation magnetic components including transformers and inductors perform functions of harmonics filtering, energy storage, level shifting, current sensing and parameter matching for power stages as well as control circuitries in a power converter. They often determine the converter size (Shen et al., 2008a, Lotfi and Wilkowski, 2001). It has been a long held view that with a continuous increase in operating and /or switching frequency a continuous decrease in physical size of magnetics would follow. However, the heat removal surface of the magnetic components decreases as a result of the higher density design; on the other hand, core and winding loss densities increase correspondingly. Therefore attention needs to be paid to magnetic material selection and associated core loss calculations, especially for high frequency high density magnetics and power converter design(Pavlovsky et al., 2005).

The selection of suitable core material out of several Ferrite grades and Nanocrystalline materials is discussed in this paper with modern approaches of estimating core losses in each



type under non sinusoidal excitations of high frequencies such as 50kHz. The advantages of Nanocrystalline that was discussed in for 20kHz applications reduce to some extent at this 50kHz application. The effects that high frequency currents such as 50kHz square and triangular waveforms have on conductor losses are explained. A novel winding technique that brings down the significance of proximity effect at high frequencies in transformer windings is presented in this paper. Several core material options such as Ferrite and Air cored inductor are discussed for the series inductor of converters operating in the range of 50kHz. Further a method of minimizing high frequency conductor losses of inductor windings carrying 50kHz currents of significant amplitudes is presented.

A novel cooling technique for these compact magnetics with high power densities is discussed. A set of prototypes were developed based on the theoretical findings and tested on a DC/DC converter. Verification of theoretical findings based on practical observations is carried out.

#### 4.71 High Frequency Transformer 50kW, 50kHz

##### Transformer Construction

The transformer is designed to handle a power of 50kW at a square wave excitation of 50kHz. The transformer was design with a primary to secondary turns ratio of 1:2 with a single secondary.

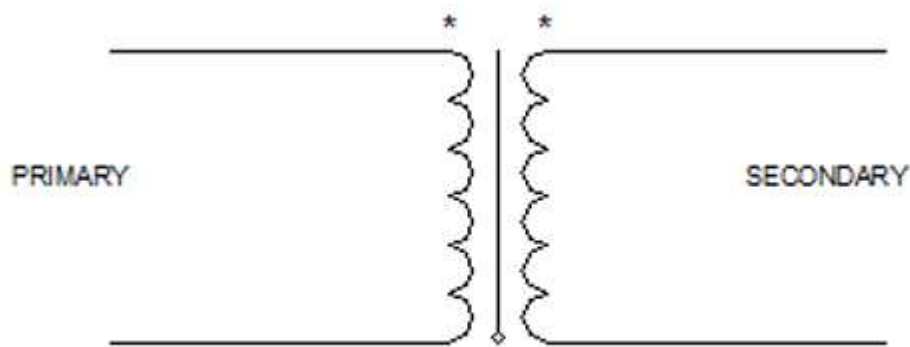


Figure 4-28 Schematic of the 50 kHz, 50kW transformer



### Transformer core selection and turns calculation

Based on the material properties of Ferrite and Nanocrystalline materials optimal operating flux densities for each material were decided based on the operating frequency of 50 kHz. The advantage having a high saturation flux density of about 1.1T in Nanocrystalline compared to about 300mT in Ferrite was considered. However higher losses in Nanocrystalline compared to ferrite avoids going in to much higher flux densities at 50kHz in comparison with 20kHz or similar applications. However, the potential advantage of Nanocrystalline against new Ferrite grade 3C97 at this frequency was considered. The Faraday's law with appropriate constants for rectangular wave excitation is used to decide on the primary turns.

### Transformer core loss estimation

An improved calculation method of core losses for non-sinusoidal waveforms based on recent publications(Venkatachalam et al., 2002), (Herbert, 2008) and (Shen et al., 2008a) was carried out. Modified and generalized versions of Steinmetz equations and a simplified graphical method discussed in these publications were used in loss estimations. Simplified equation for core loss estimation using Steinmetz parameters of the material, based on (Venkatachalam et al., 2002).

$$P_v = k_i(\Delta B)^{\beta-\alpha}/T \sum_j |V_j/(NA_c)|^\alpha (\Delta t_j) \quad 4 - 64$$

where

$$k_i = k/[2^{\beta+1}\pi^{\alpha-1} \left[ 0.2761 + \frac{1.7061}{\alpha + 1.354} \right]] \quad 4 - 65$$

and where  $N$  is the number of turns,  $A_c$  is the core cross-sectional area,  $B$  is the peak-to-peak flux of the loop under consideration.

The use of this equation gives a reasonable indication of the losses at the initial design stage. Further based on the detailed study described in (Shen et al., 2008a) it was possible to get an estimation of the losses that would be generated in Nanocrystalline material in the application of interest.

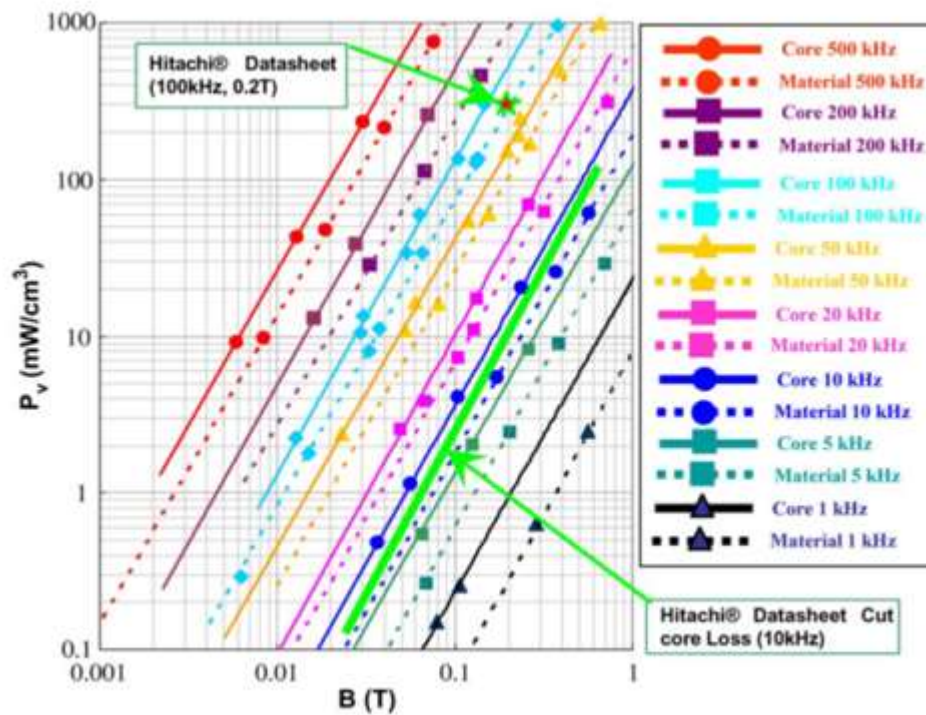


Figure 4-29 Loss densities of nanocrystalline material at different frequencies, based on (Shen et al., 2008a)

The values obtained in these calculations suggested that the Ferrite 3C90 or the latest development 3C97 stand to be more suitable in this application. Thus at the initial study it was decided to produce the sample with the Ferrite 3C97. The winding losses estimations described in the below section and the manufacturing conditions suggested that UU construction would give the best advantage in this application. Though the Nanocrystalline option was set aside at this stage it was decided to reinvestigate possibilities further size and weight reductions using different Nanocrystalline grades after the successful completion of the phase 1 of the project.

#### Conductor selection and winding losses estimations.

As discussed in the Chapter 3 of this thesis transformer windings suffer from skin and proximity effects. The current distribution within a conductor depends on its current, the surrounding currents, the type of conductor, the geometry of the winding and finally the frequency of the waveform. Thus, the determination of conductor losses is not always an easy task. If winding configuration is simple enough, like foil or coaxial conductors, the resolution of one dimensional field equations (Maxwell Equations) is usually sufficient to estimate losses. However in complex

winding arrangements magnetic field distribution, and therefore current density distribution are highly two dimensional and analytical solutions may become too complex to be solved and usually require finite element resolutions(Villar, 2010).

The option of Litz wires and foil conductors were considered for this application. The level of power and the frequency of the current in this particular application make the foil conductors a more attractive choice compared Litz wires or thin profile conductors. However the foil conductors carrying high frequency currents results in prominent occurrence of proximity effect as it was pointed out in previously. . A quick explanation of the increased losses due to the proximity effect in foil windings and its sensitiveness to the increase of frequency can be seen from the below illustrations. The details of this was discussed in the Chapter 3 of this thesis. A sample was built up and the testing was carried out on a 50kHz application.

### 4.72 High Frequency Inductor 8.5 $\mu$ H at 300A, 50kHz

#### Inductor core selection

The DC/DC converter topology used in this development requires an inductor with above listed parameters. The high current value and its high frequency makes the use of high saturation magnetization level core materials such as Amorphous, 6.5% Si steel and even Nanocrystalline not very suitable for this application. The losses at this frequency require the design flux levels to be brought down very low values making the use of these materials non-economical. Ferrite options give reasonable losses. However the requirement of operating around 250mT to 300mT makes the ferrite design bulky. Thus an air core option was considered. The air core obviously gives the advantage of eliminating the core losses. However this requires use of higher number of turns in achieving the required inductance. The larger number of layers of a conductor carrying high frequency high current results in significantly high conductor losses as discussed earlier in this paper. Below discussed approach is used to minimise the increase of conductor losses.

### Effective heat removal of high-density magnetics

With the increase in the operating frequency and with the use of loss minimization techniques discussed so far the high frequency high power magnetics can be made highly compact. These products become so compact thus their cooling surfaces are not large enough to keep the temperature rises at acceptable levels under natural cooling conditions. It is not always preferable to have forced air cooling. Water cooling techniques are not practical in many applications. In the case of the 50kW, 50kHz transformer it was decided to use an enclosure with heat sink similar walls providing several times higher cooling area figure 4-30 This makes the heat removal more efficient. Based on practical observations this method becomes very much compulsory for operating frequencies over 50kHz for high power ferrite transformers with compact designs. In the case of high power Nanocrystalline transformers the requirement comes as the operating frequency exceeds approximately 20kHz due to the high compactness in such designs.

### Prototype development and testing



Figure 4-30 Ferrite HF transformer (50kW,50kHz)



Figure 4-31 Inductor (8.5uH@ 300A, 50kHz)

A 50kHz transformer with the ferrite grade 3C97 was developed, figure 4-31. Bifilar winding technique discussed in this paper was used. The sample comfortably met the standard testing as per standards including the high voltage test between the primary and the secondary. The heat sink rating was purposely made higher as an addition precaution for avoiding excessive temperatures under the full load conditions. Similarly the inductor was manufactured, Figure 9. The measured inductance was well within the acceptable tolerance level. Prototypes were tested on a 50kW, 50kHz converter application.

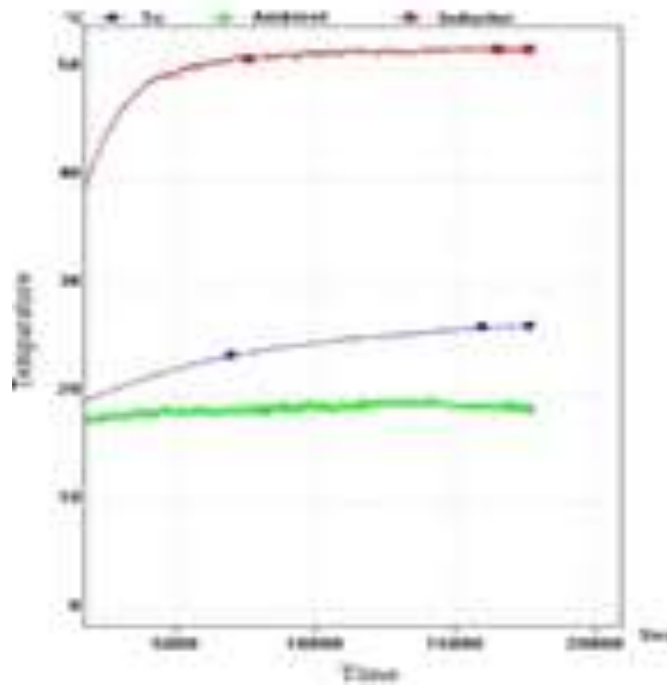


Figure 4-32 Load test temperature rise vs time

As discussed in the chapter 3 due to the difficulty of making accurate loss measurements at 50kHz the temperature rise measurements were made. The temperature rise of the each component can be seen in the figure 4-32 There were certain difficulties in arriving at the full power of 50kW in the testing set up. It was identified that certain improvements have to be made in the arrangement in order to arrive at the full power of 50kW at 50kHz. However, the testing arrangement was sufficient to make reasonable judgements of the magnetics component performance.

## Discussion

The modern developments such as SiC MOSFETs have considerably low switching losses compared to Silicon MOSFETs and IGBTs. These offer a considerable advantage over conventional silicon devices. These also make it possible to operate at 2 to 5 times higher switching frequencies compared to their conventional counter parts. As the frequency goes high the magnetics components in the power electronics systems become more and more compact. Magnetics components being usually the bulkiest components in a power electronics system and in most of the situations also the most expensive component, it is of high interest of many developers to move in this direction.

However, with the increase of operating frequency accurate approaches must be taken in the design of magnetic components. Otherwise, these can become high loss-making components in the system generating excessive heat and causing thermal runaway of the complete system. Therefore it is especially important that the magnetics designers for power electronics applications look into the fundamental theories that govern the electromagnetics behavior in the context of very high frequency levels of interest. In this study which is another step of a series of related research works a detailed investigation was made into magnetic components to be used in 50kHz high power application going down to Maxwell Equation level analysis. Based on the theoretical findings new constructional techniques were developed to address the challenges of reducing losses, making the product compact and to reduce the weight.

The test results observed on the sample testing was very much encouraging and was reasonably in line with the theoretical predictions. The High frequency transformer shows a considerably low temperature rise and a considerably low rate of temperature rise. This stands to confirm that the predicted drop in the losses due to interleaved winding has avoided a significant rise of conductor losses at high frequencies. However, when the system reaches the full power the temperature rise of the high frequency transformer can go further high. However, the calculations carried out based on the testing completed it can be concluded that the product will not reach temperature limit of the insulation class. Furthermore, it can be seen that the rating of the heat sinks of the enclosure can be brought down giving the opportunity to further reduce the overall size of the product.

The technique used in the air cored inductor also showed some positive results. However, the need was identified to develop the mathematical model giving the optimum separation of the winding layers based on the frequency and the power it is supposed to handle.

## 4.8 Development of a 100kW, 20 kHz Nanocrystalline Core Transformer for DC / DC Converter Applications

Achievement of high-power levels in a single module inverter/converter application always has number of advantages. However, high frequency magnetic components most often become the limiting factor in the achievement of such high-power levels in a single module. In this paper the achievement of 100kW in 20kHz transformer is discussed. This development is an extension of a series of developments carried out with high frequency, high power transformers of power and frequency levels such as 40kW, 20kHz and 50kW, 50kHz. The advantages and disadvantages of Ferrite and Nanocrystalline core materials at this power levels are discussed and the choice of Nanocrystalline core is explained. Further novel winding technique that mitigates high frequency conductor losses is presented in this section with a theoretical explanation on its advantages.

In order to achieve a high degree of miniaturization, designers move into significantly high operating (switching) frequencies and high-power levels in the development of modern high power converters and inverters. There is also a clear trend that the requirement of achieving high power levels in a single module will increase alongside the operating frequencies used in these applications.

Applications like traction, ship and basically any mobile platform with a converter on board require light weight and compact converters to exploit the space available on board more effectively. They often require galvanic isolation for safety and other reasons. Therefore high power high frequency transformers which offer galvanic isolation and a small volume are of increased importance(Pavlovsky et al., 2005). In addition to the galvanic isolation magnetic components including transformers and inductors perform functions of harmonics filtering, energy storage and parameter matching for power stages as well as control circuitries in a power converter. They often determine the converter size (Shen et al., 2008a, Lotfi and Wilkowski, 2001). It has been a long-held view that with a continuous increase in operating and/or switching frequency a continuous decrease in physical size of magnetics would follow. However, the heat removal surface of the magnetic components decreases as a result of the higher density design; on the other hand, core and winding loss densities increase correspondingly. Therefore, attention needs to be paid to magnetic material selection and associated core loss calculations, especially for high frequency high density magnetics and power converter design (Shen et al., 2008a).



In the initial stages of this research the advantages and disadvantages of Ferrite and Nanocrystalline materials as a core material for high frequency high power transformers were presented. Further mitigation techniques of conductor losses at high power high frequencies with novel winding techniques were presented based on developments such as 40kW, 20kHz and 50kW , 50kHz transformers.

Going forward with the findings of these studies an approach was made to achieve 100kW single module transformer that operates at 20kHz, which is used in a DC /DC converter application.

In the selection of suitable core material for this task several Ferrite grades and Nanocrystalline materials were evaluated with modern approaches of estimating core losses in each type under non sinusoidal excitations of high frequencies. The advantages of Nanocrystalline at 20kHz applications reduce to some extent at 50kHz. The challenges of mitigating high frequency conductor losses at these high current levels are explained. A novel winding technique that mitigates the high frequency losses and constructional challenges of this technique are explained.

Two design options are presented with a Nanocrystalline core for natural convection cooling applications and water plate mounting applications. Housings with specially engineered exterior are used for the natural convection cooling applications and one with specially engineered interior is used in water cooled mounting application.

### 4.81 Transformer Design

#### Transformer Construction

The transformer is designed to handle a power of 100kW at a square wave excitation of 20kHz. The transformer was designed with two parallel operating secondary windings each handling a power of 50kW.

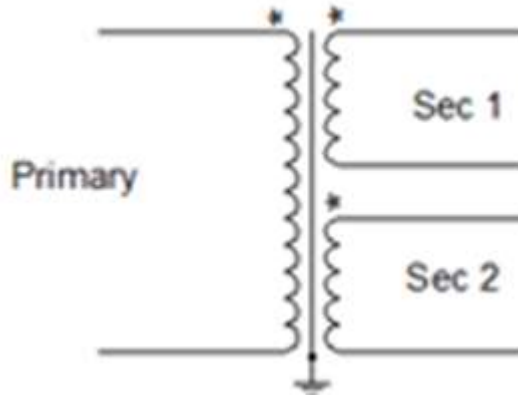


Figure 4-33 Schematic of the 100kHz, 20kW transformer

### Transformer core selection and turns calculation

The advantage of having a high saturation flux density of Nanocrystalline material was considered. Based on the material properties of Ferrite and Nanocrystalline materials optimal operating flux densities for each material were decided based on the operating frequency of 20 kHz. The Faraday's law with appropriate constants for rectangular wave excitation is used to decide on the primary turns.

### Transformer core loss estimation

An improved calculation method of core losses for non-sinusoidal waveforms based on recent publications (Venkatachalam et al., 2002, Herbert, 2008) and (Shen et al., 2008a) was carried out. Modified and generalized versions of Steinmetz equations and a simplified graphical method discussed in these publications were used in loss estimations.

Simplified equation for core loss estimation using Steinmetz parameters of the material, based on (Venkatachalam et al., 2002).

$$P_v = k_t (\Delta B)^{\beta-\alpha} / T \sum_j |V_j / (NA_c)|^\alpha (\Delta t_j)$$

4 - 66

where,

$$k_i = k/[2^{\beta+1}\pi^{\alpha-1}\left[0.2761 + \frac{1.7061}{\alpha + 1.354}\right]]$$

4 - 67

is the  $N$  number of turns,  $A_c$  is the core cross-sectional area,  $B$  is the peak to peak flux of the loop under consideration.

Conductor selection and winding loss mitigation.

The option of Litz wires and foil conductors were considered. The application under consideration handles a power of 100kW. The suitability of Litz wires including rectangular cross-section braided Litz wires were considered. However, the initial calculations carried out including poor filling factor of Litz wires showed that the foil windings are more suitable for this application. The increased conductor losses at high frequencies were considered and the significance such increased losses at the high-power level of interest were considered. The details of the conductor selection were presented in the Chapter 3 of this thesis.

Effective heat removal of high-density magnetics

Construction for the natural convection cooling

Even though a high level of minimization of losses achieved with the appropriate operating flux levels and winding techniques in this 100kW transformer the high level of miniaturization archived results in considerably high power density. This makes it challenging to maintain the temperature rise under convection conditions.

The surface area of the product or the enclosure is not sufficient for the effective removal of heat under natural convection.

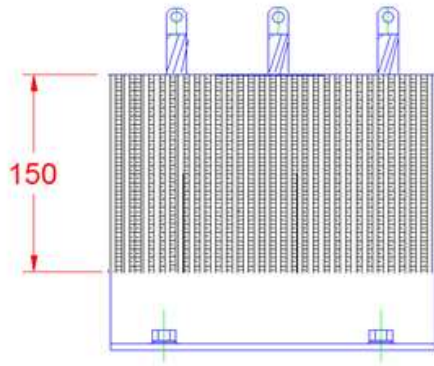


Figure 4-34 Housing construction for the natural convection cooling

Therefore, an enclosure made from heatsinks as shown in the figure 4-34 considered as a method of heat removal.

### Construction for the water-cooled plate mounting

Alternative approach considered for the effective heat removal is the use of water-cooling arrangement of the end product for the cooling of magnetic components. Under this the high frequency transformer will be mounted on a water-cooled plate as shown in the diagram below.

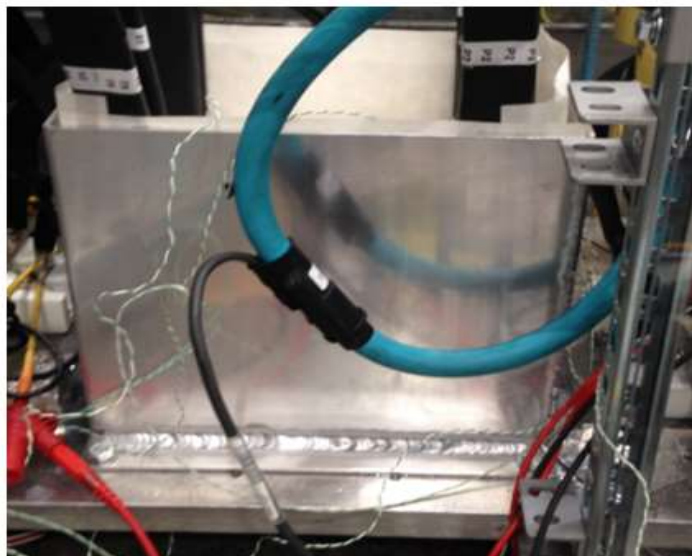


Figure 4-35 Transformer mounted in water cooled plate.

In order to effectively remove the heat generated in the inner parts of the core heat pipe and heat sheet options were considered. However, the fact that the heat has to be transferred towards the bottom direction and the short operation life of heat sheets such as 16 years in continuous operation made the use of them non suitable for the application. Therefore an enclosure with specially engineered interior was used.

### Prototype development and testing

After taking the above discussed factors into consideration a 100kW,20kHz transformer was constructed. A winding arrangement as discussed in 2.1.3 was also constructed. However, it was realised that time required for the new winding arrangement was approximately 30% higher than the sandwiched winding arrangement. The new winding arrangement provides the advantage of controlling the leakage inductance between the primary and the secondary winding. Also when duly constructed it provides a slightly better packing factor and improved performance by minimizing proximity effect. However due to the extra production time needed it was identified more research is necessary in production technique point of view for the winding arrangement to be commercially attractive.

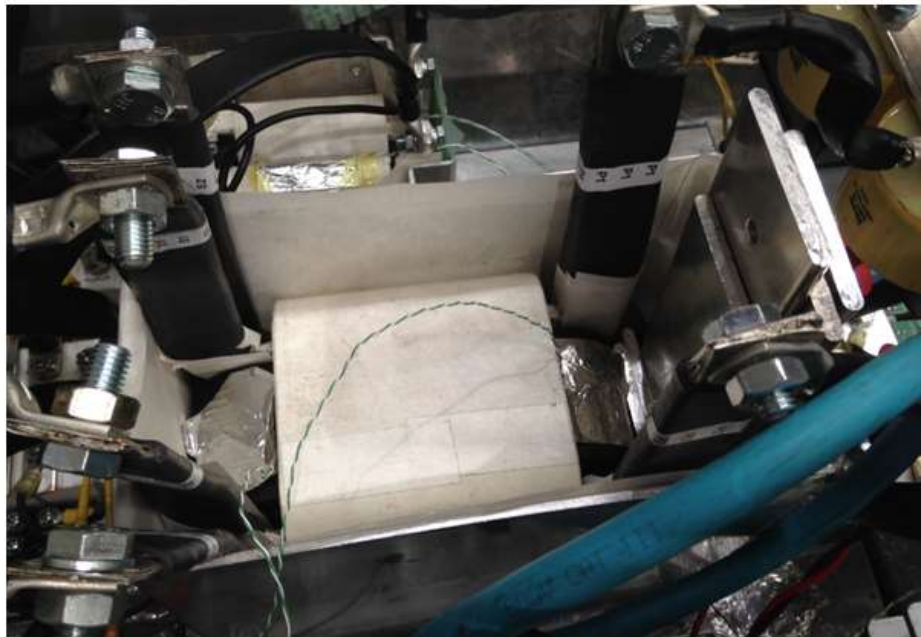


Figure 4-36 100kW, 20Hz HF transformer

A prototype with the secondly mentioned sandwich winding was also constructed as shown in the above diagram. This was tested on a 100kW DC/DC converter. As the initial step the transformer was tested inside a standard housing without any interior modifications. A power of approximately 100kW was archived. Under these conditions as it can be seen in the figure 4-35 below transformer temperature reached of 80 degrees in less than 20 minutes time.

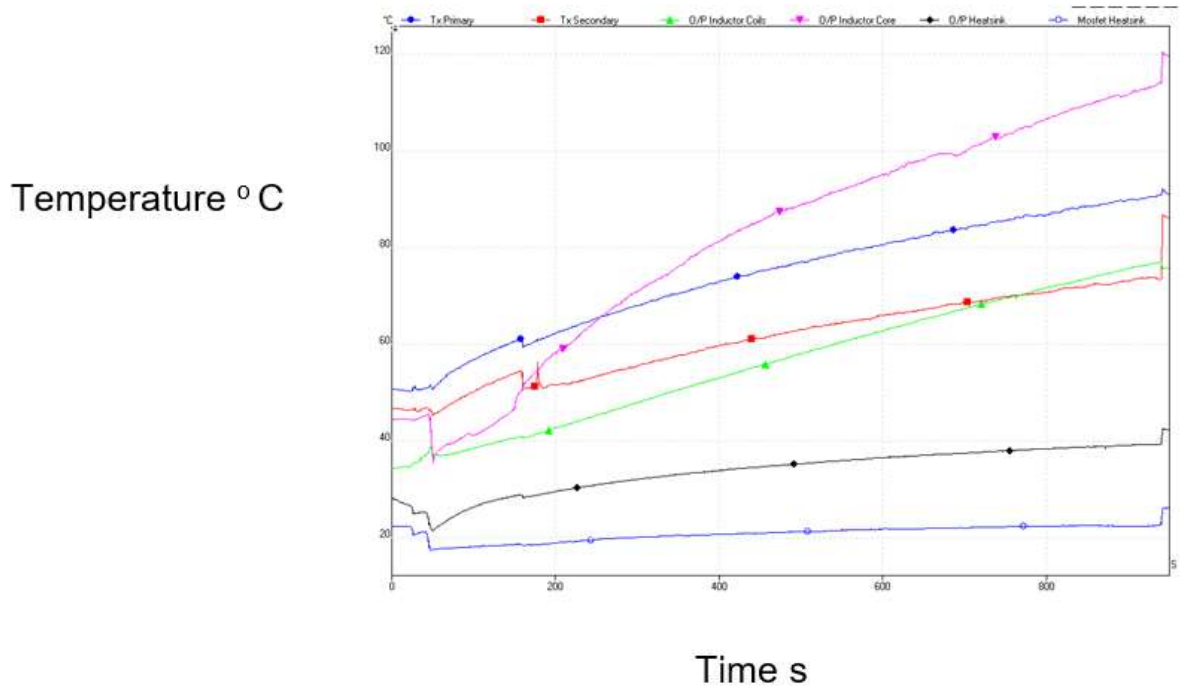


Figure 4-37 Temperature rise with a standard housing

Based on these results it was clear that in order to achieve the power of 100kW in the given volume a modified interior housing has to be used. After a further investigation on the thermal model of the arrangement the interior construction of the transformer housing was modified to effectively transfer heat from the hotspots of the transformer towards the water-cooled plate. After these improvements to the housing construction, it could be observed that more than an hour of operation at full power of 100kW was necessary for the transformer temperature to reach 80 Degrees. Further it could be seen that the temperature rise gradient was reducing significantly at this time.

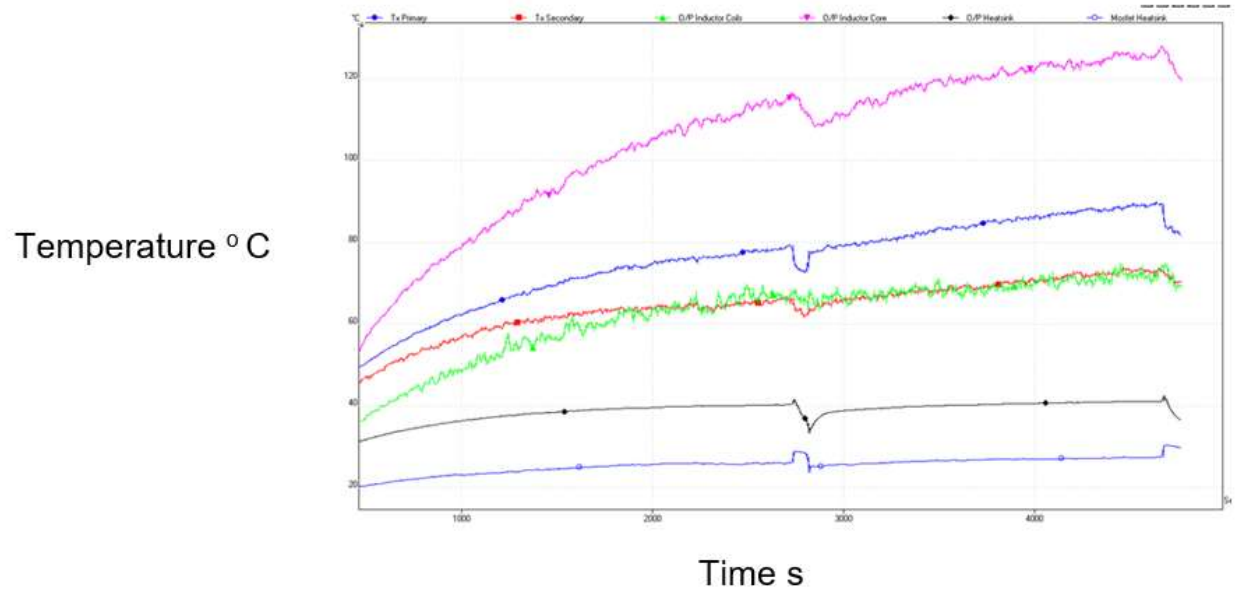


Figure 4-38 Temperature rise with modified interior housing

A further improvement of the situation and achievement of thermal stability below 90 °C could be observed when the modified interior housing was potted.

## 4.9 Comparison of core constructions

It is not useful to carry out the selection of the core construction purely on the minimization of the core losses, an appropriate compromise must be made based on conductor losses and the overall thermal management of the unit. This is a further area that the parametric approach of arriving at different solutions gives a particularly good advantage in the optimization of the design for a particular application.

A calculation sheet was developed which compares the designs for permutations of core constructions such as EI, UL with the conductor options such as “Litz” wires, foils, flat copper options etc.

As part of the commercialization of the findings researcher has already gone to the level of writing an algorithm to automate the such parametric calculation possibilities though it is outside of the scope of this study.

The patents applied relevant to this section has a close link to the thermal management of the products there for those are discussed under the Chapter 5 of this thesis.

Construction	1-Natural convection					2-Forced air cooling 2m/s					3-Forced air cooling 4m/s					4-Cold plate mounting-conventional					5-Cold plate mounting-with thermal management				
Conductor type	Cu					Al					Litz					Foil					Foil				
Cooling option	1	2	3	4	5	1	2	3	4	5	1	2	3	4	5	1	2	3	4	5	1	2	3	4	5
Design flux density	148	148				129	129				194					194					194				
Core loss (W)	100	100				188	188				80					80					80				
Winding loss Total	769	839				388	247				80					80					80				
Pri (W)	237	163				194	83				80					80					80				
Sec (W)	531	686				191	164				80					80					80				
Basic	911	970				636	517				80					80					80				
Efficiency	99.1%	99.1%				99.1%	99.1%				99.1%					99.1%					99.1%				
Temperature rise (°C)	53	75	79	65	60	53	75	70	65	60	80					80					80				
Temperature rise (°F)	80	88	80	75	70	80	88	80	75	70	80					80					80				
Weight Total (kg)	14	13				9	8				9					9					9				
Conductor weight (kg)	2.6	1.0				2.0	0.9				2.0					2.0					2.0				
Core weight (kg)	4.8	4.8				3.2	3.2				3.2					3.2					3.2				
Enclosure weight (kg)	1.8	1.8				0.8	0.8				0.8					0.8					0.8				
Potting weight (kg)	4	4				2	2				2					2					2				
kg/kW	0.14	0.09				0.09	0.08				0.09					0.09					0.09				
Dimensions (TF only)																									
Height (mm)	149	149				162	162				162					162					162				
Width (mm)	180	180				266	266				266					266					266				
Depth (mm)	170	170				130	130				130					130					130				
Volume (cm³)	4589	4589.4				5291	5291				5291					5291					5291				
cm³/kW	46	46				54	53.9				54					54					54				
Dimensions (With housing)																									
Height (mm)	164	164				177	177				177					177					177				
Width (mm)	200	200				276	276				276					276					276				
Depth (mm)	190	190				150	150				150					150					150				
Volume (cm³)	6232	6232				888	888				888					888					888				
cm³/kW	62	62				73	73				73					73					73				
Material cost (USD)																									
Labour cost (USD)																									
Prime cost (USD)																									
USD /kW																									
Selected construct	UL with PQB					Cooling method					Cold plate mounting - with thermal management					Insulation cl H (180 C)									

Figure 4-39 Design template with which a set of parametric solutions can be achieved



### Discussion

Rapid developments in the semiconductor technology and the power electronics industry enable the development of power supplies and power converters of significantly higher power levels. Considerably low switching losses of developments like SiC MOSFETs make it possible to operate at 2 to 5 times higher switching frequencies compared to their conventional counter parts. As the frequency goes high the magnetic components in such system become more and more compact. The magnetics components are usually the bulkiest components in a power electronics system and in most of the situations also the most expensive component, therefore it is of high interest of many designers to develop systems that operate at high frequencies.

The achievement of a high-power levels in a single module at high frequencies is next challenge faced by the developers of systems for high power applications. Most often the maximum power achievable with a single module is determined by the magnetic components. As a result it could be seen that constraints in the development of magnetic components make a significant influence to the miniaturization of the power electronics system. Further it is reasonably accurate to state the magnetics components have a great impact on determining the power level and the operating frequencies of power electronics applications.

The research discussed in the paper was carried out with the intention of achieving compact, high power, high frequency transformers that are capable of handling power levels in excess of 100 kW.

These studies and a series of the previous developments carried out have identified the advantages of using the materials such as Nanocrystalline for high power applications and for operating frequency levels in the range of 20 kHz to 30 kHz. With the appropriate thermal management approaches and designing at optimal operating flux levels Nanocrystalline core gives a considerable volume and weight advantage over the ferrites.

At high power levels the winding design becomes very important for the mitigation of high frequency losses. Two winding constructions are discussed in this paper. The novel method proposed with folded foils showed very good performance in mitigating the high frequency conductor losses. Further it gives the possibility of controlling the leakage inductance between the primary and secondary windings by adjusting the level of overlap. The disadvantage observed in this method was the time consumed for the proper insulation process. Through several insulating techniques were considered the amount of time savings achieved was not sufficient to adopt this method in mass production. Therefore further research is necessary to improve the production process for the successful implementation of this technique.

The second method proposed with sandwich winding could be seen as a good compromise on the performance and the amount of labor consumption.

The tests carried out with a standard enclosure showed that the amount of heat transferred to the cooled plate was not sufficient to maintain the host spot temperature below the desirable level. However, the desirable conditions could be archived with an enclosure with correctly engineered interior.

It could be concluded that with the appropriate material selection, winding techniques and with the thermal management techniques the construction of a 100kW high frequency transformer could be archived. The product showed very stable performance and presented a very compact construction giving a volume to power density of over 18W/cm<sup>2</sup> or weight to density of over 6.5kW/kg. This was a considerable reduction in the size and volume against the conventional ferrite construction considered.

Further tests studies carried out showed the possibility of achieving even higher powers such as 150kW or even 200kW in a single high frequency transformer operating at a frequency range of 20kHz to 30kHz with a compact construction is possible in a similar compact structure. In parallel with the industry demand it was intended to continue the research towards these power levels as part of future work.

## 4.10 Summary

A detail study was carried out on the losses occurring in the magnetic core of transformers. Several theoretical and empirical methods developed by various industry leading researchers were discussed in the sections 1 to 4 of the chapter 4. In the section 5 of the chapter 4 an explanation was given on the potential gap losses in magnetics core. From chapter 4.6 to 4.9 the studies carried out by the researcher are presented. This includes comparison of magnetic materials such as Nanocrystalline and ferrite to understand the ideal application areas for those materials. Further the studies carried out in this section includes different core constructions topologies, construction arrangements etc.

The test results observed in the study under the section 4.6 discussed high frequency high power application for Nanocrystalline and Ferrite was very much encouraging and was reasonably in line with the theoretical predictions. In this study nanocrystalline transformer was designed at an approximately three times higher flux density compared to the ferrite one. The temperature rise of the cores under the 20kHz excitation was at a reasonable level and Nanocrystalline version showed only a slight increase in the rate of temperature rise compared to Ferrite version. This proves that the estimation made based on theoretical calculations for the suitable operating flux density for nanocrystalline was reasonable. Further no considerable audible noise was observed in either of the products. This could be partly due to the fact that the significant part of any noise generated goes over the human audible range.

The weight of the nanocrystalline version designed under these criteria was approximately 6kg compared to approximately 15kg of the ferrite version. However large mass and the wider radiating area of the ferrite version give the advantage of reduced overall temperature rise at the condition of thermal equilibrium. In order to account for this fact it is required that a winding wire with a wider cross section is used for the nanocrystalline version. This results in increase in the weight of the nanocrystalline version slightly reducing the weight ratio advantage over ferrite. Further all the disadvantages of a thicker conductor in high frequency applications discussed in the paper need to be considered in increasing the conductor cross section of nanocrystalline version.

Based on the results obtained in this study it could be concluded that a considerable reduction in the weight and size could be reached by the use of nanocrystalline material as a core for a high-power high frequency transformer and it was intended to construct a 200kW transformer operating at 20kHz as the next step of the study. However, it should also be noted that the cost of each version highly depends on various commercial aspects.

In this section the optimum design of high power high frequency magnetics is discussed based on a 50kW application operating at 50 kHz. An in depth theoretical explanation on minimizing the losses at high frequency is discussed

In the section 4.8 of this thesis the achievement of 100kW in 20kHz transformer is discussed. This development is an extension of a series of developments carried out with high frequency, high power transformers of power and frequency levels such as 40kW, 20kHz and 50kW, 50kHz. The advantages and disadvantages of Ferrite and Nanocrystalline core materials at this power levels are discussed and the choice of Nanocrystalline core is explained.

The results of these studies are discussed in detail in the chapter. The patented constructions developed that are also relevant to the core less management is discussed in the chapter 5 as that relates to the thermal management of the overall product as well.

## Chapter 5

### Thermal Management of High-Power High Frequency Magnetics

## Chapter 5 Thermal management of High-power High Frequency Magnetics

Although hot spot temperature is a performance parameter (Pierce, 1996), to be met by the manufacturer, there are currently no test methods or requirements that this parameter be measured on production or prototype transformers. This seems extremely peculiar since it is the fundamental parameter determining the life of the equipment and the thermal evaluation standards give test methods for determining the rated hot spot temperature of an insulation system. Most manufacturers of dry type transformers simply add 30 °C to the average temperature rise (calculated using empirical equations) and claim this is "per the standards", although the IEEE standards do not state that this is permissible practice. IEEE standard (37.12.01-1989 requires that both average winding temperature rise and hot spot temperature are limits to be met at rated kVA. The difference between these two limits is 30 °C but the 30 °C does not appear as a separate number. Many dry-type transformer manufacturers would like users to believe that the subject of dry type hot spot temperatures is a mysterious subject. They would like you to believe that almost nothing is known on this subject with no published papers, etc. They also claim that the hot spot temperature is difficult to measure and that since there is no IEEE test method, they are under no obligation to conduct testing, etc. They also convey the impression that temperatures in transformer windings are somewhat uniform and the 30 °C allowance is for localized heating at a spot which cannot be predicted. They also try to give the impression that the 30 °C allowance was adopted in standards as a maximum number and that it is usually less than this value. Some even claim that most manufacturers take steps to see that the allowance is always less than 30 °C in their designs. ANSI/IEEE Standard 1 supports these arguments by stating that the hot spot allowance value is arbitrary, difficult to determine, and depends on many factors, such as size and design of the equipment. The hot spot is simply the highest temperature in the transformer windings. It is a naturally occurring phenomena due to the generation of losses and the dissipation of those losses by the heat transfer mechanisms. All transformers have a hot spot since at some place in the winding the temperature is the highest. Many commercial computer programs are advertised to predict temperatures in equipment. Readers of magazines such as Machine Design or Design News in which these programs are described would naturally expect manufacturers to have the capability to calculate the maximum temperature in the transformer windings. Similarly readers of magazines such as the IEEE Spectrum would naturally expect manufacturers to have the

ability to calculate the eddy loss distribution within the windings. With modern computer technology it should be possible to predict the hot spot temperature. Dry type transformers have unique heat transfer characteristics which are not well known. For this reason, a proprietary 3-D program for heat transfer calculations in dry type windings was developed. The program was refined by tests on windings and prototype transformers with embedded thermocouples.

There have been extensive investigations of liquid filled transformer heat transfer phenomena with many published papers. Some companies have chosen not to publish their test results and computer calculation methods and expertise depends on the manufacturer. Harold Moore, a consultant, recently reported that information submitted by manufacturers of large transformers during design reviews show that some have detailed computer analysis of the thermal design but others calculate the hot spot simply by adding 15 °C to the average temperature rise. An accurate electromagnetic and thermal analysis is essential for transformers designed for non-sinusoidal load currents. An example of this type analysis for liquid immersed transformers is given by the paper of Preiningerova, Kahoon, and Doiezel(Preiningerova et al., 1983, Karsai et al., 1987)and in the book by Karsai, Kerenyi, and Kiss (Karsai et al., 1987). Heating due to harmonic currents may also occur in utility transformers(Dugan and Mcdermott, 2002).

## 5.1 Thermal Investigations for Dry Type Transformers

### History of the 30 °C Allowance

Based on the 1944 experimental works of Stewart and Whitman(Stewart and Whitman, 1944) and Satterlee (Satterlee, 1944), NEE standards used a hottest spot allowance of 30 °C for 80 °C average temperature rise. The conclusion of Stewart and Whitman from 1944, that the ratio of hottest spot temperature rise to average temperature rise was constant, appears to have been forgotten in present industry standards for ventilated dry type transformers. The 30 °C hottest spot temperature allowance established in 1944 for 80 °C average temperature rise was approximately correct. At that time average kVA ratings were less than the present. The 150 °C average winding temperature rise for the 220 °C insulation temperature class was extended to ventilated units initially in NEMA Standards and later in IEEE standards and the 30 °C hottest spot allowance incorrectly retained. The 1989 IEEE standard used a constant 30 °C hottest spot allowance for all insulation temperature classes and all size transformers. The

IEC standard uses a variable hottest spot allowance from 5 °C to 30 °C. B. Recent Hot Spot Investigations-Dry Type Transformers following tests on dry type transformer windings and prototypes have been carried out and the results have been shared with the industry (Pierce, 1996):

1. 2000 kVA cast resin transformer, 300 imbedded thermocouples, 22 test runs.
2. Six thermal test coils of different duct sizes, 142-171 thermocouples, 97 test runs for fundamental heat transfer data.
3. 2 500 kVA prototype with disc high voltage windings and embedded thermocouples.
4. 2 500 kVA prototype with sheet conductor low voltage winding containing embedded thermocouples.

The above investigations represent the most comprehensive investigation of dry type transformer heat transfer since that of Stewart and Whitman (Stewart and Whitman, 1944) 50 years ago. Stewart and Whitman were the only investigator to determine the effect of core loss on the hot spot temperature by conducting comparative loading back and short circuit heat run tests. The Stewart and Whitman discovered that the ratio of hot spot rise to average rise was essentially constant for a given winding and depended on duct size and winding height. C. Hot Spot Temperature of Cast Resin Transformers

The author's test data by Stewart and Whitman indicated a ratio of hot spot rise to average rise of 1.20 to 1.25 for the cast resin transformer design tested. This is lower than the ratio of 1.4 to 1.5 for large ventilated dry type transformers due to the extremely large cooling duct sizes and the large amount of winding surface area available for radiation heat loss. Cast resin designs with smaller internal cooling ducts would be expected to have hot spot ratios similar to ventilated dry type transformers.

#### Hot Spot Temperatures of Ventiladed Dry Type Transformers

Stewart and Whitman discovered that there is a large thermal gradient from the bottom to the top of the windings of large (above 500 kVA) dry type transformer". This gradient is dependent on the height (length) of the winding. IEEE standards utilize a constant 30 °C allowance between the hot spot temperature rise and the average temperature rise. To meet hot spot temperature rise limits requires that the average temperature rise be reduced below guarantees because the difference between hot spot and average temperature rise may be more than 30 °C. The recent data indicated that the hot spot increment may be up to 60 °C on large transformers (generally above 500 kVA). A comparison of the Stewart and Whitman test results with the



IEEE assumed temperature gradient for a typical winding is shown in Fig.5.1 Changes in IEEE standards to more accurately reflect the relationship between average temperature rise and hot spot rise in large (above 500 kVA) dry type transformers has been proposed. An IEEE Working Group has been formed to review these proposals for a future revision of (37.12.01 Table 4A. It will be difficult to reconcile the divergent opinions on this subject and most manufacturers are unwilling to change IEEE standards since it increases their transformer cost(Institute, 1989).

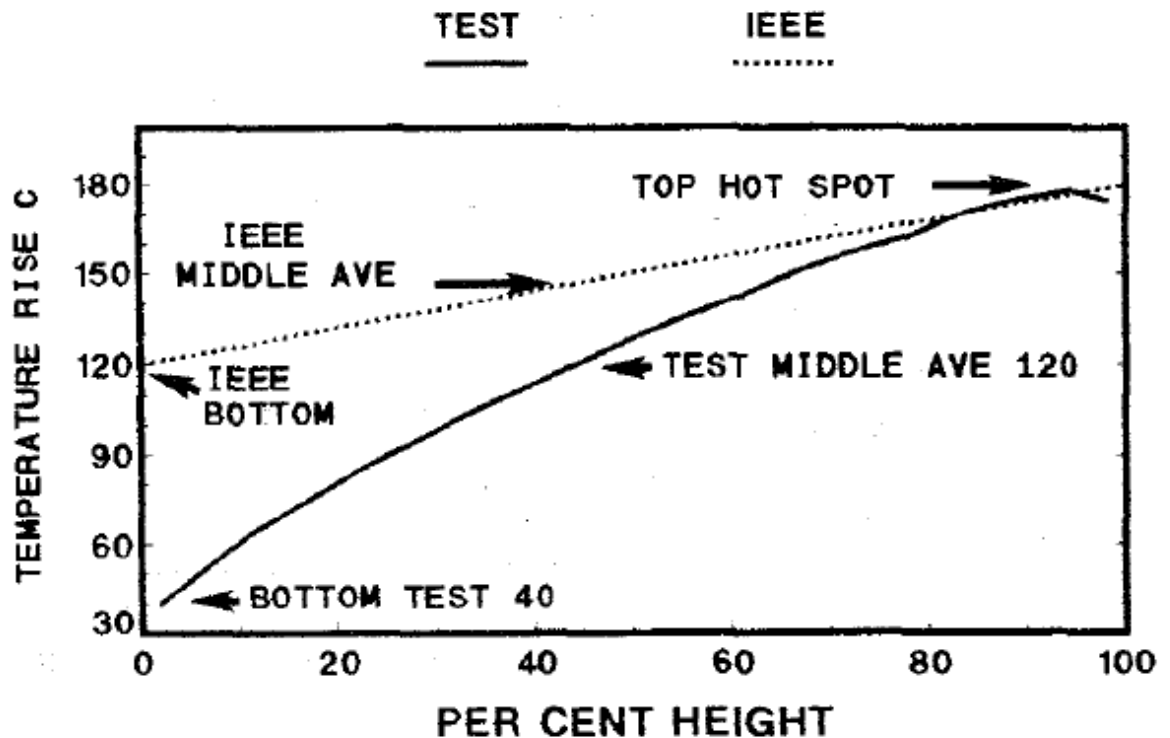


Figure 5-1 Comparison of test data with IEEE standards

#### Example calculations for ventilated dry type transformers

A dry type transformer was required rated AA-T-60-300-13800-950 with a harmonic current content equivalent to a k-Factor of 13. Loss data was as follows:

Resistive losses LV 7650 watts

Resistive losses HV 15 446 watts

Eddy Loss LV 326 watts

Eddy Loss HV 225 watts

Stray Loss 1 744 watts

For this transformer the high voltage winding had a higher hot spot temperature even though the eddy loss was lower than the low voltage winding. The low voltage winding used a sheet conductor which provided good heat conduction from the high eddy loss region. The electromagnetic analysis indicated a eddy loss of 1.46 % of the ohmic loss for the high voltage winding. The three-dimensional mathematical model [W] developed to predict hot spot temperatures in ventilated dry type transformers allows for eddy loss variation throughout the winding. The computer program was used to perform a sensitivity analysis of the relationship of eddy loss magnitude and distribution on the average and hot spot temperature rises. The distribution of the eddy loss for two cases is described in Table 5.1

The analysis was performed with the calculated average eddy loss of 1.46 percent of the ohmic loss for K-factors of 1 and 13. A calculation was performed with a slightly higher eddy loss of 2 % to show the effect of the uncertainty on the hot spot rise and average rise. The results are summarized in Table I1 and the temperature distribution for eddy loss distribution case number 2 is shown in Fig.5.2 The sensitivity analysis indicates that the hot spot temperature rise is influenced considerably more than average winding rise by changes in eddy loss magnitude and location. Test methods which simply increase sinusoidal current to give the same losses will give approximately the same average temperature rise but hot spot temperatures may vary considerably.

Distribution	Description
Case 1	Eddy loss was distributed throughout the winding and the eddy loss at the top and bottom five per cent of the winding was four times the average eddy loss distribution.
Case 2	All the eddy loss was assumed to be at the top and bottom five percent of the winding

Table 5-1 Eddy loss distribution

Table 5-2 Calculated temperature rise variation with eddy loss magnitude and distribution

K-factor	Dist. Case	EL %	Ave. rise °C	Hot spot rise °C
1	1	1.46	80.2	128.1
1	1	2.00	80.5	128.7
1	2	1.46	80.2	129.7
13	1	18.98*	89.0	151.9
13	2	26.00**	92.3	160.7
13	2	18.98*	87.5	176.9
*1.46 x 13 = 18.98      **2.0 x 13 = 26.0				

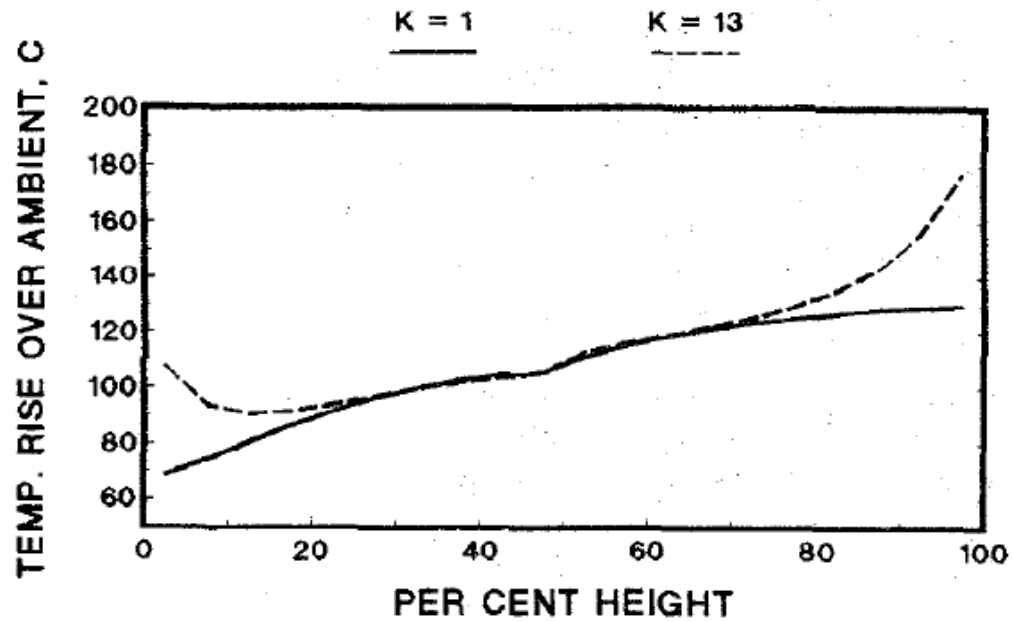


Figure 5-2 Effect of harmonic losses on temperature rise.

## 5.2 Hot spot investigations for liquid filled transformers.

In the decade of the 1990's the technology focus in the transformer industry was on thermal performance and load ability. Many transformers undergo planned overloading by electric utilities to maximize the return on the investment in this expensive equipment. As reported recently by W. J. McNutt(McNutt, 1992), "all load ability decisions are based on hottest conductor temperature, but that parameter is never measured during a thermal test, and some manufacturers never actually calculate what it would be for rated loading.

The thermal equations provided in the loading guide are recognized to be grossly inaccurate for some cooling modes and not precisely correct for others". Since the loading guide equations were first proposed in 1945, many papers and trade press articles have been written on transformer loading using these equations. It is generally stated that the equations are conservative without giving test data to substantiate this statement. The equations have been incorporated into computer programs by consultants and utilities. Until recently little research has been performed on measurements of hot spot temperatures in windings of full-size transformers during transient loading. Thermal research has centered on computer modeling of steady state performance with tests on model windings to obtain data to validate the models. The purpose of these studies was to predict thermal performance more accurately at nameplate ratings to minimize the manufacturer's cost. Transformer manufacturers have investigated liquid filled transformer heat transfer phenomena for over a hundred years with many published papers. Many of the design equations are based on proprietary test data obtained by many researchers. The recently reported investigation on a full-size test winding with embedded thermocouples to investigate transient loading on the hot spot temperature. The tests indicated that the industry loading guides were not valid for all modes of cooling and all loading conditions. During overloads there is a time lag between the top oil temperature rise in the tank and the oil rise in the winding cooling ducts. Thermal tests were also performed on a 5 600 kVA prototype transformer at various loads to compare the hot spot temperature with oil and silicone fluids. The test data was used to refine an analytical computer program to calculate hot spot temperature(Pierce, 1992b, Pierce, 1992a).

Modern computer technology now permits more refined calculations of loading capability. An improved system of equations was developed (Pierce, 1992a) for inclusion in the next loading guide IEEE Guide for loading Mineral Oil Immersed Transformers. The improved system of loading equations is based on the fluid flow conditions occurring in the transformer during transient conditions. The equations and computer program also incorporated an improved

method of calculation for variable load cycles and variable ambient temperatures. The properties of the low flammability fluids polydimethylsiloxane (silicone) and high temperature hydrocarbon (hthc) were also incorporated into the improved loading equations.

In the 1980s direct measurement of winding hot spot using fiber optic detectors became feasible. In the 1990's thermal research is moving into studies of overload performance using these fiber optic hot spot detectors. Due to the high cost and poor reliability of the fiber optic devices their use appears to be primarily as a research tool to measure hot spot during factory thermal tests on transformers and for use on selected units to obtain dynamic loading data under actual field conditions. Due to the poor reliability, redundant probes must be used. Experience such as that reported in a recent Doble paper by Troisi (Troisi, 1992) indicates that even with extreme care in installation, about 25 to 33 percent of the probes can be expected to fail due to damage. Reported data indicated that the location of the hot spot is difficult to determine. A recent survey reported that two to eight sensors would be adequate if placed in the winding where the higher temperature is expected but for prototype transformers it was estimated that twenty to thirty sensors would be required.

### Example calculation for liquid filled transformer

An oil immersed transformer rated OA-T-60-3600 kVA-22000Y-575 was designed for a specified harmonic current content. After installation actual harmonic currents were measured and the current spectrum supplied to the manufacturer with a request to check the temperature rises.

At rated load and 60 Hz. the tested losses were:

No Load 4072 watts

PR 27 821 watts

Stray and eddy loss 4 060 watts

Total loss 35 953 watts

Temperature rises above ambient were:

HV Ave. Rise 48.1 °C

LV Ave. Rise 47.6 °C

Top Oil Rise 47.2 °C

Hot Spot rise 55.3 °C

A calculation using the harmonic current distribution gave;

$$\sum_{h=1}^{h=h_{max}} \left[ \frac{I_k}{I_R} \right]^2 k^2 = 6.28$$

5 - 1

$$\sum_{h=1}^{h=h_{max}} \left[ \frac{I_k}{I_R} \right]^2 h = 1.62$$

5 - 2

Engineering analysis indicated the division of the eddy and stray loss to be;

eddy loss 316watts

stray loss 3 744 watts

With the harmonic load currents the losses are;

No Load 4 072 watts

I\* 27 821 watts

eddy loss 6.28 x 316 = 1 984 watts

stray loss 1.62 x 3 744 = 6 065 watts

Total loss 44 014 watts

As indicated by equations in the IEEE Loading Guide "IEEE Guide for loading Mineral Oil Immersed Transformers" , for the OA cooling mode, the top oil rise is proportional to the losses to the .8 exponent and may be estimated for the harmonic losses from the test data at rated load and losses as shown below:

$$TOR = \left[ \frac{44\ 014}{35\ 953} \right]^{0.8} 47.2 = 55.5\ ^\circ C$$

The maximum per unit eddy loss occurred in the high voltage winding and was calculated to be 2.0 per cent of the ohmic loss. Assuming that the maximum eddy loss at the hot spot region to be four times the average eddy loss would give an eddy loss of 8.0 per cent of the ohmic loss density at the hot spot location. The hot spot rise over top oil can be calculated as,

$$HS\ OVER\ TO = \left[ \frac{1 + (6.28)(0.08)}{1 + 0.08} \right]^{0.8} (55.3 - 47.2) = 10.5\ ^\circ C$$

The hot spot rise over ambient = 55.5 + 10.5 = 66.0 'C.

This is less than the permissible hot spot rise of 80 "C

### 5.3 Temperature Rise for High Frequency Transformer under Forced-air Convection

Transformer design plays an important role in high-frequency switch mode power supply design. The most important limiting factors for high frequency transformer design are the core saturation and temperature rise induced by core losses and winding losses. The temperature rise is dependent on its surface area, cooling environment and power losses. To verify that temperature does not exceed material specification and can meet safety requirements, an estimation of power losses and temperature rise becomes an important design step during its preliminary design process. In the conventional design process, the power losses and temperature rise of the transformer are often ignored in preliminary design. This is because the power losses are too complicated to calculate and the evaluation tool for temperature rise is not available to get an accurate result. The skin effect describes that current distribution within the conductor and can be found by solution of Maxwell's equations. For high frequency sine wave current, the result is that the current density is greatest at the surface of the conductor. The current density is an exponentially decaying function of distance into the conductor. The current crowds near the surface of the conductor, the center of the conductor is not utilized, and the effective conductor cross-section area is reduced.

However, the skin effect alone is not sufficient to explain the increased high frequency winding losses observed in multiple-layer windings. The proximity effect illustrates that the externally applied magnetic field, which is built by the multiple-layer windings will induce eddy currents to flow in a conductor, and thereby induce loss in adjacent conductors. To avoid the skin effect and proximity in the winding, the copper foil and Litz wire are generally used to replace the round wire. The copper foil with a width equal to the core window width is often applied for low voltage, high current windings with few turns and large conductor area. The thickness of copper foil can be similar to or smaller than skin depth to reduce the eddy current losses. Litz wire is another means of increasing the conductor area while maintaining low skin effect and proximity effect. Tens, hundreds or more strands of small-gauge insulated round wire are bundled together, and externally connected in parallel. For Litz wire, it is assumed that the individual wires of the strands are interleaved and twisted along the entire divided conductor. This ensures that the current will divide equally among the separate strands, and can greatly decrease the loss induced by skin effects and proximity effect. In the past years, some analytical models for winding losses with solid conductor windings have been studied

(Dowell, 1966, Vandelac and Ziogas, 1988, Tourkhani and Viarouge, 2001, Carsten, 1986). The first analytical model, which has been proposed by Dowell (Dowell, 1966), is restricted to foil conductor windings. Then, Vandelac (Vandelac and Ziogas, 1988), which arrange the winding geometry, have been proposed for extending the analytical model of foil conductor winding to round wire windings. However, this will be too pessimistic the winding loss of round wire (Tourkhani and Viarouge, 2001). For the round wire and Litz wire study, in (Carsten, 1986), the 1D solution of foil conductor is applied to round Litz wire winding, providing that a foil conductor is equivalent to a stack of thinner foils. In (Tourkhani and Viarouge, 2001) an analytic model of winding for Litz wire is derived based on the linear distribution of the leakage field across the winding layers. In (Vandelac and Ziogas, 1988) and (Tourkhani and Viarouge, 2001), the analytic models can be applied to calculate the multiple layer winding loss of foil conductor and Litz wire, respectively. However, these two models are starting with zero magneto-motive forces (MMF) boundary conditions. In most application, there may be multiple outputs for converter design and this will result in multiple secondary windings, not only single secondary winding in transformer.

In considering eliminating the proximity effect, the winding strategies may select interleaving or partially interleaving. All of these designs will cause the winding model starting with non-zero magneto-motive boundary conditions. The high frequency winding losses for multiple-layer copper foil and Litz wire windings with MMF boundary conditions has been studied in (Chang et al., 2010).

To extend results based on (Chang et al., 2010), this paper develops analytical models of winding losses for multiple-layer copper foil and Litz wire windings with MMF boundary conditions.

In these two models, geometric parameters of conductor and distribution of magneto-motive forces are considered in the formulation of the winding losses equation. Then, the thickness of copper foil and strand diameter of Litz wire is considered to obtain the minimum winding losses. Because of the skin effect and proximity effect, the winding losses in high frequency transformer are significantly in excess of the dc loss. In this study, analytical models of winding losses for multiple-layer copper foil and Litz wire windings with MMF boundary conditions are derived, respectively. In these two models, geometric parameters of conductor and distribution of magneto-motive forces are considered in the formulation of the winding losses equation.

Comparing with the FEM simulation result, it shows that these two models have good accuracy. Then, the thickness of copper foil and strand diameter of Litz wire is discussed to obtain the minimum winding losses. It reveals that the characteristic of Litz wire is similar to copper foil.



As the duty cycles decrease or the MMF boundary condition increase in positive tendency, the proximity effect will increase. Hence decreasing the thickness of copper foil or strand diameter can eliminate the proximity effect and reduce the winding losses.

## 5.4 Numerical Analysis of Winding Temperature Field for Dry Type Transformer

Because the insulating media in dry type transformers are mainly epoxy resin and air, the dry type transformer has the advantages of safety and environmental protection. But its heat performance is not so good as that of an oil-immersed type transformer. Hot spot temperature is the principal reason for affecting transformer life span(Susa and Nordman, 2009). Nevertheless, the demand in performance and economy cannot be met by testing or traditional design methods of hot spot temperature now. Under the case of both transformer capacity and failure problems caused by local overheating increasingly, numerical analysis on temperature field distribution of windings is very important for dry type transformer design and its reliable operation(Pradhan and Ramu, 2003, Jing et al., 2012).

Based on the analysis of winding structure features for a 2500kVA dry type transformer, a reasonably simplified model of winding temperature field is established. Then, the winding temperature field is calculated by using FVM and validation of hot pot temperature is confirmed by comparison of both calculating and testing results. Some useful distribution rules are analyzed for dry type transformer design (Jing et al., 2012)

### 5.41 The simplified model and boundary conditions

The analyzed dry type transformer is three phase, two winding structure with many layer cylinders along radial direction and its low voltage (LV) winding with foil conductor is divided into four layers, its high voltage (HV) winding with ordinary wire being divided into two layers. They have cool air way with epoxy resin material between the core and windings, and the layers of windings (WANG et al., 2010, Swift et al., 2001).

A. The Simplification and Assumption of The Model On the bases of analyzing structure and performance for a 2500kVA dry type transformer, the main simplifies and assumptions are the following when winding temperature field is calculated(Jing et al., 2012)

- Assuming that temperature distribution of transformer windings along circumferential direction had no gradient change. Then, steady temperature field can be approximately

calculated by using axial symmetry FVM and the simplified model composed of a half along center plane of a phase is shown in figure 5-3, according to the structure symmetry of three phase transformer windings and cores(Jing et al., 2012).

- Heat sources are produced by the losses of both core and windings respectively. According to the loss distribution, heat source in core is approximately uniform, and heat source in windings is divided into some subregions along their axial height of every layer (in figure 5-3 each layer LV is divided into seven subregions and each layer HV is ten subregions), because of uneven eddy current losses in two ends of windings. and the windings losses or heat sources vary with itself temperature. The effects of the clamp and tie-plate are ignored.
- The boundaries of air fluid are far enough from the core and the windings.
- When the heating and cooling achieve to a thermal balance in the operation process of dry type transformer, the temperatures of both winding and air fluid don't vary with time.
- The density, specific heat, thermal conductivity of both solid material and air in dry type transformer and ambient temperature are constant. The dynamic viscosity of air fluid is constant.

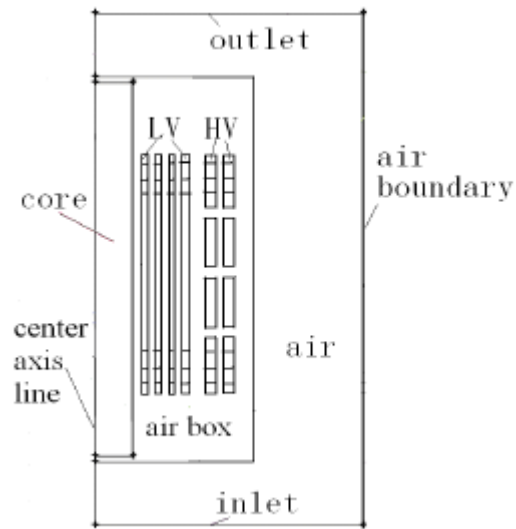


Figure 5-3 The simplified model

### Heating and Cooling Analysis of Dry-Type Transformers

The heat source analysis: Heat sources in dry type transformers are mainly the core and windings. The heat sources in the HV and LV windings are mainly composed of two parts of loss, the one being the DC resistance loss and the other being winding eddy current loss caused by the leakage flux. The distribution of the former is uniform and that of the latter is uneven. The total loss of two parts is called as load loss of dry type transformer. Because the resistivity of winding conductor varies with the temperature, the loss of winding is a function of temperature and the heat source is nonlinear, represented generally by using loss value of 120 degrees. According to the loss distribution characteristic, the heat source in core is approximately uniform and equivalent heating object. The heat sources in the windings are composed of the losses of some subregions and every part is regarded as uniform and equivalent heating object. Then, heat source density of every heating object can be obtained by the following formulae:

$$q_v = \frac{P}{V}$$

5 - 3

Where,  $q_v$  is heat source density of the transformer core or winding subregions(w/m<sup>3</sup>);  $P$  is the loss of of heating source (w);  $V$  is the volume of heating source(m<sup>3</sup>). For the insulating part, it is set to  $q_v = 0$ . 2) The heating and cooling analysis: The ways of heating and cooling in dry-type transformers have heat conduction, convection, and radiation. The inner heat quantity of both transformer core and winding is transferred to the outer surfaces which are in contact with air by heat conduction from the hottest point, so there is a temperature difference between the outer surface of heating object and air fluid. Then, the outer surface heat quantity of heating object is transferred to surrounding air by convection and radiation. The cooling of windings has a great relation to the structure of winding surface and the status of surface fluid when the transformer is operating. Because the temperature, fluid velocity and roughness of winding surface along its axial height is not same, so is the heat transfer coefficient along axial height of winding. In this paper, the heat transfer coefficient of the winding surface not to be constant is set by automatic coupling way of both fluid and solid using temperature field software solver. The heat transfer coefficient determined by this coupling way varies with the change of both air temperature and velocity, thus, the calculation results are more accurate.

### The Governing Equation and Boundary Condition

1) The governing equation and boundary condition: By the above assumption and simplification, thermal conduction equation of the steady-state temperature field in transformer winding is as follows(Jing et al., 2012, Wang and Tao, 2008):

$$\frac{\partial^2 t}{\partial r^2} + \frac{1}{r} \frac{\partial t}{\partial r} + \frac{\partial^2 t}{\partial z^2} + \frac{q_v}{\lambda} = 0$$

5 - 4

where,  $t$  is temperature (°C);  $\lambda$  is thermal conductivity of the material (w/m-k).

The air fluid boundaries of upper, down, and right in figure 5-3 are all first type condition ( $t$  equals environmental temperature) and its left boundary is second type condition depending on core loss density. The internal boundaries with convective and radiative heat transfer are the third kind of boundary condition and can be obtained by the following formulae:

$$-\lambda \left( \frac{\partial t}{\partial n} \right)_w = h(t_w - t_f)$$

5 - 5

Where,  $n$  is the vertical direction,  $h$  is the integrated heat transfer coefficient,  $t_w$  is the temperature of solid object wall,  $t_f$  is the air medium temperature of the surrounding fluid.

2) Initializing the boundaries and setting material properties: According to the ambient temperature and air velocity at hot spot temperature testing, the three boundaries temperature of upper (air outlet), down (air inlet) and right (air fluid) in figure 5-3 is 15.0 (°C), and velocity of fluid inlet is 0.15 (m/s). The relative pressure stress of fluid outlet is 0.

3) Setting material properties: The density of air fluid is 1.225(kg/m<sup>3</sup>); The viscosity coefficient is 1.7894e-05 (kg/m·s); The thermal conductivity and specific heat of air is 0.1242(w/m-k), 1006.43(J/kg·K) respectively. The density, the specific heat and thermal conductivity of winding conductor is 2719(kg/m<sup>3</sup>), 900(J/kg·K), 287(w/m-k) respectively. The density, specific heat and thermal conductivity of the insulating resin is 980(kg/m<sup>3</sup>), 1400(J/kg·K) and 0.25(w/m-k) respectively.(Wang and Tao, 2008, Zhang and Li, 2004)

## 5.5 Effective heat removal of high-density magnetics

### 5.51 Construction for the natural convection cooling

Even though a high level of minimization of losses achieved with the appropriate operating flux levels and winding techniques in this 100kW transformer the high level of miniaturization archived results in considerably high-power density. This makes it challenging to maintain the temperature rise under convection conditions.

The surface area of the product or the enclosure is not sufficient for the effective removal of heat under natural convection.

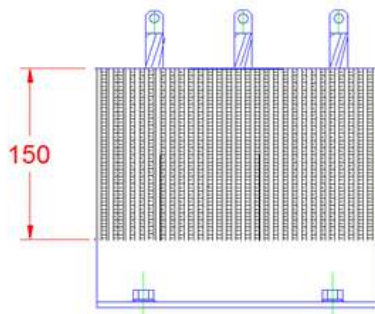


Figure 5-4 Housing construction for the natural convection cooling

Therefor an enclosure made from heatsinks as shown in the figure 5-4 considered as a method of heat removal.

### 5.52 water cooled plate mounting

Alternative approach considered for the effective heat removal is the use of water-cooling arrangement of the end product for the cooling of magnetic components. Under this the high frequency transformer will be mounted on water cooled plate as shown in the diagram below.

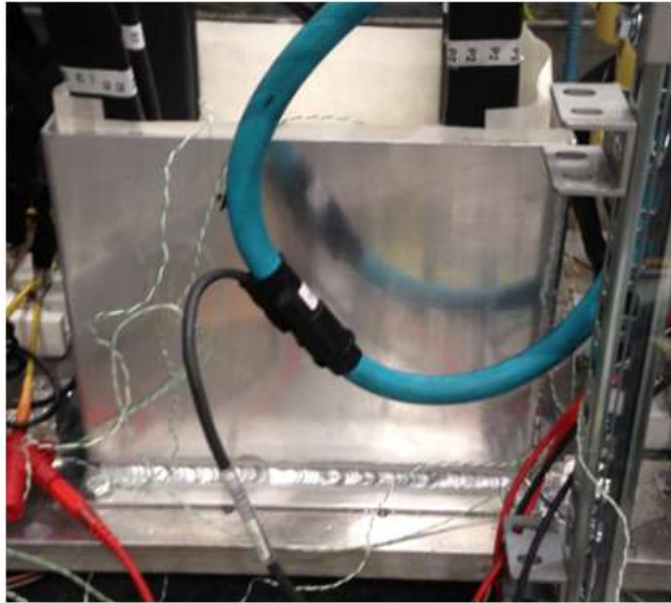


Figure 5-5 Transformer mounted in water cooled plate.

In order to effectively remove the heat generated in the inner parts of the core heat pipe and heat sheet options were considered. However, the fact that the heat must be transferred towards the bottom direction and the short operation life of heat sheets such as 16 years in continuous operation made the use of them non suitable for the application. Therefore, an enclosure with specially engineered interior was used.

After taking the above discussed factors into consideration a 100kW,20kHz transformer was constructed. A winding arrangement as discussed in 2.1.3 was also constructed.



Figure 5-6 100kW, 20Hz HF transformer

The research discussed in this section was carried out with the intention of achieving compact, high power, high frequency transformers that are capable of handling power levels in excess of 100kW. These studies and a series of the previous developments carried out have identified the advantages of using the materials such as Nanocrystalline for high power applications and for operating frequency levels in the range of 20kHz to 30kHz. With the appropriate thermal management approaches and designing at optimal operating flux levels Nanocrystalline core gives a considerable volume and weight advantage over the ferrites. At high power levels the winding design becomes very important for the mitigation of high frequency losses. Two winding constructions are discussed in this paper. The novel method proposed with folded foils showed very good performance in mitigating the high frequency conductor losses. Further it gives the possibility of controlling the leakage inductance between the primary and secondary windings by adjusting the level of overlap. The disadvantage observed in this method was the time consumed for the proper insulation figure 5-8. Temperature rise with modified interior housing Temperature in °C. Time in s Through several insulating techniques were considered the amount of time savings archived was not sufficient to adopt this method in mass production. Therefore further research is necessary to improve the production process for the successful implementation of this technique. The second method proposed with sandwich winding could be seen as a good compromise on the performance and the amount of labor consumption. The tests carried out with a standard enclosure showed that the amount of heat transferred to the cooled plate was not sufficient to maintain the hot spot temperature below the desirable level. However the desirable conditions could be archived with an enclosure with correctly engineered interior. It could be concluded that with the appropriate material selection, winding techniques and with the thermal management techniques the construction of a 100kW high frequency transformer could be archived. The product showed very stable performance and presented a very compact construction giving a volume to power density of over 18W/cm<sup>2</sup> or weight to density of over 6.5kW/kg. This was a considerable reduction in the size and volume against the conventional ferrite construction considered. Further tests studies carried out showed the possibility of achieving even higher powers such as 150kW or even 200kW in a single high frequency transformer operating at a frequency range of 20kHz to 30kHz with a compact construction is possible in a similar compact structure. In parallel with the industry demand it was intended to continue the research towards these power levels as part of future work

## 5.6 Estimation of Temperature Rise in MVA Range Dry-Type Transformers and Practical Verification Based on Simulated Loading

Dry-type transformer becomes the preferable choice in many applications due to its construction specific advantages over oil-cooled transformers. However, they inherent low thermal conductivity giving the rise to high operating temperatures. The temperature rise of a transformer is an important factor deciding its safe operation and the useful life span. With the increase of the power rating of the transformers the amount of heat generated during its operation increases. Thus the construction of large dry type transformers requires a details understanding of their thermal behavior. In this paper the development of a 1.2MVA single phase dry-type transformer is discussed. The constructed product was tested for a 1.2MVA loading condition base on simulated loading method. Practical vales are compared with the theoretical predictions.

Transformer, as an important part of the transmission and distribution system, plays an important role in the safe operation of power grids(Ning and Ding, 2012). In comparison with the oil-cooled transformer, dry-type transformer shows a good performance in fireproof performance, mechanical properties, die-electric strength, anti-short-circuit ability, heat resistance etc. Further, the feature of less pollution and convenient installation make it widely used. However, the low thermal conductivity of the dray-type transformer makes its operating temperature higher than the oil-type/oil-cooled transformers. This directly influences the performance and the service life of dry-type transformers (Ding and Ning, 2012).The temperature rise is an important indicator of the safe operation of dry-type transformers. The excessive temperature is a main factor that shortens the service life of dry-type transformers(Ding and Ning, 2012). Further, the modern applications often require high power transmissions which inevitably require a greater capacity and larger size. This increased the single capacity of a transformer causes higher losses, the resulting local overheating problems, inconvenience due to larger size and costs. Therefore, it is necessary to make a good thermal design in order to manufacture compact size and efficient transformers (Li et al., 2013b).

The study discussed in the papers is based on a 1.2MVA single phase transformer developed for a laboratory application. This transformer is to be used in a partial accelerator arrangement in a research facility in the United Kingdom. The requirement of handling a power of 1.2MVA in single phase itself made the design of the transformer outstanding. Further, the proper operation of the unit over a long period was a vital factor due to the nature of the application.



Therefor a detail study of the thermal model was carried out in arriving at the suitable design that gives the required compact size and reasonable temperature rise that ensures a long-life operation.

The developed product was subjected to a load test to evaluate the accuracy of the theoretically predicted temperature. It is generally not practical to carry out a full load test of a MVA range transformer under laboratory conditions. This situation is well identified in the transformer standard BS EN 60076-11(Power Transformers Dry-Type Transformers) and a simulated loading method is defined for the load tests of larger transformers.

Even under the simulated loading conditions the transformer is supposed to be loaded with a power exceeding 85kVA. It is a quite challenging task to obtain a single-phase power of 85kVA in practice. Therefore, a test transformer was developed with the open delta vector configuration. This transformer was used as a phase conversion transformer for converting the three-phase power into a single-phase power so that the single phase 1.2MVA transformer can be loaded.

The temperature rise obtained from this simulated loading method is compared with the theoretically predicted values.

## 5.61 Theoretical background

### Thermal Modeling

The temperature rise of the transformer components is caused by all of the device electrical losses, which are the no-load and load losses. It is known that the thermal behavior within the electromagnetic device is composed by conduction, convection (also known as heat advection) and radiation (Arjona et al., 2014, Lu et al., 2003).

The transformer can be considered to have a geometrically symmetric structure. Therefor a simplified model can be established. One of the limbs in a three-phase transformer can be taken as the main research object in calculation. In the case of a single-phase transformer with a high power rating similar to the product discussed in this paper where the UI construction is used (UI construction is suitable for single phase transformers with much lower power rating than the one discussed in this paper) one of the two limbs can be considered as the main research object (Gao et al., 2012). The construction of the limb of a transformer similar to the

one investigated is illustrated in the Fig. 1. This simplified construction is very much useful in the thermal analysis especially in the analysis of the thermal field distribution.

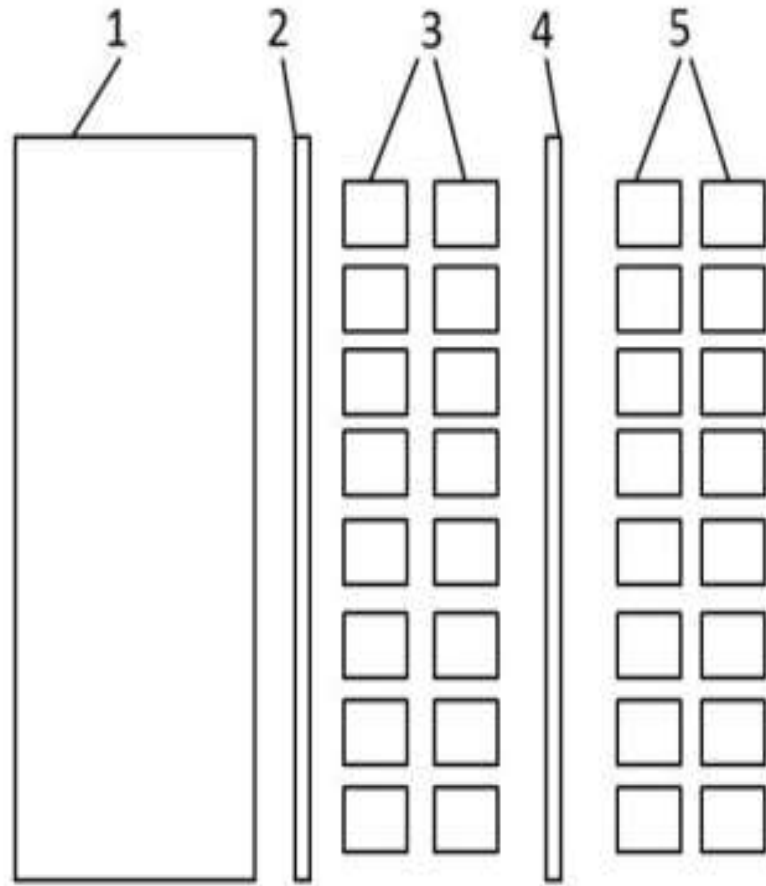


Figure 5-7 Simplified diagram of a transformer coil structure . 1. Si-Steel core, 2. Primary winding to core insulation barrier, 3. Primary winding 4. Primary winding to Secondary winding insulation barrier, 5. Secondary winding; note: Depending on the design specific conditions designers use air ducts in between any of the above layers

The transformer coil construction described in figure 5-8 can be illustrated with the three dimensional model developed for the evaluation of the overall construction as shown in the figure 5-9 The exposure of the Si-steel core and the windings to the environment can be seen in this figure.

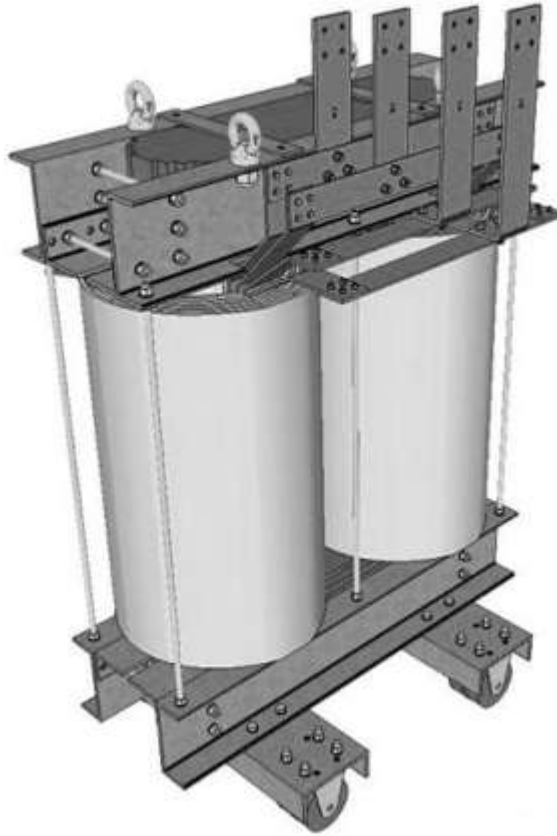


Figure 5-8 Three-dimensional model of the 1.2MVA transformer

When the transformer is in operation, part of the electromagnetic energy is transferred into heat energy, i.e., the transformer generates energy loss in the windings and other components, which is converted to heat. One part of the heat increases the transformer temperature and the other part distribute to the sounding medium. The heat generating elements can be roughly divided into two parts which are the windings and the Si-steel core of the transformer (Ding and Ning, 2012).

#### Transformer core temperature rise

In a dry-type transformer as shown in the figure 5-9 Si-steel core is one of the heating elements and these losses that generates the heat are called core losses, iron losses or no-load losses of the transformer. These no-load losses refer to the hysteresis loss and eddy current loss. The

two losses are associated with Si-steel sheet material, magnetic density values and have a great relationship with the silicon sheet processing.

The heat dissipation area of the core can be divided into the exposed part and non-exposed part. The exposed area includes the upper surface of the iron yoke; figure 5-9, the side surfaces of the upper and lower iron yokes and vertical outer surfaces coming out of the windings. Non exposed area includes sides of the air ducts in the core and the surface of the iron core column, which is surrounded by the winding or insulation, and so on. The thermal load of the transformer core can be expressed as follows (Ding and Ning, 2012).

$$q_c = \frac{P_c}{\sigma_a + k_d \sigma_b} \quad 5 - 6$$

where

$$k_d = 0.56^4 \sqrt{a^{1.6}/H} \quad 5 - 7$$

$q_c$ ; A core of the effective surface load (W/m<sup>2</sup>),

$P_c$ ; The core loss (W),

$\sigma_a$ ; Exposed area, (m<sup>2</sup>)

$\sigma_b$ ; Non-exposed area (m<sup>2</sup>)

$a$ ; Width of the air duct (mm)

$H$ ; The average height of the core

Now the engineering practice is the most commonly used empirical algorithm of core temperature rise calculation, which to a certain extent can satisfy the need of engineering(Ning and Ding, 2012, Lu et al., 2003). The empirical coefficients are generally different for the different core materials and structures . In the calculation of average temperature rise for a core made of stacked silicon steel sheets, the empirical coefficients k, n take the values of 0.36,0.8. Thus the core temperature rise model is as follows(Ning and Ding, 2012).

$$\tau_c = 0.36 q_c^{0.8} = 0.36 \left( \frac{P_c}{S_c} \right)^{0.8} \quad 5 - 8$$

where

$\tau_c$ ; The core temperature rise (oC),

$q_c$ ; A core of the effective surface load (W/m<sup>2</sup> ),

$P_c$ ; The core loss (W),

$S_c$ ; The core and the effective radiating area (m<sup>2</sup>),

The core loss  $P_c$  mainly consists of two parts: the hysteresis loss  $P_h$  and the eddy current loss  $P_e$

$$P_h = \eta f B_{max}^{1.6} V \times 10^{-3} \quad 5 - 9$$

$$P_e = \eta d^2 f^2 B_{max}^{1.6} V \times 10^{-3} \quad 5 - 10$$

$$P_c = P_h + P_e \quad 5 - 11$$

where

$\eta$ ; The coefficient of the hysteresis of the core material,

$f$ ; Is the frequency (Hz),

$B_{max}$ ; The maximum flux density (T),

The temperature rise of the transformer windings

The dry-type transformer windings are the main components of heat generating elements (Ding and Ning, 2012). The heat of the primary winding and the secondary windings are mainly caused by the respective load losses. The load loss includes the basic loss and additional loss. The basic loss refers to the winding DC resistance component of the conductor loss. DC resistance loss is the main reason leading to the winding temperature, so during normal engineering practice, only DC resistance loss is considered in computing (Ning and Ding, 2012, Lu et al., 2003). However, based on previous research work in this particular study additional factor of 5% was added to account the additional AC losses due to the presence of winding eddy current losses.

Winding temperature rise calculation model and the core temperature rise calculation model use the same principle, just with different values of empirical coefficients. The winding temperature rise calculation is as follows (Ning and Ding, 2012).

$$\tau_w = k q_w^n = k (P_w / S_w)^n \quad 5 - 12$$

where

$\tau_w$ ; The winding temperature rise (oC),

$q_w$ ; The winding surface load (W/m<sup>2</sup>),

$S_w$ ; The effective winding cooling area (m<sup>2</sup>),

The calculation process for the winding loss is as follows:

$$P_w = P_k \beta^2 = P_k \left( \frac{S_{js}}{S_e} \right)^2$$

where

$P_k$ ; The transformer short circuit active power (kW),

$S_{js}$ ; The transformer computational load (kVA),

$S_e$ ; The rated capacity of the transformer (kVA),

$k$  and  $n$  are empirical coefficients and they are related to the winding process and the materials. For low voltage windings, when all surfaces are in contact with the inner air ways generally  $K=0.66$  For windings with subsection cylindrical windings, which is vertical air duct therefor there two axial radiating surfaces where  $K$  becomes 0.46(Ding and Ning, 2012).

The values of  $K$  and  $n$  are also calculated based on the historical test results of the Carroll & Meynell Transformers Ltd.

## 5.62 Product construction

The 1.2MVA single phase transformer was designed constructed as per requested specific per turn induction ratio. It was required to maintain specific voltages in the primary side of the transformer and the secondary side of the transformer as described in the transformer schematic diagram in the Fig. 3, which made the selection of the number of turns and the size of the core restrictive to some extent.

The transformer was constructed utilizing the 'UI' type core construction. Given the size of the transformer it was decided to base the core area profile on a step system of cross-sections to give a cylindrical coil construction. The material chosen for the coil former was a silicone coated glass mat that is wound to the required thickness. This material meets the Class H insulation system requirement.

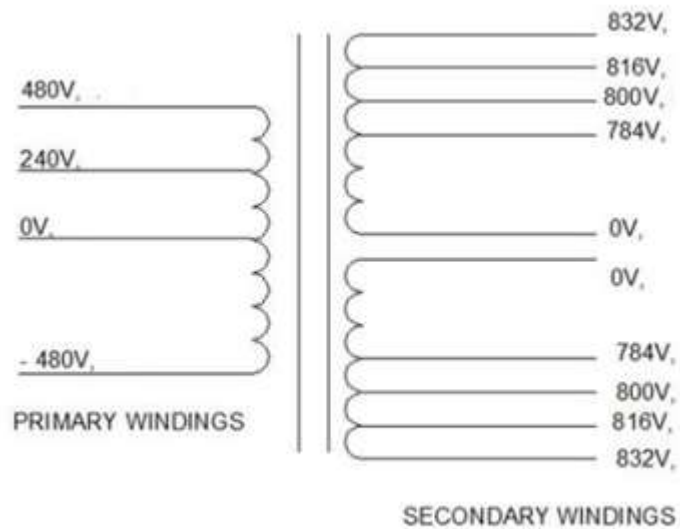


Figure 5-9 Transformer schematic diagram

The conductors consisted of multiple sections of rectangular copper strips were bunched together to obtain the acceptable current density. In deciding the appropriate conductor cross-section, the temperature rise was estimated as explained in the section II C and a certain iterative approach was used to arrive at the most suitable conductor cross-section. In order to avoid issues of circulating currents between the inner and outer strips of the conductor bunch being generated a single transposition of the wires in the middle of the coils was used; the optimum number of transpositions for the size of the transformer was decided based on a detail study on the construction explanation of which goes beyond the scope of this paper. This transposition balances the total lengths and winding areas to within a  $\pm 1\%$  tolerance for all conductors. This balances the individual resistances and inductances of the windings which reduces any additional heat generated due to circulating currents. The drawing in the figure 5-10 illustrates the construction of the coil.

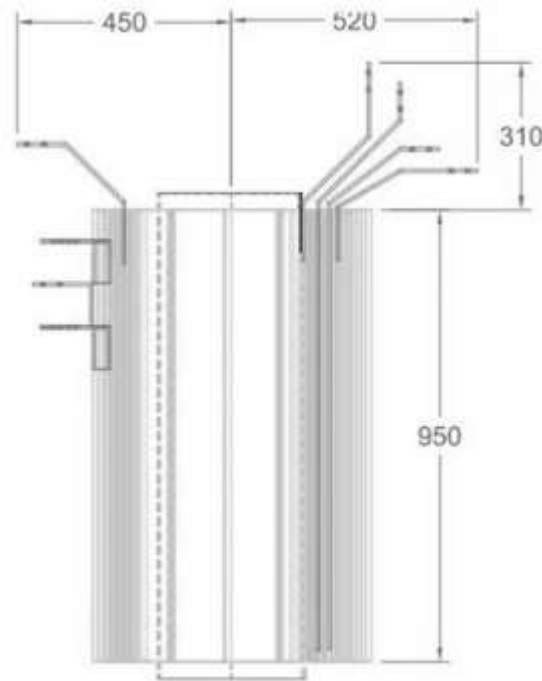


Figure 5-10 Construction of one of the two coils

The core material and the operating flux density was decided based on the amount of heat generated due to core losses described in above equation. Based on the calculated temperature rise as explained in section II B an iterative approach was made to decide on the optimum design flux density for the application. Though the transformer was constructed with a class H insulation system it was decided to limit the temperature rise to the vales of a class F system. This was to ensure the expected long-life operation of the transformer and to account for any potential over load possibilities due to the nature of the application in the particle accelerator laboratory setup where the transformer intended to be used.

### 5.63 Experimental procedure

#### Simulated loading method

It was decided to carry out a load test on the constructed transformer. One of the objectives was to get a verification of the theoretically predicted values of the temperature rise. The second objective was to subject the transformer to the full load condition and to stress it for the



design thermal condition as a certain quality assurance step before it goes through the expensive installation in the laboratory.

Carrying of a load test on a MVA range transformer is not very much practical in a laboratory set up due to the amount of power involved. This situation is addressed in the standard BSEN60076-11 where a simulated load test is defined.

In the simulated load test method temperature rise is established combining the short-circuit (load loss-winding losses) and open circuit test (no-load loss – core losses). The winding short circuit test is carried out with a rated current of 1160A in the primary and 670A in the secondary. The windings were loaded under this condition until the steady state of the transformer core and the windings was researched. The temperature rise is measured based on the resistance method. The testing arrangement is shown in the figure 5-12



Figure 5-11 1.2MVA transformer testing arrangement

The open circuit test was carried out by loading the primary of the open circuit transformer with a voltage of 960V at the rated frequency of 50Hz. Test was continued until the steady state condition of the windings and the magnetic core was achieved. The total winding temperature that would be researched at a power of 1.2MVA is then calculated as per the formula given below [BSEN 60076-11].

$$\Delta\theta_c^1 = \Delta\theta_c \left[ 1 + \left( \frac{\Delta\theta_e}{\Delta\theta_c} \right)^{\frac{1}{k_1}} \right]^{k_1}$$

5 - 13

where

$\Delta\theta_c^1$ ; is the total winding temperature,

$\Delta\theta_c$ ; is the winding temperature rise at the short circuit test,

$\Delta\theta_e$ ; is the individual winding temperature rise at the open circuit test,

$k_1$ ; =0.8 for natural air cooling and 0.9 for forced air cooling.

#### Supply of high single-phase power

Even though the load test was carried out based on the simulated loading method due to the high-power rating of the transformer required supply power level for the load test comes to about 85kVA. Since the product under discussion is a single-phase transformer this power has to be obtained in one phase. Obtaining a power of 85kVA in a single phase was a considerable challenge in making the testing setup. In order to achieve this 90kVA open delta phase conversion transformer was constructed. Figure 5-12.



Figure 5-12 90kVA open delta phase conversion transformer

This is a transformer constructed with a three phase 3UI type core only with two windings. The center limb of the core is left open without a winding on it. However elimination of the center limb is not possible for the operation of the magnetic circuit. The primary is supplied with a three phase supply with an open delta arrangement and the two secondary windings are connected in series to form the required single phase supply. By the use of this transformer the required single phase power of about 85kVA was obtained.

### Load testing process

With the use of the above open delta phase conversion transformer the core of the 1.2MVA transformer was loaded as explained in the section IV A. The temperature was recorded over a period of 25 hours. As the temperature of the core had reached the level of its rise per hour is below one 0C the core test was stopped at this stage. The measured temperature values were corrected for the ambient temperature variations.

Immediately after the above no-load test the short circuit test was started as explained in section IV A. When the secondary winding was loaded to the rated current of 670A primary voltage of about 76V could be seen indicating a power of approximately 88kVA. This also shows a short circuit impedance of about 7.9% in the 1.2MVA transformer which is well over the 5% minimum requirement for a transformer of this power range as per BSEN 60076. The short circuit test was also carried out for a period of approximately 24 hours and the measured temperature was corrected for the ambient temperature variations. Here again it could be seen that after about 24 hour period the rise in the windings were coming below one degree per hour. Further based on the plotted graphs and extrapolated lines of best fit it could be seen that the temperature of the windings had researched well over 95% of the steady state conditions.

In addition to recording the measured temperature the resistance of each winding was recorded. As per the definition in BSEN 60076 the temperature of each section of the coils were calculated based on the resistance method.

### Discussion

The temperature rise of the core obtained during the no-load test is shown in the Table 5-3. Based on the equations (3), (4), and (5) and with the data obtained from the core material manufactures the core loss was calculated which amounted to approximately 958W. The estimated temperature rise of the core based on the equation (2) and the calculated core loss value was 75.52 0C. The measured value on the experiment was 66 0C. It could be seen that the predicated value of the core temperature was slightly higher than measured value. However,

considering the overall practical assumptions made during the calculation process level of accuracy researched can be considered as very satisfactory.

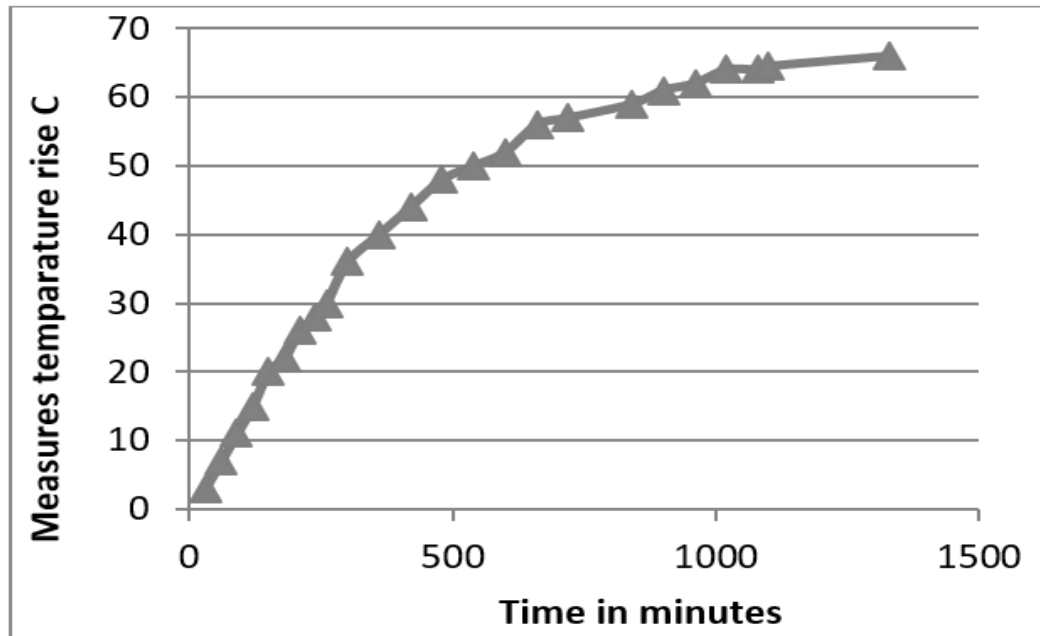


Figure 5-13 Temperature rise of the core at the open circuit test

The measured temperature rise of outer surface of the coils were as shown in the figure 5 -14

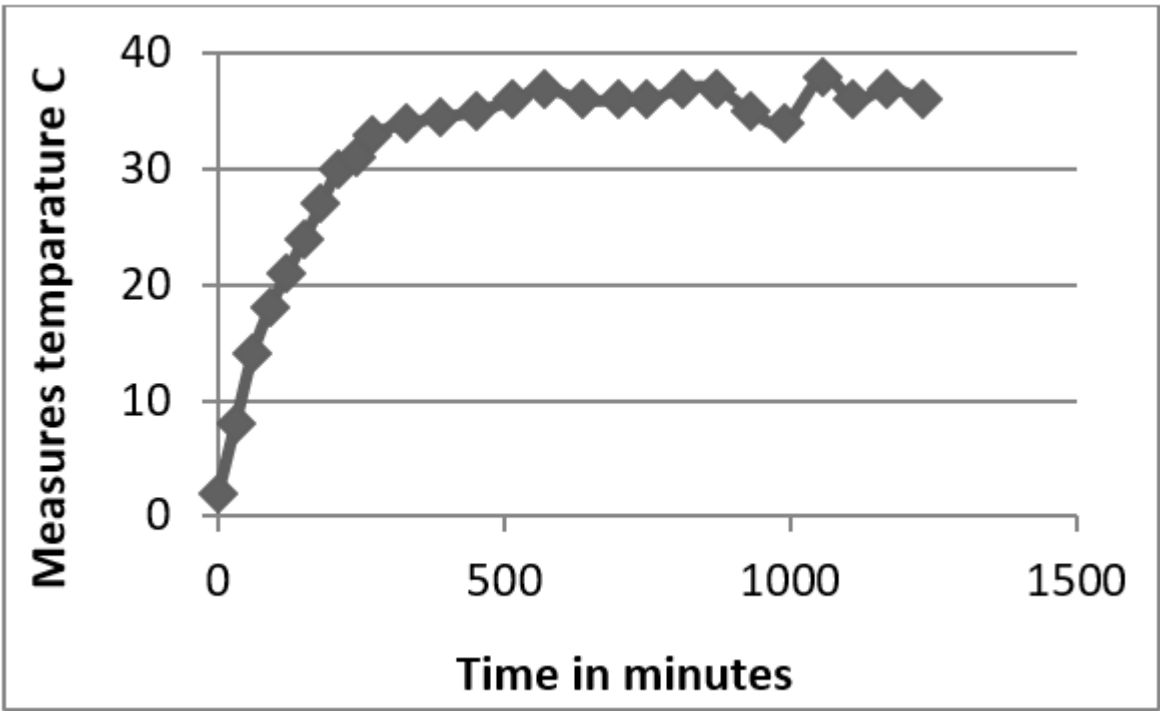


Figure 5-14 Temperature rise of the windings at the open circuit test

The values obtained for the temperature rise of the windings based on resistance method is shown in table 5-3

Table 5-3 Calculated temperature rise of coils based on resistance method

COIL	CALCULATED TEMPERATURE RISE IN °C RESISTANCE METHOD
PRIM LEFT COIL	95.6
PRIM RIGHT COIL	104.5
SEC LEFT COIL	93.8
SEC RIGHT COIL	110.1

The above temperature values were extrapolated based on the simulated load test formula; this gives the temperature rise of the windings as shown in the table 5-4

Table 5-4 The temperature rise of coils based on simulated load test method

COIL	TEMPERATURE RISE OF THE COILS AS PER SIMULATED LOAD TEST METHOD °C
------	--

PRIM LEFT COIL	110.7
PRIM RIGHT COIL	112.5
SEC LEFT COIL	96.4
SEC RIGHT COIL	112.18

The calculated temperature rise of the windings at the design stage based on the above equation and with the parameters adjusted based on experience at Carroll & Maynell Transformers Ltd was 102.40C.

As far as the prediction of the winding temperature rise is concern the actual values show about 100C higher value than the predicted vales. It could be assumed that this is due to additional eddy current loess happening in the windings with high thickness. Though an additional provision of 5% loses was added to the conductor loses it might be required to look into this correction factor in more detail in the case of large transformer with thick winding conductors where the possibility of increased eddy current losses is present. It was intended to investigate this factor in the future research work.

#### Summery

The theoretical predictions made for the temperature rise in both the core and windings in the 1.2MVA transformer showed reasonably accurate when compared with the actual values obtained based on the simulated loading method. There is a certain deviation amounting up to about +/- 100C for the 1.2MVA transformer investigated. These could be due to potential errors in estimating the total winding losses, core losses and due to the limitations in the thermal models. This level of verified accuracy gives reasonable confidence in finalizing the designs of transformers of this power range. However, authors intend to make further improvements to the thermal models to arrive at a better accuracy specially taking the eddy current losses in the windings into account.

This work was carried out based on a product developed for a leading research facility in the United kingdom. The product was designed, manufactured and tested at the manufacturing facility of Carroll and Meynell Transformers Ltd in Stockton on Tees, United Kingdom. The research work was carried out under the supervision of Professor F. Nabhani of the Teesside University, United Kingdom. Science thanks are expressed to Mr. Mike Meynell, the Managing Director of the Carroll & Meynell Transformers Ltd, its management and the staff for financing and providing the opportunity to carry out the study. Further, Kapila Warnakulasuriya expresses science thanks to Professor F. Nabhani and the Teesside University for the continuous guidance in the research activities.

## 5.7 Novel thermal management approaches for high power density transformers.

Patent internal no P82227.GB01(M20-02249)

*This application relates to thermal management of an electromagnetic device such as a transformer, and in particular to an electromagnetic device and a core assembly suitable for an electromagnetic device.*

The detailed analysis of core and conductor losses makes it possible to achieve the theoretically minimum level of high frequency conductor losses in high power high frequency transformers. However, as the demand for power levels increase the need for very high power levels in a compact structure is required. This results in a very high power / loss densities in high power high frequency transformers. Therefore effective removal of heat from such transformers make the products operating at a much lower temperature rise for a given size and make it possible to further miniaturize the high power high frequency transformers. The disk nature of windings patented under WO2019234453A1 (Winding arrangement for an electrical transformer) also facilitates the improved thermal management approaches.

- Efficient removal of heat from the center and interior of the magnetic core
- Reduction of the hot spot temperature of the core

Reduction of heat generated in the core getting transferred to the windings and increasing the winding temperature.

Efficient removal of heat from the winding utilizing a further advantage of windings patented under WO2019234453A1 (Winding arrangement for an electrical transformer).

This type of cooling channel approach has not been used in the conventional high frequency transformer constructions. Thus the core and the dimensions have been increased as per the results of the thermal models to maintain a reasonable temperature rise of the unit.

As it is found during the prior art search a cooling channel in the middle of the core has been used in the case of power transformer with an EE core assembly. In this innovation EE cores are not used and an assembly of UU cores are used thus it is physically a different construction. Further The use of cooling channels in between the core blocks as seen in the below pictures is not used in the prior arts. However, the introduction of those cooling channels improves the effectiveness of the thermal management system significantly.

Aluminum cooling channels provide a path for the heat generated in the core to flow in to the radiation surfaces. Aluminum channels can be changed to Copper channels for space critical applications for the further improvement of the efficacy. This path has a heat conductivity of over 50times than that of the core material if Aluminum is used as the cooling channel material and nearly 100 times if Copper is used.

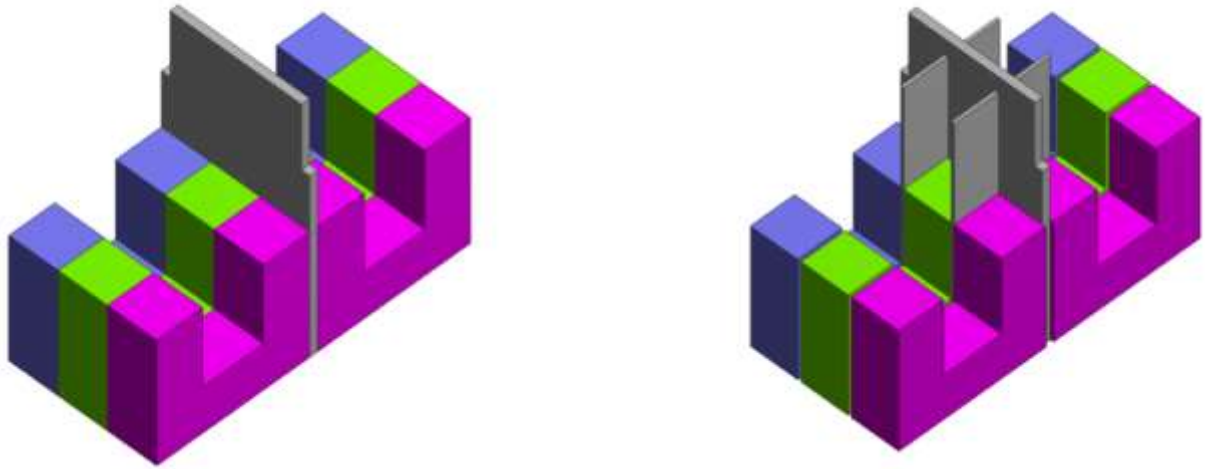


Figure 5-15 Aluminum cooling channel arrangement

Aluminum cooling channels placed in the right orientation to have no effect to the magnetic circuit. This reduces the hot spot temperature of the transformers by more than 20 degrees. These cooling channels provide the low thermal resistance path for the heat generated in the windings to flow to the radiation surfaces. This is an arrangement that can also be used in combination with windings patented under WO2019234453A1 (Winding arrangement for an electrical transformer) which further utilizes the advantages of those windings.

This concept can be used in any high-power high frequency transformers that are constructed with a UU core assembly that provides a middle separation in magnetic path parallel to the flow of the direction of the flow of the magnetic flux.

Further improvements to the heat conduction path and improvements to heat radiation surfaces as seen below can be done as illustrated in the diagrams below.



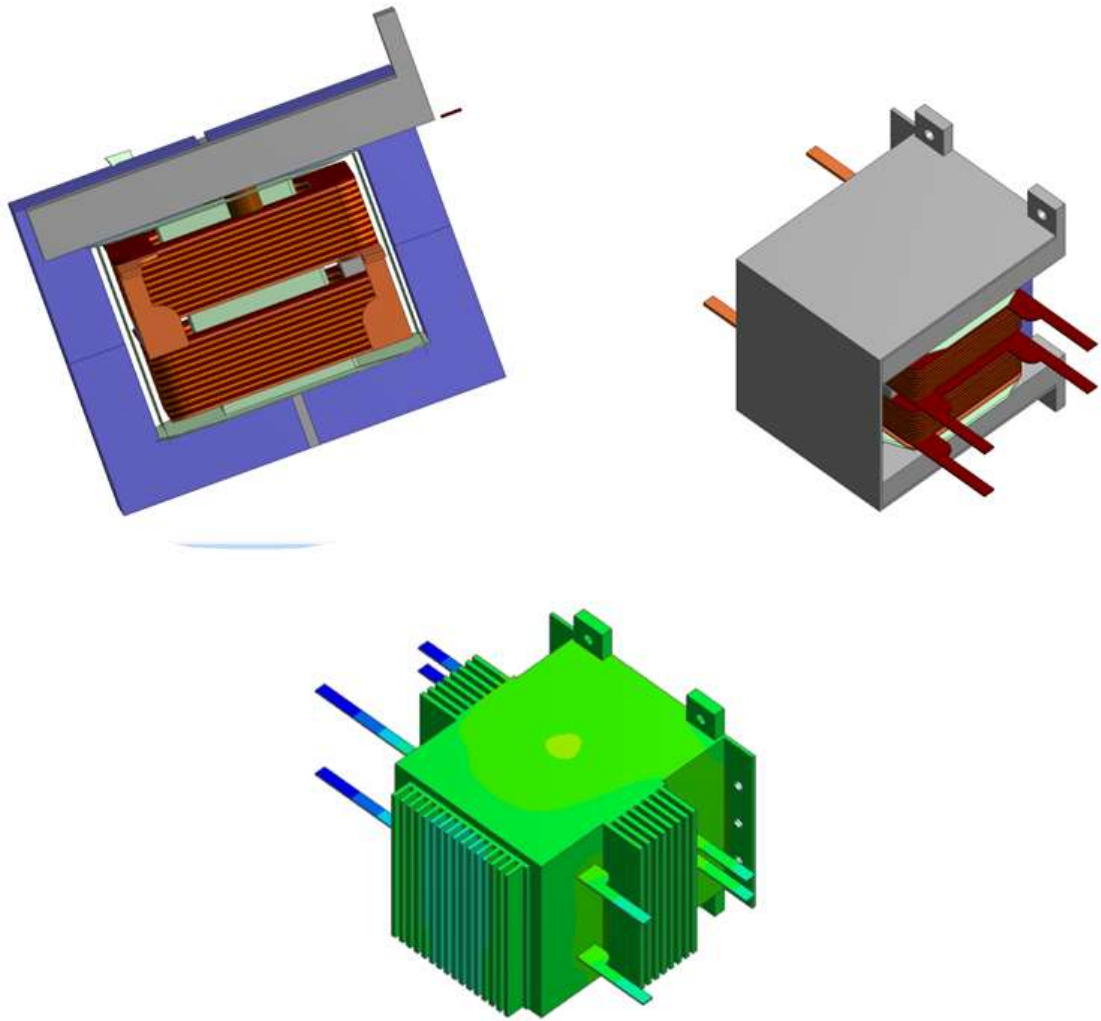


Figure 5-16 improvements to the heat conduction paths and improvements to heat radiation surfaces.

## 5.8 Novel approach to extract heat from the windings of transformers with high isolation requirements.

Patent internal no P82228.GB01 (M20-02413)

*The invention relates to a winding assembly for a transformer, and a transformer device including the winding assembly, and to the thermal management of transformer windings.*

“Cast resin” is used in the transformers as a dielectric material especially in the case of high voltage transformers where the isolation requirement between the input and the output circuits is high. The isolation requirement is such transformers usually range from several tens of kV to several hundreds of kV.

- The thick layers of cast resin material used to maintain the isolation requirement creates a barrier for the heat flow from the windings. Therefore this method is usually suitable for transformers with reasonably low winding loss densities.
- As a result cast resin material is not often used in high frequency or medium frequency transformer windings where the losses density is considerably high.
- The cooling channel approach proposed in this innovation provides a method to extract the heat generated in the windings in a very efficient manner without degrading dielectric strength between the input and output windings.
- This opens up the possibility of achieving very high isolation levels between the windings of high frequency transformers.

The cast resin is not often used to maintain the isolation requirement in high frequency transformers. Conventional paper insulation is typically used in maintaining the isolation requirements of high frequency transformers. This has limited the level of isolation that can be achieved in high power high frequency transformers.

The proposed innovation eliminates this limitation in the industry.

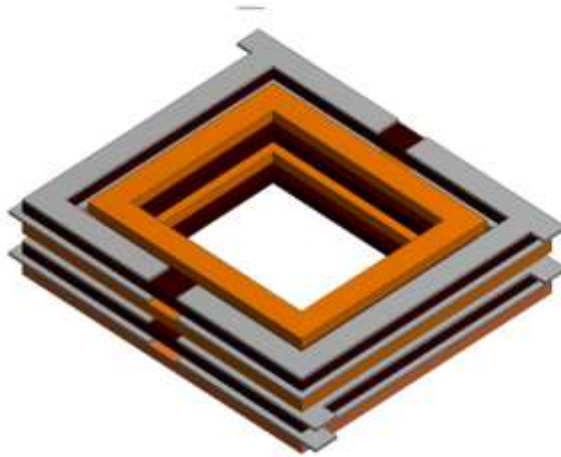


Figure 5-17 Aluminum cooling channel arrangement with radiators

Separated cooling channels are used in input and output windings as shown above; a gap is maintained to avoid the situation of having a shorted turn.

The separation of these two cooling channel systems are maintained all the way out to the radiating surfaces as shown in the below picture with the use of two colors.

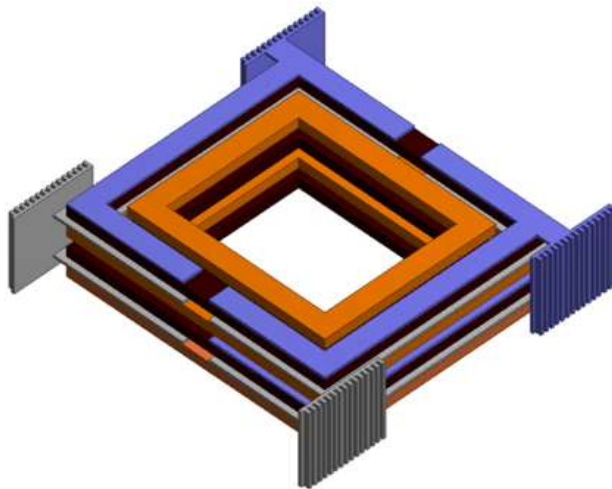


Figure 5-18 Aluminum cooling channel arrangement with radiators

As it can be seen in the picture the proposed construction allows maintaining the required distance through insulation all the way up to the radiation surfaces. Therefore, this approach

makes it possible to extract the heat out of the windings without degrading the isolation properties of the transformer.

Once the cast resin process is complete the product will look as shown in the below picture.

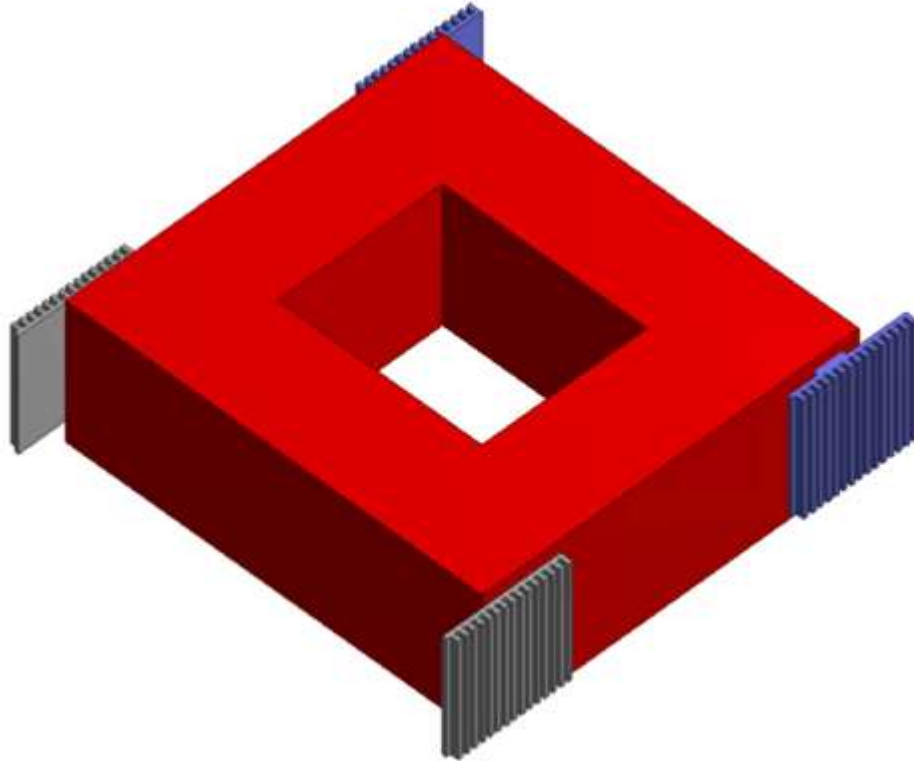


Figure 5-19 Cast resin high voltage medium frequency winding.

## 5.9 Summary

Theoretical aspects of transformer thermal management is discussed in the sections 5.1 to 5.5 of this chapter. This includes the theoretical aspects of thermal investigation of dry type transformers, calculations for ventilated dry type transformers, hot spot investigations for liquid filled transformers, temperature rise for high Frequency transformer under Forced-air convection etc

From the sections 5.6 to 5.8 the studies carried out under based on 100 kW transformer with novel method of effective heat removal, thermal management of larger transformer structures are discussed. The theoretical predictions made for the temperature rise in both the core and windings in the 1.2MVA transformer showed reasonably accurate when compared with the actual values obtained based on the simulated loading method. There is a certain deviation amounting up to about  $\pm 100^\circ\text{C}$  for the 1.2MVA transformer investigated. These could be due to potential errors in estimating the total winding losses, core losses and due to the limitations in the thermal models. This level of verified accuracy gives reasonable confidence in finalizing the designs of transformers of this power range. However, it is intended to make further improvements to the thermal models to arrive at a better accuracy specially taking the eddy current losses in the windings into account.

The thermal management approaches introduced during the research which are now patented are discussed towards the end of chapter 5. Novel approach to extract heat from the windings of transformers with high isolation requirements are also discussed. The section 5.7 explains the method introduced in this study which has proven very effective. Further the patented approach discussed in section 5.8 under “The novel approach to extract heat from the windings of transformers with high isolation requirements” is particularly suitable for high voltage high frequency transformers which require high insulation requirements.

# Chapter 6

## Inductance, impedance, leakage inductance

## Chapter 6 Inductance, impedance, leakage inductance

Leakage inductance is an inductive element in a transformer that results from the imperfect magnetic linking of one winding to another. Leakage inductance plays a critical role in the switching-mode power supply design. It makes the switching current at the device vary at a slower rate and increases the commutation time between output diodes. Moreover, the stored energy in the leakage inductance leads to voltage spikes in the switches. Consequently, it creates electromagnetic interference problems, increases switching losses, and reduces power efficiency (Ouyang et al., 2014, Choi et al., 2012, Chen and Kumar, 2014, Muhammad and Lu, 2013, Stadler and Albach, 2006, Biela and Kolar, 2004).

Today's new technology pushes the switching frequency into the megahertz range in order to minimize the size of the inductive components, making the switching loss more severe. Therefore, an accurate prediction of leakage inductance at high frequency is needed, to implement an optimized design. The accurate prediction of leakage inductance at high frequency is also critical for resonant converters because a well-matched resonant frequency is often required (Fu et al., 2010, Jung, 2012). Many publications contain excellent analysis and calculations for leakage inductance in the conventional and planar transformers (Dowell, 1966, De León et al., 2013). However, these papers rarely consider the high-frequency effects due to the skin effect and the proximity effect. Most of the conclusions assume that the current is homogeneously distributed within the conductors, and thus, the leakage inductance calculation is frequency independent.

Several aspects of the operation of power-electronic circuits with transformers are significantly influenced by the leakage inductance of the respective transformer. For instance, it concerns power transfer capability of the circuit and power semiconductor stress parameters. The tendency to higher switching frequencies of power-electronic apparatuses results in an increasing relevance of low transformer leakage inductance values. Mostly, the so-called interleaving of windings (i.e., the fragmentation of the primary and the secondary windings into a certain number of sub-windings and alternate interleaving of primary and secondary sub-windings) is used to meet this requirement. Using an appropriate approximation method, it is possible to determine the leakage inductance of a transformer already in the design phase on the basis of predicted geometry parameters. Thus, circuit simulation can be used to shorten the development process of power-electronic apparatuses. Formulas which are given in

literature generally rely on an approximation method for leakage inductance determination which has been established by Rogowski (Ouyang et al., 2014, Choi et al., 2012). It is based on the consideration of the energy of the leakage magnetic field and applies to a transformer design with windings arranged on the same leg. The basic formula of this method is

$$L_L = \mu_0 N^2 l_{mc} \lambda k_\sigma$$

6 - 1

with  $L_L$  leakage inductance,  $\mu_0$  absolute permeability,  $N$  number of turns of the winding to which the leakage inductance refers,  $l_{mc}$  mean length per turn for whole arrangement of windings,  $\lambda$  relative leakage conductance (depending on geometry parameters and on the degree of interleaving of windings),  $k_\sigma$  Rogowski factor (also depending on geometry parameters).

The formulas which can be found in contemporary technical literature mostly represent simplified variants of the mentioned basic formula. Usually the Rogowski factor (whose value is nearly 1 in most arrangements) is omitted and the formula describing the relative leakage conductance is included in the main formula. Often, constant factors like absolute permeability and numerical values are merged into one coefficient, so that the physical background of the formula is not recognizable anymore, e.g., in (Chen and Kumar, 2014). In some cases, different formulas are given for a transformer design without interleaving of windings and for transformer arrangements with interleaving of windings, e.g., in (Muhammad and Lu, 2013).

The degree of interleaving is considered in literature by the number of the couples of sub-windings (Stadler and Albach, 2006, Biela and Kolar, 2004) or by the number of interfaces (insulating interspaces) between the single sub-windings of an arrangement of windings (Fu et al., 2010, Jung, 2012). Furthermore, the aim to present a universal formula which is valid for transformer versions with concentric and with pie windings arrangements often causes some confusion. It also results from the diversity of terms which are used for the dimensions of windings (e.g., breadth, width, traverse, build, height, length) comparing the formulas and their descriptions which are given in different books and papers.



## 6.1 Theoretical Estimation and Practical Verification of the Impedance and Leakage Inductance of MVA Range Single Phase Transformers

Theoretical estimation of Impedance and leakage inductance of transformers is a challenge that design engineers in the transformer manufacturing industry often face. Both these parameters depend on the physical construction and the geometry of the transformer. The accurate prediction of values becomes more and more difficult as the physical size of the transformer increases. This is due to the increased significance of the construction and the geometry of the product on these parameters. Further, the maneuvering of construction and geometry targeting specific values of impedance is difficult due to the lack of predictability. In this paper a mathematical approach is used to estimate the impedance and leakage inductance of a large single phase MVA range transformer. The effects of the coil geometry, cooling channels, the transposition of the parallel wound conductors etc. are addressed in this mathematical approach. Verification of the theoretically estimated values is made based on measurements on actual transformers. The testing carried out on a single-phase 1.2MVA transformer, which is of a considerably large power rating for a single-phase transformer is used to compare the theoretical predictions and realization of values in actual manufacturing. A transformer which is mainly composed of windings and core parts is a static electrical device that transfers energy from one circuit to another by mutual magnetic coupling. The transformer is ideal if the magnetic coupling is perfect, and the energy transfer is lossless. For a transformer to be ideal, 1) the resistance of the windings must be zero and thereby no losses in the windings. 2) The magnetic coupling must be perfect or in other terms the coupling factor must be 1 thereby giving no leakage inductance in the transformer. 3) The permeability and the resistivity of the core material must be infinite giving no energy stored or no losses situation in the core (Niemela et al., 1989). However, the winding resistance is inherent in the transformer. Further leakage of flux from the common path is inevitable even in a perfectly layered winding arrangement which gives the rise to an imperfect coupling. Since the invention of the transformer considerable theoretical and empirical research have been carried out by scientists and engineers to estimate and optimize the losses in transformers.

Transformer modelling however is a broad topic and models are widely used for simulation of transient behaviors. An accurate representation of every transient situation requires a model valid for a wide frequency range. This is exceedingly difficult and, in most cases, not feasible.

Transformer models can be developed to be accurate for a specific range of frequencies (Chiesa, 2010).

Transformer models have been developed using different approaches depending on the simulation or evaluation requirement. Transformer models based on magnetic circuits, models based on an equivalent electric circuit and models based on hybrid approaches are some examples for those. Furthermore, these models have been extended to high frequency evaluations. The most commonly used transformer model for low frequency evaluation can be represented as shown in the Figure 6-1. Where  $R_1$ ,  $R_2$  represent the winding resistance,  $X_1$  and  $X_2$  leakage reactance in primary and secondary,  $R_0$  is the core or iron losses representation,  $X_0$  is the Magnetizing reactance,  $E_1$  and  $E_2$  are the Electromotive (EMF) of primary and the secondary,  $V_1$  and  $V_2$  are the primary and secondary voltages of the transformer and  $I_1$ ,  $I_2$ ,  $I_0$ ,  $I_w$ , and  $I_u$  represent the primary, secondary, core loss, eddy current and magnetising components of the currents.

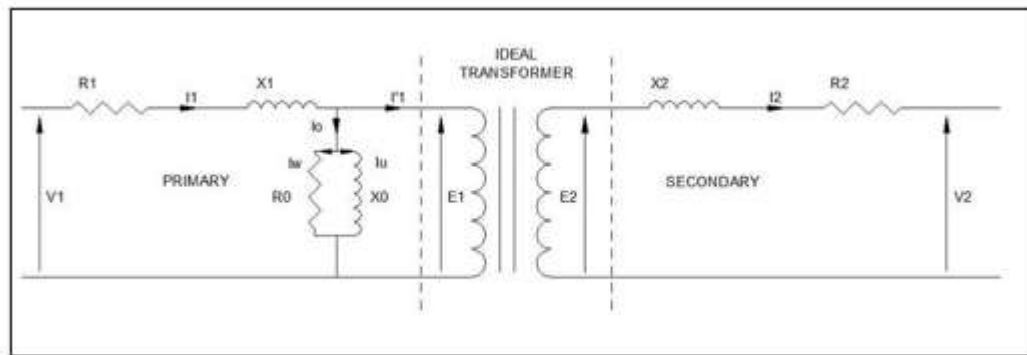


Figure 6-1 Equivalent Circuit of a Transformer

Power transformer and its limitation caused by internal losses or voltage drops are important aspects in all applications of power transformers. This is true in the case of mains frequency operated transformers and even more relevant in medium or high –frequency transformers. Copper losses are influenced by the cross section and (because of the skin and proximity effect with influences of the frequency and the field distribution) also by the arrangement of the windings. Imperfect magnetic coupling occurring in each real transformer is expressed by the term 'leakage' and represented by leakage inductances in equivalent circuits of the transformers (Doebbelin et al., 2009). The performance of a transformer can be calculated from its equivalent circuits (Dowell, 1966). In the case of existing transformers, leakage inductance can be determined by measurements. However, more often it is necessary to predict leakage induct of a transformer in design phase, especially if the circuit simulation is intended. This can

be done applying certain approximation methods in which the geometry parameters of the transformers are used to calculate its leakage inductance. Which approximation method has to be applied depends on the given arrangement of windings.

In this study theoretical estimation of transformer impedance and leakage inductance is made for a 1.2MVA transformer. Theoretically arrived at values are then compared with the measured values of the actual transformer.

### 6.11 Leakage Inductance Calculation

The leakage inductance of a transformer represents the field that leaks from the core and returns through the air, not linking both windings and causing imperfect coupling. This effect is modeled by a series leakage inductance in the primary ( $X_1$  in the Figure 1) as well as in the secondary ( $X_2$  in the figure 6-1 of a transformer (Niemela et al., 1989). If the couple of coils whose leakage inductance is to be calculated are on the same leg of the transformer, method of Rogowski and the method of Petrov can be used considering certain further aspects (Doebbelin et al., 2009). This is the situation that can be commonly seen in the shell type transformer constructions e.g. figure 6-1a.

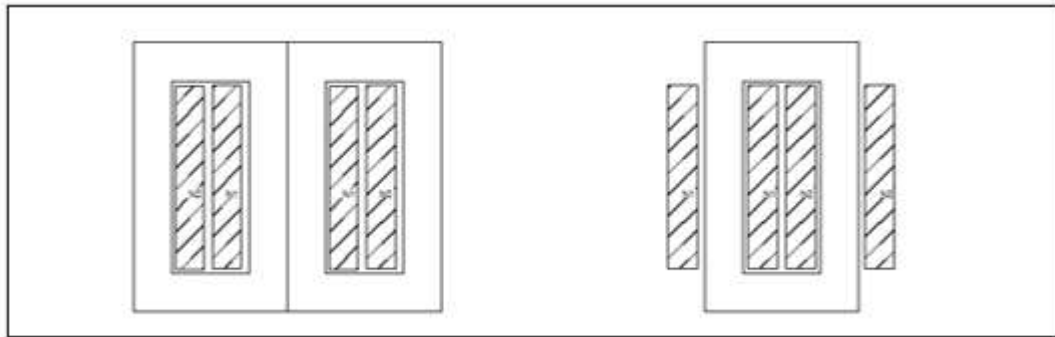


Figure 6-2 a) Shell type transformer construction    b) Core type transformer construction

In the case of high power single phase (e.g. MVA range) transformers core type construction become inevitably become advantageous over the shell type construction. Therefore the 1.2MVA single phase transformer discussed in this paper was constructed as a core type transformer. In this construction where the coils are arranged on different legs of the transformer leakage inductance can be calculated based on an approximation method developed by Lebedev. A basic assumption of this method is that the leakage field can be

considered to consist of three leakage flux components (Doebbelin et al., 2009). This is illustrated in Fig 6.3 bellow based on (Doebbelin et al., 2009, Doebbelin et al., 2008).

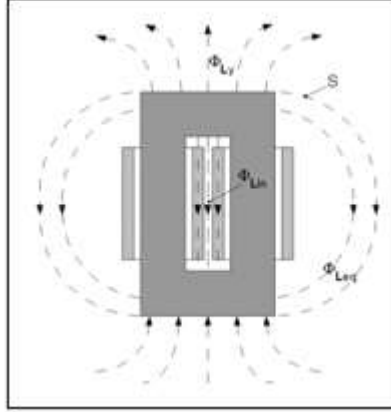


Figure 6-3 Components of leakage flux of a core - type transformer

#### Calculation Method

Taking the field configuration in to account the windings N1 and N2 are replaced by the equivalent winding N1-2 and a notional winding Nn is added to the transformer.as explained in (Doebbelin et al., 2008, Lebedev, 1958) the leakage inductance can be calculated as the sum of the three parts:

$$L_L = L_{L\,in} + L_{L\,y} + L_{L\,eq} \quad 6 - 2$$

The parts are the inner leakage inductance related to the leakage inductance component belonging to the section of the transformer of the windings which is located within the core window and the leakage flux which occurs in the region. This leakage inductance component shall be calculated according to the method of Rogowski using,

$$L_{L\,in} = \mu_0 \cdot w_1^2 \cdot d_c \cdot \lambda \cdot k_\sigma \quad 6 - 3$$

With  $w_1$ -number of turns of the primary winding to which the leakage inductance refers ,  $\lambda$  relative leakage conductance and Rogowski factor to be determined

The leakage inductance component which is related to the yoke leakage flux can be calculated according to

$$L_{Ly} = \mu_0 \cdot w_1^2 \cdot g_y$$

6 - 4

The specific yoke conductivity  $g_y$  varies with the width and the height of the core.

The leakage inductance of the equivalent transformer  $L_{eq}$  needs to be determined. To enable the calculation of this leakage inductance component, the notional winding  $N_n$  is subdivided into sections  $N_3$ ,  $N_4$  and  $N_5$  and section  $N_4$  is divided into two equal partitions which are assigned to  $N_3$  and  $N_5$  respectively. Based on the method of mean geometric distances (Doebbelin et al., 2008) this leakage inductance component can be calculated according to

$$L_{Leq} = \frac{\mu_0}{\pi} \cdot w_1^2 \cdot l_{mn/(1-2)} \cdot (1.1 + \log hc/b + 2a_{1-2})$$

6 - 5

where

$$l_{mn/(1-2)} = \frac{1}{2} \cdot (l_{mn} + l_{m(1-2)})$$

6 - 6

mean length per turn to be calculated considering the geometry of the winding  $N_n$  and the equivalent winding  $N_{1-2}$  representing the average of their mean length per turn values  $l_{mn}$  and  $l_{m(1-2)}$

To predict the total leakage inductance of a transformer with interleaved windings, the leakage inductance values of the different couples of coils have to be calculated (by means of the method of Rogowski or Petrov if both coils are located on the same leg, by means of method of Lebedev if the coils are located on different legs of the transformer). Then the leakage inductance values of these couples of coils have to be merged in to the total leakage inductance of the transformer using specific formulas which are related to the respective combination of the coils of the transformer. In a transformer design with two primary and two secondary coils (connected in series in each case), the total leakage inductance can be calculated according to below equation (Doebbelin et al., 2008).

With  $w_{xx}$  number of turns of the respective coil,  $w_{ref}$  with reference number of turns to which the single leakage inductance values  $L_{Lxx,yy}$  of certain couples of coils  $N_{xx}$  and  $N_{yy}$

$$L_{l,total} = \frac{w_1^2}{w_{ref}^2} \cdot \left( \frac{w_{11} \cdot w_{21}}{w_1 \cdot w_2} \cdot L_{L11,21} + \frac{w_{12} \cdot w_{21}}{w_1 \cdot w_2} \cdot L_{L12,21} + \frac{w_{11} \cdot w_{22}}{w_1 \cdot w_2} \cdot L_{L11,22} + \frac{w_{12} \cdot w_{22}}{w_1 \cdot w_2} \cdot L_{L12,22} \right. \\ \left. - \frac{w_{11} \cdot w_{22}}{w_1^2} \cdot L_{L11,12} - \frac{w_{12} \cdot w_{22}}{w_1^2} \cdot L_{L21,22} \right)$$

6 - 7

Evaluation based on Dowell's Equations.

If a two winding transformer is considered based on Dowell's and later Dauhajre works the following equation can be arrived at [152] for a configuration similar to the figure 6-1

$$l = 2\pi\mu_0 N_1^2 \frac{1}{b} \left[ h_1 \left( \frac{r_0}{3} + \frac{h_1}{4} \right) + \delta \left( r_0 + h_1 + \frac{\delta}{2} \right) + h_2 \left( \frac{r_0 + h_1 + \delta}{3} + \frac{h_2}{12} \right) \right]$$

6 - 8

In order to evaluate the difference in the two-transformer construction a theoretical calculation of inductance based on this equation was carried out. In this method in order to compensate the difference in the construction the leakage inductance of the individual coils were calculated and the total was arrived at assuming that each leakage inductance operate as parallel to each other. This assumption is understood to be reasonable as two primary coils are connected in series in this particular transformer design. A further assumption was made that the mutual dependence of the leakage inductance was minimum. The validity this second assumption needs to be further verified theoretically. However, the measurements made after the transformer construction implied that this assumption was reasonable.

## 6.12 Short Circuit Impedance Calculation

Short circuit Impedance is an important parameter of power transformer performance indicators. The value of short circuit impedance can influence the efficiency, cost, voltage regulation, mechanical strength and short circuit current of a transformer, so the deviation between measured value and the estimated value is very significant(Li et al., 2013b).

### 3D Model

Various researchers have established 3D FEM models for the evaluation of the short circuit impedances. These have been done mainly for multi MVA range large transmission type transformers for example the reference(Li et al., 2013a) explains a 3D model for an 88MVA transformer. The transformer under the discussion of this paper is a single phase 1.2MVA one. Therefor it was decided to carry out a simplified calculation method for the estimation of short circuit impedance. This was based on the leakage inductance estimations carries out under the above sections. However, it was intend to carry out a 3D simulation for this transformer as a future work and to verify the values against obtained practical data.

### Calculation Method.

In a multi winding transformer, there is one short circuit or leakage impedance for each possible pair of windings, totaling  $K(K - 1)/2$  impedances for a transformer having  $K$  windings. The short circuit impedance,  $Z_{(jk)}$  is the impedance seen at the terminals of winding  $j$  during short circuit test  $(jk)$ , where winding  $j$  is excited is excited at an angular frequency  $\omega$ , winding  $k$  is short circuited, and remaining windings are open circuited (Niemela et al., 1989).

$$Z_{(jk)} = R_{(jk)} + j\omega L_{(jk)} = \left(\frac{N_j}{N_k}\right)^2 Z_{(kj)}$$

6 - 9

The core loss is assumed to be negligible. The magnetizing inductance of the core is neglected as it is assumed to be much larger than the leakage inductance. With the aid of the design calculations and the 3D drawings produced the actual length of the Cu windings and thereby the DC resistance of the windings could be estimated with a good degree of accuracy. With these data the short circuit impedance and thereby the impedance voltage and it as a percentage of the nominal voltage is calculated.

## 6.13 Experimental Results

### Transformer construction.

A single phase transformer with a power rating 1.2MVA was constructed. The Figure 4 below shows the schematic diagram of the transformer. In order to address demands of the application UI construction with a step core arrangement was used. The selected construction provides several other constructional and cost advantages which go outside the subject area of this paper.

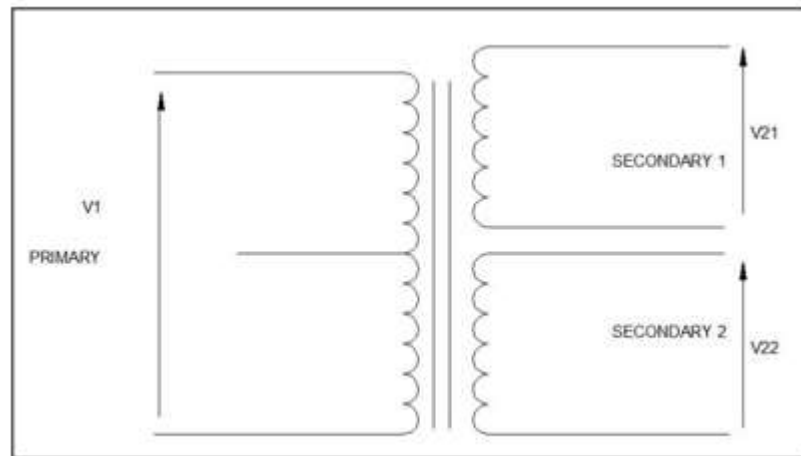


Figure 6-4 The schematic of the developed 1.2MVA transformer

#### 6.14 Practical measurements

Figure 6-5 shows the constructed 1.2MVA transformer and the measuring set up made for the leakage inductance and the impedance measurements. The impedance voltage was measured with the secondary winding short-circuited and letting a current equal to the rated current through the primary. Inductance values were measured on the primary side when the secondary coil is short circuited with the use of an LRC meter.



Figure 6-5 Constructed 1.2MVA single phase transformer and the testing set up



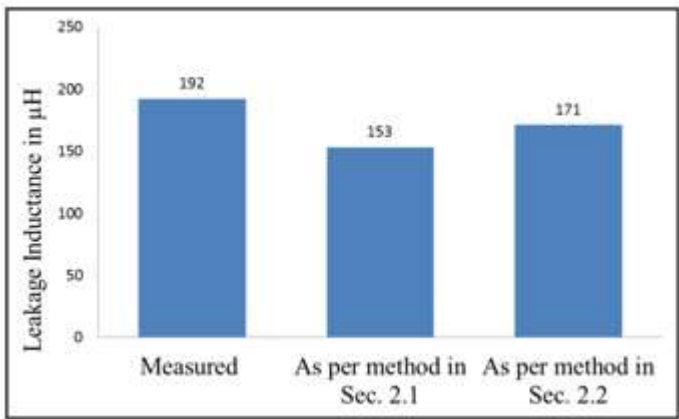


Figure 6-6 Leakage Inductance Measured and Estimated

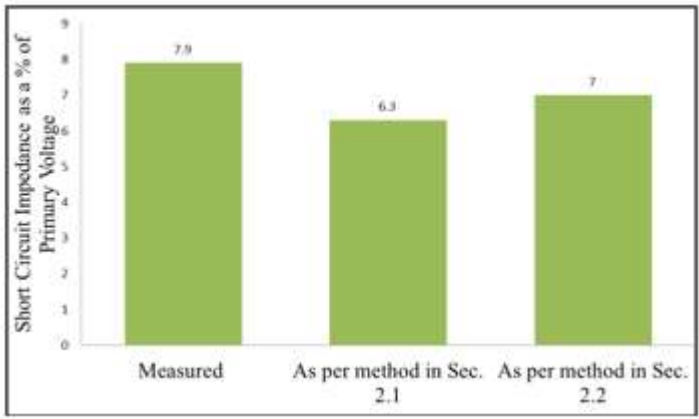


Figure 6-7 Short Circuit Impedance, Measured and Estimated

Measured leakage inductance value was tabulated together with the theoretically calculated values figure 6-6 . Based on the voltages measured as described above the percentage impedance was calculated. This was tabulated with the theoretically calculated vales as shown in the figure 6-7

### 6.15 Discussion

The requirement of single-phase transformers with a power rating in MVA range is not very much common in the industry. However, in special situations such as research laboratory applications it is somewhat common that large single-phase transformers are used. When the

requirement for such a transformer arise, it is very useful if the leakage inductance as well as the impedance values can be estimated with a good degree of accuracy prior to the actual production of the unit. Further the ability of such a prediction gives the designers the facility to alter the construction parameters to achieve the desired leakage inductance and impedance values.

Through a reasonable amount of work have been carried out by various researchers most of those works have been carried out based on small single-phase transformers or exceptionally large three phase transformers. These include certain Finite Element Methods discussed in the references (Xie et al., 2007, Bala and Morega) and (Doebbelin et al., 2008). It has been identified that there is a certain lack of research or at least a lack of verification of the existing theories on actual MVA range single phase transformers. Further the existing developments do not necessarily cover different winding configurations that may be used in such constructions. In this study several available estimation methods were considered, and it was decided to proceed with the two methods discussed in section 2 and 3. Neither of the methods fully covers the situation discussed in this study. So certain assumptions and extensions were necessary to arrive at quantifiable figures. As it could be seen in the graphs in figure 6-6 and figure 6-7 the estimations made prior to any physical construction have shown accuracy in the range of 20% or even 15%.

The parameters, leakage inductance and the short circuit impedance of a transformer (certainly these parameters are very closely linked) depend on the physical construction of the product to a great extent. As a result arriving at a higher degree of accuracy in predicting them based on purely on a computational method is quite challenging. Further certain additional phenomena such as the effect of the high frequency components in the excitation waveforms and extra eddy current losses in the windings especially with the increase of the high frequency content would result in actual values deviating from to the estimated values. However in this study a higher level emphasis was not given on the effect of high frequency harmonics due to the available information on the nature of the application. If the application demands the product to work under high frequency harmonic content the modes discussed need to be extended to get a better accuracy in the results.

Theoretical estimations made for the leakage inductance and the short circuit impedance of the 1.2MVA single phase transformers discussed in this paper showed an accuracy level in the range of 20% and 15%. Due to the nature of these parameters arriving at a prediction with this level of accuracy can be considered as reasonable as it is acceptable for industry applications. However if a better degree of accuracy level is needed it is required to address the effect of

high frequency content, eddy current losses proximity effect etc. Further a Finite Element Analysis could also provide a better accuracy in the prediction. Though the level of analysis carried out has met the requirements of the present study the it is intended to extend the discussed models to accommodate high frequency content in the excitation waveforms and different winding configurations. Further it is also intended to adjust the mathematical models to accommodate partial interleaving conditions, fractional layer winding situation etc. These discussed later publications.

## 6.2 Optimization of 12 and 18 pulse rectifier systems by the selection of optimum parameters for magnetics

In this study an approach is made to arrive at optimum designs for 12 and 18 pulse rectifier systems by defining the optimum parameters and configurations of magnetics. The approach is based on the definition of the parameters for magnetics considering the system impact on actual magnetics designs and the performance of the system with the set parameters of magnetic components. The several possible situations of unbalanced supply are also considered and optimum magnetic parameters to minimize the effect of the supply imbalance are discussed. Based on a series of simulations which were verified by practical testing a quantitative explanation of the size of the magnetics against the quality of the output and robustness to supply imbalances is presented. This explanation gives a measure on the degree of compromise that can be made on magnetics and the quality of the output. Situations where the magnetic designs are made larger or the requirement of using special magnetic materials that make the magnetic components more expensive are also discussed.

As technology grows, the study of power systems has shifted its direction to power electronics to produce the most efficient energy conversion (Hernadi and Anwari, 2008). Large harmonics, poor power factor and high total harmonic distortion (THD) in the utility interface are common problems when nonlinear loads such as adjustable speed drives. Power supplies, induction heating systems, UPS systems and aircraft converter systems are connected to the electric utility (Choi et al., 1996). In most power electronics applications, diode rectifiers are commonly used in the front end of power converter as an interface with the electrical utility. The nonlinear operation of the diode bridge rectifiers causes highly distorted input current. The non-sinusoidal shape of the input current drawn by the rectifiers causes a number of problems in the sensitive electronic equipment (Anandpara et al., 2014). Several methods have been proposed for harmonics reduction in utility line currents. A conventional 12-pulse diode bridge rectifier results in 5th & 7th harmonics cancellation in utility line current. Many multi-pulse converters have been introduced to achieve clean power such as 12-pulse 18-pulse & 24-pulse systems. These multi-pulse converters are formed by combination of 6-pulse converters & isolation transformer (Lee et al., 1999).

Multi-pulse rectifier systems contain a front-end poly phase transformer. When it is required to achieve galvanic isolation, this must be made as an isolation transformer, otherwise a poly phase auto transformer can be used which gives significant advantage on the size of the transformer. This point is described in the system with actual design details.

Two or three of three phase rectifier bridges depending on 12 pulse or 18 pulse system are connected via an inter-phase balancing reactor. Improper selection of inductance value for the interface transformer can result in unnecessarily larger unit or a unit that is subjected to higher order harmonics. Therefore, considering the actual magnetic design in deciding the values of inter phase reactors give an additional dimension for the optimization of multi pulse rectifier systems.

A series of simulations were carried out with different inter phase transformer reactance values and respective magnetic designs were carried out based on the inductance value and the waveform that these magnetic components are subjected at those particular values of inductance.

Simulation results were verified with a practical prototype built and the conclusions are presented in this paper. Further the effect of an unbalanced three phase input is evaluated for the different interphase reactance values considered above and the results were verified with the prototype built up.

### 6.21 Magnetics selection

Poly phase transformer selection.

Isolation transformer vs Auto transformer

It is required to use an isolation transformer if the system requires galvanic isolation. However, depending on the input output voltage ratio an auto transformer can give a significant weight and size advantage.

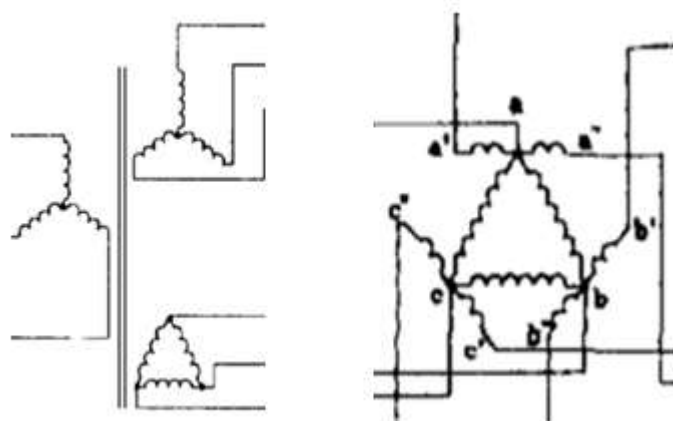


Figure 6-8 Isolation and Auto polyphase transformer

### Delta vs Star transformer

Another consideration in designing a 12pulse system is the section between the delta and star confirmation.

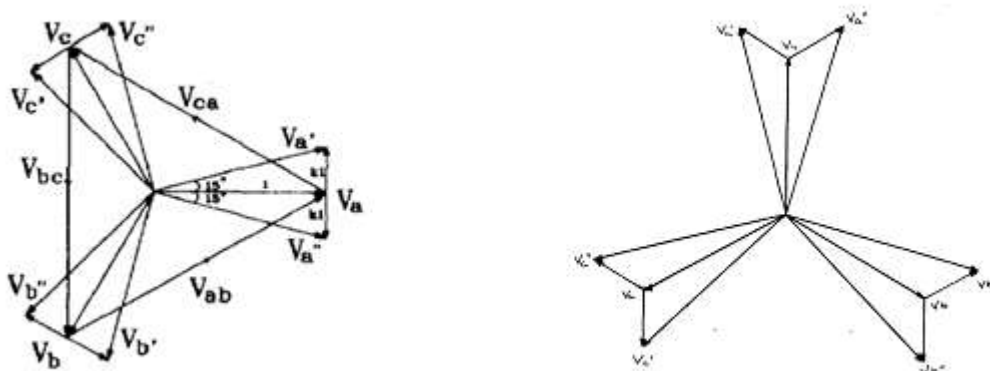


Figure 6-9 Vector diagram for Delta and Star Auto polyphase transformers

The selection of an Auto Delta transformer can result in over 35% smaller transformer compared to the selection of an Auto Star transformer. Below table makes a comparison of the sizes of an auto Delta 12 pulse transformer and an auto star 12pulse transformer based on actual designs carried out.

Table 6-1 Weight Comparison of Delta and Star Transformers in 12 Pulse Rectifications

<b>Transformer weight(kg) / power</b>	<b>10kVA</b>	<b>50kVA</b>	<b>500kVA</b>
Auto Delta Transformer	33.5	105	615
Auto Star Transformer	45	163	990
Percentage saving in weight in Delta Configuration	25.5%	35.5%	37.8%

It could be seen from the above table that the weight advantage of the star configuration become significant as the power increases.

#### Interphase transformer for 12 pulse system

In order to active the high power requirements the parallel operation the two six pulse rectifier converter systems that form the 12 pulses is required. In this parallel operation of two systems which have waveforms with a phase displacement of 300 proper care has to be taken to address any voltage variations. These voltage variations can result in one of the consisting 6 pulse systems getting overloaded causing them to the thermal runaway situations and other failures. This situation can be effectively addressed by the use of interphase rectifiers which ae also called as interphase transformer.

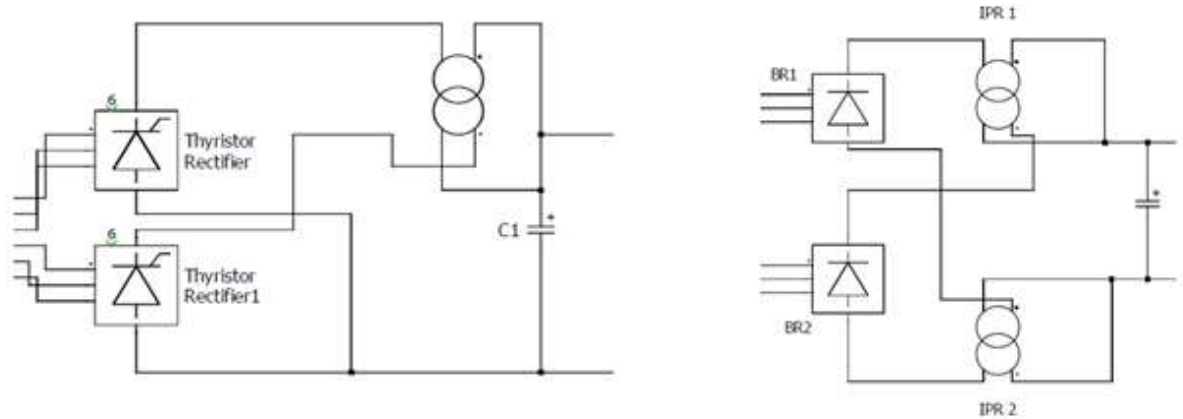


Figure 6-10 Parallel connection of two 6 pulse converters with the use of one and two interphase reactors

As shown in the above figure 6-10 this can be achieved with a use of one or two interphase reactor arrangements.

#### Interphase transformer for 18 pulse system

18 pulse systems are also used in many applications such as heating, air conditioning etc. These systems are achieved by the parallel or series connection of three 6 pulse converter systems. In the series configuration three, six-pulse systems having a third of the output DC voltage are connected in series. The series connection does not have the issues associated with current sharing and a requirement of having an interspace reactor. However, this has the disadvantage of the requirement of having high current capability rectifier systems. 18pulse systems with parallel connected 6pulse rectifier systems require appropriate interphase reactors and these can be connected in a number of configurations.

## 6.22 Simulations

During the study, a number of simulations were carried out for different conditions of the supply voltages. Balanced and unbalanced supply voltages are considered and the performances of the system under these conditions are evaluated for different interface reactor values. The changes in the interphase current waveform under different interphase reactor values were



studied and impact of these current on the actual magnetic design of such interphase reactors were investigated.

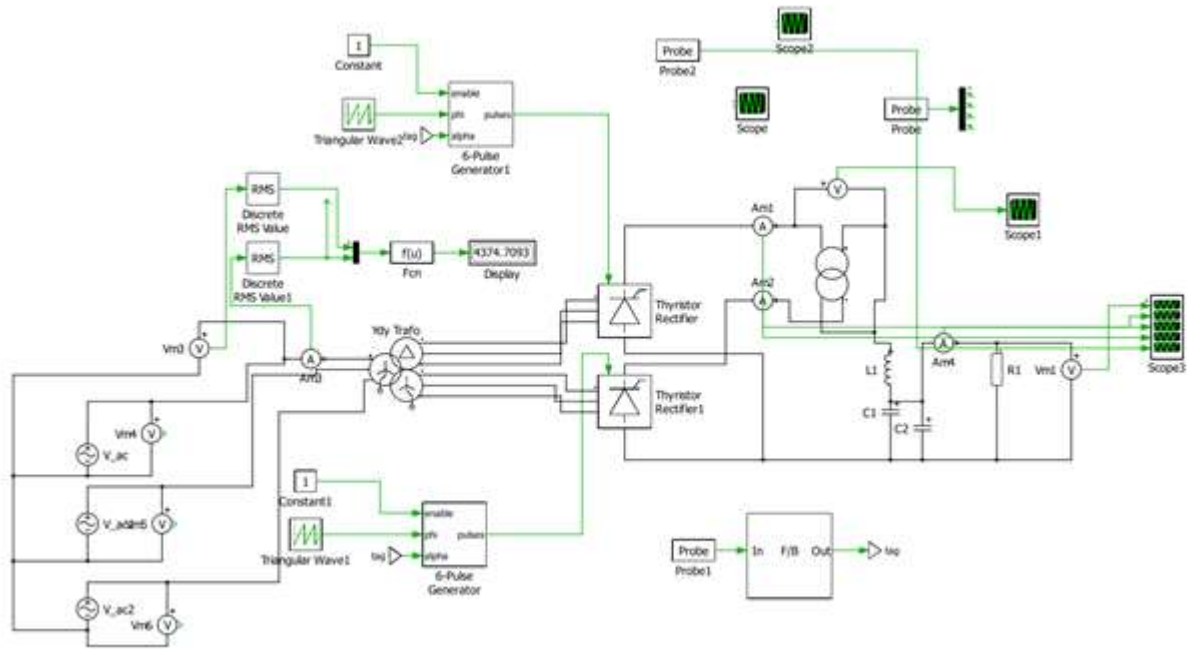


Figure 6-11 Simulation arrangement

## Simulations of a balanced three-phase input

Simulations were carried with the inter phase reactor values of 50  $\mu\text{H}$ , 200  $\mu\text{H}$  and 800  $\mu\text{H}$  with a balanced three phase input. The harmonic content of the inter phase reactor currents were studied.

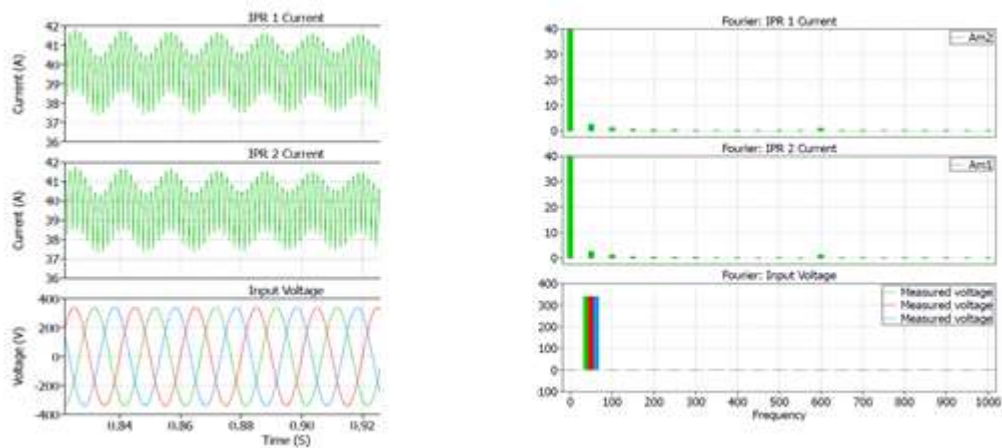


Figure 6-12 Simulation results with a 50µH interphase reactor

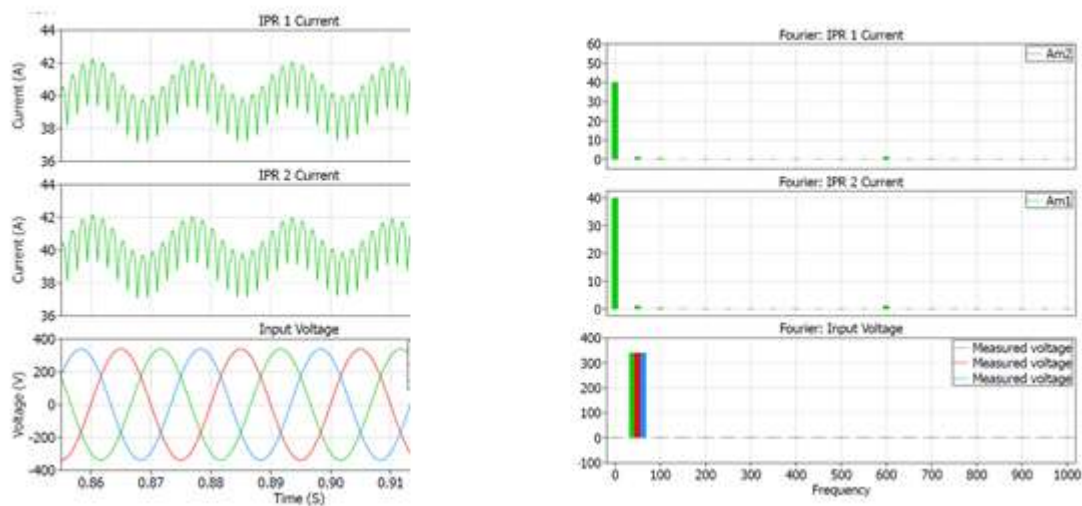


Figure 6-13 Simulation results with a 200µH interphase reactor

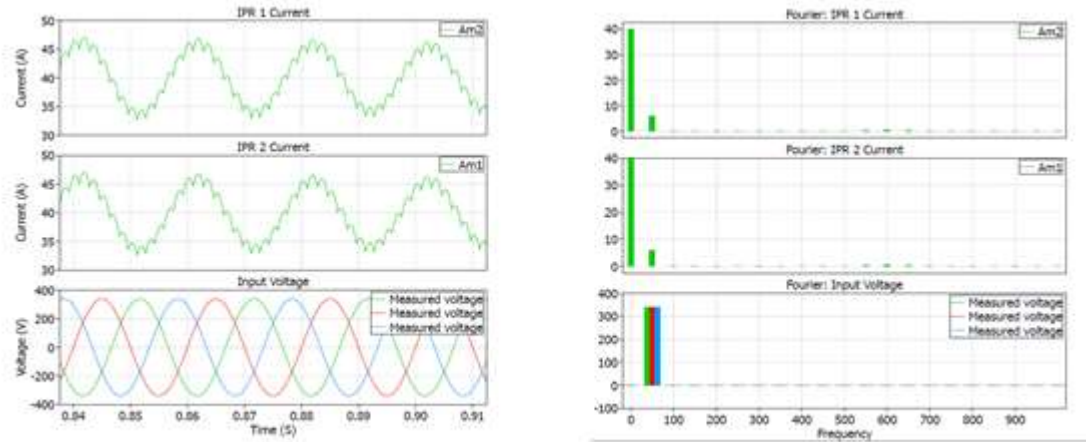


Figure 6-14 Simulation results with an 800 $\mu$ H interphase reactor

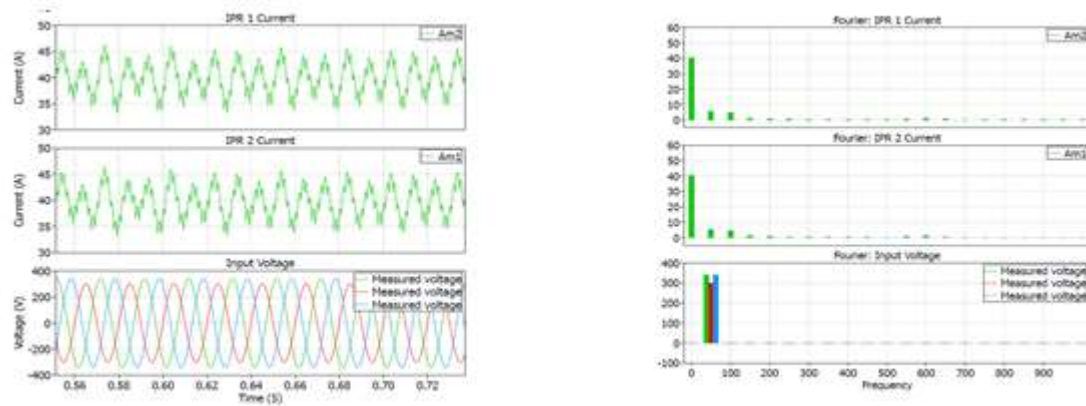


Figure 6-15 Simulation results with a 50 $\mu$ H interphase reactor with unbalanced input

### Simulations of an unbalanced three-phase input

The performance of the system was evaluated with the interphase reactor values of 50 $\mu$ H, 200 $\mu$ H, 600 $\mu$ H and 800 $\mu$ H when the three phase input is unbalanced. The harmonic content of the inter phase reactor currents were studied.

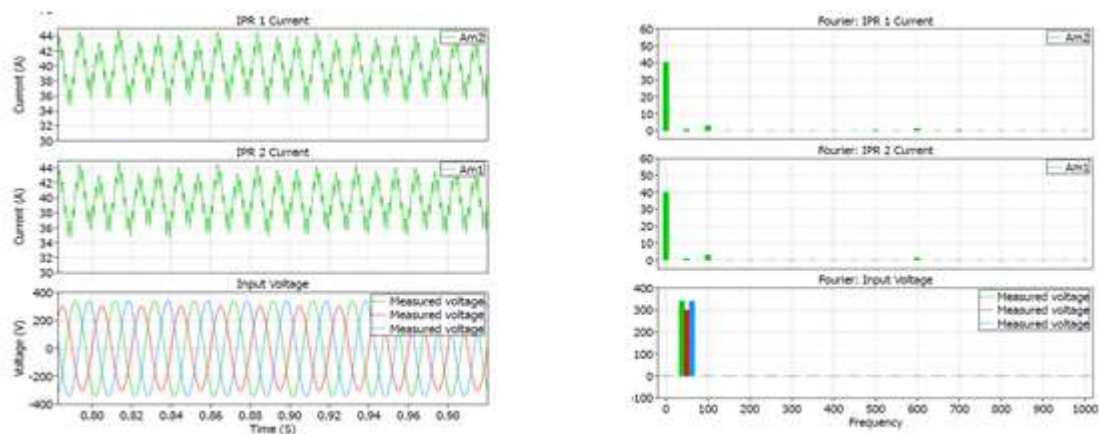


Figure 6-16 Simulation results with a 200µH interphase reactor with unbalanced input

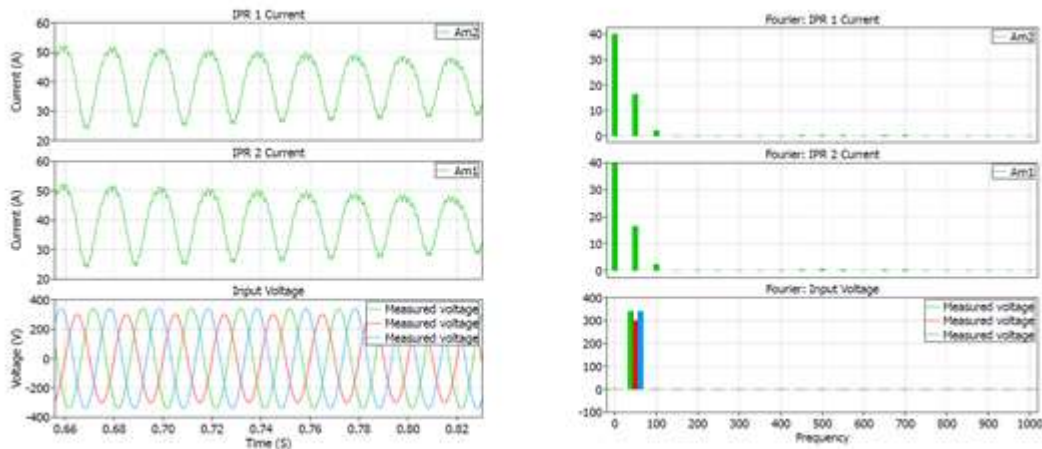


Figure 6-17 Simulation results with a 600µH interphase reactor with unbalanced input

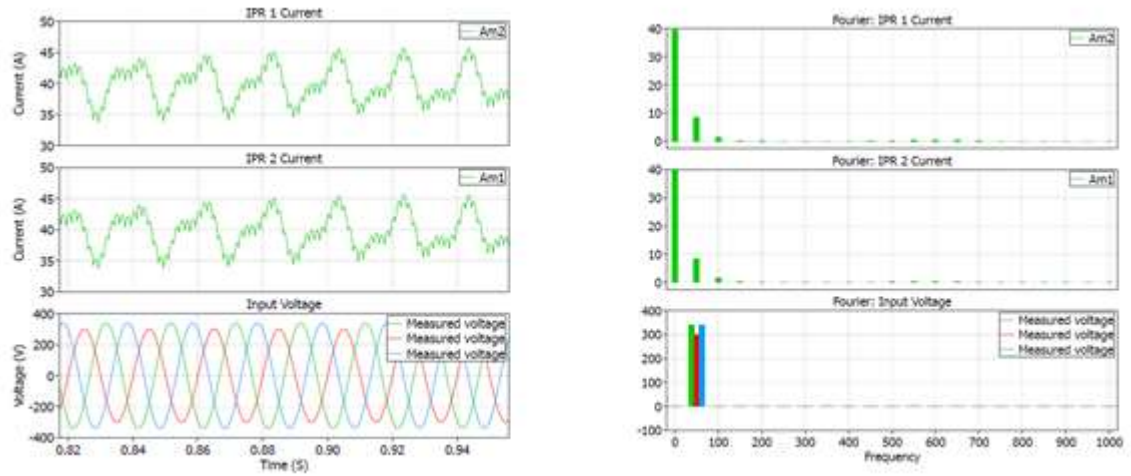


Figure 6-18 Simulation results with an 800 $\mu$ H interphase reactor with unbalanced input

### 6.23 Prototype development and testing

After the detailed analysis of the situation with the use of simulation tools two prototype interphase reactors were built. These were constructed such that the inductance of each inter phase reactor can be adjusted to the values of 50 $\mu$ H, 200 $\mu$ H, 600 $\mu$ H and 800 $\mu$ H by adjusting the air gap thickness in the magnetic path. These were developed to be suitable for a 2kW 12pulse rectifier system. In designing the interphase reactors appropriate selection of magnetic materials were made based on their exciting waveforms through simulations. As it could be seen from the waveforms and their Fourier spectrums the presence of the higher order harmonic currents content was not extremely high. Therefore the requirement of using high performance magnetic core materials was not identified.

However, attention was given to the increase in the physical size and the weight of the interphase reactors with the increased values of their inductance in contrary to contribution given by the high inductance for the reduction of harmonic content.

The 12pulse rectifier system was tested with these interphase reactors for each of the above-mentioned inductance values with a balanced three phase input voltage. Same tests were carried out for the system with a three-phase input supply of unbalanced conditions. The phase imbalance conditions were achieved with the use of a three-phase variable transformer. Obtained results were recorded and compared with the simulated results.



Figure 6-19 Prototype and testing arrangement

## 6.24 Discussion

Magnetic components play a vital role in any power electronic system. Usually, they become the bulkiest components in a system and on most occasions they become a major contributor for the cost of the system. This study was carried out with the intention identifying the optimum parameters for the magnetic components used in the multi pulse rectifier systems such as 12 pulse and 18 pulse systems. In the case of designing multi-pulse rectifier systems, it is a common practice in the industry to finalize the parameters for magnetic components based on the desirable output conditions and with a rough understanding of the physical size based on equivalent power rating.

In this study an approach is made to add an additional dimension for the multi-pulse system optimization by taking the actual magnetic designs, rather than the just the equivalent power approach in defining the parameters for the vital magnetic components such as interphase reactors. A series of simulations were carried out and the current waveforms through the inter phase reactor was analyzed. The test results obtained on a 2 kW 12 pulse rectifier system showed the simulation results were very much in line the actual values obtained for the current waveforms.

The considered 2 kW 12pulse system showed reasonable performance in the simulation as well as in the actual testing even with a 50 $\mu$ H inductance inter phase reactor. Actual magnetic



design showed a weight less than a 1kg in such an inter phase reactor. However, when the unbalanced supply situation was considered it could be seen that 100Hz and 600Hz components of the current wave form increases. Though an actual magnetic design of a considerably small size can be active even with this increased harmonic content especially in high power application it is advisable to increase the inductance and reduce the harmonic content which enables a reduction in high frequency losses in magnetic components.

The increase the inductance up to about 200  $\mu\text{H}$  resulted in a further reduction in the harmonic content of the current and this situation could be seen both in the simulation and the actual measurements. This results in an actual component size of about little over 2 kg for the system under consideration. Further increase of the interphase reactor values up to 600  $\mu\text{H}$  and 800  $\mu\text{H}$  resulted in a considerable drop in the 600Hz and higher harmonic content. However, increase of actual size of the interphase reactor makes it less attractive to increase the inductance values to this level.

Based on the series of testing and simulations carried out it could be concluded that an optimum value of inductance can be achieved for a system and it is advisable to do in by taking the actual designs of magnetic components. A smaller value that may still give the required total harmonic distortion can result in a higher high frequency content in the inter phase reactor current making it more loss making and larger value will result in a much bigger component size. For the considered example of 2 kW 12 pulse rectifier, it could be seen that the best compromise is archived little over 200  $\mu\text{H}$  level considering both system performance and actual magnetic designs.

The requirement of continuing the study for several other configurations of 12 and 18 pulse system and for several power levels and arrive at table of optimum interphase reactor values that gives the best system performance and optimum magnetic components designs were identified and it is expected to carry out this as part of future research work.

## 6.3 Summary

Several aspects of the operation of power-electronic circuits with transformers are significantly influenced by the leakage inductance of the respective transformer. In this section a study on This aspect is discussed in detail in this chapter based on large constructions. Theoretical estimations made for the leakage inductance and the short circuit impedance of the 1.2MVA single phase transformers discussed in this paper showed an accuracy level in the range of 20% and 15%. Due to the nature of these parameters arriving at a prediction with this level of accuracy can be considered as reasonable as it is acceptable for industry applications. However if a better degree of accuracy level is needed it is required to address the effect of high frequency content, eddy current losses proximity effect etc. Further a Finite Element Analysis could also provide a better accuracy in the prediction.

Further the optimization of magnetics for 12 and 18 pulse rectifier systems are discussed here. This is done by defining the optimum parameters and configurations of magnetics. The approach is based on the definition of the parameters for magnetics considering the system impact on actual magnetics designs and the performance of the system with the set parameters of magnetic components. The several possible situations of unbalanced supply are also considered and optimum magnetic parameters to minimize the effect of the supply imbalance are discussed. Based on a series of simulations which were verified by practical testing a quantitative explanation of the size of the magnetics against the quality of the output and robustness to supply imbalances is presented. This explanation gives a measure on the degree of compromise that can be made on magnetics and the quality of the output. Situations where the magnetic designs are made larger or the requirement of using special magnetic materials that make the magnetic components more expensive are also discussed.

Based on the series of testing and simulations carried out on 12 and 18 pulse rectifier systems it was concluded that an optimum value of inductance can be achieved for a system and it is advisable to do in by taking the actual designs of magnetic components. A smaller value that may still give the required total harmonic distortion can result in a higher high frequency content in the inter phase reactor current making it more loss making and larger value will result in a much bigger component size. For the considered example of 2 kW 12 pulse rectifier, it could be seen that the best compromise is archived little over 200  $\mu\text{H}$  level considering both system performance and actual magnetic designs.



# Chapter 7

## Summary

## Chapter 7 Summary

### 7.1 Evolution of magnetics

Magnetism is one of the most amazing phenomena that mankind has ever discovered. Though magnetism was first discovered over 2500 years ago and went through a great level of discoveries and understandings over the last two centuries, However, some phenomena such as Faraday's paradox that indicate some of the fundamental laws which are the basis for the operation of practical magnetic components may predict incorrect results are left open. Most electronics engineers even today do not attempt to understand the basic principles of magnetics due to its theoretical and complicated nature. The innovation and developments in the electronics industry took place at a very rapid pace during the last several decades. This includes the developments that took place in the power conversion technologies, communication technologies, the technologies related to the miniaturization of consumer electronic products, developments in technologies related to the internet of things (IOT) etc. In this context one could reasonably argue that the deployment of magnetic components has not happen at a competitive rate to that of electronics or semiconductor devices. As a result of this magnetic components still remain as the bulkiest components in an electronics system. In most of the cases they also remain to be the most expensive single component in an electronics system. It is generally believed in the industry that no considerable change in the magnetic components is possible as they are first level components which are very close to the physics of magnetism and to make a significant change in the nature of them would require shaking the basic laws of physics. Through this situation is explained in such ways and it has its own arguments the magnetics designers are put under pressure to come up with smarter solutions for magnetics in power electronics applications.

The main limitation for achieving both high frequency and high current in many of today's DC/DC converters is the magnetic components design. The magnetic is typically the largest component in converters, and at high frequencies it becomes increasingly difficult to have high current output and remain competitive with the size of silicon(Li et al., 2010).Magnetic components, namely inductors and transformers, are necessary for most commercial power electronic circuits such as DC/DC converters. Often the magnetic components represent some of the largest and most expensive parts in these circuits. With the continual push to shrink the size and cost of commercial electronic devices, numerous research efforts over the past decade have focused on new materials and manufacturing techniques to help address these

limitations. Examples range from low profile magnetic cores with conventional wire wound technology; to integrating planar transformers and embedded passives into the substrate of a printed circuit board (PCB)(Roesler et al., 2010). These efforts in the magnetic research have been able to take magnetic components through several generations which brought up several advantages to the industry including considerable size, weight, and cost savings of electronics systems.

## 7.1 Evolution of magnetics in power electronics applications

### 7.11 Wire wound components.

Wire wound magnetic components existed for number of decades if not for centuries since the first invention of the transformer. Despite the limitations associated with such conventional wire wound magnetic components they still constitute a very large percentage of magnetic components produced in the world. They are associated with number of limitations due to the nature of construction. These can be seen in the point of view of production engineering as well as in the point of view of the device performance. The considerable amount of production time needed in wire wound components and the very limited possibility of automation of the complete production process drive the price of wire wound components high. Further these require the introduction of foil insulation materials in order to maintain the dielectric strength between the parts of the components requiring isolation. This is also a contributor for the increase in the production time and the cost.

Further in the applications of high frequency operations the inevitable presence of skin effect and the proximity effect causes additional winding losses. Numerous efforts have been carried out by magnetics researchers including advanced theoretical analyses and computer simulations in order to explain these situations and to mitigate the losses due to them. These aspects have been discussed in detail in some of the previous publications.

Further a number of steps have been taken for the improvement of the insulation properties of magnet wires. These include developments such as multiple insulated wires as well as more novel developments such as fully insulated wires (FIW).

The other disadvantage in the wire wound components is the requirement of having to provide sufficient winding window for the wires themselves and for the winding tools or machinery in the case of toroidal and similar constructions. This makes it inevitable to have a large core. Having a large core in a magnetic component means that a large amount of magnetic material

has to be magnetized and demagnetized in every cycle of operation. This results in increased core losses in the magnetic component. As a result of the research work carried out on magnetic materials over a large period of time significant improvements have been achieved in the case of the performance of the magnetic core materials.

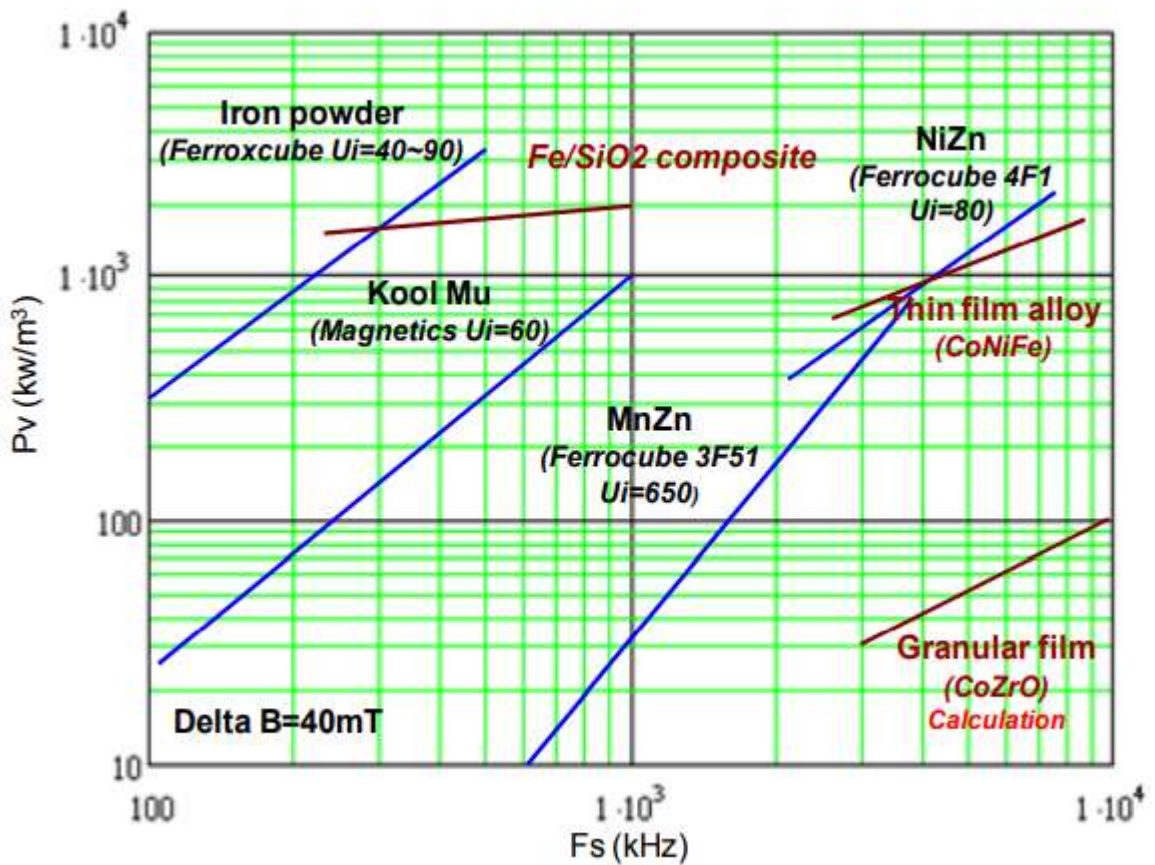


Figure 7-1 Core loss density of different magnetic material (Li et al., 2010)

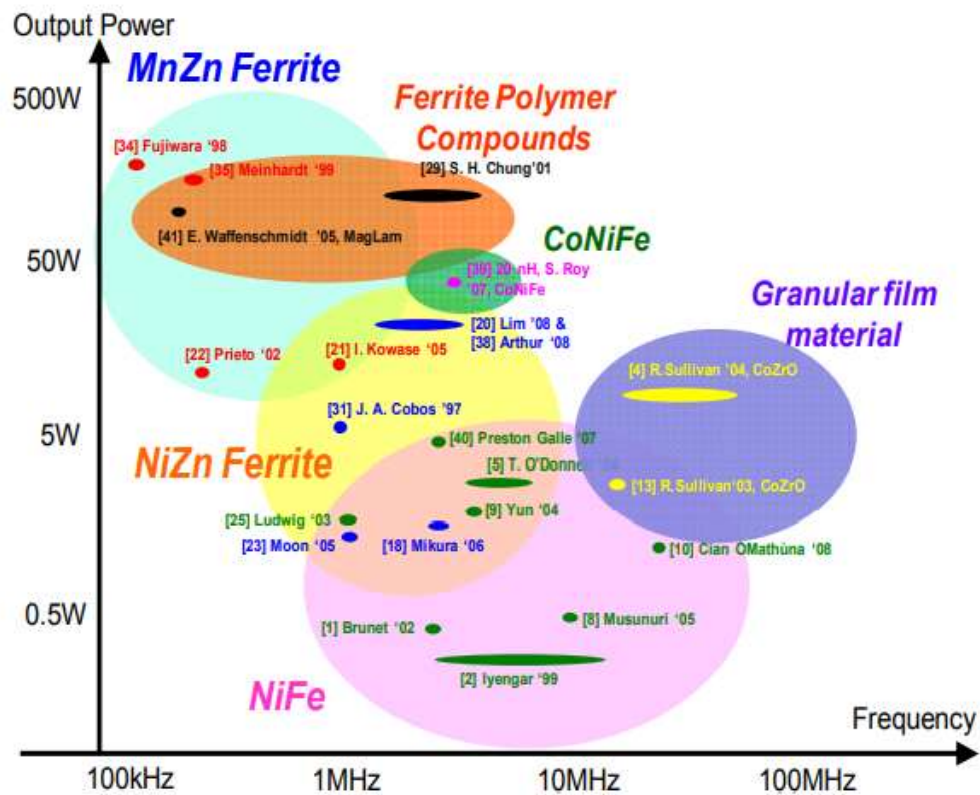


Figure 7-2 Integrated converter with different magnetic material (Li et al., 2010)

The figure 7-1 above provides useful information on the core loss performance of magnetic materials in high frequency applications. As it can be seen in the above figure the latest developments such as granular film materials provide considerably low core losses even under high frequency magnetic excitations. However, as it can be seen in the figure 7-2 limitations still exist in the achieving high power level with these magnetic materials.

Nevertheless, because of the advantages of these developments in the core materials as well as magnetic wire properties it is unlikely that the wire wound magnetic components will become completely obsolete even for the application in miniaturized electronics systems. However the other technologies such as planar magnetics have already taken over some of the wire wound component applications.

## 7.12 Planar magnetic components

The momentum toward high efficiency, high frequency, and high-power density in power supplies limited the wide use of conventional wire-wound magnetic component structures. For instance, winding loss is significantly increased due to the eddy current effect in conventional

round conductors particularly at frequencies above 100 kHz. Moreover, wire-wound magnetic components have resisted the trend toward integration and planarization. Planar magnetic components intrinsically provide lower profiles than conventional wire-wound components, aiding the miniaturization of power converters (Ouyang and Andersen, 2013).

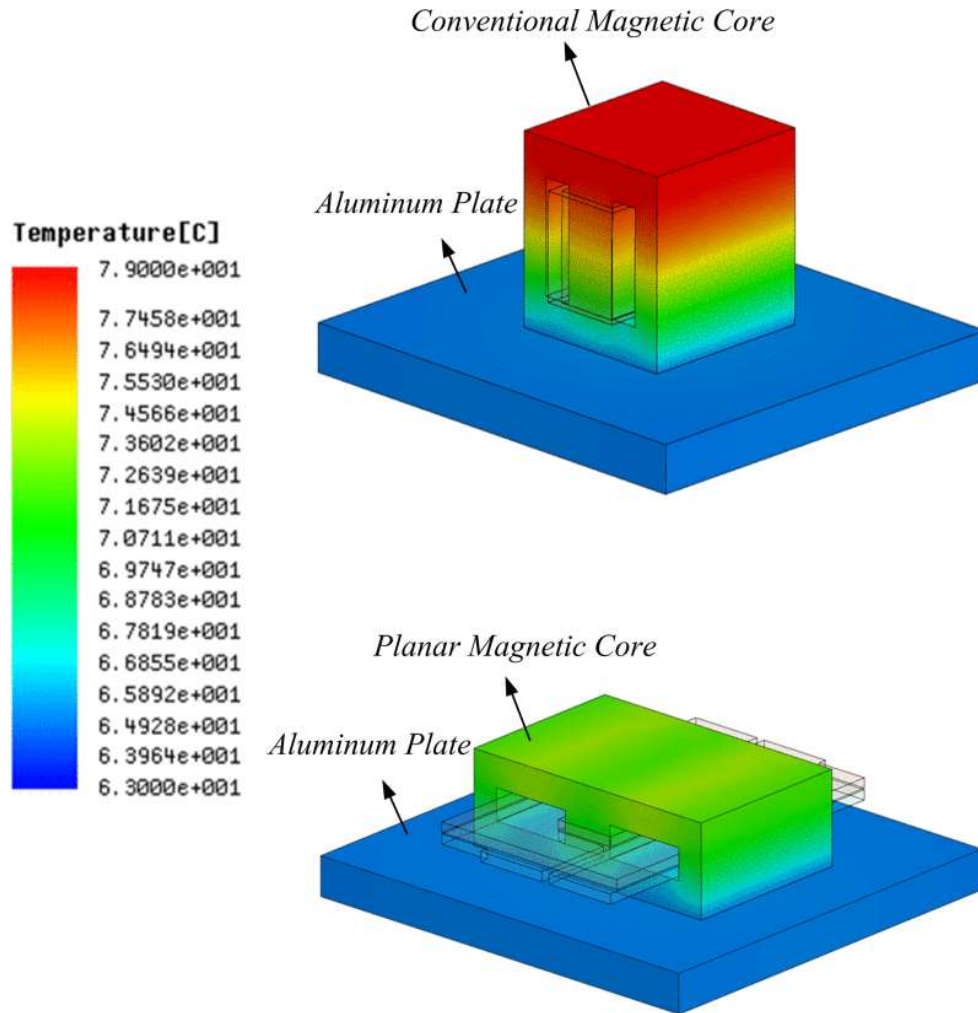


Figure 7-3 Comparison of thermal behavior between conventional core and planar core (Ouyang and Andersen, 2013)

The advantages that planar magnetics brought in to the magnetic component optimization are the reasons for them to take the place of some of the wire wound components.

The construction of planar magnetics in its nature provides a high frequency friendly performance. That is the nature of the planar construction itself beings the laws of physics related to magnetism in line to provide a basis for the mitigation of high frequency losses commonly known as skin effect and proximity effect in the industry. The theoretical aspects of these have been discussed in depth.

In addition to the provision of low conductor losses the planar magnetics provides a far better control over the parasitic effects in the components. This helps to maintain the consistent performance in mass production.

Further as it is illustrated in the figure 7-2 the planar construction provides better thermal performance.

The major disadvantage spoken about the planar magnetics is the cost of them in comparison with the conventional wire wound counterparts. However, with the amount of research put on to these type of magnetics it is expected for the price of these to go down considerably in the near future. Therefore it is expected that planar magnetics will take over a further share of wire wound magnetic components.

### 7.13 .PCB Integrated magnetics

Many low-power applications require miniaturized, flat components. This can be done by scaling down conventional wire wound/planar components using mechanical fabrication methods like powder blasted E cores in combination with flex circuit windings or the total integration of both the winding and magnetic core [164].

As the demand for flat and ultra-flat power converters increased during the last couple of decades more and more research efforts have been put in to the development of highly compact and flat systems. Magnetics components being the major barrier in achieving electronics systems of such flatness many companies and researches looked in to the possibility of arriving at flat magnetic components.

The idea of PCB integration of magnetics provided a revolutionary solution for this. Several magnetic integration technologies are used in the development of PCB integrated magnetics. The PCB embedded magnetic components achieved using these technologies provide a level of constancy and control over the variations of parasitic effects to a level that cannot be achieved by any of the previously discussed generations of magnetic components.

Further these provide the basis for the highest level of automation in the fabrication of them resulting more cost saving options.

The applications can already be seen in the areas of up to several MHz range switching frequencies and power levels in the range of 500W.

### 7.14 Magnetics on silicon

Future applications such as magnetics in Internet of Things (IoT) applications as well as modern application in ultra-flat mobile consumer electronics applications require ultra-thin and ultra-small magnetics components. The demand of these has become considerably high in the last few years and it is expected to have a high commercial need for them in the near future. In order to achieve such requirements magnetics integrated to packaging or on chip magnetics are being introduced as the next generation of magnetics. The developments in this branch of magnetics drive the construction of magnetic components to a completely new phase.

In addition to providing several advantages that PCB integrated magnetics or Planar magnetics provide the magnetics on silicon is becoming a technology that enables several branches of electronics applications. This also includes the applications related to the internet of things, micro level energy harvesting, development of self-sufficient electronics with inbuilt energy harvesting and converter systems etc.

It is expected to present detail fact on these technologies in the future publications.

### 7.15 Ultra-high-power magnetics in excess of 100kW

As it was discussed in the previous section the since the invention of the first magnetic components they have gone through several generations. Through it could be seen that the field of magnetics did not go significant evolution until couple of decades at present they are evolving at a much rapid rate. The developments discussed in this paper have contributed to these to a considerable extent. Those are developments have been welcome by the electronics industry.

However, with the development of semiconductor devices such as SiC MOSFETs high power DC DC convertors with power levels in excess of 100kW are attempted in the today's industry. Most of the techniques discussed in the new generations of magnetics still inherent the limitations developing efficient magnetics for this power levels and for the operating frequencies. Thus certain integration of several technologies and manufacturing techniques are required for the development of such magnetics components. In the continuous research in magnetic developments, magnetics components for ultra-high power levels such as 50kW, 50kHz DC DC converters and to a 100kW, 20kHz DC DC converters have been developed. In the development of such magnetic components the advantages of several techniques discussed above were combined to achieve these power levels in the required compact sizes.



These techniques are used to mitigate the high conductor losses happening at high frequencies.

## 7.2 Contributions of the research

### 7.21 Challenges that magnetics industry faced at the beginning of the research.

Rapid developments in the semiconductor technology and the power electronics industry enable the development of power supplies and power converters of significantly higher power levels. Considerably low switching losses of developments like SiC MOSFETs make it possible to operate at 2 to 5 times higher switching frequencies compared to their conventional counter parts. As the frequency goes high the magnetic components in such system become more and more compact. The magnetic components are usually the bulkiest components in a power electronics system and in most of the situations also the most expensive component, therefore it is of high interest of many designers to develop systems that operate at high frequencies.

The achievement of a high-power levels in a single module at high frequencies is next challenge faced by the developers of systems for high power applications. Most often the maximum power achievable with a single module is determined by the magnetic components. As a result, it could be seen that constraints in the development of magnetic components make a significant influence to the miniaturization of the power electronics system. Further it is reasonably accurate to state the magnetics components have a great impact on determining the power level and the operating frequencies of power electronics applications.

The design of magnetic components that meets the requirements of the modern applications face several major challenges as discussed in this thesis. These challenges made most of the magnetic designs not possible at certain power levels at certain frequencies. These are mainly

- 1.) Mitigation of excessive conductor losses generated in the conductors carrying high frequency high currents.
- 2.) Maintaining a core losses at the minimum possible level.
- 3.) Thermal management of the magnetic components and effective removal of heat generated.
- 4.) Evaluating multiple possible solutions for a particular application

- 5.) Control of other parameters such as leakage inductance, impedance, interwinding capacitance etc

## 7.22 Overcoming the challenges in mitigating conductor losses

In the chapter 3 of thesis a detail theoretical explanation is given for the significant increase of losses in conductors of magnetic components which are excited by waveforms containing high frequency components of considerable magnitudes. Analytical estimation is also made for simplified practical cases. The theoretically looked at situations were tested by the construction of series of high power high frequency transformers as discussed in the section 3.4 of the chapter 3.

At high power levels the winding design becomes very important for the mitigation of high frequency losses. Two winding constructions are discussed in the chapter 3.4 of this thesis. The novel method proposed with folded foils showed very good performance in mitigating the high frequency conductor losses. Further it gave the possibility of controlling the leakage inductance between the primary and secondary windings by adjusting the level of overlap. The disadvantage observed in this method was the time consumed for the proper insulation process. Through several insulating techniques were considered the amount of time savings archived was not sufficient to adopt this method in mass production for practical applications. Therefor further research is necessary to improve the production process for the successful implementation of this technique.

The second method proposed with sandwich winding could be seen as a good compromise on the performance and the amount of labor consumption.

As a result of these continued work the it was possible to arrive at a winding arrangement that enables the handling of high frequency large currents in high frequency magnetics. Details of this was discussed in this chapter under the section 3.5. This method is now patented and considered as a game changer as this technology very much eliminates the practical difficulties in achieving high power levels even up to MW range at frequencies as high as 50 kHz.

Several actual designs have already been manufacture using this method up to 200 kW of power operating at 30 to 50 kHz operating frequency. Further designs are made up to 2000 kW ( 2 MW ) operating at 20 kHz which was not possible at all at the time of the start of the reasearh. Further drivations of this approch has been namde giving the possibility of applyind thid technology for high power high frequency high voltage transformers.

### 7.23 Minimization of core losses and the selection of appropriate core material

A detail study was carried out on the losses occurring in the magnetic core of transformers. Several theoretical and empirical methods developed by various industry leading researchers were discussed in the sections 1 to 4 of the chapter 4. In the section 5 of the chapter 4 an explanation was given on the potential gap losses in magnetics core. From the sections 4.6 to 4.9 in the chapter 4 the studies carried out by the researcher are presented. This includes comparison of magnetic materials such as Nanocrystalline and ferrite to understand the ideal application areas for those materials. Further the studies carried out in this section includes different core constructions topologies, construction arrangements etc.

In this section the optimum design of high power high frequency magnetics is also discussed based on a 50kW application operating at 50 kHz.

In the section 4.8 of this thesis the achievement of 100kW in 20kHz transformer is discussed. This development is an extension of a series of developments carried out with high frequency, high power transformers of power and frequency levels such as 40kW, 20kHz and 50kW, 50kHz. The advantages and disadvantages of Ferrite and Nanocrystalline core materials at this power levels are discussed and the choice of Nanocrystalline core is explained.

These studies and a series of the previous developments carried out by the researcher have identified the advantages of using the materials such as Nanocrystalline for high power applications and for operating frequency levels in the range of 20 kHz to 30 kHz. With the appropriate thermal management approaches and designing at optimal operating flux levels Nanocrystalline core gives a considerable volume and weight advantage over the ferrites.

The results of these studies are discussed in the chapter 4. The patented constructions developed that are also relevant to the core less management is discussed in the chapter 5 as that relates to the thermal management of the overall product as well.

## 7.24 Thermal management of high power high frequency magnetic components

Theoretical aspects of transformer thermal management is discussed in the sections 5.1 to 5.5 of this chapter. This includes the theoretical aspects of thermal investigation of dry type transformers, calculations for ventilated dry type transformers, hot spot investigations for liquid filled transformers, temperature rise for high Frequency transformer under Forced-air convection etc

From the sections 5.6 to 5.8 the studies carried out based on 100 kW transformer with novel method of effective heat removal, thermal management of large transformer structures are discussed.

As discussed in the chapter 3 and 4 the detailed analysis of core and conductor losses made it possible to achieve the theoretically minimum level of high frequency conductor losses in high power high frequency transformers. However, as the demand for power levels increase the need for very high power levels in a compact structure is required. This results in a very high power and loss densities in high power high frequency transformers. Therefore effective removal of heat from such transformers make the products operating at a much lower temperature rise for a given size and make it possible to further miniaturize the high power high frequency transformers. Thermal management approaches developed and patented during the study are discussed in the section 5.7. These provide a very effective way of extracting the heat generated in the transformers.

Further the patented approach discussed in section 5.8 under novel approach to extract heat from the windings of transformers with high isolation requirements is particularly suitable for high voltage high frequency transformers which require tough insulation requirements.

## 7.25 Leakage inductance and other parameters that influence the system optimization.

Several aspects of the operation of power-electronic circuits with transformers are significantly influenced by the leakage inductance of the respective transformer. In the chapter 6 of this thesis a detail study on this aspect is discussed based on large constructions. Theoretical estimations made for the leakage inductance and the short circuit impedance of the 1.2MVA single phase transformers discussed in this paper showed an accuracy level in the range of 20% and 15%. Due to the nature of these parameters arriving at a prediction with this level of

accuracy can be considered as reasonable. as it is acceptable for industry applications. However if a better degree of accuracy level is needed it is required to address the effect of high frequency content, eddy current losses proximity effect etc. Further a Finite Element Analysis could also provide a better accuracy in the prediction.

Further the optimization of magnetics for 12 and 18pulse rectifier systems are discussed in the chapter 6. This is done by defining the optimum parameters and configurations of magnetics. The approach is based on the definition of the parameters for magnetics considering the system impact on actual magnetics designs and the performance of the system with the set parameters of magnetic components. The several possible situations of unbalanced supply are also considered and optimum magnetic parameters to minimize the effect of the supply imbalance are discussed. Based on a series of simulations which were verified by practical testing a quantitative explanation of the size of the magnetics against the quality of the output and robustness to supply imbalances is presented. This explanation gives a measure on the degree of compromise that can be made on magnetics and the quality of the output. Situations where the magnetic designs are made larger or the requirement of using special magnetic materials that make the magnetic components more expensive are also discussed.

Based on the series of testing and simulations carried out on 12 and 18pulse rectifier systems it was concluded that an optimum value of inductance can be achieved for a system and it is advisable to do in by taking the actual designs of magnetic components. A smaller value that may still give the required total harmonic distortion can result in a higher high frequency content in the inter phase reactor current making it more loss making and larger value will result in a much bigger component size. For the considered example of 2 kW 12 pulse rectifier, it could be seen that the best compromise is archived little over 200  $\mu\text{H}$  level considering both system performance and actual magnetic designs.

## 7.26 Parametric design approach

The details of the large number of design parameters that have to be taken into consideration in arriving at the optimum design of a magnetic component was discussed in the chapter 2 of this thesis. It is rarely the case that the values of all the parameters or at least the suitable range of values for all these parameters are known at the time of the start of the design. In certain applications depending on the level of circuit simulations carried out by the application engineers the ideal values for certain parameters are known. In certain other applications the application engineers and system designers would like to have practically achievable parameters of the magnetic components for them to use as an input for the electronics system design.

In each section of the research discussed in different chapters the focus was on eliminating or reducing the impact key limitations experienced in magnetic designs. However, when it comes to the final design of magnetic products it is not just one solution exist that will satisfy the input criteria. Therefore the concept of parametric design was taken as a concept that governs the overall research, which enables the multiple possible solutions for a particular application. This approach benefits industry giving an additional dimension for the system optimization.

The manual tools that facilitate the generation of parametric designs solutions are discussed in the chapter two of this thesis. These have enabled the design of engineering samples discussed in different chapters in this thesis.

The possibility of providing multiple solutions by the adjustment of design as well as input parameters is a feature very welcome by the system designers.

As a future work that goes beyond the scope of this study the researcher intended to develop a software program based on the development made during this research which will make it possible automatically generate multiple design solutions.

Though it was out of the scope of the PhD and was seen as a part of future works out of the interest of the researcher an algorithm has already been developed to automate the magnetic design process which the researcher expects to commercialize in the near future. This will in several minutes generate thousands of design solution solutions for a particular application. These designs will be optimised based on different criteria defined by the designer of the application. For example, optimization can be based on maximizing the efficiency, minimizing the weight, minimizing cost, minimizing the space etc.

## 7.27 Magnetics are no longer the barrier for the development of power electronics.

This research was aimed at facing this change by carrying out a comprehensive study that extends to the analysis fundamental principles behind these limitations. At the end of this research work it became possible to eliminate the barriers of achieving high power levels and to make the power level that can be achieved in a transformer almost independent from the operating frequency. The use of a combination of several patented technologies developed during this study which are explained in this thesis made it possible to arrive at design of transformers with power levels as high as 2.5 MW operating at frequencies over 50 kHz.

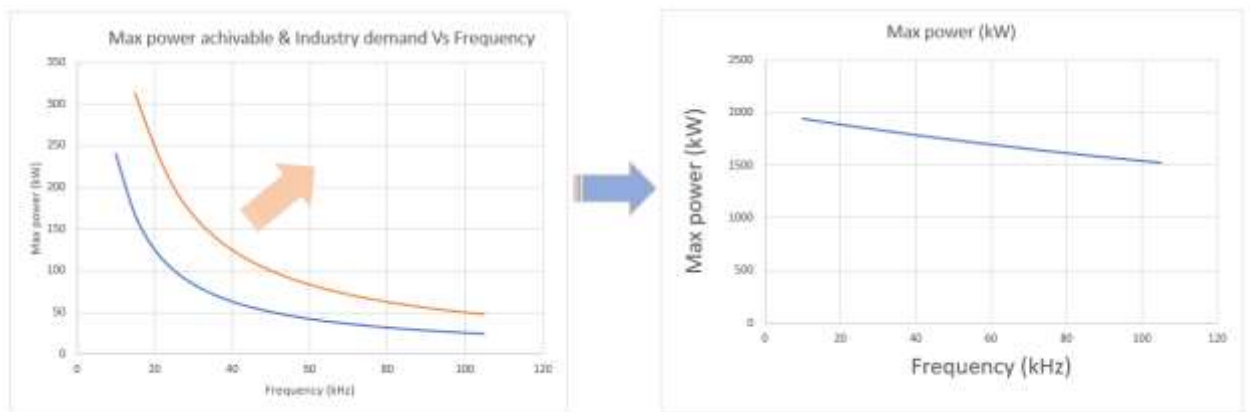


Figure 7-4 Change in power level that can be achieved at a given frequency before and after the research -Kapila Warnakulasuriya own charts

The achievement of this condition has made a transformation of the magnetics industry and the commercialization has already started. The path to achievement condition is discussed in this thesis. This study does not limit at the level of giving a single solution for a particular application, but also it goes to the extent of providing a whole set of parametric solutions that would fulfill the requirements of a particular application. An example of the multiple solution is explained in chapter 2.

### 7.3 Future work

The study has made it possible to achieve power levels at high frequencies far beyond the industry requirements at present. Therefore it is suggested to focus on areas such as incorporating further adjustable leakage inductance, which will be an attractive aspect for many modern power electronics applications. Another area of research interest is the accurate prediction and reduction of inter winding capacitance of high-power high frequency transformers.

Carrying out research on new core materials is another area of high use for the future of the magnetics industry.



## Chapter 8 References

- ACERO, J., ALONSO, R., BURDÍO, J. M., BARRAGÁN, L. A. & PUYAL, D. 2006. Frequency-dependent resistance in Litz-wire planar windings for domestic induction heating appliances. *IEEE Transactions on Power Electronics*, 21, 856-866.
- ALBERS-SCHOENBERG, E. 1958. Ferrites. *Journal of the American Ceramic Society*, 41, 484-489.
- AMMOURI, A., SALAH, T. B. & KOURDA, F. Modeling and simulation of a high-frequency planar power transformers. 2015 4th International Conference on Electrical Engineering (ICEE), 2015. IEEE, 1-6.
- ANANDPARA, M., PANCHAL, T. & PATEL, V. An active interphase transformer for 12-pulse rectifier system to get the performance like 24-pulse rectifier system. 2014 Eighteenth National Power Systems Conference (NPSC), 2014. IEEE, 1-6.
- ARJONA, M., HERNANDEZ, C., ESCARELA-PEREZ, R. & MELGOZA, E. Thermal analysis of a dry-type distribution power transformer using FEA. 2014 International Conference on Electrical Machines (ICEM), 2014. IEEE, 2270-2274.
- BAHMANI, M., THIRINGER, T. & KHAREZY, M. Optimization and experimental validation of medium-frequency high power transformers in solid-state transformer applications. 2016 IEEE Applied Power Electronics Conference and Exposition (APEC), 2016. IEEE, 3043-3050.
- BAHMANI, M. A., THIRINGER, T., RABIEI, A. & ABDULAHOVIC, T. 2015. Comparative study of a multi-MW high-power density DC transformer with an optimized high-frequency magnetics in all-DC offshore wind farm. *IEEE Transactions on power delivery*, 31, 857-866.
- BALA, C. V. & MOREGA, A. M. A high short-circuit impedance electrical transformer. 2011 7TH INTERNATIONAL SYMPOSIUM ON ADVANCED TOPICS IN ELECTRICAL ENGINEERING (ATEE).
- BARRIOS, E. L., URTASUN, A., URSÚA, A., MARROYO, L. & SANCHIS, P. 2014. High-frequency power transformers with foil windings: maximum interleaving and optimal design. *IEEE Transactions on Power Electronics*, 30, 5712-5723.
- BARTH, D., KLAUS, B. & LEIBFRIED, T. Litz wire design for wireless power transfer in electric vehicles. 2017 IEEE Wireless Power Transfer Conference (WPTC), 2017. IEEE, 1-4.
- BARTOLI, M., NOFERI, N., REATTI, A. & KAZIMIERCZUK, M. K. Modeling litz-wire winding losses in high-frequency power inductors. PESC Record. 27th Annual IEEE Power Electronics Specialists Conference, 1996. IEEE, 1690-1696.
- BERNARDONI, M., DELMONTE, N., COVA, P. & MENOZZI, R. 2010. Thermal modeling of planar transformer for switching power converters. *Microelectronics Reliability*, 50, 1778-1782.
- BERTOTTI, G. 1986. Some considerations on the physical interpretation of eddy current losses in ferromagnetic materials. *Journal of magnetism and magnetic materials*, 54, 1556-1560.
- BERTOTTI, G. 1988. General properties of power losses in soft ferromagnetic materials. *IEEE Transactions on magnetics*, 24, 621-630.
- BERTOTTI, G. 1992. Dynamic generalization of the scalar Preisach model of hysteresis. *IEEE Transactions on Magnetics*, 28, 2599-2601.
- BIELA, J. & KOLAR, J. W. Electromagnetic integration of high power resonant circuits comprising high leakage inductance transformers. 2004 IEEE 35th Annual Power

- Electronics Specialists Conference (IEEE Cat. No. 04CH37551), 2004. IEEE, 4537-4545.
- BIRO, O., LOWTHER, D. A., ALOTTO, P., CAMPELO, F., WATANABE, K. & IGARASHI, H. 2007. 3D topology optimization using an immune algorithm. *COMPEL-The international journal for computation and mathematics in electrical and electronic engineering*.
- CAMPELO, F., GUIMARÃES, F., IGARASHI, H., WATANABE, K. & RAMIREZ, J. An immune-based algorithm for topology optimization. 2006 IEEE International Conference on Evolutionary Computation, 2006. IEEE, 3204-3211.
- CAMPELO, F., OTA, S., WATANABE, K. & IGARASHI, H. 2008. Generating parametric design models using information from topology optimization. *IEEE transactions on magnetics*, 44, 986-989.
- CARSTEN, B. High frequency conductor losses in switchmode magnetics. IEEE Proc. High Frequency Power Conf. 1986, 1986. 155-176.
- CHAN, J. H., VLADIMIRESCU, A., GAO, X.-C., LIEBMANN, P. & VALAINIS, J. 1991. Nonlinear transformer model for circuit simulation. *IEEE Transactions on Computer-Aided Design of Integrated Circuits and Systems*, 10, 476-482.
- CHANG, R.-C., CHEN, C.-K., WANG, C.-Y. & TZOU, Y.-Y. Calculation of losses and temperature rise for high frequency transformer under forced-air convection. IECON 2010-36th Annual Conference on IEEE Industrial Electronics Society, 2010. IEEE, 1-6.
- CHEN, K. & KUMAR, N. 2014. Influence of isolation transformer leakage inductance on constant current output of Class D series-parallel LCC-type resonant converter for light-emitting diode lighting application. *IET Power Electronics*, 7, 1362-1373.
- CHENG, K. W. E. 2000. Computation of the AC resistance of multistranded conductor inductors with multilayers for high frequency switching converters. *IEEE Transactions on Magnetics*, 36, 831-834.
- CHIESA, N. 2010. Power transformer modeling for inrush current calculation.
- CHIN, G. 1971. Review of magnetic properties of Fe-Ni alloys. *IEEE Transactions on Magnetics*, 7, 102-113.
- CHOI, J.-M., BYEN, B.-J., LEE, Y.-J., HAN, D.-H., KHO, H.-S. & CHOE, G.-H. 2012. Design of leakage inductance in resonant dc-dc converter for electric vehicle charger. *IEEE transactions on magnetics*, 48, 4417-4420.
- CHOI, S., ENJETI, P. N. & PITEL, I. J. 1996. Polyphase transformer arrangements with reduced kVA capacities for harmonic current reduction in rectifier-type utility interface. *IEEE Transactions on Power Electronics*, 11, 680-690.
- ĆUK, S. New topology eliminates magnetic cores at 50 kHz NOT 50MHz! 2017 International Conference on Green Energy Conversion Systems (GECS), 2017. IEEE, 1-9.
- DAI, X.-B., DONG, Y.-D. & QIN, L. 2014. Research on Variable Structure, Parametric Design System of Ceramic, Tile Mould Based on Modular [J]. *Computer Aided Drafting, Design and, Manufacturing*, 24, 67-73.
- DAS, A. K. & FERNANDES, B. G. Accurate Capacitance Calculation of Multi-layer Foil Windings in a Medium/High-frequency High-power Transformer. 2020 IEEE Energy Conversion Congress and Exposition (ECCE), 2020. IEEE, 5834-5841.
- DAS, A. K., WEI, Z., VAISAMBHAYANA, S., CAO, S., TIAN, H., TRIPATHI, A. & KJÆR, P. C. Thermal modeling and transient behavior analysis of a medium-frequency high-power transformer. IECON 2017-43rd Annual Conference of the IEEE Industrial Electronics Society, 2017. IEEE, 2213-2218.

- DE LEÓN, F., PURUSHOTHAMAN, S. & QASEER, L. 2013. Leakage inductance design of toroidal transformers by sector winding. *IEEE Transactions on Power Electronics*, 29, 473-480.
- DELLA TORRE, E. & VAJDA, F. 1994. Parameter identification of the complete-moving-hysteresis model using major loop data. *IEEE Transactions on Magnetics*, 30, 4987-5000.
- DEN BOSSCHE, A., VALCHEV, V. & GEORGIEV, G. Measurement and loss model of ferrites with non-sinusoidal waveforms. PESC 2004 IEEE 35th Annual Power Electronics Specialists Conference, 2004. 4814-4818.
- DIMITRAKAKIS, G., TATAKIS, E. & RIKOS, E. A new model for the determination of copper losses in transformer windings with arbitrary conductor distribution under high frequency sinusoidal excitation. 2007 European Conference on Power Electronics and Applications, 2007. IEEE, 1-10.
- DIMITRAKAKIS, G. S. & TATAKIS, E. C. Investigation of high frequency effects on layered coils. 2008 13th International Power Electronics and Motion Control Conference, 2008. IEEE, 1301-1308.
- DIMITRAKAKIS, G. S. & TATAKIS, E. C. 2009. High-frequency copper losses in magnetic components with layered windings. *IEEE Transactions on Magnetics*, 45, 3187-3199.
- DING, X. & NING, W. Analysis of the dry-type transformer temperature field based on fluid-solid coupling. 2012 Second International Conference on Instrumentation, Measurement, Computer, Communication and Control, 2012. IEEE, 520-523.
- DIXON, L. H. Eddy current losses in transformer windings and circuit wiring. SEM600 Unitrode Seminar, 1988. R2-1.
- DOEBBELIN, R., BENECKE, M. & LINDEMANN, A. Calculation of leakage inductance of core-type transformers for power electronic circuits. 2008 13th International Power Electronics and Motion Control Conference, 2008. IEEE, 1280-1286.
- DOEBBELIN, R., TEICHERT, C., BENECKE, M. & LINDEMANN, A. 2009. Computerized calculation of leakage inductance values of transformers. *Piers Online*, 5, 721-726.
- DOWELL, P. Effects of eddy currents in transformer windings. Proceedings of the Institution of electrical Engineers, 1966. IET, 1387-1394.
- DUGAN, R. C. & MCDERMOTT, T. E. 2002. Distributed generation. *IEEE industry applications magazine*, 8, 19-25.
- EL SHAFEI, A., OZDEMIR, S., ALTIN, N., JEAN-PIERRE, G. & NASIRI, A. A High power high frequency transformer design for solid state transformer applications. 2019 8th International Conference on Renewable Energy Research and Applications (ICRERA), 2019. IEEE, 904-909.
- EMPRINGHAM, L., DE LILLO, L. & SCHULZ, M. 2013. Design challenges in the use of silicon carbide JFETs in matrix converter applications. *IEEE transactions on power electronics*, 29, 2563-2573.
- ERICKSON, R. & MAKSIMOVIC, D. 2001. Fundamentals of Power Electronics Norwell. MA: Kluwer-Academic.
- FELDTKELLER, E. 1984. 100 years' magnetic contributions to electrical engineering. *IEEE Transactions on Magnetics*, 20, 2057-2090.
- FERREIRA, J. Appropriate modelling of conductive losses in the design of magnetic components. 21st Annual IEEE Conference on Power Electronics Specialists, 1990. IEEE, 780-785.
- FERREIRA, J. Analytical computation of ac resistance of round and rectangular litz wire windings. IEE Proceedings B (Electric Power Applications), 1992. IET, 21-25.
- FERREIRA, J. A. 1994. Improved analytical modeling of conductive losses in magnetic components. *IEEE transactions on Power Electronics*, 9, 127-131.

- FILCHEV, T., WHEELER, P., CLARE, J., VALCHEV, D. Y. V. & VAN DEN BOSSCHE, A. A LCL resonant dc-dc converter for electrical power distribution systems. European Power Electronics, EPE-PEMC Conference, Riga, 2004.
- FISH, G. E. 1990. Soft magnetic materials. *Proceedings of the IEEE*, 78, 947-972.
- FU, D., LEE, F. C. & WANG, S. Investigation on transformer design of high frequency high efficiency dc-dc converters. 2010 Twenty-Fifth Annual IEEE Applied Power Electronics Conference and Exposition (APEC), 2010. IEEE, 940-947.
- FUKUNAGA, H., EGUCHI, T., KOGA, K., OHTA, Y. & KAKEHASHI, H. 1990. High performance cut cores prepared from crystallized Fe-based amorphous ribbon. *IEEE transactions on magnetics*, 26, 2008-2010.
- FUKUNAGA, H., EGUCHI, T., OHTA, Y. & KAKEHASHI, H. 1989. Core loss in amorphous cut cores with air gaps. *IEEE transactions on magnetics*, 25, 2694-2698.
- GAO, H. B. & YANG, Z. J. Dynamic Analysis and Research of Motor's Elastic Shaft of the Large Miner High Shearer's Cutting Parts. Applied Mechanics and Materials, 2012. Trans Tech Publ, 105-110.
- GAO, L., LUO, Q., XU, Y., JING, G.-Q. & JIANG, H.-K. 2015. Discrete element method of improved performance of railway ballast bed using elastic sleeper. *Journal of Central South University*, 22, 3223-3231.
- GAO, S.-W., ZHANG, M., SUN, X.-T., YUAN, C.-H., WANG, N. & LI, X. The research on calculation of temperature field of winding in dry type transformer. 2012 Fifth International Conference on Intelligent Networks and Intelligent Systems, 2012. IEEE, 185-188.
- GRADINGER, T. B. & DROFENIK, U. Managing high currents in litz-wire-based medium-frequency transformers. 2018 20th European Conference on Power Electronics and Applications (EPE'18 ECCE Europe), 2018. IEEE, P. 1-P. 10.
- GRADINGER, T. B., DROFENIK, U. & GRECKI, F. Enabling foil windings of medium-frequency transformers for high currents. 2020 22nd European Conference on Power Electronics and Applications (EPE'20 ECCE Europe), 2020. IEEE, 1-10.
- GUILLOD, T., HUBER, J., KRISMER, F. & KOLAR, J. W. Litz wire losses: Effects of twisting imperfections. 2017 IEEE 18th Workshop on Control and Modeling for Power Electronics (COMPEL), 2017a. IEEE, 1-8.
- GUILLOD, T., KRISMER, F. & KOLAR, J. W. Electrical shielding of MV/MF transformers subjected to high dv/dt PWM voltages. 2017 IEEE Applied Power Electronics Conference and Exposition (APEC), 2017b. IEEE, 2502-2510.
- HE, R., ZHANG, Y., ZHANG, D. & XIE, D. An improvement of core losses estimation model in power electronic transformer. 2018 IEEE Student Conference on Electric Machines and Systems, 2018. IEEE, 1-5.
- HERBERT, E. 2008. User-friendly data for magnetic core loss calculations. *Unpublished., August.*
- HERNADI, A. & ANWARI, M. Modeling and simulation of 6-pulse and 12-pulse rectifiers under balanced and unbalanced conditions with impacts to input current harmonics. 2008 Second Asia International Conference on Modelling & Simulation (AMS), 2008. IEEE, 1034-1038.
- HERZER, G. 1997. Amorphous and nanocrystalline soft magnets. *Magnetic Hysteresis in Novel Magnetic Materials*. Springer.
- HSU, M.-H. & HSU, Y.-L. 2005. Interpreting three-dimensional structural topology optimization results. *Computers & structures*, 83, 327-337.
- HUGO, N., STEFANUTTI, P., PELLERIN, M. & AKDAG, A. Power electronics traction transformer. 2007 European conference on power electronics and applications, 2007. IEEE, 1-10.

- HUI, S. & ZHU, J. 1995. Numerical modelling and simulation of hysteresis effects in magnetic cores using transmission-line modelling and the Preisach theory. *IEEE Proceedings-Electric Power Applications*, 142, 57-62.
- HURLEY, W. G. & WÖLFLE, W. H. 2013. *Transformers and inductors for power electronics: theory, design and applications*, John Wiley & Sons.
- IMAN-EINI, H., FARHANGI, S. & SCHANEN, J. A modular AC/DC rectifier based on cascaded H-bridge rectifier. 2008 13th International Power Electronics and Motion Control Conference, 2008. IEEE, 173-180.
- INSTITUTE, A. N. S. 1989. *IEEE Guide for Loading Dry-Type Distribution and Power Transformers*, IEEE.
- ISLAM, M. R., GUO, Y. & ZHU, J. 2013a. A high-frequency link multilevel cascaded medium-voltage converter for direct grid integration of renewable energy systems. *IEEE Transactions on Power Electronics*, 29, 4167-4182.
- ISLAM, M. R., GUO, Y. & ZHU, J. 2013b. A medium frequency transformer with multiple secondary windings for medium voltage converter based wind turbine power generating systems. *Journal of Applied Physics*, 113, 17A324.
- ISLAM, M. R., GUO, Y. & ZHU, J. 2014. A multilevel medium-voltage inverter for step-up-transformer-less grid connection of photovoltaic power plants. *IEEE journal of photovoltaics*, 4, 881-889.
- JIAN-NENG, C. & YING, W. 2012. Reverse Solution and Parametric Design of, the Conjugate Cam Weft Insertion, Mechanism Based on VB .NET and, UG [J]. *Journal of Donghua University (English, Edition)*, 29, 166-170.
- JIE, R., HONG, N., XIAOHUI, W. & YONGFENG, F. 2013. PARAMETRIC MODELING OF COMPONENT LIBRARY FOR LANDING GEAR BASED ON CATIA/CAA. *南京航空航天大学学报 (英文版)*, 02.
- JILES, D. C. & ATHERTON, D. L. 1984. Theory of ferromagnetic hysteresis. *Journal of applied physics*, 55, 2115-2120.
- JILES, D. C., THOELKE, J. & DEVINE, M. 1992. Numerical determination of hysteresis parameters for the modeling of magnetic properties using the theory of ferromagnetic hysteresis. *IEEE Transactions on magnetics*, 28, 27-35.
- JING, C., WANG, J., CUI, W., ZHAI, Y., HAN, D., WANG, X., HOU, J. & CHENG, Z. Numerical Analysis of Winding Temperature Field for Dry Type Transformer. 2012 Sixth International Conference on Electromagnetic Field Problems and Applications, 2012. IEEE, 1-4.
- JOHN, N., JAMES, J. & KOSHY, D. E. The Concept of Power Electronic Traction Transformer For Indian Railway. 2018 International Conference on Control, Power, Communication and Computing Technologies (ICCPCT), 2018. IEEE, 340-346.
- JOSHI, A. & NATH, S. Estimation of Core Loss of High Frequency Nanocrystalline Transformer for Non-sinusoidal Excitation. 2019 National Power Electronics Conference (NPEC), 2019. IEEE, 1-6.
- JUNG, J.-H. 2012. Bifilar winding of a center-tapped transformer including integrated resonant inductance for LLC resonant converters. *IEEE transactions on power electronics*, 28, 615-620.
- KARSAI, K., KERÉNYI, D. & KISS, L. 1987. Large power transformers.
- KHAN, A., WAHEED, D., SIDDIQUI, M. B., ANWER, M. S., HUSSAIN, S. W. & MAKDA, I. A. Design and Comparative Analysis of Litz and Copper Foil Transformers for High Frequency Applications. 2018 20th European Conference on Power Electronics and Applications (EPE'18 ECCE Europe), 2018. IEEE, P. 1-P. 10.

- KIEFERNDORF, F., DROFENIK, U., AGOSTINI, F. & CANALES, F. Modular PET, two-phase air-cooled converter cell design and performance evaluation with 1.7 kV IGBTs for MV applications. 2016 IEEE Applied Power Electronics Conference and Exposition (APEC), 2016. IEEE, 472-479.
- KRAWCZYK, A. & TEGOPOULOS, J. A. 1993. *Numerical modelling of eddy currents*, Oxford University Press.
- KYAW, P. A., DELHOMMAIS, M., QIU, J., SULLIVAN, C. R., SCHANEN, J.-L. & RIGAUD, C. 2019. Thermal modeling of inductor and transformer windings including litz wire. *IEEE Transactions on Power Electronics*, 35, 867-881.
- LA GANGA, A., REYHAN, S., RE, R., DALBAVIE, J.-M. & GUGLIELMI, P. Losses and thermal considerations on an IPOS structure with 20kW high-frequency planar transformers. 2020 International Conference on Electrical Machines (ICEM), 2020. IEEE, 921-926.
- LAI, J.-S., MAITRA, A., MANSOOR, A. & GOODMAN, F. Multilevel intelligent universal transformer for medium voltage applications. Fourtieth IAS Annual Meeting. Conference Record of the 2005 Industry Applications Conference, 2005., 2005. IEEE, 1893-1899.
- LAMMERANER, J. & ŠTAFL, M. 1966. *Eddy currents*, CRC Press.
- LANCAROTTE, M. S. & PENTEADO, A. D. A. 2001. Estimation of core losses under sinusoidal or nonsinusoidal induction by analysis of magnetization rate. *IEEE Transactions on Energy Conversion*, 16, 174-179.
- LEBEDEV, V. 1958. Calculation of the short-circuit resistance of welding transformers with yoke leakage (russ.). *Automatic Welding*, 11, 37-44.
- LEE, B. S., HAHN, J., ENJETI, P. N. & PITEL, I. J. 1999. A robust three-phase active power-factor-correction and harmonic reduction scheme for high power. *IEEE Transactions on Industrial Electronics*, 46, 483-494.
- LEE, R. 1988. *Transformers and Circuits*, John Wiley & Sons.
- LEE, R. & STEPHANS, D. Measurement of gap loss in current limiting transformers. Proc. Workshop Appl. Magn., 1972. 77-81.
- LEE, R. & STEPHENS, D. 1973. Influence of core gap in design of current-limiting transformers. *IEEE Transactions on Magnetics*, 9, 408-410.
- LEIBL, M., ORTIZ, G. & KOLAR, J. W. 2016. Design and experimental analysis of a medium-frequency transformer for solid-state transformer applications. *IEEE Journal of Emerging and Selected Topics in Power Electronics*, 5, 110-123.
- LI, J., ABDALLAH, T. & SULLIVAN, C. R. Improved calculation of core loss with nonsinusoidal waveforms. Conference Record of the 2001 IEEE Industry Applications Conference. 36th IAS Annual Meeting (Cat. No. 01CH37248), 2001. IEEE, 2203-2210.
- LI, Q., LIM, M., SUN, J., BALL, A., YING, Y., LEE, F. C. & NGO, K. Technology road map for high frequency integrated DC-DC converter. 2010 Twenty-Fifth Annual IEEE Applied Power Electronics Conference and Exposition (APEC), 2010. IEEE, 533-539.
- LI, Y., LI, L., JING, Y., HAN, F., LI, S. & ZHANG, F. Calculation and analysis of leakage magnetic field and short-circuit impedance in split-winding transformer. 2013 International Conference on Electrical Machines and Systems (ICEMS), 2013a. IEEE, 2263-2266.
- LI, Y., LI, L., JING, Y., LI, S. & ZHANG, F. Calculation and analysis of hot-spot temperature-rise of transformer structure parts based on magnetic-thermal coupling method. 2013 International Conference on Electrical Machines and Systems (ICEMS), 2013b. IEEE, 2259-2262.

- LI, Z. Development of transformer CAD system based on parametric technology. 2010 Second International Workshop on Education Technology and Computer Science, 2010. IEEE, 625-627.
- LI, Z., SHEN, Z., PAN, P. & JIN, L. Electromagnetic Dynamic of Medium-frequency Transformer in Electrostatic Precipitation. 2019 IEEE 4th International Future Energy Electronics Conference (IFEEEC), 2019. IEEE, 1-6.
- LIN, D., ZHOU, P., FU, W., BADICS, Z. & CENDES, Z. 2004. A dynamic core loss model for soft ferromagnetic and power ferrite materials in transient finite element analysis. *IEEE Transactions on magnetics*, 40, 1318-1321.
- LIU, R., MI, C. C. & GAO, D. W. Modeling of iron losses of electrical machines and transformers fed by PWM inverters. 2007 IEEE Power Engineering Society General Meeting, 2007. IEEE, 1-7.
- LIU, X., WANG, T., HU, L., CHEN, X., LIU, N. & CHEN, L. Design and Optimization of High Frequency Transformer with Nanocrystalline Core. 2019 4th International Conference on Intelligent Green Building and Smart Grid (IGBSG), 2019. IEEE, 246-249.
- LIU, X., WANG, Y., ISLAM, M. R., LEI, G., LIU, C. & ZHU, J. Comparison of electromagnetic performances of amorphous and nanocrystalline core-based high frequency transformers. 2014 17th International Conference on Electrical Machines and Systems (ICEMS), 2014. IEEE, 2028-2032.
- LIU, Z., ZHU, J. & ZHU, L. 2018. Accurate calculation of eddy current loss in litz-wired high-frequency transformer windings. *IEEE Transactions on Magnetism*, 54, 1-5.
- LOTFI, A. W. & LEE, F. C. A high frequency model for litz wire for switch-mode magnetics. Conference Record of the 1993 IEEE Industry Applications Conference Twenty-Eighth IAS Annual Meeting, 1993. IEEE, 1169-1175.
- LOTFI, A. W. & WILKOWSKI, M. A. 2001. Issues and advances in high-frequency magnetics for switching power supplies. *Proceedings of the IEEE*, 89, 833-845.
- LU, C., GUO, Z. & LIU, W. 2003. Theory and Calculation of Dry-Type Power Transformer.
- MA, Y., MENG, P., ZHANG, J. & QIAN, Z. Detailed losses analysis of high-frequency planar power transformer. 2007 7th International Conference on Power Electronics and Drive Systems, 2007. IEEE, 423-426.
- MAYERGOYZ, I. 1986. Mathematical models of hysteresis. *IEEE Transactions on magnetics*, 22, 603-608.
- MCLYMAN, C. W. T. 2017. *Transformer and inductor design handbook*, CRC press.
- MCLYMAN, C. W. T. 2018. *Magnetic Core Selection for Transformers and Inductors: A User's Guide to Practice and Specifications*, CRC Press.
- MCNUTT, W. 1992. Notes from Bill McNutt. *The Doble Exchange*, 10, 9-10.
- MEEKER, D. C. 2012. An improved continuum skin and proximity effect model for hexagonally packed wires. *Journal of Computational and Applied Mathematics*, 236, 4635-4644.
- MEYER, H. W. 1971. A history of electricity and magnetism.
- MOUAWAD, B., ESPINA, J., LI, J., EMPRINGHAM, L. & JOHNSON, C. M. Novel silicon carbide integrated power module for ev application. 2018 1st Workshop on Wide Bandgap Power Devices and Applications in Asia (WiPDA Asia), 2018. IEEE, 176-180.
- MUHAMMAD, K. S. & LU, D. D.-C. 2013. Magnetically isolated gate driver with leakage inductance immunity. *IEEE Transactions on Power Electronics*, 29, 1567-1572.
- MÜHLETHALER, J. 2012. *Modeling and multi-objective optimization of inductive power components*. ETH Zurich.

- NABHANI, F., ASKARI, V. & WARNAKULASURIYA, K. Determination of Losses in Conductors Carrying Higher Order Harmonics of Significant Amplitudes. WCE (World Congress in Engineering), London, England July, 2014.
- NAJAFI, A. & ISKENDER, I. Reducing losses in distribution transformer using 2605SA1 amorphous core based on time stepping finite element method. 2015 International Siberian Conference on Control and Communications (SIBCON), 2015. IEEE, 1-4.
- NAN, X. & SULLIVAN, C. R. An improved calculation of proximity-effect loss in high-frequency windings of round conductors. IEEE 34th Annual Conference on Power Electronics Specialist, 2003. PESC'03., 2003. IEEE, 853-860.
- NAN, X. & SULLIVAN, C. R. 2009. An equivalent complex permeability model for litz-wire windings. *IEEE Transactions on Industry Applications*, 45, 854-860.
- NIEMELA, V. A., SKUTT, G., URLING, A. M., CHANG, Y.-N., WILSON, T. G., OWEN, H. & WONG, R. C. Calculating the short-circuit impedances of a multiwinding transformer from its geometry. 20th Annual IEEE Power Electronics Specialists Conference, 1989. IEEE, 607-617.
- NING, W. & DING, X. Three-dimensional finite element analysis on fluid thermal field of dry-type transformer. 2012 Second International Conference on Instrumentation, Measurement, Computer, Communication and Control, 2012. IEEE, 516-519.
- OATES, C. & BASSETT, R. Future t&d technology. 2006 12th International Power Electronics and Motion Control Conference, 2006. IEEE, 2144-2148.
- ORTIZ, G., BIELA, J. & KOLAR, J. W. Optimized design of medium frequency transformers with high isolation requirements. IECON 2010-36th Annual Conference on IEEE Industrial Electronics Society, 2010. IEEE, 631-638.
- OUYANG, Z. & ANDERSEN, M. A. 2013. Overview of planar magnetic technology—Fundamental properties. *IEEE Transactions on Power Electronics*, 29, 4888-4900.
- OUYANG, Z., THOMSEN, O. C. & ANDERSEN, M. A. 2010. Optimal design and tradeoff analysis of planar transformer in high-power DC–DC converters. *IEEE Transactions on Industrial Electronics*, 59, 2800-2810.
- OUYANG, Z., ZHANG, J. & HURLEY, W. G. 2014. Calculation of leakage inductance for high-frequency transformers. *IEEE Transactions on Power Electronics*, 30, 5769-5775.
- OVERSHOTT, K. 1979. Amorphous ribbon materials and their possibilities. *Electronics & Power*, 25, 347-350.
- OVERSHOTT, K. 1991. IEE Science Education & Technology Division: Chairman's address. Magnetism: it is permanent. *IEE Proceedings A (Science, Measurement and Technology)*, 138, 22-30.
- PAVLOVSKY, M., DE HAAN, S. & FERREIRA, J. Partial interleaving: a method to reduce high frequency losses and to tune the leakage inductance in high current, high frequency transformer foil windings. 2005 IEEE 36th Power Electronics Specialists Conference, 2005. IEEE, 1540-1547.
- PETZOLD, J. 2002. Advantages of softmagnetic nanocrystalline materials for modern electronic applications. *Journal of Magnetism and Magnetic Materials*, 242, 84-89.
- PICANÇO, A., DE SALLES, C., MARTINEZ, M., ROSA, P. & DE OLIVEIRA, H. Development of Economical Analysis and Technical Solutions for Efficient Distribution Transformers. 6th Mediterranean Conference and Exhibition on Power Generation, Transmission, Distribution and Energy Conversion—MedPower, 2008.
- PIERCE, L. Predicting liquid filled transformer loading capability. [1992] Record of Conference Papers Industry Applications Society 39th Annual Petroleum and Chemical Industry Conference, 1992a. IEEE, 197-207.



- PIERCE, L. W. 1992b. An investigation of the thermal performance of an oil filled transformer winding. *IEEE Transactions on Power Delivery*, 7, 1347-1358.
- PIERCE, L. W. 1996. Transformer design and application considerations for nonsinusoidal load currents. *IEEE Transactions on industry applications*, 32, 633-645.
- POLLOCK, J. D., ABDALLAH, T. & SULLIVAN, C. R. Easy-to-use CAD tools for litz-wire winding optimization. Eighteenth Annual IEEE Applied Power Electronics Conference and Exposition, 2003. APEC'03., 2003. IEEE, 1157-1163.
- POPOVIĆ, Z. B. & POPOVIĆ, B. D. 2000. *Introductory electromagnetics*, Addison-Wesley.
- POVEDA-LERMA, A., MARTINEZ-LA-OSA, P., RODRIGUEZ-MANEZ, E., PUCHE-PANADERO, R. & PINEDA-SANCHEZ, M. Improved Interleaved Layer Distribution for High-Frequency High-Power Planar Transformer. 2019 19th International Symposium on Electromagnetic Fields in Mechatronics, Electrical and Electronic Engineering (ISEF), 2019. IEEE, 1-2.
- PRADHAN, M. & RAMU, T. 2003. Prediction of hottest spot temperature (HST) in power and station transformers. *IEEE Transactions on Power Delivery*, 18, 1275-1283.
- PREININGEROVA, V., KAHOUN, V. & DOLEŽEL, I. 1983. Thermal analysis of large oil-immersed transformer windings. *Electric Machines and Power Systems*, 8, 89-102.
- PREISACH, F. 1935. Über die magnetische Nachwirkung. *Zeitschrift für physik*, 94, 277-302.
- PRYOR, L., SCHLOBOHM, R. & BROWNELL, B. 2008. A comparison of aluminum vs. copper as used in electrical equipment. *GE Consumer and Industrial*, 1-7.
- RABIUL ISLAM, M., GUO, Y., WEI LIN, Z. & ZHU, J. 2014. An amorphous alloy core medium frequency magnetic-link for medium voltage photovoltaic inverters. *Journal of Applied Physics*, 115, 17E710.
- RAZAK, A. A., TAIB, S. & DAUT, I. Design and development of high frequency high power transformer for renewable energy application. International conference on robotics, vision, information and signal processing, 2005. 375-379.
- REATTI, A. & KAZIMIERCZUK, M. K. 2002. Comparison of various methods for calculating the AC resistance of inductors. *IEEE Transactions on Magnetics*, 38, 1512-1518.
- REINERT, J., BROCKMEYER, A. & DE DONCKER, R. W. 2001. Calculation of losses in ferro-and ferrimagnetic materials based on the modified Steinmetz equation. *IEEE Transactions on Industry applications*, 37, 1055-1061.
- REN, X., ZHOU, Y., WANG, D., ZOU, X. & ZHANG, Z. 2016. A 10-MHz isolated synchronous class- $\Phi$  2 resonant converter. *IEEE Transactions on Power Electronics*, 31, 8317-8328.
- RIOS, M., VENKATARAMANAN, G., MUETZE, A. & EICKHOFF, H. Thermal performance modeling of foil wound concentrated coils in electric machines. 2016 IEEE Energy Conversion Congress and Exposition (ECCE), 2016. IEEE, 1-8.
- ROBERT, F., MATHYS, P. & SCHAUWERS, J.-P. The layer copper factor, although widely used and useful, has no theoretical base [smmps transformers]. 2000 IEEE 31st Annual Power Electronics Specialists Conference. Conference Proceedings (Cat. No. 00CH37018), 2000. IEEE, 1633-1638.
- ROBERT, F., MATHYS, P. & SCHAUWERS, J.-P. 2001. A closed-form formula for 2-D ohmic losses calculation in SMPS transformer foils. *IEEE Transactions on Power Electronics*, 16, 437-444.
- ROESLER, A., SCHARE, J. & HETTLER, C. Integrated power electronics using a ferrite-based low-temperature co-fired ceramic materials system. 2010 Proceedings 60th Electronic Components and Technology Conference (ECTC), 2010. IEEE, 720-726.
- ROPOTEANU, C., SVASTA, P. & IONESCU, C. A study of losses in planar transformers with different layer structure. 2017 IEEE 23rd International Symposium for Design and Technology in Electronic Packaging (SIITME), 2017. IEEE, 255-258.

- ROSHEN, W. A. 2007. A practical, accurate and very general core loss model for nonsinusoidal waveforms. *IEEE Transactions on Power Electronics*, 22, 30-40.
- ROßKOPF, A., BÄR, E., JOFFE, C. & BONSE, C. 2015. Calculation of power losses in litz wire systems by coupling FEM and PEEC method. *IEEE Transactions on Power Electronics*, 31, 6442-6449.
- ROSSMANITH, H., DOEBROENTI, M., ALBACH, M. & EXNER, D. 2011. Measurement and characterization of high frequency losses in nonideal litz wires. *IEEE Transactions on Power Electronics*, 26, 3386-3394.
- RYLKO, M. S., LYONS, B. J., HAYES, J. G. & EGAN, M. G. 2011. Revised magnetics performance factors and experimental comparison of high-flux materials for high-current DC–DC inductors. *IEEE Transactions on Power Electronics*, 26, 2112-2126.
- SATTERLEE, W. 1944. Design and operating characteristics of modern dry-type air-cooled transformers. *Electrical Engineering*, 63, 701-704.
- SHEN, W. 2006. *Design of high-density transformers for high-frequency high-power converters*. Virginia Tech.
- SHEN, W., WANG, F., BOROYEVICH, D. & TIPTON, C. W. 2008a. Loss characterization and calculation of nanocrystalline cores for high-frequency magnetics applications. *IEEE Transactions on Power Electronics*, 23, 475-484.
- SHEN, W., WANG, F., BOROYEVICH, D. & TIPTON IV, C. W. 2008b. High-density nanocrystalline core transformer for high-power high-frequency resonant converter. *IEEE Transactions on Industry Applications*, 44, 213-222.
- SHEN, Z., SHEN, Y. & WANG, H. Thermal Modelling of Planar Transformers Considering Internal Power Loss Distribution. 2019 IEEE 4th International Future Energy Electronics Conference (IFEEEC), 2019. IEEE, 1-5.
- SHU-FANG, W. 2011. Parametric Collaborative Design of Network-based Mechanical Products.
- SHUAI, P. & BIELA, J. Design and optimization of medium frequency, medium voltage transformers. 2013 15th European Conference on Power Electronics and Applications (EPE), 2013. IEEE, 1-10.
- SIEGEL, D. M. 2003. *Innovation in Maxwell's electromagnetic theory: Molecular vortices, displacement current, and light*, Cambridge University Press.
- SPYKER, R., HUTH, J., MEHDI, I. & BROCKSCHMIDT, A. 300C ferrite material for high temperature magnetics. 2004 IEEE 35th Annual Power Electronics Specialists Conference (IEEE Cat. No. 04CH37551), 2004. IEEE, 155-160.
- STADLER, A. & ALBACH, M. 2006. The influence of the winding layout on the core losses and the leakage inductance in high frequency transformers. *IEEE Transactions on Magnetics*, 42, 735-738.
- STEINER, M. & REINOLD, H. Medium frequency topology in railway applications. 2007 European Conference on Power Electronics and Applications, 2007. IEEE, 1-10.
- STEINMETZ, C. P. 1892. On the law of hysteresis. *Transactions of the American Institute of Electrical Engineers*, 9, 1-64.
- STEWART, H. & WHITMAN, L. 1944. Hot-spot temperatures in dry-type transformer windings. *Electrical Engineering*, 63, 763-768.
- STYSKIN, A. V. & URAZBAKHTINA, N. G. Parametric transformer designs with improved technical characteristics. 2020 International Conference on Electrotechnical Complexes and Systems (ICOECS), 2020. IEEE, 1-6.
- SULLIVAN, C. R. 1999. Optimal choice for number of strands in a litz-wire transformer winding. *IEEE transactions on power electronics*, 14, 283-291.

- SULLIVAN, C. R. & ZHANG, R. Y. Analytical model for effects of twisting on litz-wire losses. 2014 IEEE 15th Workshop on Control and Modeling for Power Electronics (COMPEL), 2014a. IEEE, 1-10.
- SULLIVAN, C. R. & ZHANG, R. Y. Simplified design method for litz wire. 2014 IEEE Applied Power Electronics Conference and Exposition-APEC 2014, 2014b. IEEE, 2667-2674.
- SUSA, D. & NORDMAN, H. 2009. A simple model for calculating transformer hot-spot temperature. *IEEE transactions on power delivery*, 24, 1257-1265.
- SUZUKI, K., MAKINO, A., INOUE, A. & MASUMOTO, T. 1991. Soft magnetic properties of nanocrystalline bcc Fe-Zr-B and Fe-M-B-Cu (M= transition metal) alloys with high saturation magnetization. *Journal of Applied Physics*, 70, 6232-6237.
- SWIFT, G., MOLINSKI, T. S. & LEHN, W. 2001. A fundamental approach to transformer thermal modeling. I. Theory and equivalent circuit. *IEEE transactions on Power Delivery*, 16, 171-175.
- TANG, X. & SULLIVAN, C. R. Stranded wire with uninsulated strands as a low-cost alternative to litz wire. IEEE 34th Annual Conference on Power Electronics Specialist, 2003. PESC'03., 2003. IEEE, 289-295.
- TAUFIQ, J. Power electronics technologies for railway vehicles. 2007 Power Conversion Conference-Nagoya, 2007. IEEE, 1388-1393.
- TOURKHANI, F. & VIAROUGE, P. 2001. Accurate analytical model of winding losses in round Litz wire windings. *IEEE Transactions on magnetics*, 37, 538-543.
- TROISI, J. 1992. Experience with fiber optic hot-spot sensors in 450 MVA SMIT autotransformer. *DOBLE Proc*, 6, 1-16.
- VANDELAC, J.-P. & ZIOGAS, P. D. 1988. A novel approach for minimizing high-frequency transformer copper losses. *IEEE Transactions on power electronics*, 3, 266-277.
- VENKATACHALAM, K., SULLIVAN, C. R., ABDALLAH, T. & TACCA, H. Accurate prediction of ferrite core loss with nonsinusoidal waveforms using only Steinmetz parameters. 2002 IEEE Workshop on Computers in Power Electronics, 2002. Proceedings., 2002. IEEE, 36-41.
- VILLAR, I. 2010. Multiphysical characterization of medium-frequency power electronic transformers. *Lausanne, Switzerland: Ecole Polytechnique Fédérale de Lausanne*.
- WANG, D., MAO, C. & LU, J. 2007. Modelling of electronic power transformer and its application to power system. *IET Generation, Transmission & Distribution*, 1, 887-895.
- WANG, J.-M., WANG, Y.-X., HAN, D.-J., JIA, J.-G., ZHANG, W. & ZHU, F.-S. 2010. Numerical Analysis of Leakage Magnetic Field and Its Characteristic Parameters of Foil Winding in Transformer [J]. *Transformer*.
- WANG, X.-C. & TAO, J.-P. 2008. Temperature field research of large forced-directed oil cooling transformer. *Transformer*, 7, 6-10.
- WANG, Y., CALDERON-LOPEZ, G. & FORSYTH, A. J. 2016. High-frequency gap losses in nanocrystalline cores. *IEEE Transactions on Power Electronics*, 32, 4683-4690.
- XIE, B., LI, X., CHEN, Q., ZHANG, Y. & WANG, J. Calculation of the circulating current and short-circuit impedance of a 3000kVA HTS transformer with split types of windings. 2007 International Conference on Electrical Machines and Systems (ICEMS), 2007. IEEE, 1291-1295.
- YONG-XIANG, D., DONG-HONG, S., YU-JUN, X. & JI-SHUN, L. Parametric Design of Complex Elastic Components. 2017 Second International Conference on Mechanical, Control and Computer Engineering (ICMCCE), 2017. IEEE, 87-91.
- YOSHIZAWA, Y. OGUMA., and YAMAUCHI, K., 1988. *J. appl. Phys*, 64, 6044.
- ZHANG, H., LEE, J.-H., IYER, N. M. & CAO, L. New analytical equations for skin and proximity effects in interconnects operated at high frequency. 2017 IEEE Electron Devices Technology and Manufacturing Conference (EDTM), 2017. IEEE, 39-41.

- ZHANG, J., HURLEY, W. G., WOLFLE, W. H. & DUFFY, M. C. Optimized design of LLC resonant converters incorporating planar magnetics. 2013 Twenty-Eighth Annual IEEE Applied Power Electronics Conference and Exposition (APEC), 2013. IEEE, 1683-1688.
- ZHANG, J. & LI, X. 2004. Coolant flow distribution and pressure loss in ONAN transformer windings. Part II: Optimization of design parameters. *IEEE Transactions on Power Delivery*, 19, 194-199.
- ZHANG, J., OUYANG, Z., DUFFY, M. C., ANDERSEN, M. A. & HURLEY, W. G. 2014a. Leakage inductance calculation for planar transformers with a magnetic shunt. *IEEE Transactions on Industry Applications*, 50, 4107-4112.
- ZHANG, K., CHEN, W., CAO, X., SONG, Z., QIAO, G. & SUN, L. Optimization design of high-power high-frequency transformer based on multi-objective genetic algorithm. 2018 IEEE International Power Electronics and Application Conference and Exposition (PEAC), 2018. IEEE, 1-5.
- ZHANG, K., WU, T., KUTKUT, N., SHEN, J., WOODBURN, D., CHOW, L., WU, W., MUSTAIN, H. & BATARSEH, I. Modeling and design optimization of planar power transformer for aerospace application. Proceedings of the IEEE 2009 National Aerospace & Electronics Conference (NAECON), 2009. IEEE, 116-120.
- ZHANG, R. Y., WHITE, J. K., KASSAKIAN, J. G. & SULLIVAN, C. R. Realistic litz wire characterization using fast numerical simulations. 2014 IEEE Applied Power Electronics Conference and Exposition-APEC 2014, 2014b. IEEE, 738-745.
- ZHAO, L., GE, Q., ZHOU, Z., YANG, B., WANG, K. & LI, Y. Calculation and Analysis of the Winding Loss of High-Frequency Transformer Based on Finite Element Method. 2018 21st International Conference on Electrical Machines and Systems (ICEMS), 2018. IEEE, 2655-2658.
- ZHAO, S., LI, Q., LEE, F. C. & LI, B. 2017. High-frequency transformer design for modular power conversion from medium-voltage AC to 400 VDC. *IEEE Transactions on Power Electronics*, 33, 7545-7557.
- ZHENG, J. 2000. *Transformer ac winding resistance and derating when supplying harmonic-rich current*. Michigan Technological University.
- 陈建能, 王英, 雷昌毅, 赵雄 & 林万焕 2012. Reverse Solution and Parametric Design of the Conjugate Cam Weft Insertion Mechanism Based on VB .NET and UG. *Journal of Donghua University (English Edition)*.